THE MODIFICATION OF RESIDUAL GAS ANALYZERS TO PRODUCE MASS-SELECTED ION BEAMS

by

Jeffrey Ross Gilbert

A DISSERTATION

Submitted to
Michigan State University
in partial fulfillment of the requirements
for the degree of

DOCTOR OF PHILOSOPHY

Department of Chemistry

1990

ABSTRACT

THE MODIFICATION OF RESIDUAL GAS ANALYZERS TO PRODUCE MASS-SELECTED ION BEAMS

by

Jeffrey Ross Gilbert

We have constructed an instrument designed to trap mass-selected ions at low temperatures within a solid inert gas matrix for spectroscopic analysis. Our goal was to construct a flexible instrument that would permit the study of a wide variety of mass-selected positive ions, and which could also be used to investigate the role that counterions play in the effective trapping of ionic species in inert cryogenic hosts. This type of experiment requires the production of two mass-selected ion beams, a beam of mass-selected cations that are deposited simultaneously with a beam of anions to reduce space-charging within the matrix. The instrument was designed to utilize both laser-induced fluorescence (LIF) and Fourier transform infrared (FTIR) spectroscopies to identify and investigate the structure of the trapped species. The sources employed in this experiment must produce high current ion beams for extended periods to allow the accumulation of a significant number of absorbers in the optical beam for FTIR investigation. Residual gas analyzers (RGAs) were selected as the basis for the mass-selected ion sources for this instrument. An RGA is a specialized high vacuum pressure gauge that consists of a high efficiency electron impact ionization source, injection optics, a miniature quadrupole mass filter, and a detector.

This dissertation focuses on the modification of two RGAs to produce controlled beams of mass-selected positive and negative ions that can be directed onto a remote surface for matrix isolation experiments. The discussion includes descriptions of the modifications made to the RGA ion sources and to a commercially available chemical ionization source to produce ions by surface emission, chemical ionization, and negative surface ionization. The mass-selected beams produced by the RGA quadrupoles were focused and deflected using a series of electrostatic optics. The design of these elements was optimized using computer modeling and ion beam visualization techniques. The modifications to the ion sources, quadrupole mass filters, and electrostatic optics of these systems have allowed these RGAs to produce mass-selected ion beams that have been effectively used in the isolation of mass-selected ions within solid inert gas matrices.

In dedication to my parents
whose lives continue to provide inspiration in all that I do
and in memory of
Carbon
the best friend I ever had

ACKNOWLEDGMENTS

This project has been a conglomeration of the efforts of many individuals, all of whom have been invaluable in its completion. First of all I would like to thank Mark Sabo who has made my graduate experience more than just a bunch of lab work (even if at times it was more odiferous than I might have desired). I think that the all night experiments watching "The Big Brawl" movies will always be my favorite memory of lab 'work'. I started this project with little or no experience in the hardware side of mass spectrometry, and I'd like to thank Paul O'Connor for all his help in running these experiments. Finally I'd like to thank John Allison and George Leroi for their guidance and supervision. In this project I was working toward a goal of their conception, and I hope that my efforts have aided in the completion of that goal.

I'd also like to thank all the support staff for the hundreds of hours that they have spent trying to interpret my somewhat confused needs. Russ Geyer and Dick Menke made many of my convoluted designs into something that actually worked. Their help with my work and in the overall construction of the matrix isolation instrument was truly invaluable. Marty Rabb and Ron Haas put up with uncounted hours of pestering when I had incorrectly designed or misconnected various electrical components, and I'd like to thank them for both their help and tolerance.

Last, but far from least, I'd like to thank all the people here at State that made graduate school an experience that I will always look back on fondly. I'd like to thank Berly for putting up with me these last few months while I've been under a lot of stress, and for all the support/stress relief efforts she has made. I will always miss 'the gang' here at MSU.

Kris, Sabo, Jason, D.G., Laura, Karen, Ed and Maria, Judy, Jim D., Gary, Tom, Nurt, and the rest of the gang have made grad school fun. I'll always remember the rowboat party my first year, Mac's Bar fall of my second year, poker parties in cigar smoke filled rooms, keg parties in our old apartment, wild friday nights of pre, during, and post-hockey partying, and other fun events too numerous (or embarrassing) to mention here. I don't think that I would have survived without you guys.....thanks!!!

Table of Contents

LIST OF TABLES

LIST OF FIGURES

Figure **Page**

Chapter 1. Introduction

One of the most powerful modern analytical techniques available is mass spectrometry. Mass spectrometry utilizes the mass-to-charge ratio of ions, produced through gas phase ionization of an analyte molecule, to obtain both qualitative and quantitative information. The combination of information about the molecular ion, and the fragment ions which are produced by unimolecular decomposition of the molecular ion has proven especially useful in identifying the structures of unknown compounds. The formation of these fragment ions is generally explained using accepted unimolecular decomposition mechanisms. These mechanisms are based upon thermodynamically and structurally reasonable pathways through a series of parent ion, intermediate ion, and product ion structures.

Mass spectrometrists often utilize indirect methods, such as isotopic labeling and collision-induced dissociation, to verify the structures of these ions.. For organometallic systems, ligand displacement reactions can be used to identify the ligands attached to a central metal ion. By combining these techniques, the proposed structures of many ions have been verified. One example was the identification of the $NiC_4H_8^+$ ion produced through the interaction of Ni^+ ion with n-butane. Beauchamp and co-workers performed a series of ion beam and ion cyclotron reactions of Ni^+ with n-butane [1]; some of the observed product ions for this reaction were:

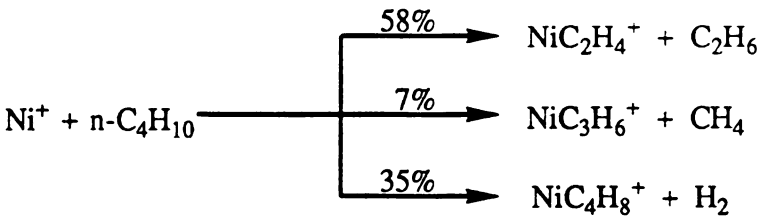

Two mechanisms were proposed to explain the formation of the $NiC_4H_8^+$ ion, a 1,2-elimination process and a 1,4-elimination process. The proposed

first step in the 1,2-elimination mechanism is the oxidative addition of Ni^+ across a secondary C-H bond of a butane molecule, shown below [2]. This insertion is followed by the shift of a ß-hydrogen onto the metal ion to form a butene-ion complex. Finally, the reductive elimination of H_2 results in the formation of the Ni-butene ionic complex, $NiC_4H_8^+$, of unknown geometry.

1,2-elimination mechanism

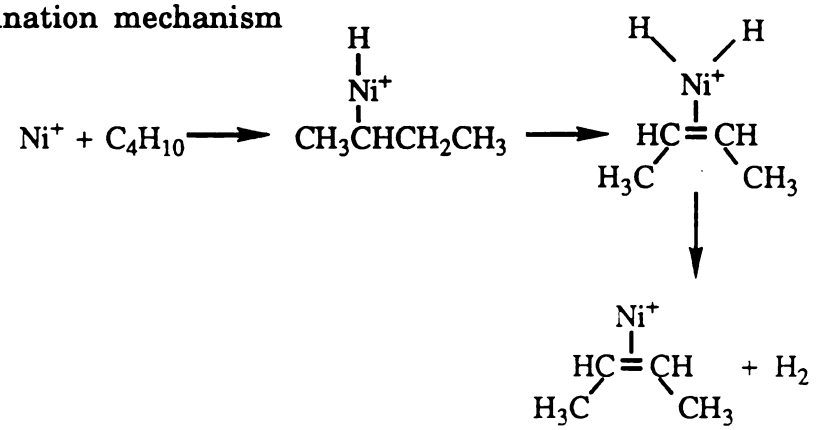

The proposed first step in the 1,4-elimination mechanism is the oxidative addition of Ni^+ across the central C-C bond of a butane molecule. This is followed by two successive ß-hydrogen shifts onto the metal ion. Finally, the reductive elimination of H_2 results in the production of the bis-olefin ionic complex shown below.

1,4-elimination mechanism

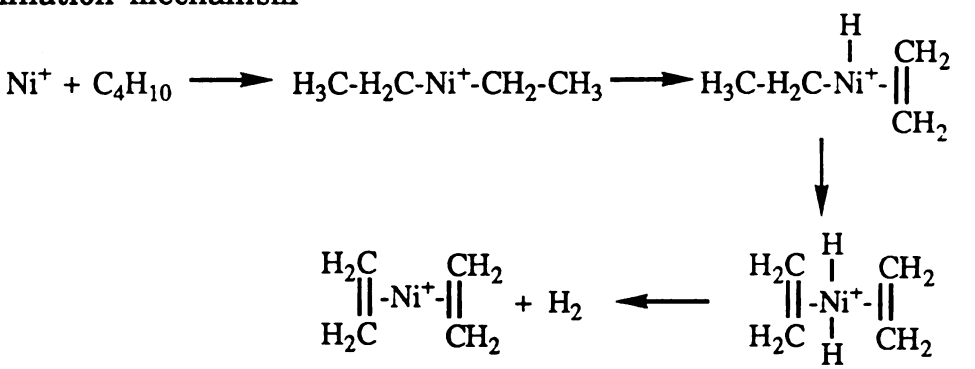

Both of these proposed mechanisms would result in the production of ions

with identical masses. To determine which mechanism was responsible for the formation of the $NiC_4H_8^+$ ion, a series of isotopic labeling, ligand exchange, and collision-induced dissociation experiments were performed. The reaction was repeated using butane with deuterium atoms substituted for the hydrogens on the terminal butane carbons. If the $NiC_4H_8^+$ ion was formed through the 1,2-elimination mechanism, a neutral loss of HD or H_2 would be observed. If, however, the $NiC_4H_8^+$ is formed through the 1,4-elimination mechanism the result should be a loss of D_2. When Ni^+ was allowed to react with the labeled butane neutral a loss of D_2 was observed; this suggested that the $NiC_4H_8^+$ ion had a bis-olefin ionic structure and was formed through the 1,4-elimination mechanism.

In previous studies the two ligand displacement reaction of $Ni(C_4H_4)_2^+$ with HCN to form $Ni(HCN)_2^+$ was determined to be exothermic by 10 kcal [3]. However, reactions of Ni^+ with HCN did not produce $Ni(HCN)_n^+$ ionic complexes. ICR ligand exchange experiments were performed using HCN to further investigate the structure of $NiC_4H_8^+$. Ni^+ was again reacted with n-butane, this time in the presence of HCN, and the rapid formation of $Ni(C_2H_4)(HCN)^+$ and $Ni(HCN)_2^+$ ions from $NiC_4H_8^+$ was observed. Through double resonance experiments, these ions were linked to the initial formation of $NiC_4H_8^+$ which again indicated that the $NiC_4H_8^+$ ion was formed through the 1,4-elimination mechanism. The sequential displacement of C_2H_4 from $NiC_4H_8^+$ also confirmed that the $NiC_4H_8^+$ ion had a bis-olefin structure.

In a separate study, collision induced dissociation experiments were performed on the $NiC_4H_8^+$ ion using a Fourier transform ion cyclotron mass spectrometer [4]. Ni^+ was reacted with neutral n-butane to form $NiC_4H_8^+$. All other ions were ejected from the FTMS cell, and the $NiC_4H_8^+$ ion was collided with neutral argon molecules at varying collision energies. At low collision energies the neutral loss of C_2H_4 was observed. As the collision energy was increased a loss of C_4H_8 was observed along with the loss of C_2H_4. Throughout all the collision energies investigated, the

dominant neutral loss was C_2H_4. These results confirmed that the $NiC_4H_8^+$ ion had a bis-olefin structure, and could sequentially lose one or two of the C_2H_4 ligands depending upon the energy of collision.

Through the combination of these three indirect methods the $NiC_4H_8^+$ ion was confirmed to have a bis-olefin structure, indicating its formation through a 1,4-elimination mechanism. These indirect methods for structural elucidation have been used to confirm proposed structures for fragment ions formed through unimolecular decomposition as well as ions produced through ion/molecule reactions. More conclusive results could be obtained if the structures of ions could be determined directly through spectroscopic methods, but this type of study is limited by difficulties associated with concentrating ionic species in the gas phase due to Coulombic repulsion. Instead, a combination of indirect methods for structural elucidation is generally applied.

Several other indirect experimental methods exist for the determination of ionic structures. These have recently been reviewed [5], and are often used in combination to ensure that accurate conclusions are drawn [6]. Some of these methods include:

Isotopic labeling studies
Ligand exchange studies/ ion-molecule reactions
Collisionally induced dissociation
Photodissociation
Kinetic energy release
Metastable ion characteristics

Isotopic labeling methods, described above, can yield useful information, but require the use of labeled compounds and can be complicated by internal scrambling if the ion is formed with high levels of internal energy. Collision induced dissociation (CID) can be used to determine both the mass and appearance potential of the collisionally

formed fragments, but the internal energy of the fragment ions is not well defined. Rearrangements can also occur in CID if large amounts of energy are present in the fragment ions, and the CID technique requires specialized instrumentation. Photodissociation is a powerful technique for the determination of appearance potentials of molecular and fragment ions. These can be used in combination with neutral heats of formation data to infer ionic structures [7]. Unfortunately the excess energy of the ions formed through photodissociation or other appearance potential methods is often unknown which can complicate these structural inferences. The observation of metastable ion peak widths and onset energies can be used to compare the kinetic energy release and rate constants for the degradation of ions [8]. This information can be used to confirm the presence of different structures for isomass ions, but yields little direct structural information. Through combination, these indirect techniques can be used as powerful techniques for investigating ion structures.

Direct methods also exist for the investigation of ion structures; several of these have been recently reviewed [9,10]. Microwave spectroscopy of ions formed in plasma discharges has proven a powerful technique for the study of the rotational absorptions bands of molecular ions [11]. Coulombic explosion experiments can be used to determine the nuclear positions of ions through high energy collisions (MeV) of ion beams with solid targets [12]. Photoelectron spectroscopy has been used to perform low resolution analysis of ion structures [13]. Infrared laser spectroscopy has recently emerged as an extremely powerful, high resolution technique for studying ion structures [14]. This technique generally obtains infrared absorption bands for ions using tunable infrared lasers. The laser beam is sent coaxially through a high energy ion beam, and the infrared absorption of ions in the beam is monitored using mode-locked detection. Mode-locked detection is performed by applying an ac signal to the accelerating voltage of the ion source, which allows discrimination against absorptions from

neutral molecules in the ion beam. This technique is extremely powerful, but the wavelength region that can be scanned is limited to the tunability of the IR laser, or the ion velocity range that can be tuned for velocity modulation tuning. In general only a range of 0.25 cm^{-1} can be scanned in a single experiment.

Reactive species, such as ions, can also be studied using the technique of matrix isolation. In a matrix isolation experiment a reactive species is trapped within an inert solid matrix maintained at extremely low temperatures. This technique, first introduced by George Pimentel in 1954 [15], has been used to study a variety of highly reactive transient species by electron spin resonance, Fourier transform infrared and laser induced fluorescence spectroscopies [16,17]. For ionic species, it has been stated that "modern laser experiments have shown that some of the more detailed infrared studies made in crystals do, in fact, produce reasonable approximations to gas phase structures and vibrational frequencies..." [18]; thus matrix isolation spectroscopy of ions has proved to be a useful complement to high resolution laser spectroscopy experiments. Matrix isolation experiments are generally performed at temperatures of ~10 K, and therefore must be conducted within a high vacuum chamber using cryogenic techniques. The analyte sample or ion is generally co-deposited with an unreactive matrix gas, commonly argon or neon, onto an appropriate substrate maintained at $\leq$10 K. If the matrix gas is deposited at the correct matrix to host ratio, often 10,000:1, ions can be trapped within an unreactive noble gas 'cage' and stored for extended periods. This allows the accumulation of higher concentrations of ions than can be obtained using gas-phase methods.

Various methods have been used to generate ionic species within low temperature noble gas matrices and have been described in several reviews [19,20,21,22,23]. Ions formed through these methods are generally classified as either bound ion pairs or isolated ions (ions trapped in separate matrix cavities). Some of the methods used to produce isolated

ions include;

Vacuum ultraviolet (VUV) photoionization [24]
γ and x-ray irradiation [25]
Windowless discharge [26]
Proton radiolysis [27]
Electron bombardment [28]
Fast atom bombardment [29]
Laser vaporization [30]
Chemical ionization sources [31]
Deposition of mass-selected positive ions [32]

VUV photoionization experiments are performed by co-depositing the sample precursor molecule and the matrix gas upon the cold substrate. Following deposition, the matrix is bombarded with high energy VUV photons from a mercury, hydrogen, or argon lamp. These high energy photons can photoionize the sample molecules, forming ions in the matrix. Gamma irradiation, x-ray irradiation, proton radiolysis, and electron bombardment techniques are similar techniques that utilize other energy sources to form ions during or after deposition of the matrix. Fast atom bombardment (FAB) and laser sputtering have both been used to produce ions that are co-deposited with the matrix gas. FAB has been used to directly produce ions from metal targets, and laser sputtering has been used to produce clusters from metal surfaces that are deposited and ionized using VUV photoionization. Another method recently used to deposit both positive and negative ions within a noble gas matrix is chemical ionization. A mass spectrometer high pressure chemical ionization source was adapted for production of ions in a matrix isolation experiment, with argon utilized as the source buffer gas. From this high pressure source both positive and negative ions were effectively trapped in an argon matrix. All of these techniques have been successfully used to produce ions trapped

within noble gas matrices, but with all of these methods a variety of ions can be formed from the matrix gas, precursor molecule, and contaminants in the matrix, making the exact determination of ion structure difficult. Matrix isolation experiments have recently been performed by depositing high energy (50-350 eV) mass-selected positive ions produced by a quadrupole mass spectrometer [32]. This method of ion production allows the unambiguous deposition of specific ions within the matrix for subsequent spectroscopic analysis.

The goal of the matrix isolation project currently in progress within the Allison and Leroi groups is to isolate mass-selected ions produced by quadrupole mass spectrometers for spectroscopic investigation. Most methods currently in use for the production of matrix isolated ions can produce a variety of ionic species, at times making the identification of trapped species ambiguous. By trapping the mass-selected ions emanating from quadrupole mass spectrometers we have greatly increased the selectivity of the ion trapping process. It is also generally true that most ion formation conditions are accompanied by the production of oppositely-charged counter-ions. In processes such as VUV photoionization these ions are assumed to result from the capture of electrons released through ionization by electrophilic contaminant molecules, such as H_2O, trapped in the noble gas matrix. The formation and/or need for these counter-ions in the effective trapping of ions in noble gas matrices is not well understood. We have designed an instrument that enables both positive and negative ions to be co-deposited within the matrix gas to allow the study of the role of counter-ions in effective ion trapping.

The instrument that has been constructed for these studies is shown in Figure 1.1. A more detailed discussion of the design and operation of the entire instrument is forthcoming [33], and the overall instrument will be outlined only briefly in this manuscript. The instrument is based upon an 8" diameter ultrahigh vacuum chamber constructed of stainless steel and conflat flanges which is pumped by a Leybold-Heraeus 1500 l/sec cryopump

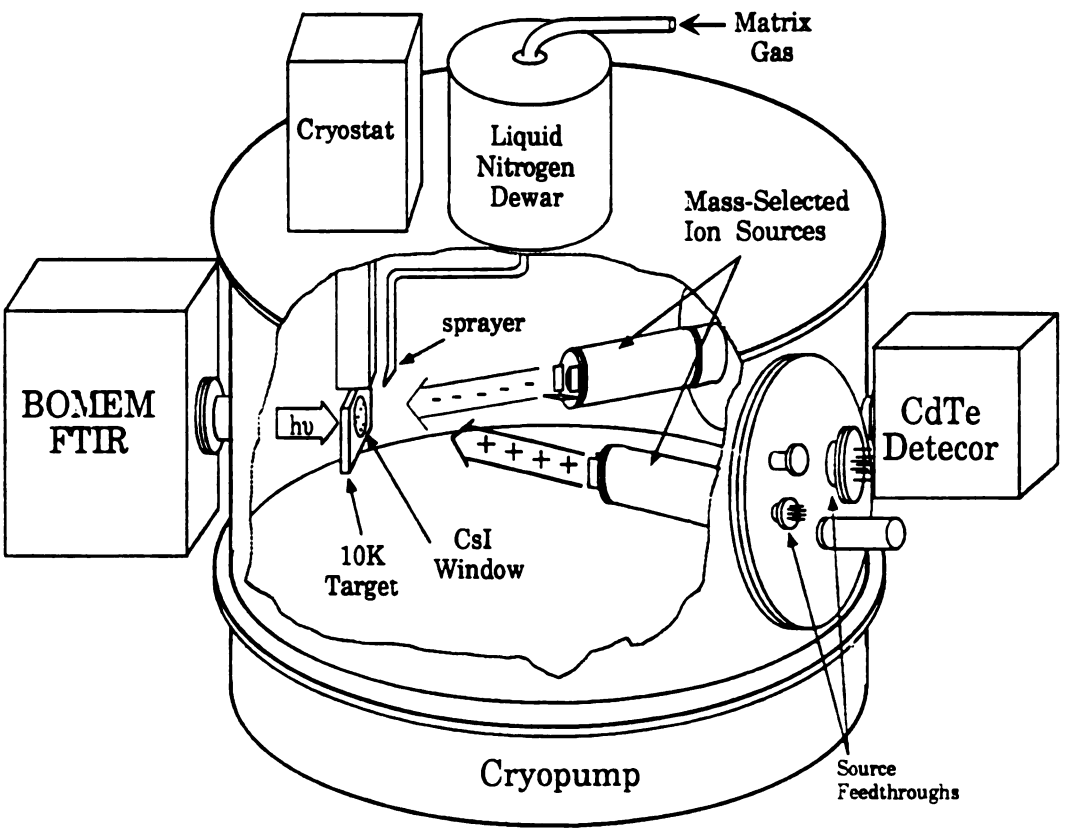

Figure 1.1 The matrix isolation instrument designed for the isolation of mass selected ions followed by spectroscopic analysis (LIF and FTIR).

to maintain clean deposition conditions. This chamber houses an Air Products Displex 202 cryostat head which can achieve temperatures down to 10 Kelvins. This cold head is in thermal contact with an optical substrate upon which both ions and matrix gas are co-deposited. The matrix gas, in this case argon, is introduced through a high precision leak valve to a sprayer that directs the gas onto the cryostat window. Two 6" conflat flanges, used to mount the ion sources, are located opposite the cryostat window as shown in Figure 1.1. Ion sources have been fabricated that can produce low energy positive and negative mass-selected ion beams which are directed onto the cryostat window using a series of electrostatic optics. Using these ion sources, mass-selected positive and negative ions are co-deposited with matrix gas to allow the accumulation of ions for extended periods, in some cases over a period of days. A linear motion feedthough (LMF), not shown in the figure, can be inserted between the cryostat window and the ion sources. An electrically isolated Faraday plate is mounted onto the LMF and can be positioned directly in front of the optical substrate. This Faraday plate can be inserted to measure ion current at the cryostat window, thus allowing the operator to optimize the ion sources and deflection optics for maximum ion deposition current. Following optimization, the Faraday plate is withdrawn to allow the deposition of ions within the noble gas matrix.

The chamber also houses window flanges that allow the introduction of infrared or visible laser light into the high-vacuum chamber, through the optical substrate/matrix, and out of the chamber. Infrared analysis can be performed using a BOMEM DA 3.02 Fourier transform infrared spectrophotometer. Infrared light from one of the operator-selectable beam paths of the BOMEM instrument passes through the matrix and is collected at a detector installed outside the exit window mounted in-line with the beam path. For mid-IR analysis a mercury-cadmium telluride detector is used. A liquid helium-cooled germanium bolometer detector is also available for far-IR studies. High sensitivity, laser induced fluorescence

(LIF) studies were also performed using this instrument. These studies utilized a Nd:YAG pumped dye laser located within the LASER laboratory in the Michigan State University Chemistry Department as a wavelength-variable excitation source. For LIF studies the infrared assembly was removed, and the laser beam was introduced through apertures which serve to reduce stray light, and into the matrix chamber along the same axis as the infrared beam. The fluorescence signal produced by ions trapped in the matrix was collected through an off-axis window (not shown). Cutoff filters were employed to discriminate against scattered laser radiation, and the fluorescence signal was detected with a PMT.

The focus of this dissertation is the modification of residual gas analyzers (RGAs) to produce the beams of mass-selected ions necessary for these matrix isolation studies. RGAs are specialized high vacuum pressure gauges that are often employed as an alternative to ion gauges. The are designed to measure both total and partial pressures of residual gases within high vacuum chambers from $1x10^{-4}$ torr to $1x10^{-12}$ torr. Partial pressure measurements are possible through the use of miniature quadrupole mass spectrometers. RGAs generally consist of a high efficiency ionization source, extraction optics, quadrupole mass filter, and a Faraday plate detector. RGAs are much less expensive than conventional mass spectrometers, generally costing between $5,000 and $10,000. They are small in size, often 4 to 6 inches in length, generally operate at unit resolution, and can vary in mass range from 1-60 up to 1-200 daltons. To allow their use in ultra-high vacuum environments, RGAs utilize specialized high efficiency electron impact ionization (EI) sources which can produce mass-selective sensitivities of $\sim 2.0x10^{-4}$ A/torr. The high efficiency, small size, and low cost of RGAs made them an ideal choice for modification to produce the mass-selected ion beams required for the matrix isolation instrument.

Following this introduction, Chapter 2 provides a background discussion of the ionization methods and ion sources that were used to

produce the ions prior to mass-selection, the quadrupole mass filter used to mass-select these ions, and the electrostatic optical tools used to optimize and design changes to the ion optics of these systems. Chapter 3 is a discussion of the modification of an Anavac-2 RGA to produce positive and negative ions using several ionization techniques. Chapter 4 presents the modification of a Dycor M200 RGA to produce a beam of mass-selected positive ions. Finally, Chapter 5 includes a general discussion of some conclusions drawn through the work presented in chapters 3 and 4, and some suggestions for future modifications to improve the performance of the ion sources.

Chapter 2. The theory and operation of RGA components

I. Ion Sources

A. Electron Impact Ionization

The most common type of source used for the production of ions in mass spectrometry is the electron impact ionization (EI) source. An EI source is based on the ionization of neutral molecules through interaction with a high energy (~70 eV) electron beam. The EI source was first introduced by Lenard in 1902 [34], and continues to find extensive use in many physical and analytical applications of mass spectrometry [35].

Electron impact ionization is based upon the interaction between a high energy electron and a neutral molecule to form both intact molecular ions and fragment ions. While the term impact implies a collision during ionization, the respective size differences between the electron and a molecule make an actual collision highly improbable. The actual ionization occurs due to an interaction (on a quantum-mechanical level) between the wave of the high energy electron and the electric field of the neutral molecule. When an electron is accelerated to an energy of several electron volts, it can achieve a de Broglie wavelength of ~0.1 nm [36], corresponding to short wave radiation. This wavelength is on the order of the dimensions of the electron, as a result an electron of this energy will possess a wavefunction consisting of a wide range of frequencies. As this electron comes into close proximity with a neutral molecule, its complex wave function can interact with the electrons of the neutral molecule. Some portion of the frequency components present in the electron wave will be absorbed by the neutral molecule, resulting in the transfer of energy to the molecule. If sufficient energy is transferred to the neutral molecule an electron can be ejected, resulting in the formation of an ion.

Some of the different ionization mechanisms that can occur as a result of the interaction of a high energy electron with a neutral molecule (AB) include:

Ionization	$AB + e_s \rightarrow AB^+ + e_s + e_e$	(1)
Dissociative Ionization	$AB + e_s \rightarrow A^+ + B + e_s + e_e$	(2)
Multiple Ionization	$AB + e_s \rightarrow AB^{z+} + e_s + ze_e$	(3)

Where e_s is a scattered electron and e_e is an electron ejected by the neutral molecule. An ion formed by EI following the ejection of an electron often contains excess internal energy. If this energy can be effectively dissipated within the vibrational modes of the molecule, a stable molecular ion will be formed as shown in process (1). If, however, sufficient excess energy is present in the molecular ion, the ion will break apart into fragments as shown in process (2). The vibrational energy levels within a molecule are generally much lower than the energy required for ionization; for example the largest vibrational level is for H_2^+ = 0.27 eV, and the ionization potential of H_2 is 15.426 eV [37]. As a result , ions formed through EI will often consist of a mixture of vibrationally excited states, resulting in the formation of several different fragment ions. One of the principal advantages of EI is that it produces a characteristic distribution of fragment and molecular ions (cracking pattern) that can be used to identify and determine the structure of an analyte molecule.

The production of a molecular ion in EI depends strongly upon the amount of energy the neutral molecule absorbs through interaction with an electron. At electron energies close to the ionization potential of the neutral molecule EI generally produces only the molecular ion. As the electron energy is increased more energy is transferred to the ionized molecule, and the formation of fragment ions increases. A plot of ion intensity versus electron energy for a given molecule is called a clastogram, an example of which is shown in Figure 2.1.

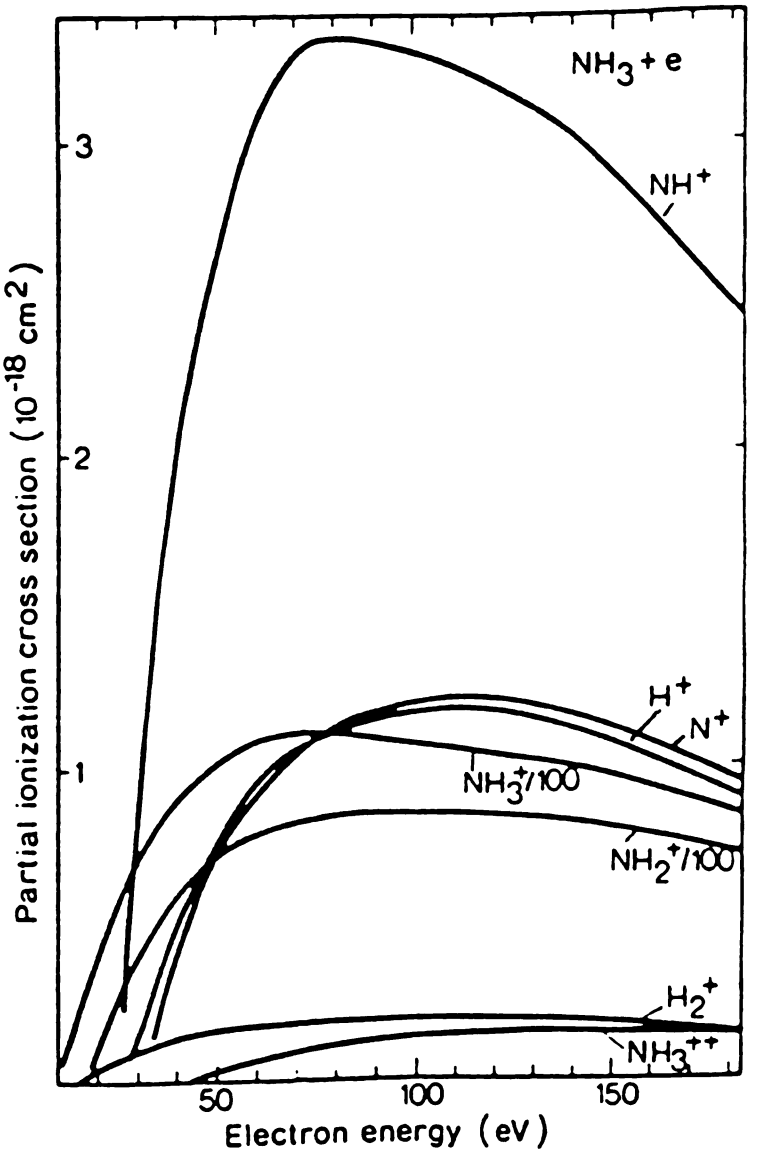

Figure 2.1 An example of a clastogram for ammonia adapted from Mark et al. [38].

This clastogram shows the production of the molecular ion and fragment ions from ammonia with increasing electron energy [38]. The onset electron energy for the production of the molecular ion, or the ionization energy for the intact molecule, occurs below 10 eV for NH_3. At this electron energy very little fragmentation occurs. As the electron energy increases different fragment ions begin to appear. The electron energy corresponding to the initial appearance of a fragment ion is called its appearance energy. If the energy of the electron beam is increased further, the relative intensities of the fragment ions become less sensitive to electron energy. For most molecules the fragmentation pattern stabilizes at electron energies above 50 eV. For this reason reference mass spectra, used to identify unknown compounds from their fragmentation patterns, are generally taken at an electron energy of 70 eV [39]. The disadvantage to operating at these high electron energies is that it may be difficult to observe the intact molecular ion. There is often an inverse relationship between the molecular weight of a molecule and the intensity of the molecular ion produced using EI [40]. For this reason EI is considered a 'nonsoft' ionization technique, and often proves to be unsuitable for the analysis of large molecules.

The interaction of a high energy electron with a neutral molecule can produce highly excited molecular ions. If the molecular ion contains sufficient energy, and no effective pathway is present to dissipate this excess energy, multiple ionization (3) can occur. This process generally occurs only at high electron energies, with the partial ionization cross section for the multiply charged ions (most often +2) rarely exceeding 1-5% of the primary singly charged peak intensity [41].

Most EI sources are based upon the design originally devised by Dempster [42], and further optimized to its modern configuration by Nier [43]. A block diagram of a Nier configuration EI source is shown in Figure 2.2. The Nier type EI source generally consists of a source housing of square or cylindrical geometry, depending on the desired symmetry of the

ion beam. A filament is mounted on one side of the source and heated until it emits free electrons. These electrons are attracted toward the source housing by a potential applied between the source and the filament, commonly 70 V. Although most of these electrons are neutralized on the source housing, a small percentage enter the source through the electron entrance aperture. These electrons continue on their initial trajectories through the source, and can impinge upon the collector located opposite the electron entrance aperture as shown in Figure 2.2.

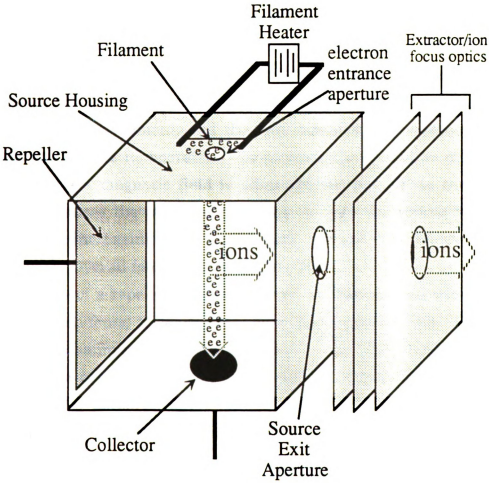

Figure 2.2. A drawing of the conventional Nier style EI source

If these 70 eV electrons encounter neutral molecules as they traverse the source volume, ions can be formed as previously described. A repeller is commonly placed opposite the ion exit aperture. An electric field can be created within the ion source by applying a potential to the repeller, this electric field causes ions that are formed through interaction with the electron beam to drift toward the source exit aperture. If the ions pass through this aperture they can be accelerated, focused using a lens system, and injected into the mass spectrometer.

The operating conditions of the source filament can be monitored using several methods. If the electron current at the collector is measured, an accurate assessment of the electron current within the source volume can be obtained. This collector current is generally on the order of 10-100 μA [44]. It is also possible to monitor the heating current applied across the filament, and the total emission of electrons from the filament to evaluate its operation. To increase the ionization efficiency of the ion source a magnetic field is often applied parallel to the electron path. This causes the electrons traveling through the source to follow a helical path, increasing their pathlength through the source, thereby increasing the overall ionization probability [45].

The use of a repeller voltage to create an electric field within the EI source has been found to cause some mass discrimination [46]. To obtain a more uniform sampling of the ions formed within the source volume the source can be operated without this repeller potential [47]. Instead of using a repeller potential to create an electric field within the source, in this mode of operation the entire source region is held at a common potential and an extraction lens after the ion aperture is used to draw ions out of the source.

The overall degree of ionization in a Nier type EI source can be increased through: 1) Increasing the flux of electrons through the source volume, 2) Increasing the cross section of the electron beam present in the source, and 3) Increasing the pressure of the sample within the source

volume. Increasing the electron flux in the source will increase the probability of an electron/neutral "collision", but is limited by the output of the filament, the lifetime of a filament is inversely related to its output [45]. Use of a large electron aperture will increase the cross section of the electron beam, but ions formed in the source will then have a broader range of initial energies because they are formed from a wider range of positions within a region of varying electric potential. Increasing the pressure in the source will also increase electron/neutral collision probability, but can induce ion/molecule collisions and interfere with operation of the mass spectrometer. The final design and operation of this type of source is generally some compromise that depends largely upon the requirements of the overall instrument.

The Nier design EI source has proven effective for the production of molecular and fragment ions from a wide range of neutral compounds, but there are several disadvantages to its design. It has a relatively low overall ionization efficiency due to small electron beam cross section inside the source. It has been estimated that less than 1% of the neutrals that enter the ion source are effectively converted into positive ions [36]. It may also be difficult to observe the molecular ion for certain compounds due to the high energy of the ionization process. Certain samples can also decompose at the temperatures required for volatilization, precluding their use in a source of this type that requires the use of a gas-phase sample. Finally many samples of interest cannot be volatilized at all, making their analysis through EI impossible.

RGAs are designed to function as ultra-high vacuum pressure-measuring devices. As such, an RGA must utilize a source that creates a maximum number of ions at any given sample pressure. This is especially important since it determines the ultimate vacuum pressure that an RGA can measure (at present, RGAs are designed to measure pressures down to $1x10^{-12}$ torr). To obtain the necessary sensitivity for these measurements, most RGAs utilize an EI source with a

configuration that differs slightly from the original Nier design. This design was originally utilized in the early quadrupole mass spectrometer constructed by Paul et al. [48], and a drawing of a typical RGA EI source is shown in Figure 2.3.

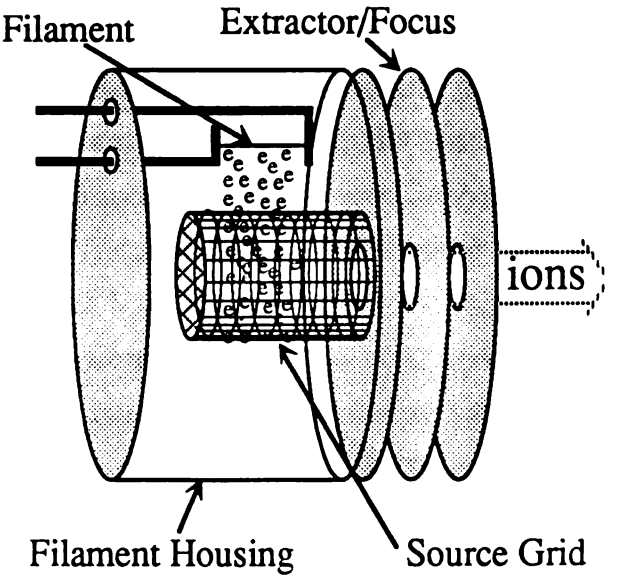

Figure 2.3. The high efficiency EI source commonly used in RGAs

RGA EI sources are commonly based upon a radially symmetric geometry, which matches the acceptance of a quadrupole mass analyzer. Similar to the Nier design, electrons are produced by heating a filament, commonly made of tungsten, rhenium, or thoriated iridium. In the RGA source these electrons are attracted to a highly transparent cylindrical source grid by the electric field between the grid and the filament. The potential between these two elements determines the electron energy. As the electrons travel through the grid they can ionize neutral molecules to form molecular and fragment ions. The grid is generally biased at +3 to +10 V, and the filament housing surrounding both the filament and grid is generally biased at -70 to -100 V. Because of the transparent nature of the grid, most electrons will travel through the entire source grid region.

After passing through this region, they slow down due to the electric field between the grid and the filament housing. This electric field eventually causes the electrons to 'turn-around' and pass through the source grid again. In this fashion, an electron can make several passes through the source grid. This greatly increases the overall efficiency for the ionization process by increasing the pathlength of the electron through the ionization region. By locating the filament close to the grid, most of the electrons emitted from the filament pass through the grid region, again increasing the efficiency of the source. Ions that are formed within the grid region feel an attractive force induced by the penetrating field of the extractor lens (commonly held at -40 V), and exit the grid region through the source aperture. This extraction is similar to that observed using an external extraction field in the Nier source (not using the repeller), and therefore also has the advantage of minimal mass discrimination gained through operation in that mode.

Another advantage gained through the use of this cylindrical grid design is the decrease in observation of ions formed by electron-induced desorption (EID). In a Nier source a large percentage of the electrons that travel through the source volume finally impact upon surfaces within the source (such as the collector or the walls of the source itself). These electrons can cause molecules adsorbed on these surfaces to desorb and ionize. As a result, peaks can appear that are not due to species present in the residual gases of the vacuum. The cylindrical grid design commonly used in RGAs minimizes these electron-surface collisions. Since electrons spend most of their time orbiting the highly transparent grid, very few come close to the source housing. This decreases the probability of electron collisions with the filament housing. As a result these high-efficiency EI sources have a much lower background signal from EID [49].

Both the cylindrical grid and the Nier style style EI sources have advantages depending upon the application. The cylindrical grid source has the advantage of increased sensitivity due to the long electron path

through the ionization region. It also suffers less from background signals due to formation of ions through EID. These criteria are especially important in the analysis of residual gases to maximize the overall sensitivity of the device and minimize background interferences at these low operating pressures. The Nier-type source can be advantageous when working with a system where the sample is introduced directly into the source volume. Because the filament lies outside the source volume, fewer electrons are generally available for ionization within the source region, but the advantage to this design is that the filament is not directly exposed to the sample gas. This is particularly important when working with thermally labile samples that would decompose if exposed to hot surfaces, or when using oxidizing samples that could attack the filament and reduce its lifetime.

B. Chemical Ionization

The technique of chemical ionization (CI) is commonly used as a complement to electron impact ionization in mass spectrometry. While EI normally forms molecular ions accompanied by a large degree of fragmentation, CI is considered a 'soft' ionization technique producing little fragmentation, and is therefore particularly useful for molecular weight determination. In CI the ionization is performed through attachment of some charged species, commonly a proton, to the intact analyte molecule. This interaction generally imparts a much smaller amount of internal energy into the product ion than EI, thereby reducing the degree of fragmentation. This effect was first described as an analytical technique by Munson and Field in 1965 [50].

The formation of the protonated analyte molecular ion is accomplished through the interaction of the neutral with reagent ions formed in a high pressure reagent gas. The two gases are introduced into the source simultaneously, with the ratio of analyte to reagent gas of

approximately $1:10^5$. Electrons are injected into the source in a fashion similar to EI. Because of the large excess of reagent gas in the source, most of the electrons will ionize reagent gas molecules. Methane was first used as a reagent gas for CI, the principal ions in the mass spectrum of methane include:

$$CH_4 + e^- \rightarrow CH_4^+ + 2e^- \quad (4)$$

$$\hookrightarrow CH_3^+ + H + 2e^- \quad (5)$$

If the pressure of the reagent gas is maintained at an extremely high level (~1 torr), ion/molecule reactions can occur to form new ions. Since the reagent gas predominates within the source, almost all of the ion/molecule reactions will be between the primary ions of the reagent gas and the neutral reagent gas. For methane the principal ion/molecule reactions that occur are [51]:

$$CH_4^+ + CH_4 \rightarrow CH_5^+ + CH_3 \quad (6)$$

$$CH_3^+ + CH_4 \rightarrow C_2H_5^+ + H_2 \quad (7)$$

If the molecular ion reacts with a neutral methane molecule the neutral molecule can accept a proton to form the ion CH_5^+, shown as process (6). If the CH_3^+ ion reacts with neutral methane, $C_2H_5^+$ can be formed through process (7). In the case of methane these ions will not further react with the reagent gas. This allows a large concentration of these "reagent ions" to accumulate within the high pressure source, eventually achieving a steady state. These reagent ion peaks, CH_5^+ and $C_2H_5^+$, are the predominant peaks in the mass spectrum for methane CI.

Most organic molecules have a stronger proton affinity than either CH_4 or the C_2H_4. If a high concentration of CH_5^+ and $C_2H_5^+$ reagent ions is present in the source the probability of an ion/molecule reaction between a reagent ion and an analyte molecule increases. Under these conditions

there is a strong probability that a analyte molecule (M) can react with a reagent ion and become protonated, forming MH^+.

$$M + CH_5^+ \rightarrow MH^+ + CH_4 \qquad (8)$$

The primary peak in the high pressure methane CI spectrum for analyte M is generally the protonated intact molecule $(M+1)^+$. The principal advantage of CI is that fragmentation occurs to a much lesser degree than with EI, and therefore much better molecular weight information can be obtained.

Other reagent gases can be used for CI; these can be especially useful for generating selective ionization conditions for a particular analyte compound. The probability that an analyte molecule will accept a proton from a reagent ion is related to the difference between the proton affinity of the analyte and the proton affinity of the molecular precursor to the reagent ion [52,53]. This difference in proton affinity can be used in the analysis of a mixture to selectively protonate one analyte over another. It can also be used to impart different amounts of internal energy into the protonated analyte ion, and thereby control the degree of fragmentation observed. If a reagent gas is selected that forms reagent ions having a much smaller proton affinity than the analyte molecule, a higher degree of fragmentation will be observed in the analyte mass spectrum [54]. This allows the ionization conditions to be chemically tuned to control the type of information obtained. By properly selecting the reagent gas used in CI, it is possible to not only selectively ionize different analyte molecules, but also to control the degree of fragmentation observed in their mass spectrum.

Under conventional EI conditions both positive and negative ions can be generated through the process of ion pair formation.

$$\text{Ion Pair Formation} \qquad AB + e^- \rightarrow A^+ + B^- + e^- \qquad (9)$$

Although this ionization mechanism could potentially prove useful for the analysis of compounds, the intensity of the negative ion signal produced through ion pair formation in EI is generally several orders of magnitude lower than the intensity for positive ion formation through single ionization and fragmentation [55]. As a result, the sensitivity of an analytical technique based on this ionization process would be quite low.

The high pressure conditions necessary for CI can also be used to produce negative ions through electron capture negative ionization (EC-NI) and negative chemical ionization (NCI). The use of high pressure EC-NI was first demonstrated by Hunt, et al. in 1976 [56], and has since proven to be an extremely sensitive technique for the analysis of certain classes of compounds. It has become especially important in the analysis of halogenated environmental pollutants because of its extreme sensitivity for this class of compounds [57].

Negative ions can be formed under high pressure conditions through several mechanisms, the three most important of which are resonant electron capture (10), dissociative electron capture (11), and negative ion-molecule reactions (12).

Resonant electron capture	$AB + e^- (\sim 0.1\ eV) \rightarrow AB^-$	(10)
Dissociative electron capture	$AB + e^- (\sim 0.1\ eV) \rightarrow A + B^-$	(11)
Negative ion-molecule reactions	$AB + C^- \rightarrow ABC^-$	(12)

Resonant electron capture involves the formation of a molecular negative ion through the capture of a low energy electron by the analyte molecule. This mode of ionization requires very low energy electrons (~0.1eV) to prevent the negative molecular ion from ejecting (autodetaching) the captured electron. Under conventional EI conditions, where ~70 eV electrons are employed, very few electrons with this low energy are available. If the pressure in the ion source is increased the likelihood that an electron will collide with a molecule can be increased.

When such a collision takes place some of the electron's energy is lost, generally the energy of a "primary" electron is reduced by ~30 eV as it ionizes a neutral molecule [58]. If several such collisions occur the electron can lose almost all of its initial energy and form a low energy (thermalized) electron. The secondary electrons ejected from the ionized molecules generally have low energies, which can also be further reduced through collisions with gas molecules. By introducing a high pressure of "buffer gas" into the source along with the analyte, it is possible to create conditions that will favor the production of a large number of these low energy electrons. These thermal electrons are then available for the production of negative molecular ions through resonant electron capture. Excess energy gained by the molecular ions as result of the electron capture process can also be dissipated through collisions with neutral buffer gas molecules. If the molecular anion contains sufficient excess energy following electron capture it can fragment to form negative fragment ions; this is called dissociative electron capture.

This mode of operation for a CI source is often called electron capture - negative ionization (EC-NI). The formation of negative ions through EC-NI has been shown to be strongly dependent upon the electron affinity of the analyte, the energy spectrum of the ionizing electrons, and the frequency of electron/molecule and ion/molecule collisions within the source region [59]. EC-NI has proven to be an extremely selective and sensitive technique (up to 1000 times greater sensitivity than positive CI) for the analysis of certain compounds, especially those compounds containing a highly electrophilic site [60].

Negative ion-molecule reactions, process (12), can also be used to produce negative ions under CI conditions. If an electrophilic buffer gas is selected and the source is operated at high pressure conditions, the buffer gas molecules can capture the thermalized electrons to form reagent ions. An example of this is the formation of Cl^- using CCl_4 or CH_2Cl_2 as a buffer gas [61]. At these elevated pressures the reagent ions can then further

react with the analyte molecules to form molecular adduct ions. This mode of operation is generally called negative chemical ionization or NCI. The advantage of NCI is the simplicity of the mass spectra produced; often only the molecular adduct ion is observed since the formation of an adduct ion is generally a low energy process. The NCI ionization technique also has excellent selectivity, the selectivity of the ionization depending upon the electron affinities of the reagent gas and the analyte molecule [62].

The source required to produce the high pressure conditions necessary for CI, EC-NI, and NCI conditions is similar in design to the Nier EI source shown in Figure 2.2. The principal modification made to the Nier design is the reduction of apertures in the source to reduce conductance, allowing the creation high pressure conditions within the source volume. The reagent or buffer gas must be present at pressures approaching 1 torr, so the entire source housing is generally sealed except for the electron entrance aperture and the ion exit aperture (shown in Figure 2.2), and the size of these apertures is generally reduced. Similar to the Nier design, the filament is located outside the source region. This is particularly important for CI and NCI work to prevent the reagent gas, which is often oxidative in nature, from attacking the heated filament. The electrons produced by heating the filament are accelerated toward the source housing by a strong electric field induced by potential applied between the filament and the source housing. For high pressure studies an electron energy greater than 100 eV is commonly used to allow the electrons to effectively penetrate the high pressure source region [63]. The output of the filament operated under these conditions is generally only monitored by observing the total emission from filament, not by monitoring the collector current. This is necessary since under these high pressure conditions only a very small percentage of the electrons that enter the source can effectively traverse the source volume and hit the collector.

Because of the high source pressures required to form ions through CI, EC-NI and NCI, special pumping is generally required. In most mass

spectrometers the analyzer region must be maintained at ~$1x10^{-6}$ torr to avoid ion/molecule collisions as the ions travel through the mass spectrometer. The extremely high pressures present in a source operated under CI conditions produces a high background pressure in the source vacuum chamber. To maintain the pressure required for effective ion formation and mass analysis, differential pumping is generally used between the source and analyzer regions. If an aperture is placed between the CI source and the mass analyzer and separate pumps are connected to each chamber, a pressure differential can be maintained between the two regions. If each region is separately pumped, the high pressure conditions necessary for CI can be maintained in the source volume without substantially elevating the pressure in the analyzer region. Most mass spectrometers that are designed to perform CI utilize this type of differential pumping.

C. Surface Ionization

Surface ionization is the process by which a material that has been coated or directed onto a heated surface evaporates in an ionic state. Surface ionization sources can be used for the production of both positive and negative ions. These ions are generated either directly from a hot surface, or as a result of the interaction of the heated surface with some neutral species. Surface emission, or thermionic emission, involves the ejection of a particle present in the matrix or substrate when the surface is heated. Surface ionization (SI) involves the emission of charged species from a molecule that is adsorbed on the surface. These molecules can be either applied directly to the surface, or adsorbed onto the surface from the gas phase. Upon heating, these adsorbed species can desorb and ionize to form either positive or negative ions.

According to Duckworth [64], the first observation of positive ion emission from a heated material was made by Elster and Geitel in 1889

[65]. This was followed closely by the work of Beattie in 1899 in which several salts were applied to a filament and heated, producing positive ions [66]. The first observation of mass-selected positive ions generated through surface ionization was made by Thomson in 1908 [67]. He observed the presence of a peak at m/z~27, corresponding to the production of Na^+, upon the heating of platinum wire. In 1936 Blewett and Jones published an extensive study in which strong currents of a variety of positive alkali ions were produced through heating alkali aluminosilicates [68]. Surface ionization has been used for the determination of ionization energies, electron affinities, and isotopic ratios, as well as for generating ion beams [69,70]. An excellent discussion the surface properties affecting the thermionic emission and surface ionization of species has recently been compiled in this laboratory [71]. The development of techniques which utilize positive surface emission (PSI) has also been discussed in the literature [72,73,74].

The overall design of a surface ionization (SI) source is shown in Figure 2.4. The source is similar in design to the Nier configuration described earlier, with the exceptions of the placement of the filament and the overall geometry of the slits. In a typical SI source a filament is placed inside the source housing and coated with a substrate to produce the desired surface (if necessary). A slit configuration is often used for SI, since this geometry is well matched to the acceptance of magnetic instruments. The filament is oriented within the source in-line with the source exit slit. The filament ends are connected to leads that run to a high current power supply which heats the filament. This assembly is also connected to a filament bias power supply that allows the filament surface to be floated at some potential. A V-shaped repeller is commonly mounted opposite the exit slit. As the filament is heated, ions are produced through surface emission or surface ionization. These ions experience a force induced by the electric field created between the repeller and the source housing, and migrate toward the exit slit. These ions are

further extracted and focused by the lenses following the source, producing an ion beam. The sample in SI can be either applied directly to the filament or introduced as a gaseous neutral through a gas inlet line.

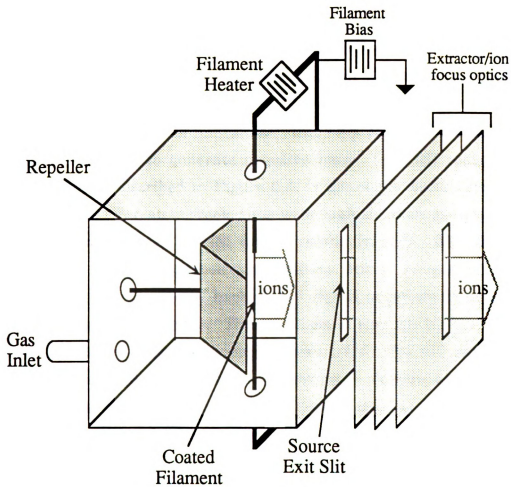

Figure 2.4. An example of a source designed for surface emission/ionization.

Negative surface ionization (NSI) has been less frequently used than PSI. It was first investigated by Owen in 1904 [75], who observed an extremely small emission of negative ions upon heating a negatively-biased filament. In 1912 Richardson detected more intense, mass-selected signals of negative ions from alkali iodides and bromides coated on

platinum filaments [76]. In general NSI has received less attention than PSI because of the weaker emission of NSI sources, interferences due to co-emission of electrons, and the limited number of ions that can be produced by NSI. Recently interest had been revived in NSI for both the generation of negative ions and the detection of neutral molecular beams [77]. Several exhaustive reviews have been written that cover the progress of NSI research; these are the source of much of the discussion that will be presented here [78,79,80,81,82].

Although NSI has some limitations , there are several advantages to using NSI as a means to generate negative ions. The NSI source, the same configuration described in Figure 2.4, is commonly quite small and simple to operate. For atoms/molecules with high electron affinities the overall ionization efficiency of NSI can be relatively high. Because NSI requires species with a strong electron affinity, the technique is highly selective and an extremely low background signal is generally obtained from residual background gases. The ions formed through NSI generally have a small initial transverse energy spread (~0.5 - 0.6 eV) and a low internal energy spread, which can be important in certain applications. Finally, relatively small amounts of sample are required for the production of ions through NSI, especially if the sample is applied directly to the surface.

Unfortunately there are several disadvantages to using NSI. Only a relatively small number of elements can be effectively converted into negative ions through NSI. NSI is only useful for producing ions from atoms or molecules with an electron affinity of > 1 eV [80]. In practice only 28 elemental negative ions have been produced using NSI [83]. In addition, the production of negative ions through NSI is often accompanied by the thermionic emission of electrons. This can be a problem unless some method is used to separate the electrons from the negative ions. Finally, the surface used for NSI can degrade and become contaminated

when the source is operated at high pressures or low surface temperatures.

The production of negative ions through NSI requires the use of a surface possessing several characteristics. It must have a low work function to allow the species that are desorbed from the surface to pick up electrons and form a negative ions. For effective negative surface ionization, the surface must be maintained at very high temperatures for extended periods, and must therefore have a high melting point. Finally the surface must be chemically stable when exposed to the molecule that is ionized. Several different materials have been tested for use as surfaces in NSI [84 ,85], a few examples of such surfaces are given in Table 2.1.

Table 2.1 The properties of some surface materials commonly used for NSI

Surface	Work Function (Φ)	Melting Point (K)	Operating Temp. (K)
Re	4.4 - 5.1 eV	3450	1500 - 2200
LaB_6	2.3 - 3.5 eV	2480	1400 - 1700
ThO_2	1.7 - 3.1 eV	3320	1500 - 1900

Rhenium is sometimes chosen because it doesn't form carbides, a problem with tungsten filaments, and has a high stability toward oxygen. Unfortunately the relatively high work function of rhenium limits its applicability for NSI systems. LaB_6 has been used for NSI work, principally because it has a relatively low work function, and high thermal and chemical stability [86]. A procedure for the preparation of LaB_6 surfaces [87], and the use of these surfaces for the detection of atmospheric iodine have appeared in the literature [88]. The principal difficulty with LaB_6 surfaces is that they are relatively brittle and sensitive to stress, and that the LaB_6 can sometimes react with the support filament. To avoid these difficulties LaB_6 surfaces have been prepared using heated graphite disks as a support [89]. Thorium oxide-coated filaments are often used as electron emitters, for example in ion gauges, due to their extremely low

work function. These surfaces have also found application in the area of NSI. A thorium oxide coating is relatively simple to prepare, and is commonly coated on a support filament such as rhenium, tungsten, or iridium [90]. Thorium oxide surfaces have high melting points, can operate at lower temperatures than other surfaces, and are relatively inert toward oxidative compounds. Cs glass surfaces, formed from a SiO_2, Al_2O_3, and $CsNO_2$ mixture, have also been used for NSI [91], These surfaces can be prepared relatively easily, exhibit low work functions, and are stable at high temperatures. Geiger investigated the emission of a series of alkali metal containing surfaces (Li, Na, Rb, Cs) that were exposed to a constant stream of halogen molecules (Cl_2, Br_2, or I_2) [92]. Of the systems investigated, the highest efficiency was obtained for the Cs amalgam with Cl_2.

The operating conditions of the NSI source can strongly influence the overall efficiency of the ionization process. If a gaseous sample is used, increasing the overall sample pressure increases the collisions of molecules with the hot surface, thereby increasing the output of the source. Increasing the operating temperature of the surface increases both the degree of ionization on the surface and the degree of dissociation of molecules from the surface. However, operating at reduced temperatures has several advantages: 1) separation of negative ions from electrons becomes unnecessary (electron emission increases exponentially above the threshold temperature), 2) the production of negative ions through gas-phase electron molecule interactions is reduced, 3) surface reactions between residual gases and the filament surface are decreased. Some compromise is often made in determining the surface temperature for NSI, generally toward higher temperature operation. NSI surfaces are most often maintained at temperatures above 1500 K [80].

The selection of a precursor molecule for NSI is also important. Generally a sample should be selected that has a relatively small M-X dissociation energy to promote dissociation on the hot surface. For

example Perskey, et. al., investigated the performance of a series of chlorine compounds under NSI conditions [84]. The negative ion output for the series was KCl > CCl_4 > C_6H_5Cl > C_2Cl_6 which follows the M-Cl dissociation energies for the parent molecules. Increasing the area of the heated NSI surface can also increase the output of the source, but the increase in output current is not proportional to the surface area increase because of difficulties in focusing ions from a large area. Most often a wire diameter of 0.1 - 0.2 mm is used as a compromise between mechanical strength, power requirements, and durability. Ribbon filaments are occasionally used, but tend to twist at high temperatures, reducing the surface area exposed to the source exit slit. Finally, a large extraction field at the surface will increase the overall ionization of an NSI source, this is especially important at high output currents where the surface ionization can become space-charge limited.

NSI sources can be used with quadrupole instruments, but certain problems may arise. Under normal operating conditions (high surface temperatures) both negative ions and electrons are emitted from the hot surface. The electric fields used by the quadrupole for mass selection of ions are not completely effective at discriminating against electrons. As a result, an NSI source often produces a background (negative) signal at the detector for all masses. This effect is especially pronounced when the quadrupole is operating at lower masses. To reduce this background signal, a weak magnetic field can be applied to the ion/electron beam between the source and the quadrupole. Another method used to discriminate against electrons is the use of a strong extraction field at the heated surface, followed by a retarding lens between the source and the quadrupole. One drawback to this method is that if the electrons exiting source react to form positive ions in the region between the source and the quadrupole, these ions can be detected as a mass-dependent background signal at the detector. A better approach is to place the retarding lens

between the quadrupole and the detector, thus eliminating the mass-dependent background signal.

A comprehensive review of surfaces, surface conditions, and precursor molecules used for NSI has been made by Kawano [82]. A few high efficiency NSI conditions for the production of Cl^- are given in Table 2.2.

Table 2.2 Some high efficiency conditions for the formation of negative ions through negative surface ionization

Sample	Surface	Temp. range (K)	Optimum T (K)	Ion	Reference
CCl_4	ThO_2-W	1650 - 2100	1740	Cl^-	Persky 1968 [84]
CCl_4	LaB_6 -Re	1550 - 1700	1600	Cl^-	Persky 1968 [84]
Cl_2	Cs	293	293	Cl_2^-	Geiger 1955 [92]
CsCl	Nb	1450	1450	Cl^-	Kawano 1971 [93]
KCl	ThO_2-W	1200 - 1500	-----	Cl^-	Trischka 1952 [94]
HCl	ThO_2-Ir	-----	1300	Cl-	Cheung 1979 [95]

II. The Quadrupole Mass filter

A. Introduction

In order to obtain partial pressure measurements for a mixture of residual gases in a vacuum chamber, the residual gas analyzer must separate the collection of ions produced in the source according to some property related to their m/z value. In a magnetic mass spectrometer the ions exiting the source enter a strong magnetic field and are dispersed along different trajectories according to their momenta. Most modern RGA's utilize a different mass selection device called a radio frequency (rf) quadrupole to perform this mass selection. An rf quadrupole has been defined as "a dynamic mass spectrometer whose ability to transmit desired ions and reject unwanted ions is based upon the principle of path stability" [96]. An rf-quadrupole RGA is simply a miniaturized quadrupole mass spectrometer. A diagram showing the principal components of a rf-quadrupole mass spectrometer is shown in Figure 2.5.

An rf-quadrupole consists of four symmetrically arranged electrodes as shown in Figure 2.5. Opposing quadrupole rods are connected, and a combination of dc and rf potentials are applied to the rods. The ions produced in the source are accelerated to an energy of 3 to 50 eV and enter the quadrupole along the Z axis of the device. The changing potentials applied to the quadrupole electrodes create a dynamic hyperbolic field within the device that effects ion stability in the X and Y planes, but not in the Z direction. As a result, ions of a limited mass range will remain stable as they traverse the quadrupole while the unstable ions will impinge upon the electrodes, and be filtered out. The stable ions are detected by a detector positioned at the exit of the quadrupole. The quadrupole functioning in this capacity acts like a variable bandpass mass filter. By varying the levels of dc and rf applied to the opposing rods, the quadrupole can electronically sweep the bandpass region of the mass

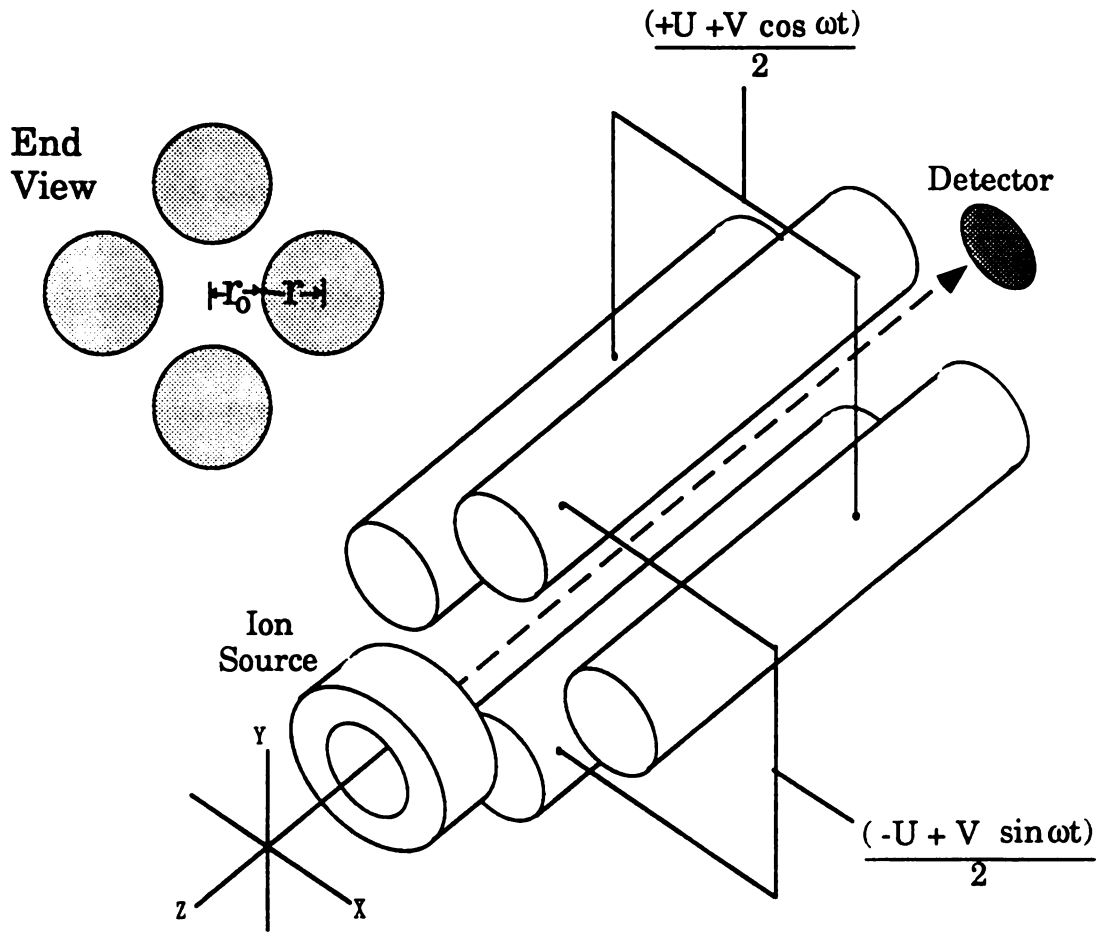

Figure 2.5 The basic components of a quadrupole mass spectrometer, both an end view of the electrodes and a drawing of the overall device is shown.

filter, allowing ions of different m/z to hit the detector. Because the quadrupole performs its mass selection through filtering rather than dispersion the quadrupole is considered a "mass filter" rather than a true mass spectrometer.

At present, quadrupole-based mass spectrometers represent over 80% of the mass spectrometer market [97]. Quadrupoles have become dominant in four main areas of research: residual gas analysis, elemental analysis, aerospace research, and organic analysis. Quadrupole residual gas analyzers have become the standard instrument for analysis of gas mixtures and contaminants in vacuum and surface science, thin films research, semiconductor manufacture, and several areas of high vacuum spectroscopy. The unique filtering properties of quadrupoles are ideally matched to important ionization techniques in elemental analysis such as inductively coupled plasma mass spectrometry (ICP-MS). Quadrupoles are also utilized in the aerospace field for upper atmosphere analysis, astronaut respiration monitoring, and space vehicle gas monitoring where light weight and ruggedness of the device are important. The majority of quadrupole mass spectrometers in operation today are used in the area of organic analysis. Quadrupoles have become important in many areas of organic analysis through coupling with separation techniques such as gas chromatography, liquid chromatography, capillary zone electrophoresis, supercritical fluid chromatography, and multi-sector mass spectrometers. The combination of the separative properties of these techniques in tandem with mass spectrometry has produced instruments capable of solving many difficult analytical problems.

The proliferation of quadrupole mass spectrometers can be attributed to several properties of the quadrupole mass filter. Because a quadrupole uses only electric fields for mass selection, there is no need for large, expensive magnets and their associated power supplies, which greatly reduces the mechanical complexity and cost of a mass

spectrometer. The filtering properties of a quadrupole are based on applied voltages which can be varied more quickly than can magnetic fields. This allows for the fast scanning of a quadrupole, which is important in techniques such as GC-MS and selected ion monitoring. It also increases the flexibility and ease of controlling the mass spectrometer, making them ideal for remote operation in residual gas analysis. Quadrupoles filter ions according to their m/z (rather than momentum) and therefore can accept a wider range of initial trajectories and energies than magnetic instruments. Quadrupoles have moderately high resolution (resolution of 3000 is fairly routine) and a relatively high mass range (up to 10^6 has been obtained with current technology) [96]. Finally the mass of a stable ion exiting the quadrupole is linearly proportional to the applied dc and rf voltages making the interpretation of detector signal fairly straightforward.

B. Theory of Quadrupole operation:

The ability of a quadrupole to filter out ions of different m/z value is based upon the motion of a charged particle in a dynamic hyperbolic field. A hyperbolic electric field is the electric field created within an array of four hyperbolic electrodes that are arranged as shown in Figure 2.6. If the opposing pairs of electrodes are connected and each connected pair is biased at opposite potentials a hyperbolic electric field will be created between the electrodes. Figure 2.6 shows a SIMION model of the electric field produced when the upper and lower electrodes are biased at -100 V and the left and right electrodes are biased at +100 V. The lines between these electrodes map out the points of equal potential for the free space region within the electrode array.

The force that a charged particle experiences is directed perpendicular to these equipotential lines. A positive ion that enters this field will experience an attractive force toward the upper and lower

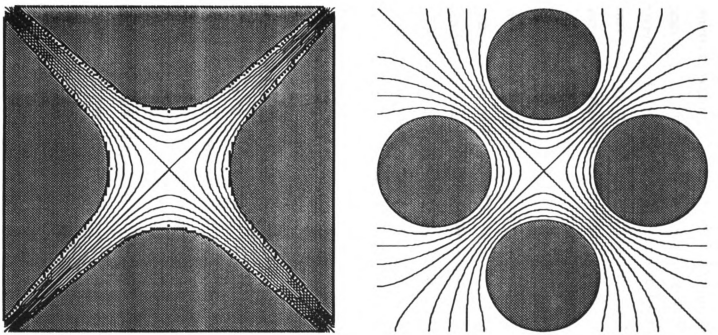

Figure 2.6 MacSIMION models of the electric field produced within hyperbolic (left) and round (right) quadrupole electrodes.

electrodes and a repulsive force from the left and right electrodes. The result is that the ion is strongly defocused (exponential defocusing) along the attractive axis and experiences harmonic motion along the repulsive axis (focusing). If the potentials on the rods are suddenly switched the effect reverses. If these potentials are alternated at the correct frequency, an overall focusing effect (toward the center of the array) will result from the alternating squeezing and relaxing forces on the ion. This focusing effect is called "strong focusing" [98]. The net restoring force on an ion is proportional to its displacement from center axis and can be achieved through the application of a sine wave ac signal to one rod pair and a cosine wave ac signal to the other rod pair. It is this effect that makes rf-only quadrupoles (and high order multipole devices) useful as beam guides. As an ion travels along the Z axis of the quadrupole (see Figure 2.5) it will experience an alternating hyperbolic field in the X and Y axes which produce an overall focusing effect. A device based on this effect was originally conceived by W. Paul in 1958 [48].

The presence of alternating potentials on the quadrupole rods results in the focusing of a broad range of different m/z ions. If dc potentials of opposite sign are applied to the opposing rod pairs at a fixed ratio with respect to the applied ac potentials, the range of stable m/z ions will be reduced (narrowing the 'bandpass' of the mass filter). By convention the y axis rod pair is defined as the pair to which the negative dc potential is applied and the x axis rod pair receives the positive potential. This mode of operation is the basis for the use of a quadrupole as a mass spectrometer.

The use of a quadrupole in this mode is more easily understood in terms of the equations of motion for a particle in a quadrupole. The potential (Φ) at any point within the free space region inside a quadrupole can be described as:

$$\Phi = [U + V\cos(\omega t)]\frac{x^2-y^2}{2r_0^2}$$

where: x = distance from center along x axis
y = distance from center along y axis
r_o = distance from quad centerline to rod as shown in Figure 2.5
ω = angular frequency ($2\pi f$) of the applied ac wave
V = magnitude of applied ac wave
U = magnitude of applied dc potential

The change in potential with distance is defined as the electric field (E) present within a region of space. By taking the partial derivative of the potential equation above with respect to movement along each of the axes of a quadrupole, one can determine the electric field that the quadrupole produces at that position. This relationship for displacement in the x(E_x), y(E_y) and z(E_z) axes is given as:

$$E_x = -\frac{\delta\Phi}{\delta x} = -[U + V\cos(\omega t)]\frac{x}{r_0^2} \qquad E_y = -\frac{\delta\Phi}{\delta y} = -[U + V\cos(\omega t)]\frac{y}{r_0^2}$$

$$E_z = -\frac{\delta\Phi}{\delta z} = 0$$

The sum of the electric field components for displacement along each axis yields the net electric field at that position. These equations show that the quadrupole produces a position-dependent electric field along both the x and y axes but not along the z axis. Therefore the ion motion along the z axis (and consequently the ion residence time in the quad) is independent of the potentials applied to the quadrupole rods. The force that an ion experiences at any position within an electric field is simply the product of the electric field and the charge on the ion (e). As a result the force on an ion in the x(F_x) and y(F_y) directions can be written as:

$$F_x = -[U + V\cos(\omega t)]\frac{ex}{r_0^2} \qquad F_y = -[U + V\cos(\omega t)]\frac{ey}{r_0^2}$$

The acceleration that a particle experiences in any direction due to an applied force is simply the force divided by the mass of the particle. Therefore, the acceleration of an ion as a result of the force induced by an applied electric field in the x(a_x) or y(a_y) direction is given as:

$$a_x = \frac{\delta^2 x}{\delta^2 t} = \frac{F_x}{m} \qquad a_y = \frac{\delta^2 y}{\delta^2 t} = \frac{F_y}{m}$$

Applying this relationship to the equations for F_x and F_y in a hyperbolic field yields the following equations describing the acceleration an ion undergoes in terms of the applied potentials, the mass, charge, and position of the ion, and dimensions of a quadrupole.

$$\frac{d^2 x}{d^2 t} = -[U + V\cos(\omega t)]\frac{ex}{m r_0^2} \qquad \frac{d^2 y}{d^2 t} = -[U + V\cos(\omega t)]\frac{ey}{m r_0^2}$$

These equations are forms of the well known Mathieu equation which was originally derived as a description of vibrational motion of a stretched membrane within an elliptical boundary [99]. The trajectory solutions to these equations for an ion traveling along the Z axis of a quadrupole can be defined as bound or unbound. A bound solution corresponds to an ion that adopts a stable periodic trajectory while traveling through the quadrupole. An unbound solution corresponds to ions that cannot adopt a stable periodic motion while traversing the quadrupole. Ions that adopt unbound trajectories will follow a path that exceeds the dimensions of the device (r_0) and impinge upon one of the quadrupole rods.

The ability of an ion to adopt a bound trajectory and successfully traverse the quadrupole depends on the values of the six terms in the equations above (including mass/charge ratio). Through extended

analysis it has been determined that the solutions to these equations can be described in terms of the two variables a and q defined below [100].

$$a=\frac{4eU}{\omega^2 r_0^2 m} \qquad q=\frac{2eV}{\omega^2 r_0^2 m}$$

The actual trajectory taken by an ion as it travels through a quadrupole is extremely complex and depends upon the initial position, trajectory, and the ac phase of entry. To simplify the description of mass scanning with a quadrupole a plot of a verses q is often made. Such a plot can be used to describe the regions of x and y stability for a quadrupole with respect to the applied dc potential (U), the applied ac potential (V), the angular frequency of the ac waveform (ω), the charge on the ion (e), and the mass of the ion (m). There are several regions of an a,q diagram in which bound solutions exist for both x and y stability, the region most commonly used for operating a quadrupole is shown in Figure 2.7.

The stability region indicated in Figure 2.7 describes a series of a and q values for which ions can attain stable trajectories (bound solutions) in both the x and y directions. This stability region is enclosed on the left by the x stability boundary and on the right by the y stability boundary. If the quadrupole is operated with dc and rf potentials in ratio corresponding to "scan line" shown in Figure 2.7, only ions of a limited mass range will remain stable within the quadrupole. Ions outside the stability region will follow unstable trajectories, impinge upon the quadrupole rods, and be filtered out. The slope of the mass scan line, given as 2U/V, is adjusted to create a small overlap with the a,q stability region. In this manner the sharp tip of the a,q region can be used as a narrow bandpass filter. By increasing the rf and dc levels at a constant ratio, ions of higher masses will be shifted upward along the mass scan line and enter the narrow stability region thus producing a mass scan.

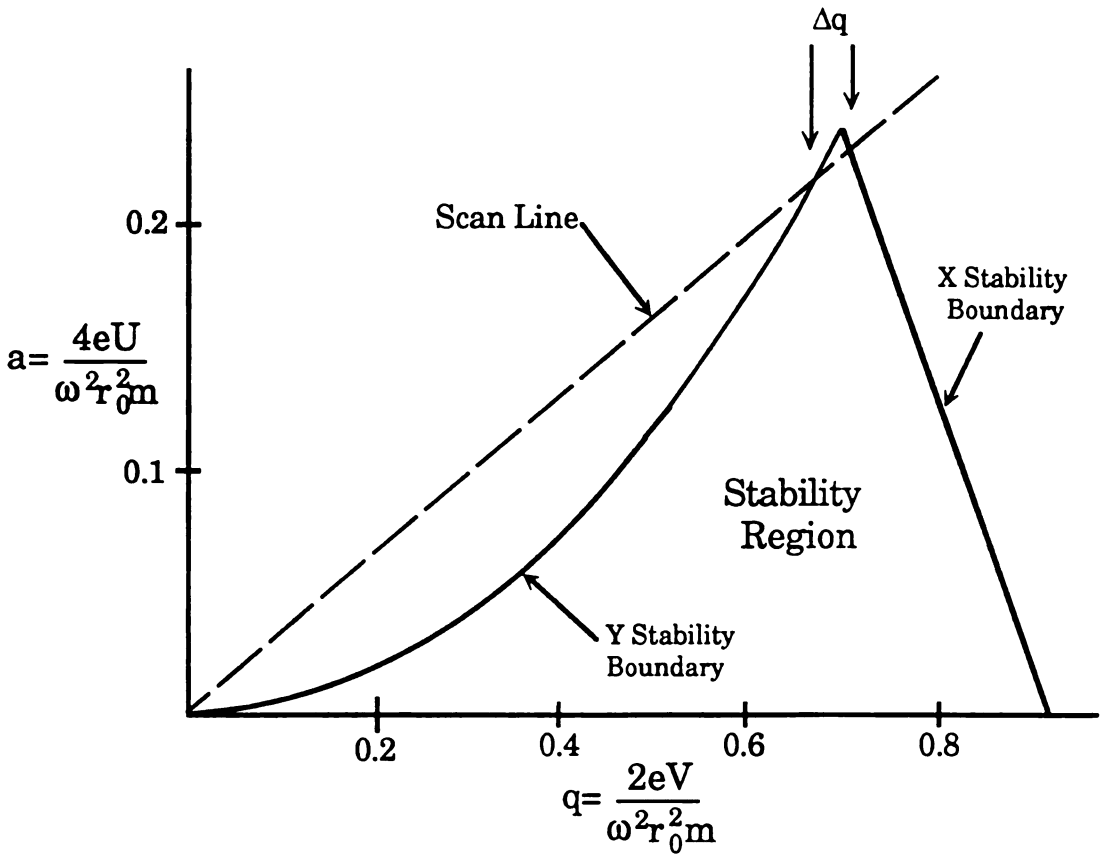

Figure 2.7 The a,q space stability diagram for a quadrupole mass filter.

The slope of the mass scan line determines the range of ion masses, or Δq, that are simultaneously stable within the quadrupole. By adjusting the slope of the mass scan line (the dc/rf level) it is possible to change this range, thereby altering the resolution of the mass spectrometer. Thus, within limits, increasing the resolution of a quadrupole is simply a matter of increasing the dc/rf ratio present on the quadrupole rods.

A quadrupole can be operated in several different modes that are distinguished by the ratio of applied dc to rf (dc/rf ratio). The two most common mass-selective modes of operation are constant sensitivity and constant peak width(ΔM) modes. If a quad is operated with a constant ratio of dc to rf then the $m/\Delta m$ for the stable ions will remain constant. This mode of operation is commonly called constant sensitivity mode. In

constant sensitivity mode the quadrupole will have approximately the same sensitivity for ions of all masses. The trade off is that as the mass of the stable ion (m) increases, Δm also increases (since U/V is constant). This causes the peak width of the quadrupole operated in this mode to increase with increasing ion mass.

If a small fixed dc potential is applied to each rod pair, it is possible to adjust the intercept of the mass scan line such that Δm will remain approximately constant. Operation of a quadrupole in this mode has the advantage that resolution remains fairly constant throughout the range of the mass spectrometer. The disadvantage to this mode is that as the ion m/z increases the sensitivity of the quadrupole decreases. The selection of an operating mode for a quadrupole depends upon the requirements of the application.

Another important mode of operation for RGA quadrupoles is rf-only mode. If the dc levels applied to the quadrupole are decreased, the slope of the mass scan line decreases and the bandpass of the mass filter increases. If no dc is present, the slope of the mass scan line will be zero which corresponds to operation along the q axis of the a,q stability diagram. Operation in this mode allows a broad range of ions to obtain stable trajectories as they pass through the quadrupole. This mode has proven useful for total pressure measurements in residual gas analysis, total ion counting in GC-MS, the application of a quadrupole as a beam guide in multi-sector instruments, and for the evaluation of source efficiency.

C. Practical Operation of a Quadrupole:

The ultimate performance of a radio frequency quadrupole is commonly described in terms of the highest mass it can select and the maximum resolution that it can obtain. The maximum m/z ion that can

be selected by a quadrupole (M_m) can be described in terms of the field radius (r_o), rf frequency (f), and maximum rf voltage between rod pairs (V_m) as:

$$M_m = \frac{7x10^6 V_m}{f^2 r_o^2}$$

A similar relationship exists between the minimum peak width (ΔM_{min}) and the ion injection energy (V_z), the rf frequency (f), and the length of the quadrupole rods (L) in meters.

$$\Delta M_{min} = \frac{4x10^9 V_z}{f^2 L^2}$$

If these two equations are combined and the operating conditions are optimized for both M_m and ΔM_{min} the following relationship is obtained.

$$\frac{\Delta M_{min}}{M_m} = \frac{r_o^2 V_z 570}{L^2 V_m}$$

Several important observations can be drawn from this relationship:

1. The ultimate performance of the quadrupole depends upon the ratio of r_o/L.
2. In theory 'any' mass range can be obtained with a quadrupole by simply lowering the rf frequency, but only by sacrificing resolution.
3. Reducing r_o will increase mass range, but will also decrease the ion acceptance of the quadrupole and make source design and contamination more critical.
4. Increasing L improves the performance of the quadrupole, but is ultimately limited by practical construction limitations.
5. Finally, V_m is limited by the levels of rf voltage that can be produced.

In the design of most modern quadrupoles some compromise has been made to allow; practical manufacture of the quadrupole electrodes, reasonable mass range and resolution, reproducible source alignment matching, and production of rf levels within the scope of modern electronics. An example of typical dimensions and operating conditions for a radio frequency quadrupole are:

$$V_z = 5\ eV \qquad L = 0.2\ m \qquad f = 2\ MHz \qquad r_0 = 0.4\ cm$$

These conditions can produce a quadrupole with $\Delta M_{min} = 0.125$ daltons and M_m of approximately $V_m/9$ (i.e. for rf $V_{p\text{-}p} = 1000$ $M_m = 222$).

The spectra produced by a quadrupole are strongly dependent not only on the value of these parameters selected in the design of instrument, but also on the precision of the rod manufacture and mounting, alignment of the source with the quadrupole, the size of source and exit apertures, the energy of the ions, and the scan rate of the quadrupole. Each of these parameters can affect not only the shape of the peaks in the mass spectrum produced by a quadrupole, but also their relative intensities and the ultimate resolution of the system.

The mechanical construction of a quadrupole is extremely important in its performance as a mass spectrometer. Most quadrupoles are constructed using round stainless steel or molybdenum electrodes. Although a hyperbolic rod shape is ideal, round rods are commonly used because they are much simpler to manufacture. If round rods are mounted so that their radius (r) is related to their spacing from the central quad axis (r_0) by the relationship $r/r_0 = 1.148$ then the field between the rods will approximate a hyperbolic field to a very high degree. This effect can be seen in Figure 2.6, in which the electric fields produced within hyperbolic and round rods are compared using the modeling program MacSIMION.

It is extremely important that the rods of a quadrupole be in precise alignment. If the rods lie at unequal distances from the center axis of the

quadrupole imperfect fields are produced within the device that can produce higher order restoring forces on an ion. These forces can cause peak splitting as the restoring force an ion experiences becomes non-linear, these field imperfections are called resonance instabilities. Field imperfections become increasingly important as an ion is displaced far from the z axis. This effect is often observed as mass discrimination against higher m/z ions (note: mass discrimination in a quadrupole is also due to the increase in number of rf cycles that an ion experiences with increasing m/z). For example, a 1% error in the positioning of the quadrupole rods would ultimately limit the resolution of the quad to 200 [97]. To insure excellent rod alignment the quadrupole rods are commonly mounted in precision ground ceramic supports. Using this mounting system the rods can be kept in alignment while the entire unit is removed for cleaning. Quadrupoles have also been constructed with each rod mounted individually using alumina or sapphire insulators. The advantage to this system is that individual rods can be removed and thoroughly cleaned. The disadvantage is that alignment jigs must be used to ensure that the rods remain in the correct position.

Field imperfections that result in peak splitting can also originate from sources other than rod alignment. If the quadrupole rods become contaminated then surface charging can occur on the rods which results in field imperfections. Thus an increase in peak splitting with time is a good indication that the quadrupole rods are contaminated and need to be cleaned. Another source of field imperfections is improper balance of the potentials applied to the rods. This imbalance can result from improper rf balancing or dc level control which is discussed in the next section.

As the resolution of a quadrupole is increased the trajectories of stable ions come closer to the rods of the quadrupole. Therefore at higher resolution settings ions must originate closer to the z axis for effective transmission. The maximum entrance aperture (D) for injected ions can be described as:

$$D = r_0(M/\Delta M)^{1/2}$$

Thus by decreasing the entrance aperture it is possible to increase the ultimate resolution of the system. The disadvantage in doing this is that sensitivity also decreases with aperture size due to the decrease in ion flux entering the quadrupole. It is common to manufacture a quadrupole with large apertures and compensate for this mass discrimination effect by increasing the sensitivity of the detector, increasing the amplification of the detector signal, as both resolution and mass range are increased.

The alignment of the ion source with the quadrupole rods can also influence the peak shape and sensitivity of the mass spectrometer. Ions that originate far from the z axis of the quadrupole can follow trajectories that will cause them to hit the electrodes even if they should theoretically have stable (bound) trajectories. The range of initial positions and trajectories that ions can have and still remain stable within the quadrupole is called the acceptance of the quadrupole. If the ion source is not in proper alignment with the quadrupole, a large number of ions will enter the quadrupole outside of the acceptance of the quadrupole and follow unstable trajectories. This results in peak splitting or multiple peak shape and significant loss of sensitivity [101].

There also exists a range of initial ion positions that can result in poor peak shape in the mass spectrum. If an ion originates exactly along the axes between the quadrupole rods the net force that it will experience as it traverses the quadrupole is approximately zero. This can be seen in Figure 2.6., the straight equipotential lines that lie along the axes between the electrodes correspond to an electric potential of zero because the electric field produced by each rod pair exactly cancels. Ions that originate at these initial positions are not properly selected by the quadrupole and can cause peak tailing on the low and high side of peaks in the mass spectrum [102]. To eliminate this problem cross wires are often attached

to the lens element directly before the quadrupole along the axis between rods Ions that would normally enter the quadrupole from these positions impinge upon the wires and are neutralized.

The energy of an ion along the z axis, or injection energy, influences the sensitivity and peak shape produced by the quadrupole. For an ion to be properly mass selected by the quadrupole it must experience a minimum number of rf cycles. The number of rf cycles (n) necessary to achieve some desired resolution ($m/\Delta m$) is given as:

$$n \gtrsim 3.6 \left(\frac{m}{\Delta m}\right)^{1/2}$$

The ion current through the quadrupole will increase as the ion injection energy is increased, but the overall resolution of the system will decrease. If the ions experience too few rf cycles, the mass peaks will split and tend to tail on the low mass side of the peak.

Another consideration in the operation of a quadrupole is the rate at which the dc and rf magnitudes are varied, or the scan rate. If a quadrupole is scanned at too high a rate, an ion that enters under stable conditions will not remain stable during the time it spends in the quadrupole. Thus if too high a scan rate is used the effect will be that no ion can remain stable as it passes through the quadrupole. The practical limit for scan rate is approximately 1000 amu/second for normal ion injection energies [97].

The quadrupoles used in residual gas analyzers are designed to achieve some compromise between the performance factors discussed above and the size and portability required for remote operation and installation. A typical RGA quadrupole consists of four round stainless steel or molybdenum rods approximately 50 to 80 mm in length with a diameter of 6 to 7 mm. These rods are generally fixed within a precision ground ceramic housing to allow their removal for cleaning and to ensure

precise alignment. The rf voltage used to operate the quadrupole ranges from 250 to 1000 volts peak to peak at a frequency of approximately 2 MHz. Injection energy can range from 5 to 10 eV and is often increased with increasing mass to overcome any mass discrimination affects in the quadrupole. For an RGA quadrupole that uses 80 mm rods with a 7 mm radius, operates with a 5 eV ion injection energy, and has a power supply that produces 250 V_{pp} at 2 MHz the ultimate performance of the system will be M_{max} = 94 and ΔM_{min} = 0.781. This produces an overall performance of $M/\Delta m$ = 120.

D. Basic Concepts in Radio Frequency Circuitry

The proper functioning of a quadrupole is dependent not only on the physical dimensions and alignment of the quadrupole rods, but also on the appearance of the proper electrical signals at the quadrupole electrodes. As discussed previously, an rf quadrupole requires a mixture of dc and large amplitude rf potentials for operation. This section will discuss generation of these signals and the circuitry required to perform scanning functions on the quadrupole.

A quadrupole functioning in mass-selective mode requires both dc and rf signals to be applied at some controlled ratio. The rf component has to be produced at high peak to peak levels to for the quadrupole to operate through a high mass range, as discussed in the previous section. This signal should have a pure sinusoidal waveform, excellent stability, and be rapidly scannable. The dc component must be applied at a precise ratio to the applied rf V_{pp}. The principal components necessary for the production of these signals including capacitors, inductors, and transformers are shown in Figure 2.8. A brief description of these components and their application to quadrupole electronics follows.

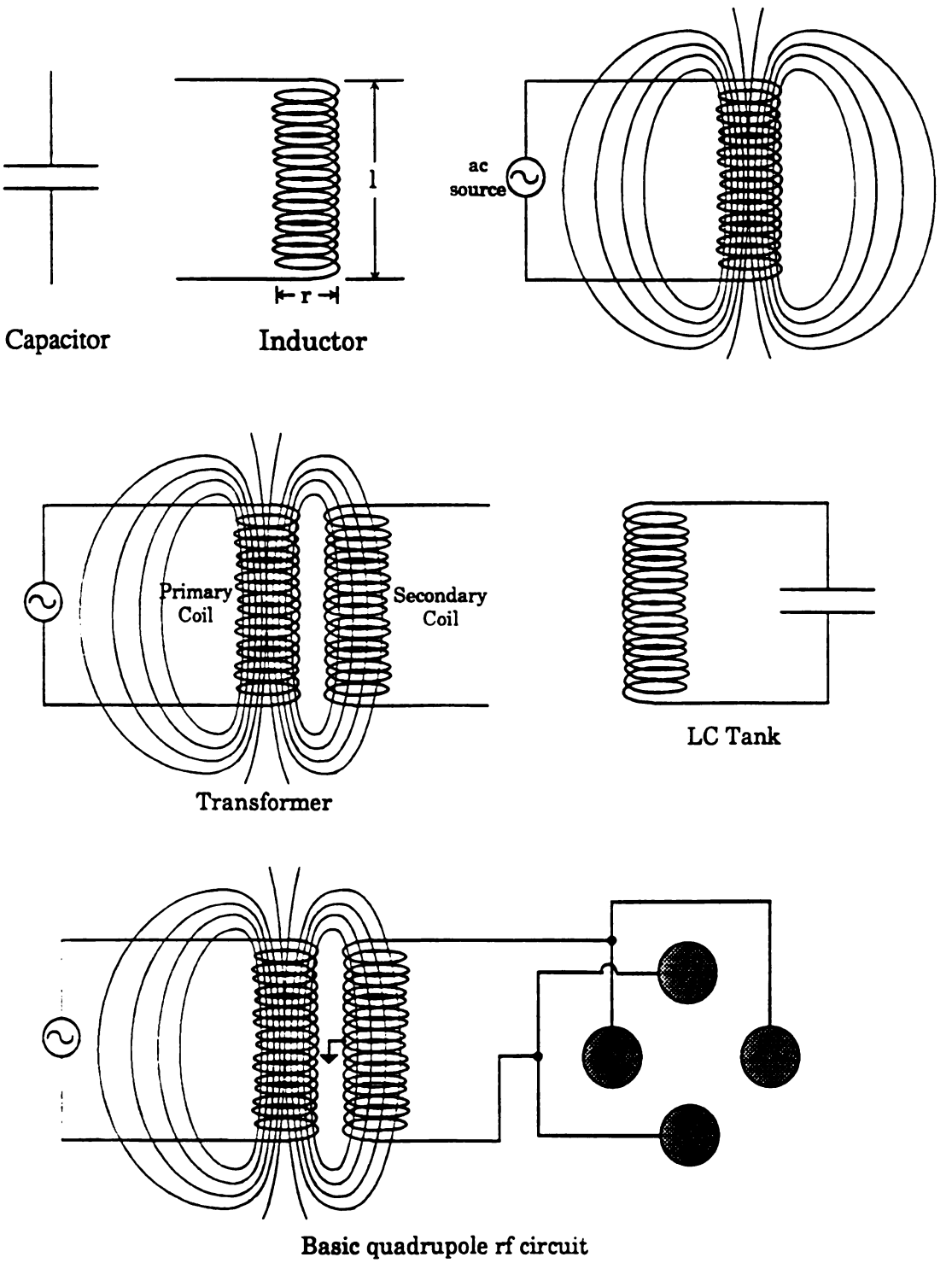

Figure 2.8 The electrical components of the radio frequency generation circuit for a quadrupole mass spectrometer.

If a potential is applied across two conductors separated by an insulator a capacitor is formed. If the potential is removed and the two conductors are isolated from each other then some charge (Q) will be stored across the two conductors. The capacitance (C) of such a system is defined as the charge (Q) stored across the capacitor divided by the potential (V) applied across the capacitor or:

$$C = Q/V$$

The unit for capacitance is the farad (F) which is defined as one coulomb/volt, a 1 farad capacitor will store 1 coulomb of charge when a 1 volt signal is applied across the two plates.

A symbolic diagram of a capacitor is shown in Figure 2.8. If a dc potential is applied to the capacitor, current will flow into the capacitor until it is charged, after which the current flow stops. If the two sides of a capacitor are connected current will flow between the two conductors until the capacitor is discharged. Therefore when a dc signal is applied to a capacitor the only time that current flows is during instances of charging and discharging.

When an alternating signal is applied across the plates of a capacitor, the changing potential results in a constant flow of current through the circuit. The capacitor requires some time to charge to a given potential. The reactance of a capacitor opposing a change in potential as result of this charging time constant is called its capacitance reactance. Since current is simply the rate of charge flow, the current flow across a capacitor is proportional to the rate of change, the frequency (f), of the ac signal. Thus capacitance reactance (X_c) is given as:

$$X_C = 1/(2\pi f C)$$

As the frequency of the applied ac signal increases, the capacitance reactance of the capacitor decreases. The overall result of the application of an ac sine wave signal across a capacitor is an induced cosine current waveform, thus in an ac capacitor circuit, current and voltage are 90° out of phase.

A capacitor is simply a device designed for its ability to hold charge. It consists of two conductors separated by an insulator. The capacitance of the device depends upon the capacitor area, spacing, and the dielectric constant of the insulating material. Increasing the surface area and decreasing the separation of the conducting plates increases the amount of charge that can be stored across the device thus increasing its capacitance. The dielectric constant of the insulating material also effects the capacitance of a capacitor. Increasing the dielectric constant of the insulator allows it to absorb more energy from the electric field between the two plates, thereby increasing it's capacitance.

A device specifically designed for its ability to resist change in current through a circuit is called an Inductor. Inductors are commonly closely wound coils as illustrated in Figure 2.8. If an ac signal is applied across a wire coil the changing current produces a varying magnetic field also shown in Figure 2.8. A change in current through the coil causes the magnetic field lines to expand or contract. This in turn induces a voltage within the coil to counter the flow of current. Through this action the inductor resists change in current through the coil.

The inductance of a coil (L) can be described in terms of the coil diameter (r) in inches, number of turns (n), and coil length (l) in inches by the following expression:

$$L(\mu H) = \frac{d^2 n^2}{18d + 40l}$$

The unit for inductance is the Henry, one Henry counters the emf of 1 volt when the current through the circuit is changing at a rate of 1 amp/second. The reactance of an inductor (resistance of an inductor to change in voltage) is given as:

$$X_L = 2\pi fL$$

If two coils are placed close to each other, a changing magnetic field produced by one coil can induce a current flow in the second coil. Under these conditions these coils are said to have mutual inductance, or mutual magnet coupling. This effect is the basis for a device called a transformer which is shown in Figure 2.8. The coil connected to the power supply of a transformer is called the primary coil. An ac signal applied to the primary coil produces an ac signal in the secondary coil. If power is removed from the secondary coil a magnetic field change that opposes the primary coil magnetic field is created. The primary coil must then draw additional current to counteract this opposing magnetic field. Through this interaction ac power is transferred between the two systems without physical connection.

If the number of turns on the primary coil differs from that on the secondary coil then the ac voltage levels produced at the two coils will be different. The voltage that appears across the secondary coil is proportional to the number of turns in the coil. By selecting the appropriate turn ratio between the primary and secondary coils a primary ac signal can be increased or decreased to a selected level. The change in ac level through a transformer can be determined from the following expression:

$$E_s = E_p(n_s/n_p)$$

where:

E_s = secondary coil EMF n_s = number of turns on the secondary coil

E_p = primary coil EMF n_p = number of turns on the primary coil

Transformers are commonly constructed by winding wire around an iron core (commonly torroidal) to increase the inductance between the two coils. Most audio frequency and lower frequency transformers use this design because of its superior magnetic coupling. Hysteresis and eddy currents within the iron core reduced the performance of this design at higher frequencies. Transformers for radio frequency signals generally use open coils with no core to eliminate problems with hysteresis and eddy currents.

If an inductor and capacitor are connected in series a circuit called an LC tank is created. An LC tank is defined as "a circuit consisting of inductance and capacitance, capable of storing electrical energy over a band of frequencies continuously distributed about a single frequency at which the circuit is said to be resonant, or tuned" [103]. A schematic drawing of an LC tank is shown in Figure 2.8. Resonance exists within an LC tank through the combination of the reactances of the inductor and the capacitor. The frequency of resonance (f) for such a circuit can be described as:

$$f = \frac{10^6}{2\pi\sqrt{LC}}$$

where: f = frequency in kilohertz (kHz)
L = inductance in microhenrys (μH)
C = capacitance in picofarads (pF)

If an ac signal of frequency (f) is applied to the system, power can be absorbed by LC tank and will be stored through resonance between the inductor and capacitor. The amount of current that flows through the LC tank depends upon the matching of the reactances of the inductor and capacitor. If these reactances match exactly the current through the inductor will be completely cancelled by an out-of-phase current through the capacitor. As a result a very high ac level will resonate through the LC tank. The ratio of the reactive voltage to the applied voltage is defined as

the Q of the circuit. Therefore a high Q circuit produces a high ac resonant signal within the LC tank for a relatively low applied ac power.

Radio frequency circuits often consist of a radio frequency power supply, rf transformer, and LC tank with the secondaries of the transformer forming the inductor of the LC tank [98]. A block diagram of a circuit used for the generation of rf levels on a quadrupole is shown in Figure 2.8. An rf signal from the rf power supply causes the production of a varying magnetic field within the transformer. This changing magnetic field induces an rf signal within the LC tank. If the resonant frequency of the LC tank closely matches the frequency of the applied rf, the LC tank will absorb the rf power. This produces a resonant rf waveform across the capacitor formed by the quadrupole rod pairs. By selecting an rf transformer with a large n_s/n_p ratio and balanced inductive and capacitive reactance, a high Q LC tank can be produced which will generate high rf levels with low rf power consumption.

If the frequency of the rf power supply does not closely match the resonant frequency of the LC tank, the LC tank will be unable to absorb power from the primary rf signal. As a result the rf signal will be reflected back from the transformer into the rf power supply, overloading the electronics and possibly damaging the unit. Proper rf power absorption can be accomplished by varying the frequency of the rf power supply to match the resonance of the LC tank. Resonance can also be matched by tuning a variable capacitor, installed between the quadrupole rod pairs, that can vary the LC tank resonant frequency to match the rf power supply frequency.

E. Quadrupole rf and dc generation:

For proper mass-selective operation the rf quadrupole requires a combination of rf and dc potentials across the two rod pairs. The electronic circuits used to produce these signals are generally a combination of the rf circuit described above and a dc production circuit coupled to the rf output.

For a quadrupole to closely produce a hyperbolic field, the signal that appears across the quadrupole rod pairs must posses several qualities:

1. A pure sinusoidal waveform must appear on one rod pair and a pure cosine waveform (90° out of phase) on the other rod pair.
2. This rf signal must have excellent frequency stability and large peak to peak amplitude.
3. A dc signal must appear on each rod pair that is accurately radioed to the applied rf level.
4. The combination of applied rf and dc signals must rapidly and reproducibly variable between differing levels.

The principal components of the rf generation portion of a quadrupole circuit are shown at the bottom of Figure 2.8. The rf signal is generated in the rf power supply shown at the far left. This signal travels through the primaries of an rf transformer and produces a varying magnetic field. Rf power from this signal is received by the LC tank consisting of the secondaries of the rf transformer and the capacitor formed between the two rod pairs. An rf transformer is utilized for two reasons: 1. It allows the amplitude of the rf signal produced by the rf power supply to be increased by selecting a transformer with the required turns ratio, and 2. By separating the LC tank from the rf power supply the dc levels can be directly applied without specialized filtering. The center of the secondary coil of the transformer is center tapped, or connected to a reference point. This results in the production of rf signals across the two rod pairs that are 90° out of phase. Proper rf power absorption between the transmitter circuit and the LC tank is maintained by varying the transmitter frequency or changing the LC tank resonant frequency as described above.

The dc levels are produced through rectification of the rf signals on each of the rod pairs. The rf signal that appears on each rod pair is fed to a rectifier (commonly a series of diodes and capacitors) that produces a dc level proportional to the rf input. The two dc signals are then fed into op-

amps that amplify them to the required levels. These dc signals are then fed back to the quadrupole.

To maintain constant rf levels a feedback loop is used between the rectification circuit and the rf power supply. The dc outputs from the rectifier are fed through another set of op-amps back to the rf power supply. The outputs are used to regulate both the rf amplitude on each rod pair and the balance of rf levels between them. The rf/dc ratio and rf balance can then be varied by changing the amplification of the op-amps between the rectification circuit and the rf power supply.

The quadrupole power supply circuit is scanned by introducing an offset signal to the reference side of the op-amps fed by the rectifier. This offset causes the op-amp output to change, which in turn induces a change in the output of the rf power supply. The result is the production of new rf/dc levels on the rod pairs at a controlled ratio. The offset signal can be varied manually by varying a sensitive potentiometer, or electronically through the production of an offset ramp (commonly 0-10 Volts) which is often produced by the controller or by some external source. As this dc ramp increases from 0 volts the rf and dc levels on the rod pairs will increase, bringing different mass ions into stability in the quadrupole. Thus a mass spectrum is produced by plotting detector signal verses offset voltage. For quadrupole operation in constant Δm mode (discussed in the quadrupole theory section) a small opposite dc bias is required on each rod pair. This is produced by applying a separate, constant bias signal to op-amp reference line.

III. Ion Optical System Design

A. Basic Concepts in Ion Optics

One important aspect of the changes made to the RGAs was the modification of ion optical elements. Ion optical systems, or electrostatic optical components, are a series of elements that are designed to manipulate charged particles through the application of electric or magnetic fields. Electrostatic lens systems employ a series of electrodes that are arranged and biased to produce controlled electric fields. Charged particles that are formed in, or travel through these fields will follow trajectories in response to the forces induced by these electric fields. Properly designed electrostatic lens systems have been used to induce beam focusing, trapping, acceleration, deceleration, and are the primary devices for manipulating charged particles within a mass spectrometer. This section will discuss some basic concepts used in the design of electrostatic optical systems, some ion optical modeling systems that can be used to optimize these designs, and a specialized method of detection that can be used to evaluate the ion beams produced by the systems.

If an ion is formed in a region that contains no electric fields (a field free region) the path that the ion follows will be dependent only upon the kinematics of its formation. If, however this ion passes through a change in electric potential it will experience an acceleration due to the force induced by that change in electric field. One important aspect of this process is that the trajectory that an ion follows as a result of applied electric fields is not mass dependent. That is, different m/z ions that are formed with the same initial energy will follow the same trajectories to some final point, but will arrive at different times. This is an important property of ion optical systems for mass spectrometry, it allows the design of ion optical systems systems that can be used regardless of the m/z of the ion being manipulated.

Electrostatic lenses are a series of elements used to focus or defocus a beam of ions within a mass spectrometer in a fashion similar to light optics. To focus a beam of ions the lens must apply some force to the ion beam in a direction radial to the propagation direction of the ion beam. Strong radial focusing can be induced through the use of static multipole lenses, but this type of lens only induces focusing in one plane. Multipole lenses can be used in series to focus ions in all planes, as is often done in high energy accelerators, the advantage of this type of systems is that it doesn't require high potentials on the elements. This type of system is too complex for use in most mass spectrometers, instead mass spectrometer lens systems are generally based upon the use of cylinder or disk lenses. These lenses can induce the symmetric focusing of an ion beam, but require the used of high potentials relative to the ion beam energy. This is often not a limitation in mass spectrometry, particularly in quadrupole instruments where the beam energy is generally on the order of 10 eV.

The simplest type of cylindrical or disk lens is the two element lens. If an ion beam travels between two regions of differing electric potential, it will experience a force not only in the transverse direction, but also in the radial direction. An example of such a system is shown in Figure 2.9.

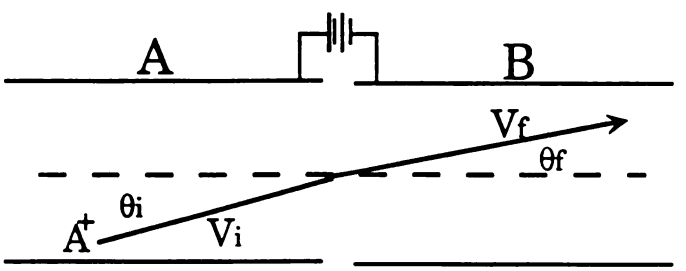

Figure 2.9 Ion refraction during transition between regions of differing potential

If an ion, A^+, is traveling from a field free region in electrode A to another another region of differing potential , electrode B, its transverse

velocity will change from V_i to V_f. This change in transverse velocity will be accompanied by a change in radial velocity causing a change in the trajectory of the ion. The initial angle of the ion relative to the transverse axis (θ_i) is related to the final angle of the ion (θ_f) by the equation:

$$V_i \sin\theta_i = V_f \sin\theta_f$$

The overall effect of using a two element electrostatic lens can be strong focusing for an ion beam, but in order to effectively focus a large beam into a small region the two element lens must accelerate the ion beam, and utilize large apertures. Ion beam focusing with a two element lens is generally accompanied by strong angular divergence, limiting its applicability.

One of the most common lens designs in mass spectrometry is the Einzel lens. The Einzel lens is a three element lens, in which the first and third lenses are held at the same potential and a separate bias is applied to the central element. This lens type, often called a unipotential lens, can be used to focus or defocus an ion beam without changing its energy. A block diagram of a unipotential lens is shown in Figure 2.10

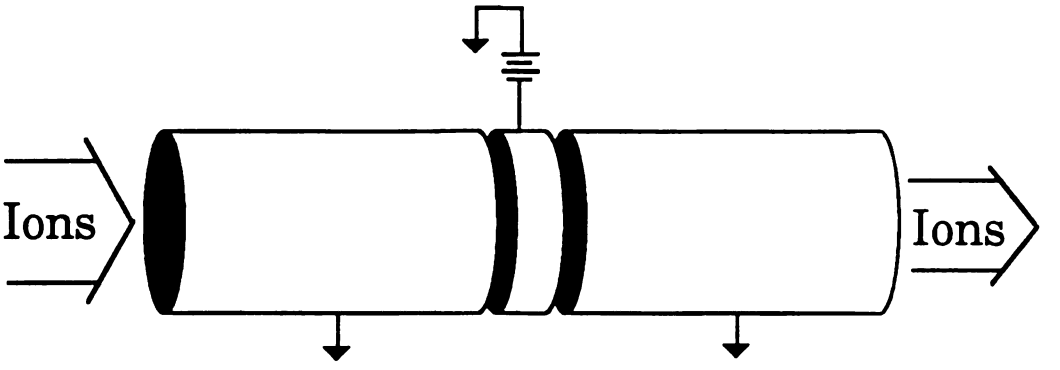

Figure 2.10 Block diagram illustrating a unipotential lens

In general any electrostatic lens that doesn't change the energy of an ion beam, such as an Einzel lens, will inducing focusing in the beam. Einzel lenses can be operated in two modes, decelerate-accelerate and accelerate-decelerate. If the central element is held at a potential that will cause the ion to decelerate as it enters this element, the lens is said to be operating in decelerate-accelerate mode. Ions entering the lens will slow down and feel a defocusing effect in the region between between the first and second elements. As a result the ion beam will spread out in the lens. As the ion beam enters the region between the second and third elements is will be accelerated and experience a focusing radial force. The overall effect on the ion beam is focusing due to the increased residence time of the ions beam in the focusing field. The advantage of the decelerate-accelerate mode of operation is that the central element need only have a potential approximately the same as the beam energy to induce focusing. When the central element of an Einzel lens is held at a potential that causes the ion beam to accelerate as it enters the center element, the lens is said to be operating in accelerate-decelerate mode. In this mode the ion beam is first focused by the transition between elements 1 and 2, and then defocused between elements 2 and 3. The advantage to using an einzel lens in accelerate-decelerate mode is that the ion beam doesn't spread out as much within the lens, and therefore the focusing properties of the lens are much less sensitive to flaws in the mechanical structure/alignment of the lens elements. The disadvantage to this mode of operation is that the central element must be maintained at a potential an order of magnitude greater than the beam energy. This can be important when working with the high energy ion (~2 kV) beams produced by magnetic instruments. Because of the low beam energies used with quadrupole instruments, quadrupole instrument einzel lenses are generally operated in accelerate-decelerate mode [98].

The design of einzel lenses for use in mass spectrometers has been investigated by several research groups [104,105]. The focusing action of

an einzel lens operated in accelerate-decelerate mode has been found to be approximately linear with increasing beam diameter. The spacing between the three electrodes was determined to be the most critical factor in determining the focal properties of an einzel lens. Also important are the diameter and thickness of the central element. The focal properties of an einzel lens have been found to be relatively insensitive to the ratio of the diameters of the central and end electrodes. The optimum relative dimensions determined for the design of an einzel lens are shown in Figure 2.11. The lens is designed with the first and third elements having a common aperture size (b), the spacing between elements and the aperture of the central element should be approximately 3b and 2d respectively [106].

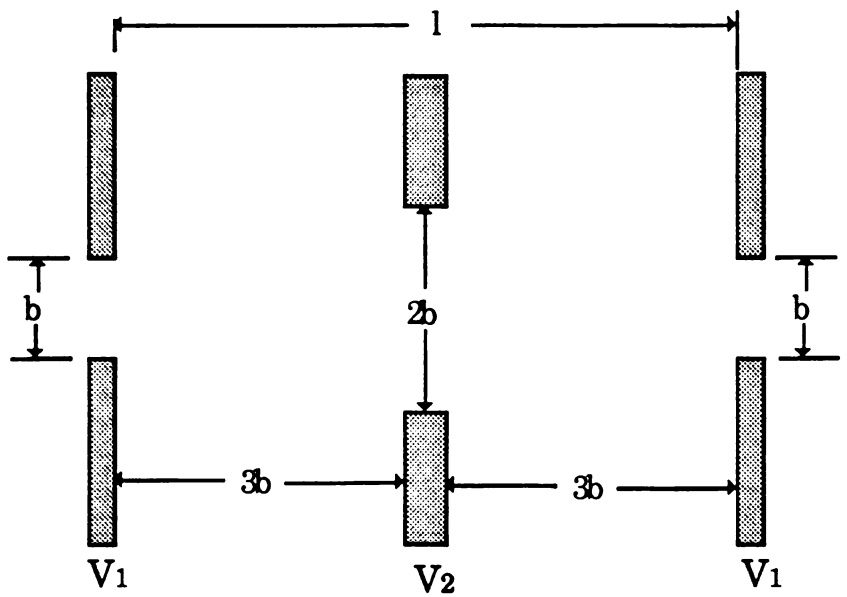

Figure 2.11 The optimal geometry for a three element Einzel lens.

The majority of the lenses that were used to manipulate the ion beams produced by the modified RGAs are based upon this Einzel lens design. The optimized geometry displayed in Figure 2.11 above was

reproduced as closely as possible with available ceramic insulators and lens materials.

The performance of an ion optical system can be evaluated in a fashion similar to light optics, in terms of its focal length, magnification, etc. One important parameter of an optical systems is the degree of aberration, or distortion, that a lens induces in an ion beam. Electrostatic optic systems are notorious for the high degree of aberration they can cause. These aberrations are generally separated into four categories, spherical aberration, chromatic aberration, ellipticity aberration, and deflection distortion.

Spherical aberrations in ion optical systems are caused by the fact that the focusing electric fields produced by a series of electrodes are stronger near the electrodes and become weaker toward the center of the lens. This causes ions near the electrodes to be more strongly focused than ions near the center of the lens, resulting in a lens that doesn't have a single defined focal point. Instead, ion lenses generally produce a region of strongest average focal point (minimal beam diameter) called the disk of least confusion. Chromatic aberration, or momentum dispersion, is caused by the sensitivity of the focal properties of an ion optical lens to the energy of the ions being focused. If a series of ions with some energy spread travel through an electrostatic lens the higher energy ions do not spend as much time within the lens. As a result they experience less of the focusing field in the lens and are more weakly focused than ions with lower velocities. This causes a spread of focal positions in the ion beam that is dependent upon the spread of initial energies. This aberration can be reduced by using an ion beam with minimal energy spread, and carefully referencing the potentials on the lens to the ion beam energy (source potentials). Elliptical astigmatism is an aberration that results from the use of asymmetric (non-circular) lens elements, or elements that are tilted with respect to the beam optical axis. These conditions result in the creation of asymmetric focusing fields within the lens, and can

generally be identified through the observation an asymmetric ion beam image.

The final aberration of interest is deflection distortion. If an ion beam must be deflected to some off-axis remote location, it is common to bias a set of X and Y deflection plates to control the beam position. These plates are positioned in series with one set controlling horizontal deflection (X) and another controlling vertical deflection (Y). When an ion beam is deflected in this fashion the linear deflection is accompanied by some distortion of the symmetric beam shape due to several optical aberrations. As a result a beam that presents a round profile before deflection can be distorted into an elliptical shape following deflection. Some distortion due to this phenomena is unavoidable, but this effect can be minimized by using a pair of plates for each deflection direction. These plates should be operated in push-pull mode by placing an attractive potential upon the plate the beam is deflected toward, and a repulsive potential upon the plate opposite the deflection direction.

One final phenomena encountered in the design of ion optical systems is space charging. If a high enough concentration of ions is present within an ion beam, an electric field can be produced between the ions that will cause the beam to expand in diameter. This becomes increasingly important when the ion beam is strongly focused because of the increase in the number of ions per unit volume, and can produce spherical aberrations in the ion beam. In general, for most ion beams this spreading due to space-charge effects is not an important factor. This is true for the manipulation of the ion beams performed in this research. Assuming a worst case where a 10 eV, 3 mm radius, 50 nA beam of m/z=30 ions must travel the complete distance from the ion source to the cryostat (~200 mm) the spreading of this ion beam due to space charge effects is negligible relative to the beam diameter [106]. This is primarily due to the low ion density of the ion beams produced by these sources.

B. Practical Ion Optical Design Tools:

Most of the early electrostatic lens systems used in mass spectrometry were based on the lens designs of Nier [107]. As mass spectrometers became more sophisticated the need for better ion-optical lens systems arose. Most early ion optical lenses were designed empirically or using analog ray-tracing techniques [108]. The analog ray tracing methods involved the painting of possible electrode arrangements, in conductive paint, upon resistive paper. Potentials could then be applied to the electrodes and the electric potential of the free space region between the electrodes was measured directly. Using these electric potentials the equipotential lines within this region could be mapped out and the trajectories of ions traveling through the lens calculated. These methods were useful for ion optical lens design, but were slow, somewhat inaccurate, and couldn't be used to model combined fields and circular lens geometries. With the introduction of computers, computational methods were applied to the study of electrostatic optics.

Computation methods, especially modeling programs, have been applied to several areas of ion-optical design. Modeling programs have been used to calculate the optical properties of electrostatic lenses including, object and image positions, magnifications, focal points, chromatic aberrations, and transfer efficiencies. These programs generally calculate the electric potential and/or magnetic field for free space points within an electrostatic lens using the LaPlace equation. Ion trajectories are calculated from these potentials using simple Newtonian relationships, and focal points and spherical aberrations are evaluated by integration of the paraxial ray equation. The final result of these calculations can include focal lengths, magnification, figure of merit, and aberration coefficients for the lens system of interest [109].

Much of the early electrostatic lens design was performed using the results of a series of lens models calculated and tabulated by Harding and

Read [110]. They modeled a series of 24 possible electrostatic lenses to compare the performance of each of these systems. The electric potential for points within the lens systems were calculated by solving for the LaPlace equation, and the paraxial ray equation was integrated to determine focal points and spherical aberration for the lenses of interest. From these results a series of equations were obtained that allow the general determination of focal lengths, magnification, and aberration coefficients for each lens design. The overall behavior of each system could then be evaluated for a particular application using an arbitrary comparison term called the figure of merit.

As the availability of computer systems increased, several different ion-optical simulation programs were developed. Complex programs such as TRIO [111] and GIOS [112] were used in the design of several systems including optimized einzel lens systems for ion kinetic energy spectrometry (IKES) [113]. Other programs were developed to allow the design of ion optical systems that could be automatically optimized using computer algorithms. One example of this type of application was the use of the modeling program CYLENS [114] to design a series of high transmission cylindrical lenses that could be self-optimized through the use of simplex optimization [115]. This type of self-optimization has also been used to design a high efficiency thermal ion source that was also optimized through simplex optimization [116].

PC based, interactive modeling programs have recently gained wide acceptance as a tool the design of ion optics. These programs allow the user to interactively model and evaluate ion-optical systems through the graphics interface available on a personal computer. The most popular of these is the program SIMION. SIMION is an electrostatic lens analysis and design program originally developed by D.C. McGilvery [117.] It allows the user to create a 2-dimensional array of points, and to define points within the array as either electrodes of non-electrodes. Voltages are then assigned to the electrodes and SIMION can calculate the electric

potential of each of the non-electrode points in the array using a technique called self-adjusting over-relaxation. Once these potentials have been calculated, SIMION can then calculate the trajectories for charged particles within the array. This trajectory information can then be used to customize the optical system to the needs of a specific application. McGilvery's original SIMION program has been modified to allow its use through an interactive graphic interface on an IBM-AT/PS2 type machine [118,119] as well as on a MacIntosh [120]. This user-friendly interface has made SIMION a practical design tool for anyone interested in the study of electrostatic optics. Since its inception SIMION has been used in variety of ion-optical design projects including: the optimization and design of wide acceptance-angle ion lenses [121], the design of a surface emission ion source for a quadrupole instrument [122], time-of-flight modeling [123], and the design of a short residence time ion lens [124].

The self-adjusting over-relaxation technique used by the SIMION program to calculate the potential of non-electrode points within its 16,000 point array has been described in detail in the literature [111]. This technique calculates the electric potential value for a point , P_0, from the average of its four nearest neighboring points, P_1-P_4 , as shown below.

$$\begin{array}{ccc} & P_4 & \\ P_1 & P_0 & P_2 \\ & P_3 & \end{array} \qquad P_{0new} = (P_1 + P_2 + P_3 + P_4)/4$$

This calculation is an approximate solution to the LaPlace equation. SIMION performs this calculation for all the points within the array, this is considered one iteration. Several iterations are repeated, and as a result the changes made by each preceding iteration slowly propagate through the array. As the number of iterations increases, the change in the electric potential calculated for each point decreases. The user can determine what the maximum change should be for the final array, when

this point is reached the array is considered "refined". Refining using this technique requires a large number of iterations, SIMION decreases the number of iterations required by using an over-relaxation factor that increases the amount each point changes in each calculation. The optimum over-relaxation factor for each array is dependent upon the geometry of the particular array, SIMION uses a self-testing technique to allow the program to self-adjust the over-relaxation factor to minimize refining times. The self-adjusting over-relaxation refining method employed by SIMION greatly reduces the amount of time necessary to refine the potential array, making the evaluation of ion optical systems far less tedious.

After the electrode array had been refined, SIMION allows the user to display equipotential contour lines within the array and model the trajectories of ions/electrons originating outside or within the array. The user can define voltage intervals (or use automatic intervals) for contour display. SIMION will search through the array, locate points corresponding to those potentials, and display lines connecting those equipotential points. These contour lines can be used to evaluate the magnitude and direction of the electric fields present within the array. Ion trajectories can be defined by the user including initial energy, mass, angle, and fragmentation characteristics. SIMION determines the force an ion experiences at any point within the array due to applied electric and/or magnetic fields and calculates the acceleration an ion will experience due to that force. During the initial layout of the array the user indicates the type of symmetry present in the system, circular, planar, or planar non-symmetric. SIMION uses this information to correctly evaluate the force due to the potential on the electrodes in three dimensions. The user can also determine how often the trajectory calculations are made, the time step, to control the accuracy of the calculation. These calculations are self-adjusting to ensure that a trajectory will not pass over a 'turn-around' or zero energy point. A series,

or family, of these calculations can be performed, displayed on screen, and observed at high magnification levels to allow the user to thoroughly evaluate the optical properties of the electrostatic lens system under investigation.

Computer modeling programs have proven extremely useful for the optimization of ion-optical designs, but in order to fully evaluate these systems it is also important to be able to directly observe the ion/electron beams. Microchannel Plate Detectors (MCPs) can be used to make these observations. An MCP is a thin glass wafer that contains an array of 10^4-10^7 miniature electron multipliers. Originally developed as amplification devices for image intensifiers [125], MCPs can be used to detect and visualize beams of charged particles and energetic photons. MCPs are manufactured from extremely small, lead-doped solid glass fibers that contain an etchable core. These fibers are packed together and fused into a hexagonal array. The bound fibers are then sliced to the desired plate thickness and angle, and the etchable core is removed chemically. The wafer is then treated to enhance the secondary emission characteristics within the hollow channels, and the front and back faces of the wafer are vacuum deposited with an electrode material (Inconel) [126]. A cutaway view of a finished MCP is shown in Figure 2.12a.

The resulting MCP contains thousands of miniature 'channeltrons' with a typical channel diameter of 10-100 um, length to diameter ratio of 40-100, and separation of ~25 um. If a high voltage is placed across the two face electrodes of the plate, the collision of a high energy particle with a channel wall will produce the secondary emission of electrons within the channel. These secondary electrons can undergo further collisions with the channel wall producing more electrons, the resulting amplification is generally on the order of 1:10,000 for a single plate. MCPs can also be used in series to increase the magnification of the detector. A series of two MCPs can produce an amplification factor of 10^4 to 10^7 output electrons per incident particle. The secondary electrons produced in the MCP impinge

upon a detector, generally a metal anode/anode array or a high speed phosphor screen mounted on a fiberoptic. The phosphor screen detection is generally used to spatially resolve the ion beam profile, while the anode detector is generally used for high speed detection.

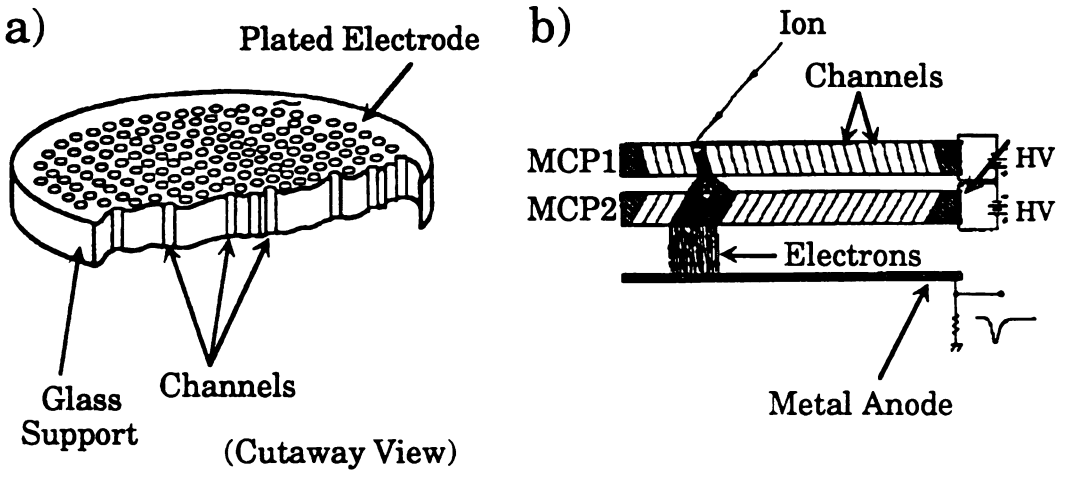

Figure 2.12 The microchannel plate detector (MCP).

MCPs can be manufactured with several channel geometries including straight channel, curved channel, and chevron configuration for a pair of MCP plates (shown in Figure 2.12b). The original straight channel design can achieve a gain of 10^3 to 10^5 for each MCP plate. The upper range of gain for the straight channel MCP is limited by ion feedback. The high flux of electrons produced within a channel can interact with gas molecules to form positive ions. These positive ions will experience the strong electric field across the channel, drift back through the channel, and produce an afterpulse at the detector. This phenomena is called ion feedback. Curved channel MCPs are often used to reduce the effects of ion feedback. Positive ions drifting through a curved channel will impinge upon the channel walls and be neutralized. This substantially reduces detector noise, and allows curved MCPs to achieve gains in the low 10^6 range [127]. The disadvantage to curved channel MCPs is that the manufacture process required to produced properly shaped channels is

much more difficult and costly. The Chevron configuration detector, shown in Figure 2.12b, most often consists of two straight channel MCPs. The channels within each plate are oriented at an offset angle, typically 8°/8°, from the axis of the detector and separated by 50 - 150 um. By using an offset angle the background noise due to ion feedback can be greatly reduced. Under normal operating conditions a chevron configuration MCP will achieve a 10^4 gain across each plate for an overall gain of ~$4x10^7$.

The detection efficiency of MCP detectors is dependent upon both the potential across the plate and the energy of the incident particles. Optimum gain is generally achieved at an operating potential between 1000 and 1100 Volts per MCP plate. The detection efficiency of an MCP ranges from 5-85% for ion energies of 200-2,000 Volts, and 60-85% for energies of 2,000-50,000 Volts. The properties and manufacture of MCP detectors have been recently reviewed by Wiza [126], and the use of MCPs as focal plane detectors in magnetic sector mass spectrometers has been presented [128].

Microchannel plate detectors were used extensively in the modification RGAs to produced mass-selected beams. Two chevron configuration MCPs with a phosphor screen/fiberoptic were used to visualize the ion beam profiles produced by the RGAs and to determine the angular divergence of those beams. This information was then used to evaluate the performance of the ion optics in the RGAs, and to make informed modeling decisions for further SIMION studies.

Chapter 3. Anavac-2 Ion Source Modifications

I. The design and performance of the Anavac-2 RGA

The first residual gas analyzer selected for modification was an Anavac-2 RGA produced by the Micromass division of VG-Gas Analysis Limited. The Anavac-2 is a small RGA, designed to measure both total pressure within a vacuum system and partial pressures of residual gases. The minimum detectable total and partial pressures for the unit are quoted as $5x10^{-12}$ torr and $5x10^{-11}$ torr respectively. The RGA uses the open EI source design described in Chapter 2.I.A, a miniature quadrupole mass filter, and a Faraday plate with a chopper amplifier for detection. The quadrupole can operate in mass-selective mode for partial pressure analysis with a mass range of 2-60 daltons and resolution quoted as better than 50% valley. The maximum operating pressure for the Anavac-2 RGA is $1x10^{-4}$ torr. Some of the features of this RGA include: external programmability of the mass filter, overpressure protection circuitry that can be used to control other equipment, complete short circuit protection of all circuitry, and program outputs voltages that allow the unit to drive an XY recorder for recording residual gas spectra. The unit was initially bought in 1979, and at that time the complete RGA cost only $4,500.

The Anavac-2 consists of three primary components, the analyzer head, the remote electronics head, and the control unit. A functional diagram of these three components is shown in Figure 3.1. The analyzer head contains the mechanical components necessary to generate, mass select, and detect the ions. The remote electronics head contains the circuitry that generates the rf and dc levels necessary to operate the analyzer head, and also the sensitive amplifier required for the detection of ions. The control unit produces the dc potentials required for the operation of the analyzer head as well as the high current levels that heat the

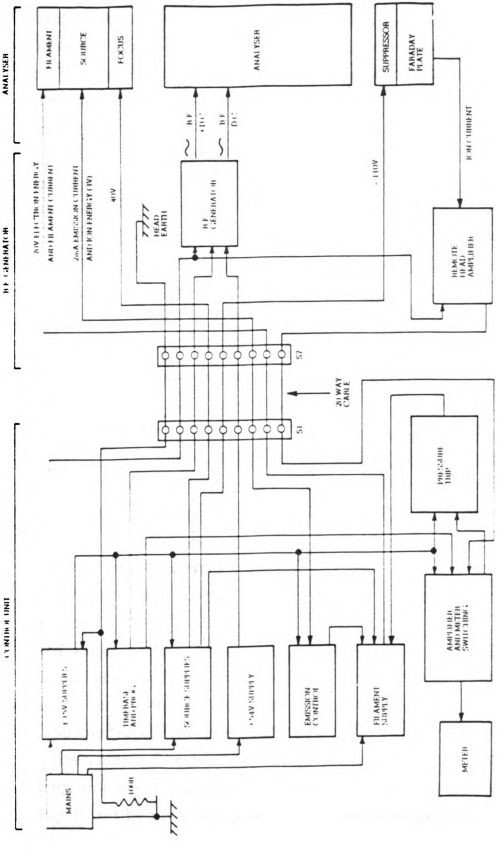

Figure 3.1 A functional schematic diagram of the Anavac-2 residual gas analyzer.

filament. The program voltages necessary to drive the remote electronics head are also produced and controlled by the control unit.

The analyzer head contains all the components that are inserted into the vacuum chamber. These include the ion source, quadrupole, and detector. Figure 3.2 shows a block diagram of the overall design of the analyzer head. The Anavac-2 source is similar in design to the source described earlier and shown in Figure 2.3. The symmetry of the unit is circular and Figure 3.2 shows a cross-sectional view of the components of the Anavac-2 system. The original RGA filament, normally tungsten, is approximately 10 mm long and oriented parallel to the Z-axis of the quadrupole. It is spot welded to two support leads that run through high current feedthroughs located in the endcap of the filament housing. One of the support leads is in electrical contact with the filament housing, allowing both the filament housing and the filament to be maintained at the same bias potential. The outside diameter of the filament housing is 29.0 mm the inside diameter is 16.8 mm. The source grid (6.6 mm diameter, 9.0 mm height) is located within the filament housing and is spot welded to a 0.5 mm stainless steel (SS) circular plate with a 3 mm center aperture. A single lens, the focus element, is positioned after the source grid. This electrode is also a 0.5 mm SS circular plate with a 3 mm central aperture. The final component of the ion source optics is the quadrupole entrance aperture plate containing a third 3 mm aperture. The source components are held in place with threaded SS rods that are isolated from the individual components of the source with ceramic sheathing tubes. 1.3 mm thick ceramic spacers are used to electrically isolate the components including the filament housing, source grid, focus lens, and quadrupole entrance plate.

The quadrupole mass filter is housed in a SS tube housing that is 53 mm long and has a diameter of 30 mm. The entrance aperture to the quadrupole, set by the quadrupole entrance aperture plate, is 3.0 mm and the exit aperture is 3.0 mm. Cutaway sections in the quadrupole housing

allow the connection of electrical leads to the quadrupole rods. The quadrupole rods are permanently mounted in a machined ceramic block designed to fit tightly inside the quadrupole housing. This ceramic block is held in place by a setscrew located in the side of the quadrupole housing. The quadrupole rods are 50.0 mm long, have a rod diameter of 6.4 mm, and a rod spacing of 5.5 mm.

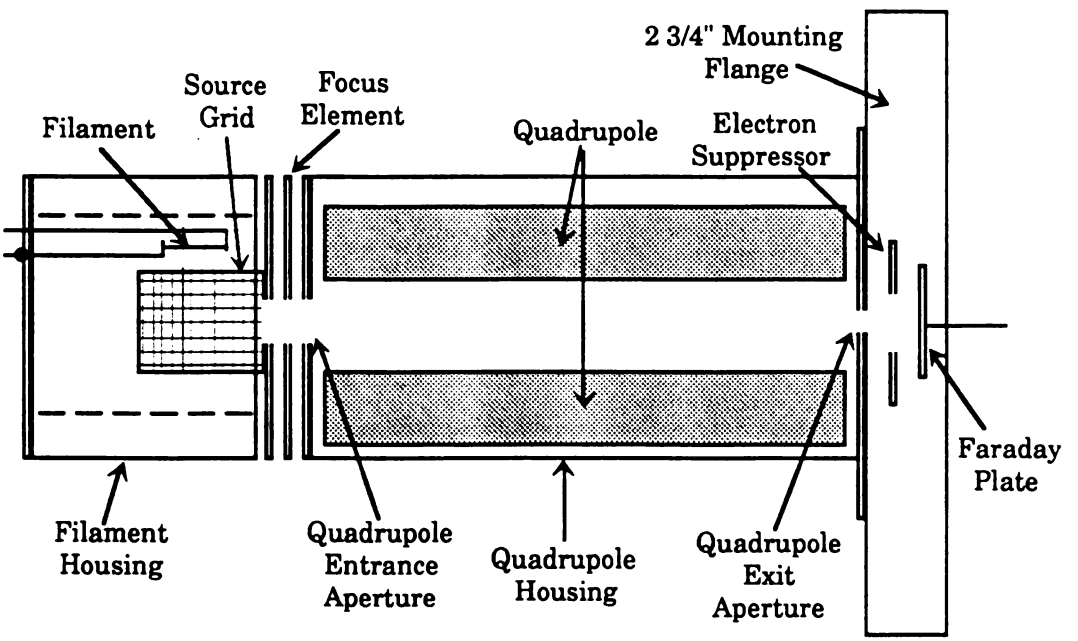

Figure 3.2 A block diagram of the Anavac-2 analyzer head

These dimensions yield a r/r_0 ratio of 1.16 which is close to the 1.148 optimum dimensions for production of a hyperbolic field within the electrode array. Using relationships described in Chapter 2.II.C, it is possible to calculate the ultimate performance that could be achieved with this size of quadrupole. For a 2 Mhz, 250 V_{p-p} rf signal the maximum mass, M_m, and minimum peak width, ΔM_{min}, that could be achieved with this system can be calculated as:

$$M_m = \frac{7x10^6 V_m}{f^2 r_o^2} = \frac{7x10^6 (500\,V)}{(2x10^6 Hz)^2 (2.75x10^{-3} m)^2} = 116 \text{ daltons}$$

$$\Delta M_{min} = \frac{4x10^9 V_z}{f^2 L^2} = \frac{4x10^9 (3\ eV)}{(2x10^6)^2 (0.050\ m)^2} = 1.2\ daltons$$

Thus the Anavac-2 quadrupole is functioning close to the ultimate resolution, or minimum peak width, that could be achieved with a quadrupole of this geometry. However the mass range that is covered by the stock Anavac-2 is approximately half of the ultimate range the quadrupole could achieve. The probable reasons the Anavac-2 is only designed to function from 2-60 daltons include; higher sensitivity obtained through operating under these conditions, decreased sensitivity to changes in mechanical alignment, and the fact that for most residual gas analysis a 2-60 mass range is sufficient to accurately monitor residual gases.

The exit aperture plate for the quadrupole also functions as a mount, allowing the coupling of the quadrupole housing to the 2 $^3/_4$" support flange. The Faraday plate used to detect ions that pass through the mass filter is located within the support flange along with an electron suppressor ring electrode used to reduce background electron noise. All the potentials supplied to the components of the analyzer head are fed through high vacuum electrical feedthroughs located in the mounting flange.

The remote electronics head contains the circuitry used to produced the dc and rf levels necessary for the operation of the quadrupole, and also the chopper amplifier used to detect the ion current at the Faraday plate. The rf generation circuit consists of three primary components: the crystal controlled oscillator that controls the rf frequency, the rf power stage that produces the rf signals, and the control stage that controls the rf output and produces the correct dc levels for the quadrupole. A block diagram of the principal quadrupole power supply components for the Anavac-2 RGA is shown in Figure 3.3

The crystal oscillator generates a square wave ac signal at a frequency of 2 MHz. This signal is fed through the control stage to the rf power stage which produces a high voltage (maximum 250 V_{p-p}) 2 MHz sine wave across the primary coil of the rf transformer. The secondary coil of the rf transformer is center tapped, producing 90° out of phase rf signals on each of the two output leads. The output leads connect to the high voltage feedthroughs on the analyzer mounting flange through which the rf signals are fed to the quadrupole.

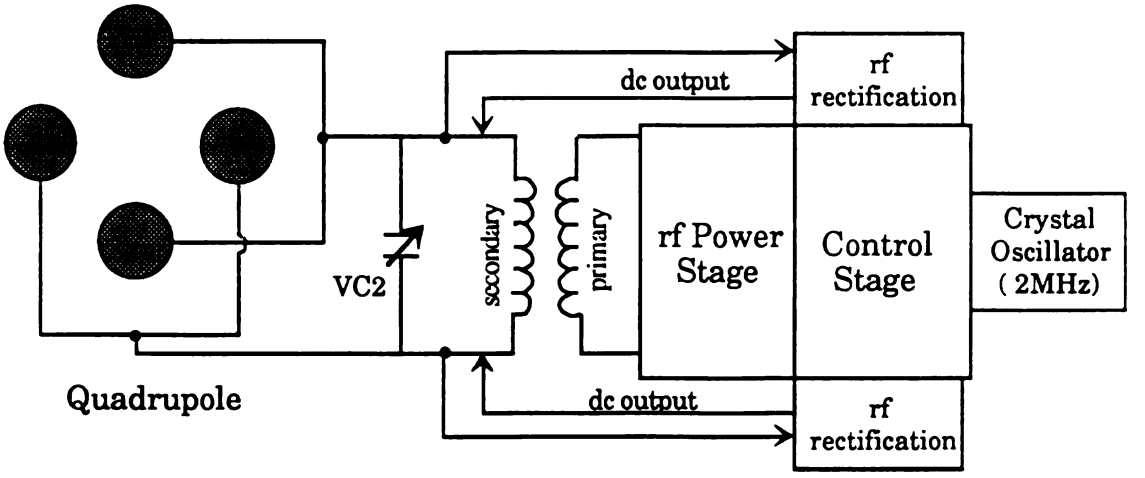

Figure 3.3 A block diagram of the quadrupole power supply circuit used in the Anavac-2 RGA.

The rf outputs from each of the two output leads are also fed back to the control stage where they are rectified to produce +dc and -dc levels. The control stage sets the dc balance between each quadrupole rod pair, and the rf/dc ratio that is produced in the rectification step. The dc levels produced by the control stage are fed back to the output leads connected to each of the quadrupole rod pairs producing the dc component on the quadrupole. These dc levels can be measured at testpoints within the remote head to verify the dc balance in the system and to indirectly monitor the rf output. A variable capacitor (VC2) is connected across the

secondaries of the rf transformer which can be varied to adjust the resonant frequency of the quadrupole/secondaries circuit to match the fixed oscillator frequency. When the RGA is operated in total pressure (rf-only) mode the dc output levels from rectification stage of the control stage are taken to ground, allowing the mass filter to pass all ions of m/z >9. A complete circuit diagram of the remote head rf generation and chopper amplifier circuits is shown in Appendix I.

The remote head also houses a sensitive chopper amplifier that acts as a current-to-voltage converter for measuring ion current at the Faraday plate. The amplifier is housed in a shielded case to reduce noise from the rf generation circuitry, and the output of the chopper amplifier is fed to the control unit for display. The control unit allows the chopper amplifier to function at several levels of amplification that can be selected using the RANGE switch on the control unit. More sensitive range settings result in higher overall amplification of the ion current, but require longer sampling times to achieve reasonable signal/noise levels. The response time, noise level, and overall gain of the chopper amplifier at each range setting is given in Table 3.1

Table 3.1 The performance of the Anavac-2 chopper amplifier

range(torr)	90% response	p-p noise (%fsd)	Gain
10^{-5}	40 ms	0.1	10^{9}
10^{-6}	30 ms	0.1	10^{10}
10^{-7}	30 ms	0.1	10^{11}
10^{-8}	40 ms	0.5	10^{12}
10^{-9}	500 ms	0.5	10^{13}
10^{-10}	500 ms	1	10^{14}

The third component of the Anavac-2 RGA, the control unit, supplies all the remaining dc and ac levels necessary to operate and control the quadrupole. These functions include the filament circuitry, mass program voltage circuits, and the dc levels required at the analyzer head. The emission of the filament in the analyzer head is regulated at 2

mA by the control unit. This emission current is measured at the source grid which is maintained at ~+3 volts. For the stock tungsten or rhenium filaments a current of approximately 4.35 amps is required to produce a 2 mA current at the source grid. The feedback circuit that regulates the filament emission is also connected to protection circuit. When the RGA is operated in filament protect mode the filament will automatically shut off should the current from the chopper amplifier exceed full scale on the control unit meter. This protection circuitry also controls the state of two relays that can be used to protect other equipment within the vacuum system. This protection circuit can be disabled by operating the RGA filament in filament override mode.

The operating mode of the quadrupole is controlled by the operating mode switch on the control unit. The TOTAL PRESSURE position causes the dc rectification circuit in the remote head to be taken to ground, allowing the detection of ions with m/z > 9. When this switch is in the PARTIAL PRESSURE mode the quadrupole is operating in mass-selective mode and the detector output is displayed on the panel meter. When the operating mode switch is is set to MASS MODE the quadrupole is operating in mass selective mode, the panel meter displays the ion mass selected by the quadrupole, and the detector output is available at the program output line on the back of the control unit. The mass dial on the unit controls the initial mass that is selected by the mass filter. This control can be used to 'sit' on a mass peak, to perform a form of selected ion monitoring, or to set the starting mass for a mass scan. The scan switch causes the control unit to produce a program voltage that will scan the filter upward from the initial setting on the mass dial. Two scan speeds are available, slow (5 sec/amu) and fast (0.5 sec/amu), that are selected depending upon the sensitivity required. The range of mass values covered by the program voltage is controlled by the span control which allows a range of 1-60 amu to be repetitively scanned. When placed in scan mode the control unit will scan the mass filter until the span limit

or the upper limit of the device (m/z = 60) is reached. At that point the scan will reset and the process will repeat. Scanning of the mass filter can also be accomplished through the use of an external input voltage. An external input port is available that allows the operator to scan from m/z =2-60 using a 0-10 volt dc input signal. The control unit also contains program outputs voltage lines for both the mass scale (X) and the detector output (Y) that can be used to drive an XY recorder. A complete diagram of the circuitry inside the control unit is shown in Appendix II.

The initial operating parameters and performance of the Anavac-2 unit prior to modification are given in Table 3.2. These values were used for comparison with the modified system to evaluate the effect that design changes had upon the performance of the RGA.

Table 3.2 Initial optimum operating conditions for the Anavac-2 RGA

Electron Energy =	70 eV	Focus Potential =	-40.3 V
Ion Energy =	3.0 eV	Suppressor potential =	-110 V
fast scan time =	61 sec	slow scan time =	337 sec

filament current limit = 4.1 A
resolution = 20% valley
sensitivity in partial pressure mode= 1.2×10^{-4} A/mb
sensitivity in total pressure mode = 1.5×10^{-3} A/mb
dc balanced at mass 60 to within 0.1 V
Mass Stability (peak top stability) drift < 0.1 amu / 8 hours

The Anavac-2 RGA that we obtained was several years old, and the first study performed was an analysis of its mass resolution and performance range. The entire analyzer head was first disassembled and cleaned with a mild abrasive followed by ultrasound baths of water and acetone. Following cleaning, the unit was assembled, tested for electrical continuity between the flange feedthroughs and the analyzer elements, and installed on a vacuum chamber. The remote head and control unit were then installed, and the program outputs on the control unit were connected to the X and Y inputs of an XY recorder. A Granville-Phillips ion gauge and Ametek M100 RGA were also installed on the vacuum

chamber for comparison with the total pressure readings from the Anavac-2. Following evacuation to ~$8x10^{-7}$ torr, an air leak was introduced into the chamber. Air was introduced to an ion gauge reading of $5x10^{-6}$ torr which yielded an Ametek M100 total pressure reading of $1.6x10^{-6}$ torr and a partial pressure reading for nitrogen of $3.5x10^{-7}$ torr. The Anavac-2 RGA was turned on and the filament was heated to an emission of 2 mA. The total pressure reading displayed when the unit was set to TOTAL PRESSURE mode was $2.1x10^{-6}$ torr. The unit was then set to MASS MODE at a sensitivity setting of $x10^{-5}$ torr and scanned at a slow setting from m/z = 2-60. The spectrum produced from the XY recorder set at Y = 100 mV/in scale is shown in Figure 3.4. The bottom trace shows the complete mass spectrum from m/z 2-60 and the upper trace shows an expanded view scanning from m/z 12-20. A peak intensity of $5.2x10^{-12}$ A for N_2^+ at m/z = 28 was calculated from the sensitivity specifications given in Table 3.1. Using the N_2 partial pressure reading from the Ametek M100 RGA and the quoted sensitivity of the Anavac-2 RGA in partial pressure mode, the optimum current that the Anavac-2 should produce with this leak is $5.6x10^{-11}$ A. This value is within an order of magnitude of the experimental value obtained, which is good agreement considering the experimental errors involved. Some experimental errors could include; different pumping speeds at each measuring device, use of an older filament on the Anavac-2, and loss of sensitivity from contaminants on the Anavac-2 source.

The resolution performance of the Anavac-2 can be best observed in the upper trace of Figure 3.4. This expanded view clearly shows the peaks at m/z = 14, 16 and, 18 resulting from the air leak and residual water on the walls of the aluminum vacuum chamber. A small peak at m/z = 17 can be seen that is formed through the fragmentation of H_2O^+ to form OH^+. This peak is poorly resolved, and although it is not an ideal comparison peak for resolution evaluation, the Anavac-2 didn't appear to be functioning at the full 20% valley resolution given in the original specification sheet. For the

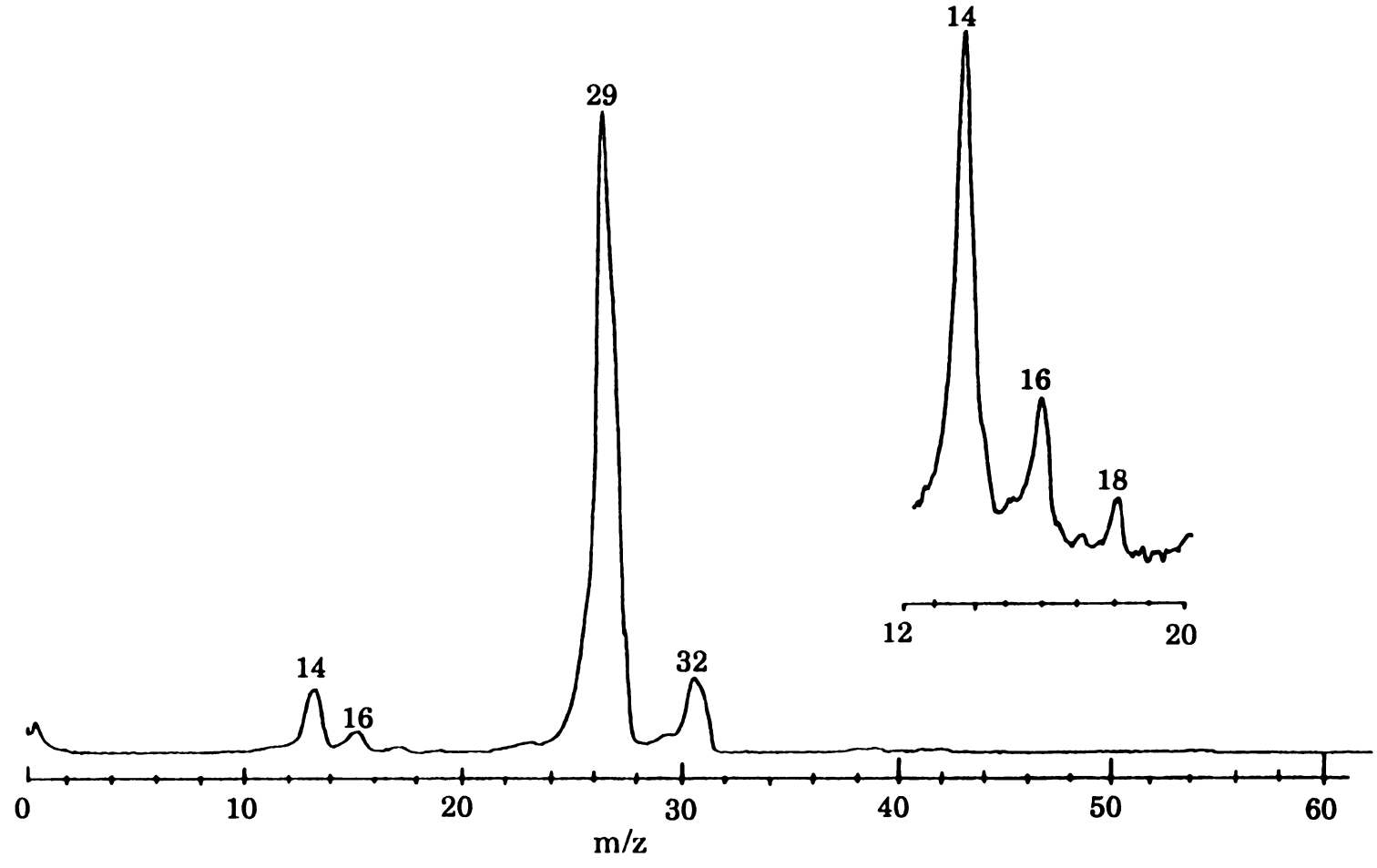

Figure 3.4 The resolution performance of the original Anavac-2 RGA with an air leak. The upper insert shows an expanded view of the region from m/z = 12 to 20.

matrix isolation studies utilizing this source, this slight loss of resolution should not be a difficulty.

II. Modification of the Anavac-2 EI source

A. SIMION modeling of design modifications

The first modification made to the Anavac-2 residual gas analyzer was the construction of a source housing to allow the direct introduction of sample gas into the source region. To minimize the amount of neutral sample gas that is trapped on the cryostat surface, the source housing must have a low conductance to the experiment chamber. A source housing was designed that could reduce the conductance from the EI source by 97%. To accomplish this reduction in conductance, a source housing was designed that enclosed the entire source region and reduced the ion exit aperture. Before undertaking the lengthy manufacture of this housing several SIMION modeling studies were performed to evaluate the effect it would have on the performance of the EI source.

The Anavac-2 source was first disassembled and all of the stock components were accurately measured. Using these dimensions a SIMION model of the EI source was constructed, this model is shown in Figure 3.5. To evaluate the performance of the original EI source it was necessary to first determine the trajectories that electrons emitted from the filament would follow in the source. From this information it was possible to determine the region within the source grid volume that had the highest probability of an electron/molecule collision that could lead to ion formation. For this reason it was necessary to include in the this model the filament and support rods shown in Figure 3.5. To include these components the source was modeled in planar-nonsymmetric symmetry, which required a larger number of array points, in this case 3,000 points,

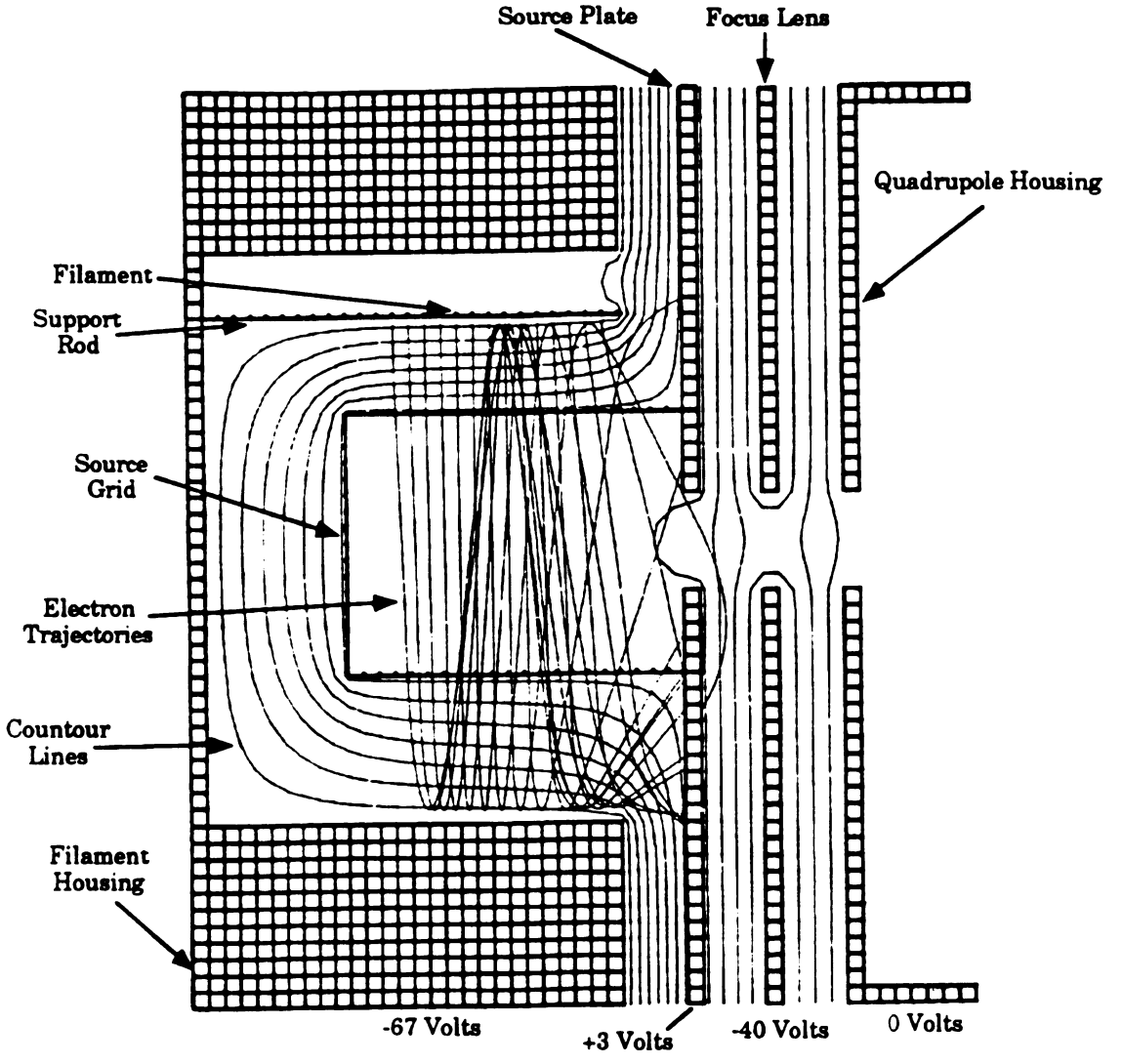

Figure 3.5 SIMION model of the Anavac source showing electron trajectories.

than do symmetric geometries. As a result, both the accuracy of the dimensions of the model and the symmetry of the model were somewhat degraded. Even with this difficulty, this model proved useful in studying the behavior of electrons in the Anavac-2 source.

The SIMION model shown in Figure 3.5 consists of four separate electrodes. The filament/support rod and filament housing are held at the same potential, in this case the normal operating potential of -67 volts. The source electrode consists of two components, a square grid region and an plate with an aperture, that are held at the normal source potential of +3 volts. With SIMION the user can create transparent electrode grids by setting the electrode thickness to 1 grid unit, the source grid is modeled in this fashion. The source plate was modeled to produce the 3 mm source exit aperture size as closely as possible within the constraints of the array size. The focus electrode,the third electrode element, it is a plate of identical dimensions to the source plate. In the model shown, the focus electrode is biased at the -40 volt potential normally used by the Anavac-2. The final electrode in Figure 3.5 is the quadrupole housing. This electrode models the quadrupole entrance aperture plate and the tube housing that contains the quadrupole. The quadrupole entrance aperture is identical to the source aperture, and the entire quadrupole housing electrode was maintained at the normal operating bias of 0.0 volts.

Following construction of the electrode array, the free space region within the array was refined to determine the electric potential at each grid point. Equipotential contour lines were then calculated at 10 volt intervals and are shown in Figure 3.5. These contour lines help the user to evaluate the force that a charged particle experiences due to the electric field created by the electrodes. Several observations can be made from these contour lines. The curved contour line penetrating the source plate aperture indicates magnitude and direction of the drawout potential created by the bias on the focus electrode. The rounded shape of the contour lines, similar to an concave optical lens, between the source plate

aperture and the quadrupole entrance aperture illustrate the focusing properties induced by this three element unipotential (einzel) lens. In the region where electrons can be produced by the filament the contour lines are fairly parallel to the source grid. Because of this, electrons emitted from the filament will gain a high transverse energy relative to the quadrupole Z-axis, but little energy in the axial direction. As a result electrons emitted from the filament will pass through the source grid on a fairly straight trajectory, with only slight motion toward the source plate. This allows the electrons to make several passes through the source grid before they impact upon the source plate.

Following the modeling of the contour lines in the source, a series of electron trajectories were calculated. These electron trajectories originated along the length of the filament and followed the path that a negatively charge particle would travel starting from those positions. These electrons generally made several passes through the source grid, as predicted from the contour lines in that region. Electrons that originated toward the left end of the filament initially experienced less axial force and made more passes through the source grid. Electrons formed closer to the source plate felt a much stronger attractive potential toward the source plate, and often only made a single pass through the source grid. Using the information from this model it was possible to determine the region within the source grid that an electron/molecule collision, and subsequent ion formation, was likely to occur.

The Anavac-2 source was then remodeled, this time using a 16,000 point circular-symmetric array geometry that better modeled the circular symmetry present within the Anavac-2 source. Symmetric geometries also require half the number of points of asymmetric arrays, therefore much more accurate dimensions can be modeled. Figure 3.6 shows the 16,000 point circular-symmetry SIMION model of the original source. The same electrodes were constructed and biased, but the dimensions of this model reproduce the real source geometry much more closely. The array

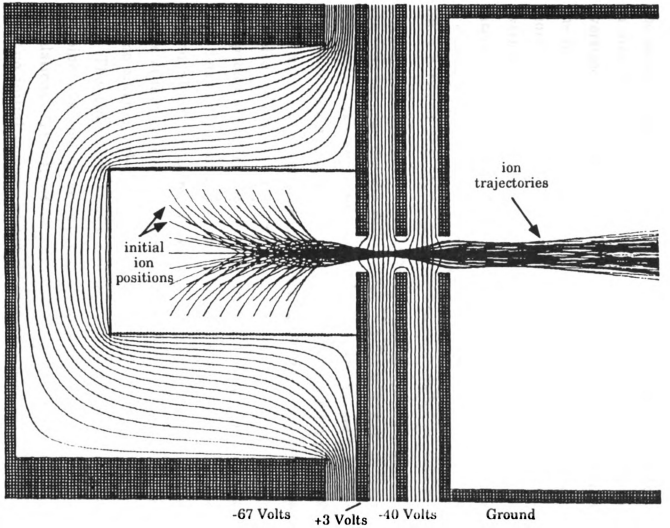

Figure 3.6 A cylindrically symmetric model of the Anavac source showing ion trajectories.

was then refined, and contour lines were calculated at 5 volt intervals. Several observations can be made from the contour lines in this model. There is less penetration of the extraction field from the focus element into the source region than in Figure 3.5. This is primarily due to the change in size of source plate aperture. The model in Figure 3.5 contains an oversized source plate aperture that was used as a compromise because of the limited accuracy of the model array. The model in Figure 3.6 much more accurately reproduces the real source plate aperture, and the extraction field produced by the focus element. The smaller contour interval combined with the larger array size also more accurately models the focal properties created within the source 'einzel' lens. The contour lines between the source and the filament housing also show much stronger curvature than in Figure 3.5. The model in Figure 3.6 is more realistic because the the actual Anavac-2 filament and support rods are relatively small and would have a much smaller effect on the electron trajectories than is indicated in Figure 3.5. Using the model in Figure 3.6, the trajectories of electrons originating at the position of the filament were modeled, and the results compared to those from the model in Figure 3.5. The potential and electric field at each of the electron starting positions was determined, and the trajectory information was tailored to the individual formation conditions of each electron trajectory modeled. The region of highest electron/molecule collision probability determined in this fashion differed little from the results obtained in Figure 3.5.

The trajectory family function in SIMION allows the user to combine a series of separate trajectory files into a single series of calculations. This function was used to model a series of ions formed, with no initial energy, within the source region of highest ionization probability. These trajectories are shown in Figure 3.6. The trajectories of 40 individual ions, reflected into 82 displayed trajectories, are shown. All of the ions that were modeled experienced sufficient drawout potential to leave the source region and pass through the quadrupole entrance

aperture. Ions formed toward the center of the source grid experienced less focusing in the lens and made up the central component of the ion beam entering the quadrupole housing. Ions that were formed in the outer region of the source grid gained more transverse energy and crossed over the center-line several times. These ions formed the outer component of the ion beam entering the quadrupole housing.

Following the evaluation of these models, the design changes involved in enclosing the ion source within a source housing were evaluated using a third SIMION model. The model of the modified Anavac-2 source is shown in Figure 3.7. The use of a source enclosure required the increase in thickness of the source plate and the reduction of the source plate aperture. The source plate aperture was reduced from the original 3 mm to 1.5 mm, and an additional 0.5 mm thickness of electrode was added to the source plate. The model used in Figure 3.6 was modified to reproduce these design changes at the same accuracy level (16,000 point cylindrically-symmetric array) used in that model. Following the construction of the array, it was refined and 5 volt contours lines were calculated, these are shown in Figure 3.7. The penetration of the extraction field into the source region of this model is slightly reduced from the original configuration. The shape and placement of the contour lines in the source lens differs little from Figure 3.6, and the contour lines between the filament housing and the source grid remain the same, as expected. The same family of ion trajectories was modeled for the modified source configuration. As in the previous model, all the ions that were formed in the source region were effectively extracted and injected into the quadrupole. Ions formed in the central region of the source grid followed approximately the same trajectories as in the previous model. Ions that were formed toward the outer region of the source grid experienced a smaller drawout potential than in the Figure 3.6, and gained less transverse energy. As a result these ions crossed the centerline less often, and remained closer to the central axis of the ion source.

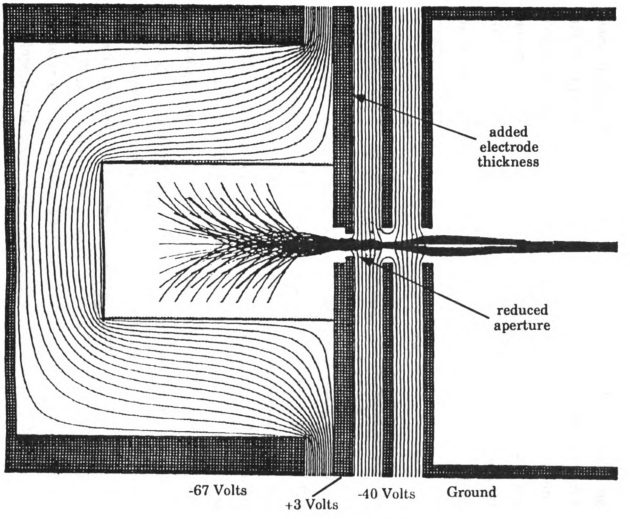

Figure 3.7 A SIMION model of the ion optical changes caused by the source housing

The observed effects of introducing the source housing elements into the SIMION model of the Anavac-2 source indicated that the modified source should produce an ion beam that is slightly more focused than the beam produced by the original source. The SIMION modeling indicates that the modified source could produce approximately the same ion beam profile as the original source by reducing the potential on the focus element to -20 volts. These results indicated that enclosed source would still be fully functional following modification, but that the total output of the modified source could be slightly reduced because of the weaker drawout potential.

B. Design and performance evaluation of modified source

A source enclosure, or source housing, was constructed using the information gathered from the SIMION modeling studies. This housing was designed to contain the source grid, filament housing, and filament assembly within a region of limited conductance to the outside chamber. To minimize the changes to the original design, the end of the housing containing the ion exit aperture had to be in electrical contact with the source grid. To avoid the mounting difficulties associated with floating the entire source housing, a Ceramaseal 807B9999-3 envelope was used to serve as the body of the source housing as shown in Figure 3.8.

This envelope is a metal/ceramic/metal tube with an outside diameter of 1.63", inside diameter of 1.25" and length of 1.4". Using this envelope as the body of the source housing allowed one end of the housing to float at the source plate potential, +3 volts, while the other end could be used to mount the source to a support flange. The source housing also had to allow the introduction of electric potentials and sample gas into the source region. To facilitate this, a gold wire seal 'flange', 1.9" in diameter, was welded to the mounting end of the source housing. A Ceramaseal 807B8177-1 quad mini-feedthrough, rated at 5 amps dc, was welded into

the removable side of the flange to allow the introduction of filament and filament housing potentials. A $^1/_4$" OD inlet line was also welded into the removable end of the flange to allow the introduction of sample gas into the source housing.

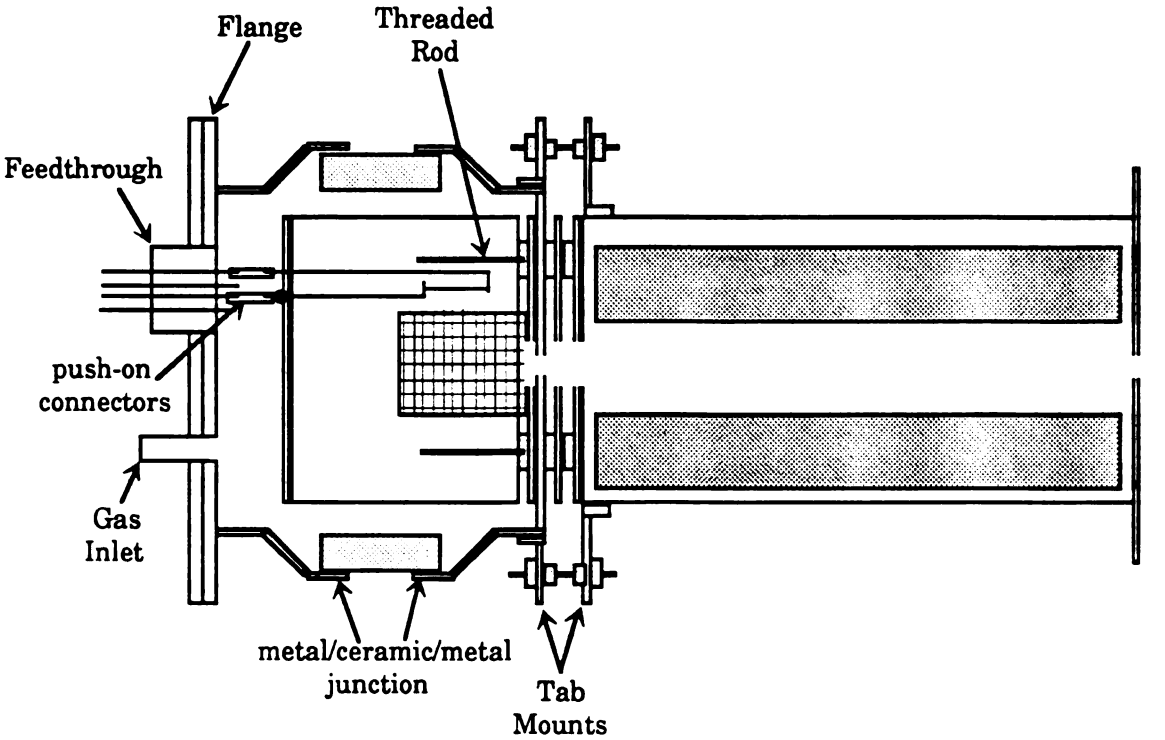

Figure 3.8 A block diagram of the source housing, source, and quadrupole.

A 1.25" plate was welded to the source plate end of the source housing. To allow the source plate to lie flat against the inside of the housing it was necessary to do some specialized welding, which was performed by a master welder at the cyclotron facility. After the endplate was attached to the source housing, a 1.5 mm hole was drilled in the center of the plate to serve as the ion exit aperture. Four 0.5" long threaded rods were installed in the plate so that a small portion of the rod (~ 1 mm) extended outside the source and the remaining rod inserted into the source housing. These rods were positioned in alignment with the mounting rods

of the source components and were used to hold the source grid and filament housing in position inside the source housing. Tab-mounts were welded to the outside of the source plate end of the housing and to the sides of the quadrupole housing. These tab-mounts contained ceramic insulators and were used to physically connect the source housing to the quadrupole while maintaining electrical isolation.

Removing the source housing flange allows the user to access the filament housing and source grid for filament replacement and source cleaning. The source plate and filament housing are held in place by the threaded rod which is isolated from these components by a ceramic sheath. Spacing between these elements is set by the ceramic washers used in the original source. After the source components are cleaned and the filament replaced, the feedthrough connections to the filament can be made using push-on Ceramaseal 841B2044-2 connectors, designed to carry up to 15 amps of current. The flange can then be tightened down with 8 hex screws, and the conductance of the source is then limited by the 1.5 mm ion exit aperture. By comparing all of the aperture areas in the original source to the aperture of the source housing, it was calculated that the source housing effectively reduced conductance from the source region by 97%. This was accomplished without sacrificing the convenience of easy access to the source components for cleaning and filament replacement.

Following the manufacture of the source housing, the performance of the modified source was evaluated. The source housing and all source components were cleaned and the filament was replaced. The source plate, and filament housing were installed in the source housing and the housing flange was sealed. The source housing was coupled to the quadrupole housing and the entire unit was remounted on the original RGA flange so that ion currents could be measured with the original detection system. All the electrical connections were made using the stock wiring, and the entire assembly was installed on a vacuum system and

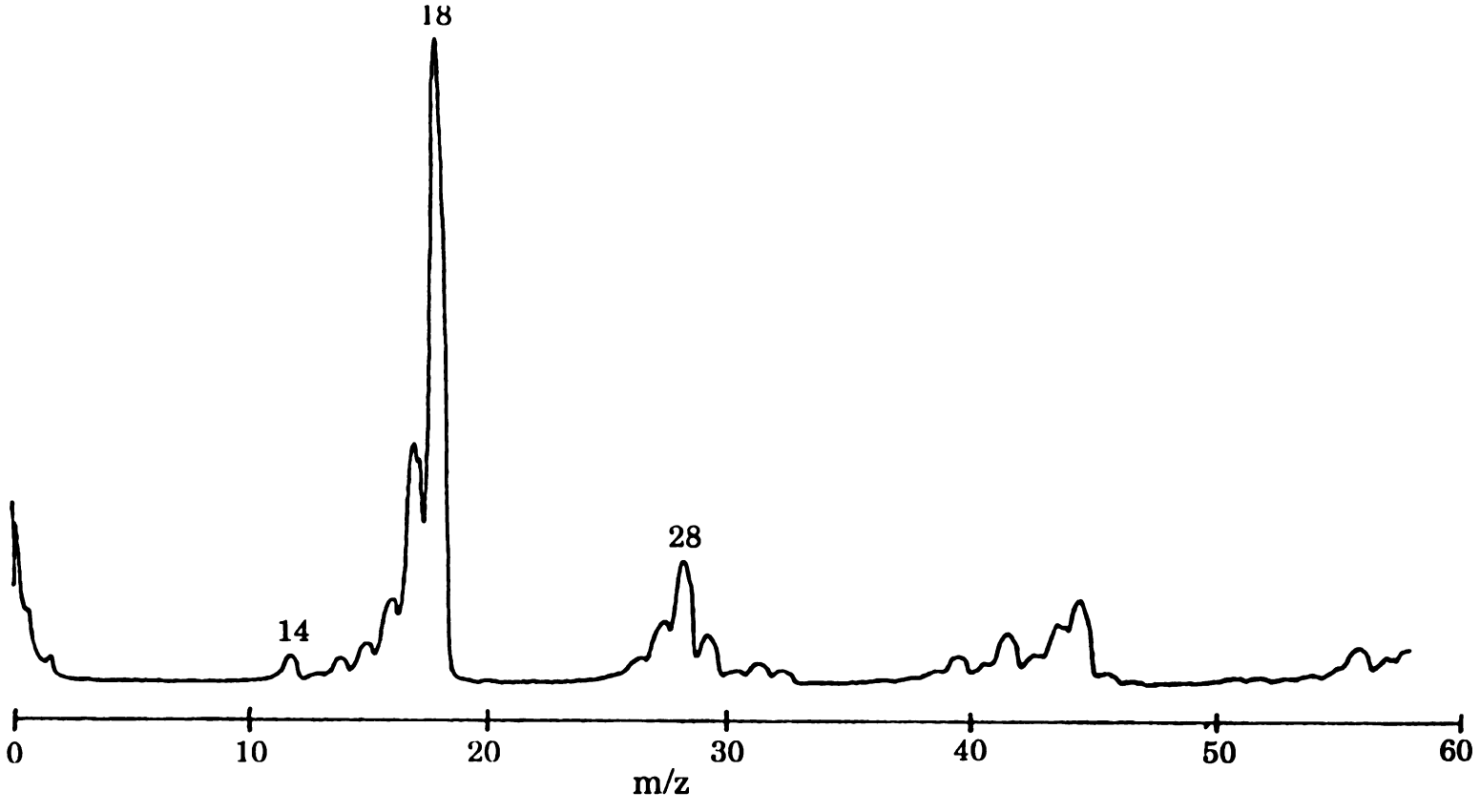

Figure 3.9 The mass spectrum of residual chamber gases taken by the modifed Anavac source.

pumped down. Following evacuation, the remote electronics head and the control unit were installed and an XY recorder was connected to the program voltage leads from the control unit. Figure 3.9 shows the mass spectrum obtained from the background residual gases in the chamber. The spectrum was taken at a chamber pressure of 1.5×10^{-6} torr measured by an ion gauge, and the total pressure reading given by the modified Anavac-2 was 2.0×10^{-7} torr. This represents a decrease in total pressure output of 79% due primarily to the reduction of the source aperture. The principle components of the residual gases in the chamber are H_20, N_2, O_2, and various hydrocarbon peaks produced from the rough and diffusion pump oil. The spectrum was taken at a sensitivity setting of $\times 10^{-8}$ torr, slow scan speed, and with a Y scale of 50 mV (variable). The peak series of m/z = 12, 14, 15, 16 , 17, and 18 clearly shows that the resolution of the quadrupole has degraded only slightly as a result of the source modifications. The quadrupole was scanned from m/z = 2-60, and peaks were observed through the entire range which indicated that the original mass range of the quadrupole had also been maintained.

III. Modification of the quadrupole wiring

The final installation of the modified Anavac-2 RGA required the modification of the analyzer head wiring. The design goal for the finished mass-selected ion source required that the entire assembly be mounted on a 6" conflat flange to allow the source to be on the matrix isolation chamber and easily removed for servicing. Another design goal was that the ion source should be mounted in a fashion that allows it to be repositioned under vacuum. To achieve this, the wiring that connects the source and quadrupole components had to be flexible, and long enough to allow a wide range of movement.

Modifying most of the analyzer head unit wiring was not critical. The dc potentials required to bias the electrodes, such as the source grid,

focus lens, and quadrupole housing, required only low current/low voltage dc signals. These components were wired using flexible, Teflon-coated cable. The wiring to the filament needed to carry high currents at low voltages. For these components 18 gauge copper wire was connected to the original filament wiring, covered with ceramic thermocouple insulators, and connected to the leads on the source housing flange with Ceramaseal 880A7332-2 connectors. The most critical stage of rewiring the analyzer head was the modification of the quadrupole wiring.

As discussed in Chapter 2.II.D, the operation of the quadrupole circuit depends upon proper matching of the rf power supply frequency with the resonant frequency of the LC tank created between the secondaries of the rf transformer and the two quadrupole rod pairs. Changing the length of the wires connecting the quadrupole rod pairs to the feedthrough flange can change the capacitance of the circuit, causing the resonant frequency of the circuit to change. If this frequency changes too much, the power transmitted from the rf power supply cannot be properly absorbed, and will be reflected back into the power supply. In the case of the Anavac-2, with its automatic overload protection, this reflected power causes the rf generation circuitry in the remote head to shut down. The resonant frequency of the quadrupole circuit can be adjusted within a limited range by adjusting a variable capacitor (VR2 in Appendix I). A study was performed to determine the practical range of wire length that could be used in wiring the quadrupole

This study was done using the original Anavac-2 mount and detector to allow direct comparison with previous studies. The source was cleaned and mounted in the source housing. This was installed on the quadrupole housing and the entire unit was attached to the mounting flange. The original wiring was connected to all components except the filament and quadrupole. An additional length of wire, described above, was used to connect the filament. To study the effect of wire length upon the behavior of the quadrupole, several lengths of wire were added to the

original quadrupole wiring. The additional wire lengths consisted of 22 gauge chromel A wire, twisted into the stock wire and covered by ceramic thermocouple insulators. The opposite end of each added wire was looped along the side of the source housing and connected to a quadrupole rod. The unit was then installed in a vacuum chamber, with the wire loops > 6 inches from any surrounding metal to reduce the effect of the chamber on the performance of the system. The behavior of the quadrupole with the wire lengths; original, 14.5 cm, 25.0 cm, and 30.0 cm was observed as the quadrupole was scanned from m/z = 2-60. With the original wire the spectrum obtained was similar to Figure 3.9. When a 14.5 cm length of wire was added, the quadrupole was still able to scan through its full range without any difficulty. The addition of 25.0 cm of wire did change the behavior of the quadrupole, the output spectrum appeared normal until m/z = 32 was reached. At this point the output of the amplifier went to baseline and repeat attempts at scanning any portion of the mass spectrum failed. When the control unit was turned off briefly and then turned back on, the normal mass scanning of values less than m/z = 32 returned. This apparent 'shutdown' behavior was also observed by monitoring the dc output testpoints in the remote head. During a normal scan the dc levels at these points increased linearly with increasing m/z. When the 'shutdown' behavior occurred the dc testpoint voltages suddenly went to ~5 volts and remained constant. This proved generally useful as an indicator of shutdown behavior in the rf power supply. Finally, a 30.0 cm length of wire was added to the stock wire. With this wire length the 'shutdown' behavior was observed at m/z = 27. An example of a spectrum displaying rf power supply shutdown is shown in Figure 3.10. This spectrum shows a mass scan from m/z = 2-60 of an air leak. A 30.0 cm length of wire has been added to the stock quadrupole wiring. The total pressure reading of $2x10^{-6}$ torr was obtained from an ion gauge installed on the system. The sensitivity scale of the control unit was set to $x10^{-8}$ torr and the Y sensitivity of the XY recorder was 50 mV full scale. Background

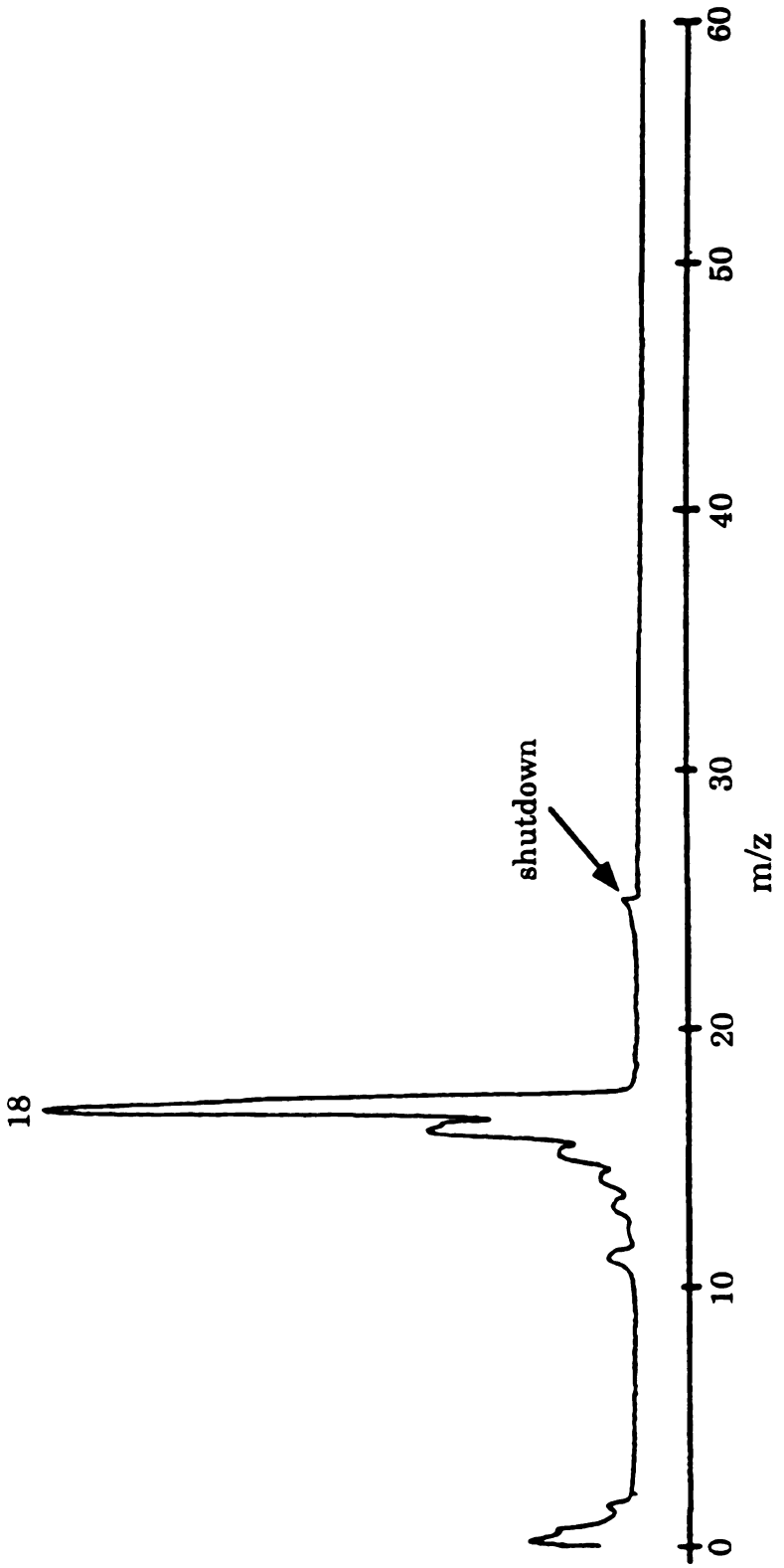

Figure 3.10 A mass spectrum from the Anavac source showing rf-feedback induced shutdown

peaks are observed in the mass spectrum for water, air, and pump oil components from m/z = 12 to 18. Shutdown occurs at ~m/z = 27 and can be seen as a sharp decrease in output on the leading edge of the m/z = 28 peak (N_2^+). After this point the control unit had to be turned off to get mass-selected output at any m/z value.

By tuning VR2 it was possible to bring the electronics back into resonance. In order to obtain optimum rf power absorption, VR2 was varied while observing the output of the dc testpoints in the remote head. By monitoring these testpoints it was possible to determine the range of VR2 settings through which no shutdown occurred. VR2 was then left at the central position within this range which corresponded to optimum rf power absorption. For the two longer wire lengths, 25 and 30 cm, varying VR2 could keep the unit from shutting down, but because VR2 was at the edge of its operating range no true central position was found. From these studies we concluded that use of an additional quadrupole wire length over 15 cm should be avoided. This length limitation was used as a guideline in designing the mount and connections for the entire source assembly.

IV. Design and construction of complete source mount/flange

The matrix isolation instrument was designed to accommodate two ion sources. Two 6" conflat flanges were installed facing the cryostat window to allow the easy removal of each source for servicing. Following the construction of the source housing, a 6" mounting flange was designed and constructed for the modified Anavac-2 RGA. This mounting flange had to provide: mechanical support for the ion source, electrical feedthroughs to provide operating potentials to the source, and a gas inlet to allow the introduction of sample gas into the source. It was also important that the operator have the ability to change the line-of-sight orientation of the source while the chamber was under vacuum. A specialized pivot-mount was devised to provide this function.

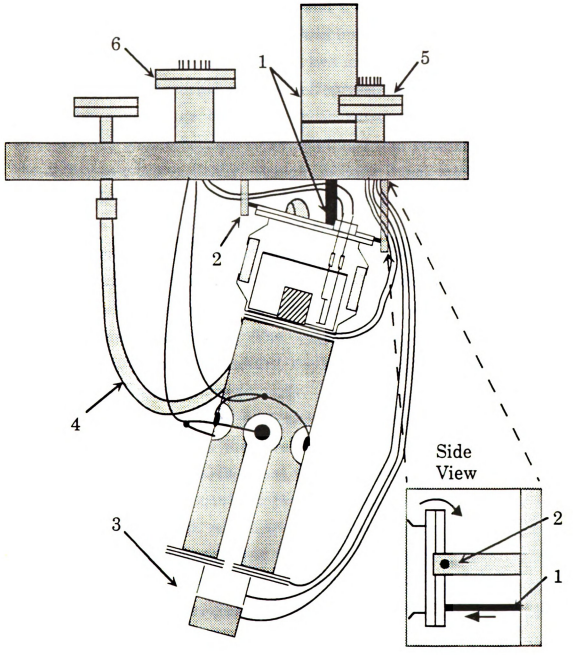

Figure 3.11 A top view drawing of the complete Anavac-2 ion source flange.

The pivot mount used to physically support the source assembly consisted of a two point bracket (2) and a linear motion feedthrough (1) shown in Figure 3.11. A 1.9" bracket was installed toward the center of the mounting flange. This bracket had two arms, each of which contained setscrews which inserted inward. Depressions were drilled into the source housing flange to accept these setscrews. By inserting the setscrews the source housing could be pinned into position, but still have the ability to move vertically. A high- vacuum linear motion feedthrough was installed in the mounting flange in a position that allowed the feedthrough rod to push against the bottom edge of the source housing flange. By inserting the linear motion feedthrough it was possible to move the source upward, this motion is shown in the side view insert of Figure 3.11. The source could also be directed downward by withdrawing the linear motion feedthrough. The weight of the source was generally enough to cause this downward motion, but a spring could also be installed to ensure proper positioning.

The source operating potentials were provided by two electrical feedthroughs installed on the mounting flange. A Ceramaseal submini octal feedthrough (808B9340-1) was installed on a miniconflat feedthrough mounted above the pivot mount, this is shown as component 5 in Figure 3.11. This feedthrough was used to provide electric potentials for the source, focus, quad housing, and deflection optics elements (3). Flexible, Teflon-coated cable, designed to carry low currents, was used to connect the feedthrough pins to each of the components. It was also necessary to provide high voltage connections to the quadrupole and high current connections to the filament. As discussed previously, is was important to minimize the changes made to the original quadrupole circuit, to accomplish this the original 2 $^{3}/_{4}$" Anavac-2 feedthrough flange was used to provide these potentials. The high current/voltage feedthroughs on this flange were also used to provide high current signals to the filament. 18 gauge copper wire was added to the original filament wire, covered with

ceramic thermocouple insulators, and connected to the housing flange feedthrough using Ceramaseal 880A7332-1 connectors. These connections could readily handle the high current loads, up to 5 amps., necessary for proper operation of the filament. To provide connections for the quadrupole, 10 cm of 22 gauge chromel A was added to the original quadrupole wire. The ends of the wire were twisted together so that no connector was added to the circuit, and the length of the wire was covered by ceramic thermocouple insulators. This wire fed to a loop of the same wire that connected the opposing rod pairs as shown in Figure 3.11. For this, and all the electrical connections, sufficient extra wire length was used to allow the source to travel through its full range of movement.

A miniconflat feedthrough was also used to provide sample gas to the source housing. A 3" section 1/4" OD SS tubing was installed through the mounting flange and welded in place. A miniconflat flange was attached to the atmosphere side of this tubing, and a swagelock SS-400-1-1 fitting was welded to the vacuum side of the mounting flange. The inlet tube on the source housing was attached to a 12" x 1/4" dia. flexible SS bellows, shown as component 4 in Figure 3.11. This bellows was looped around and connected to the swagelock fitting on the mounting flange. This arrangement allowed the direct introduction of sample gas into the source housing, and was still flexible enough to allow the source assembly to pivot.

V. Post-quadrupole focusing and deflection optics

A. Beam visualization and divergence measurements

Following the successful construction of an enclosed housing for the Anavac-2 ion source, a series of ion optical elements were fabricated to allow the manipulation of the ion beam produced by the quadrupole onto the matrix isolation window. SIMION modeling was used to investigate

and optimize these designs, but to properly use SIMION, the ion beam produced by the quadrupole first had to be characterized. SIMION PC version 3.0 was only designed to allow the modeling of static electric and magnetic fields. With the introduction of SIMION PC/PS2 version 4.0, dynamically changing electric fields could be modeled through the use of specialized 'user program' routines. Theoretically this version could be used to model the dynamic electric fields produced within the Anavac-2 quadrupole, but this would require the determination of many initial parameters such as the rf phase angle of ion injection, transverse energy of the ion, initial angle of ion injection, etc., that are extremely difficult to obtain. Instead of using modeling, an ion beam visualization experiment was performed to characterize the divergence and shape of the ion beam produced by the quadrupole. Using a CEMA detector it was possible to directly observe the size and shape of the ion beam. By placing this detector at varying distances from the quadrupole exit aperture, the change in beam size with distance, or beam divergence, was determined.

A Galileo 3025 chevron configuration CEMA detector was purchased from Galileo Electro-Optics Corporation. The design of this detector allowed the output of the CEMA to excite a P11 phosphor deposited upon a fiberoptic, thus creating an image of the ion beam on the fiber optic screen. The active area of the detector was 25 mm in diameter and the spatial resolution was 20 um. Gain for this detector was quoted at $1x10^7$ electrons per incident particle with an operating potential of 1 kV across each of the microchannel plates. In order to use this detector to visualize the beam produced by the quadrupole, a shielded mount and movable rail system were devised.

The front of the CEMA detector is normally operated at a potential of ~-1400 volts. If the detector was placed directly in line with the quadrupole exit aperture, the trajectories of ions exiting the quadrupole would be strongly influenced by this potential. To accurately determine the beam profile that the quadrupole will produce in the matrix chamber, the ion

beam must be allowed to traverse a field free region before detection. To accomplish this, a shield plate was designed and positioned before the front plate of the CEMA detector. A circular stainless steel ringplate with a 52 mm OD and 25 mm ID was used as the shield plate. A Buckby-Mears ~80% transparent SS grid was spot welded over the center of the plate and holes were drilled in the plate to accept the threaded mounting rods of the CEMA detector. This design allowed ions exiting the quadrupole to pass through a field free region between the quadrupole housing and the grid plate. Ions that passed through the grid are accelerated linearly toward the detector, and a spot was produced on the phosphor screen that corresponded to the position where the ions had penetrated the grid. The grid plate was attached to the CEMA detector at a distance of 4 mm from the front plate of the CEMA. The use of the CEMA threaded rods to attach the shield plate required that a short length of these rods, biased at -1400 V, appear in front of the shield plate. To investigate how these rods would affect ion trajectories, a SIMION model of the visualization experiment was performed. This is shown in Figure 3.12.

This model shows the quadrupole housing exit plate, shield plate with grid, and the front of the CEMA detector. In this model the shield plate was positioned at a distance of 10 mm from the quadrupole housing. The threaded support rods are shown extending 5.2 mm in front of the shield plate. After the electrode array was constructed, the CEMA electrode was biased at -1400 V and the array was refined. Contour lines were calculated at 100 V intervals, these are shown in Figure 3.12. The contour lines between the shield plate and the front of the CEMA were extremely linear, which indicated that an ion that penetrated the grid would follow a linear trajectory onto the detector. The model also showed the penetration of the electric field produced by the support rods into the "field free" region. To determine whether this field penetration would affect the trajectories of ions exiting the quadrupole, a parallel beam of 6 eV ions was modeled exiting the quadrupole. These ions, shown in Figure

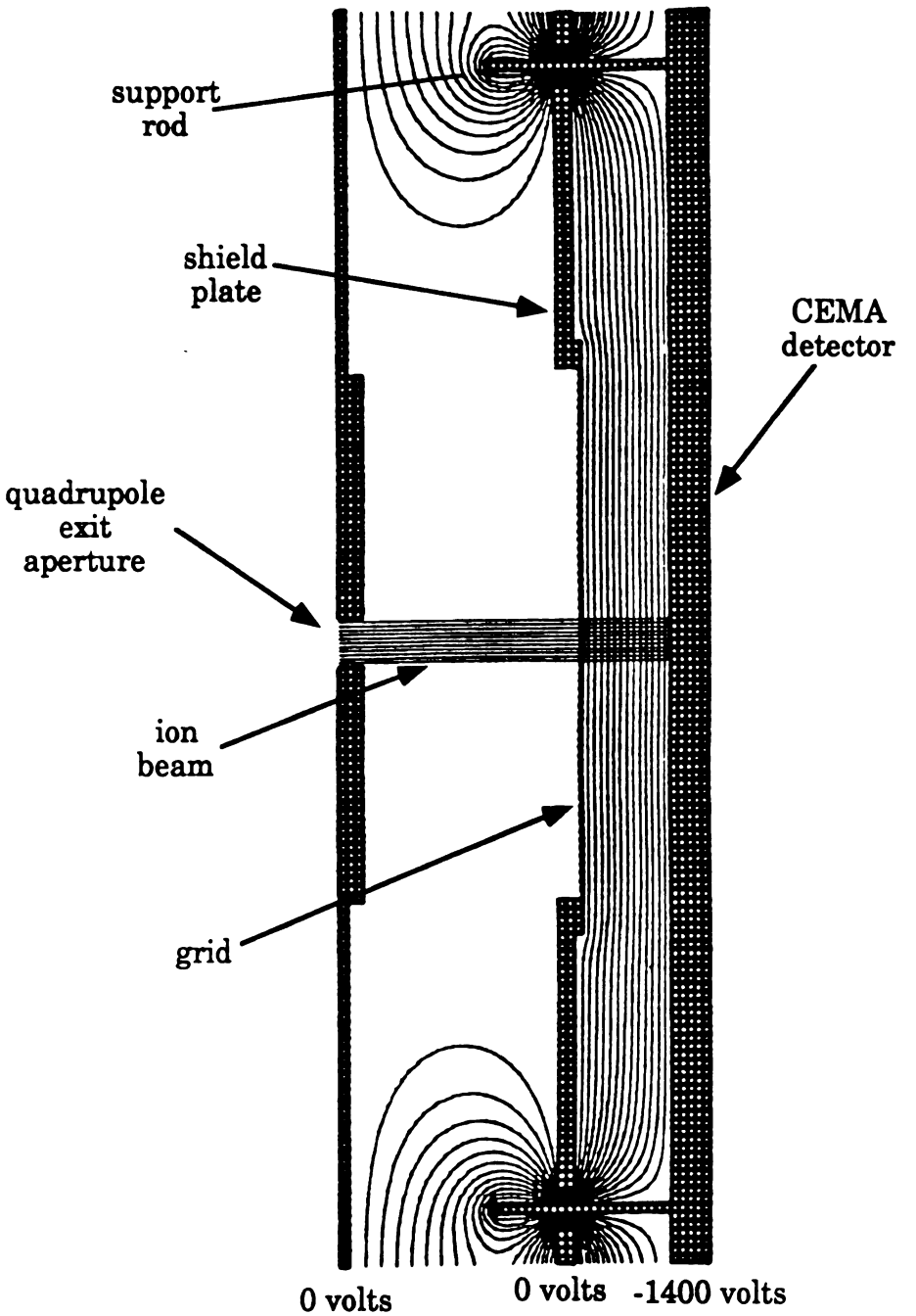

Figure 3.12 A SIMION model of the shielded CEMA detector mount.

3.12, continued on their original parallel trajectories through the region between the quadrupole housing and the shield plate. This indicated that the penetration of the electric field from the support rods would not substantially affect the shape of the ion beam exiting the quadrupole. Several similar models were evaluated, varying the distance between the quadrupole housing and the shield plate. At distances greater than 15 mm the ion beam began to diverge due to the penetration of the electric field created by the support rods. To reduce this effect, the beam divergence measurements made in this study were done at quadrupole housing to shield plate distances ≤ 10 mm and a grounded copper cage was added surrounding the support rods to provide additional shielding.

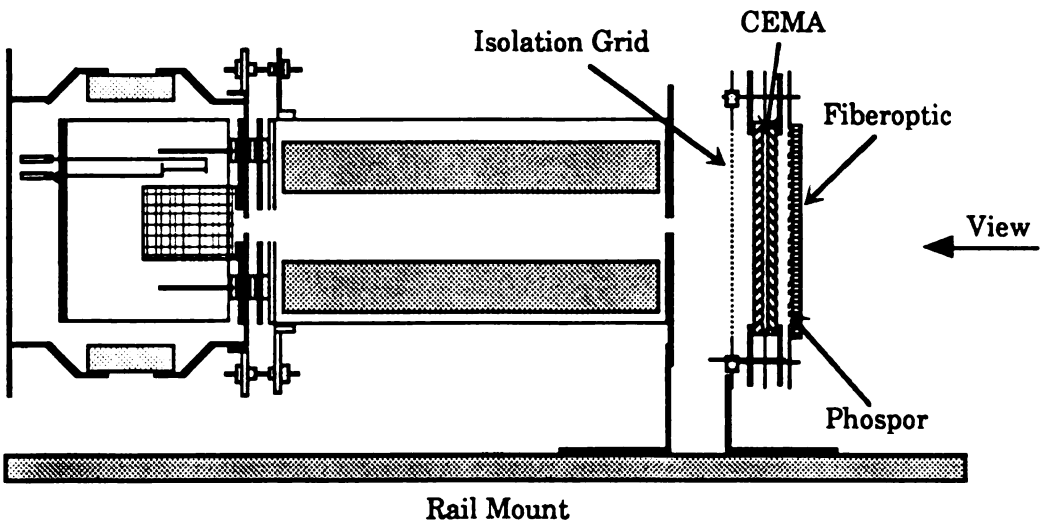

Figure 3.13 The rail mount system used for beam visualization

The shielded CEMA detector was attached to a bakeable ring and placed on a moveable rail mount shown in Figure 3.13. The source housing and quadrupole were attached to the rail mount by a bracket that could slide along the length of the rail. The endcap of the source housing flange was removed to allow the sampling of the residual chamber gases by the ion source. The entire unit was then placed in a vacuum chamber fitted with a plexiglas flange facing the fiberoptic of the detector. The electrical feedthroughs were connected from side ports on the chamber to

the source and quadrupole. External power supplies were used to provide the operating potentials to all components except for the quadrupole. A 10 cm length of 22 gauge Chromel A was used to connect the original Anavac-2 feedthrough to the quadrupole rods. The chamber was then sealed, pumped down, and the variable capacitor in the remote electronics head was adjusted to allow the quadrupole to scan through its entire mass range.

The standard operating potentials were supplied to the source and quadrupole, and the filament was heated with a 2.0 A current. Two Hewlett-Packard 6516-A high voltage power supplies were used to bias both the front and center plates. Fluke DMMs were placed between these power supplies and the plates to measure the bias current across each plate. The back of the CEMA was connected to ground, and the fiberoptic screen was connected to a Power Designs Inc. 1543A high voltage power supply. Normal operating potentials for the detector were: front plate = -1400 V, center tab = -800 V, back plate = 0.0 V., phosphor screen = +1600 V. The detector was slowly brought to these potentials, and a bias current < 0.3 mA was maintained, indicating proper operation of the detector. A combined air and argon leak was added to the chamber to an ion gauge reading of ~$3x10^{-6}$ torr. The quadrupole was operated in both rf-only and mass selected modes. The beam profiles for the peaks at m/z = 18, 28, and 40 were observed at quadrupole housing to shield grid distances ranging from 1.5 to 10 mm. The images produced at the phosphor screen were photographed on slide film for later evaluation. Figure 3.14 shows the ion beam profile produced by the quadrupole operating in mass-selected mode at m/z = 28. The distance between the shield plate and the quadrupole housing in this visualization was 5.1 mm. The quadrupole was oriented slightly off-axis from vertical, with the y rod pair (-dc) toward the vertical direction and the x rod pair (+dc) toward the horizontal direction. The cross shaped pattern observed was aligned with the quadrupole rod-pairs, with a shorter arm toward the +dc poles and an longer arm toward the -dc

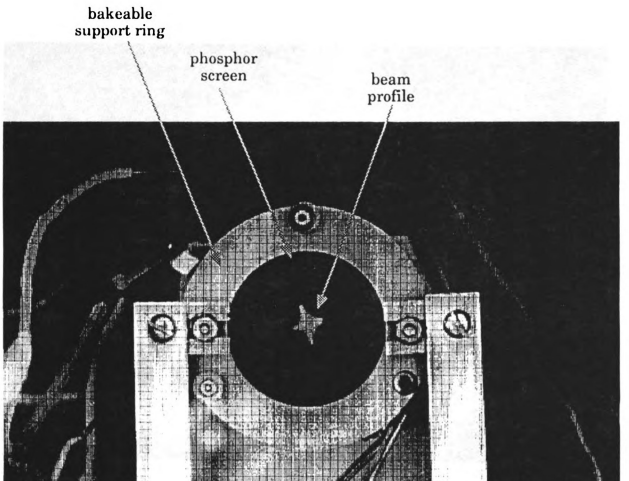

Figure 3.14 The beam profile produced at the CEMA detector by the Anavac source in mass scan mode.

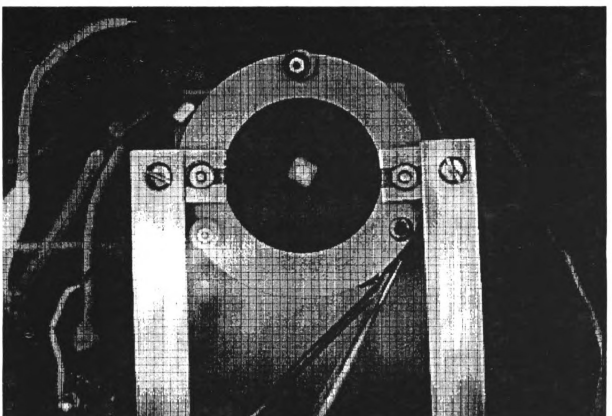

Figure 3.15 The ion beam profile produced at the CEMA detector by the Anavac source operating in total, or rf-only mode.

poles as discussed in Chapter 2.II.A. Figure 3.15 shows the beam profile obtained with the same experimental setup, but with the quadrupole operating in rf-only mode. The ion beam profile produced in rf-only mode should be fairly symmetric because an approximately equal force is exerted upon the ions by each rod pair. The profile observed in Figure 3.15 showed the expected uniform, semi-circular beam shape.

The ion beam produced by the quadrupole was characterized by comparing the dimensions of the ion beam profiles at various distances. The slides taken of the phosphor screen were projected, scaled to equal magnification using the support ring as a reference, and carefully measured. This procedure was repeated for each of the distances, and quadrupole modes, and m/z values selected. The change in these profile dimensions with increasing distance between the quadrupole housing and the shield plate was used to determine the size of the beam at a given distance, and the maximum beam angular divergence. When the quadrupole was operated in mass-selected mode two divergence values were obtained, one along the +dc rod pair axis, and another along the -dc rod pair axis. The results of these visualization studies are shown in Table 3.3.

Table 3.3. Maximum beam divergence values for the ion beam produced by the Anavac-2 quadrupole.

rf-only angular divergence = 53.8°

m/z = 18	+dc rod pair axis = 19.2°	-dc rod pair axis = 19.6°
m/z = 28	+dc rod pair axis = 28.9°	-dc rod pair axis = 56.5°
m/z = 40	+dc rod pair axis = 33.8°	-dc rod pair axis = 68.9°

B. SIMION modeling and construction of post-quadrupole optical systems

Following the characterization of the ion beam produced by the quadrupole, a series of ion optical elements were designed to allow for the focusing and deflection of the ion beam onto the cryostat window. The source housing and quadrupole were installed on the 6" mounting flange, and the unit was attached to the conflat port of the matrix chamber. The distance that the ion beam must travel from the quadrupole exit aperture to the the cryostat window was measured to be ~80 mm. The ion optical system needed to provide the operator with ability to focus the ion beam to an appropriate size at the cryostat window, and to allow the deflection of the ion beam onto the window if the source was oriented off axis. Two possible focal sizes were desired depending upon the matrix isolation experiment. For LIF experiments the laser spot size is fairly small, approximately a 4 mm diameter region is excited, and the majority of the ion beam should be focused within this region. The infrared beam produced by the BOMEM FTIR can be adjusted to fill the entire area of the 1" diameter cryostat window, in addition the central ~3 mm of the IR beam is not active. For these experiments the beam should be focused within the full area of the window for optimum overlap with the infrared beam.

Several SIMION models were investigated to determine the best ion optical system for the manipulation of the ion beams produced by the Anavac-2 ion source. Two principle components were evaluated, an einzel lens configuration to allow the focusing of the ion beam, and a series of deflection plates to control the vertical and horizontal positioning of the ion beam. Two types of einzel lenses were modeled, a two-element system and a three-element system. The two-element system used the quadrupole housing as the first element of the einzel lens with a varying potential applied to the first added element. In this system both the quadrupole

housing and second added elements were held at ground. The three-element systems added a complete einzel lens after the quadrupole, with this lens design the first and third elements were held at ground and the central element was varied. Several different versions of these two types of einzel lenses were evaluated, five of these models will be discussed here.

The einzel lens SIMION models were constructed using a 5,400 point circular symmetry array that corresponded to a modeling scale of 0.5 mm/grid unit. Different electrode configurations were constructed and refined, and the trajectories of 3, 6, 9, and 12 eV ion beams exiting the quadrupole were calculated. Parallel 2.5 mm diameter ion beams were modeled to compare the ideal focal properties of the systems, and a beam of ions with 0 to 40° angular divergence was modeled to evaluate the ability of the system to control the beam produced by the quadrupole. Three center einzel element voltages were determined for each model to allow evaluation of the different systems: 1. the minimum voltage the required to focus a parallel 2.5 mm ion beam to a point at the cryostat window (see Table 3.4), 2. the minimum voltage required to focus all the ions in a 0-40° ion beam onto the full area of the cryostat window, and 3. the minimum voltage required to focus all the ions in a 0-40° ion beam to ~3 mm on the cryostat window. The performance of each system was also evaluated in terms of focal strength and ion-optical aberrations. These aberrations are generally indicated by a poor focal spot, or ions that experience unusual trajectories and x-axis crossovers. A model with low aberration is generally able to focus a wider range of angular divergence simultaneously, this is important in the manipulation of a complex ion beam such as that produced by a quadrupole. These aberrations generally result from an ion following a trajectory that travels close to an electrode, resulting in a spherical aberration effect as discussed in Chapter 2.III.A

Table 3.4 The dimensions and performance of several SIMION lens models.

model #	# elements	aperture size	electrode spacing	min. focusing V
1	2	6 mm	2 mm	-2.9 V
2	3	6 mm	2 mm	-3.3 V
3	2	8 mm	2 mm	-6.9 V
4	3	8 mm	2 mm	-6.5 V
5	3	8 mm	3 mm	-5.9 V

The dimensions and performance of the five models presented in this discussion are shown in Table 3.4. Each model was described in terms of the number of elements that were added after the quadrupole housing, the size of the aperture in each element, the spacing between the individual elements, and the minimum voltage that must be applied to the central element to focus a 2.5 mm parallel 3 eV ion beam to a point on the window. The ability of each of these models to focus a 0-40° angular divergence ion beam is shown in Figure 3.16. The minimum voltage required to focus all ions in a 0-40° ion beam onto the window is plotted against beam energy in Figure 3.16a and the minimum voltage required to focus the same beam to 3 mm is shown in Figure 3.16b. A brief discussion of the characteristics of each of the models follows.

The first model, model 1, was a two-element system which used a 6 mm aperture size that matched the quadrupole housing aperture. The spacing between each element was 2 mm. With a 0-40° ion beam this model introduced some aberration to the outermost (40°) ion as it traveled near to the second element. The change in minimum focal voltage with beam energy for this model was linear, and this effect was found to be common to all lens models. This relationship proved useful in the prediction of new focus voltages when the energy of the ion beam was varied. This model required relatively low potentials to achieve focusing, had a reasonably low degree of aberration, and because the lens system was relatively short it could accept a wide range of angular divergence.

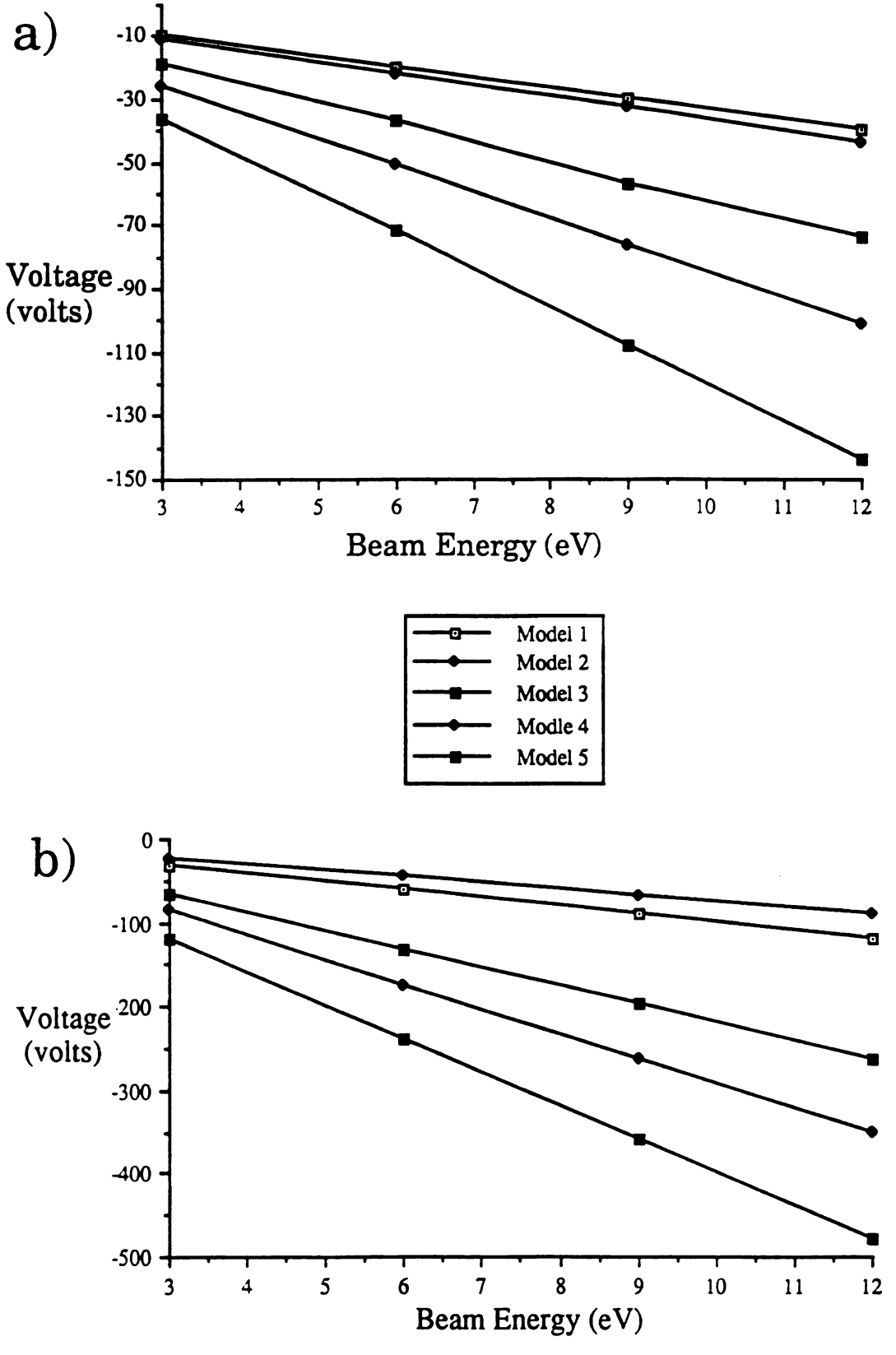

Figure 3.16 SIMION modeling results for the focusing of a 3 eV, 0-40° divergence ion beam; a) onto the cryostat window, and b) to a 3 mm region on the cryostat.

Model 1 was found to be the best system for focusing ion beams with a wide range of energies and relatively high angular divergence to within the full diameter of the matrix window, making it well suited for FTIR studies.

Model 2 was a three-element system that used a 6 mm aperture size with 2 mm inter-electrode spacing. This system produced the highest overall focusing of any of the lens systems evaluated because of the relatively small aperture size and lens length. Model 2 also introduced the highest degree of spherical aberration in the ions beam because the ions traveled very near the electrode elements. Because this model required relatively low potentials and accepted a limited range of angular divergence, it could prove especially useful for the manipulation of high energy beams with low angular divergence. Figure 3.17 shows a comparison of the degree of aberration between model 1 (a) and model 2 (b). The figure shows the trajectories of a 3 eV beam of ions with angular divergence 0-40° for each model. The minimum potential required to focus the entire ion beam onto the window was -10.5 V for model 1 and -10.9 V for model 2. The ion beam produced by model 1 had a lower degree of ion crossover which indicated a lower degree of aberration. Model 2 required a slightly higher voltage in order for the 40° ion to survive, but the overall ion beam was more strongly focused with model 2 than with model 1.

Model 3 was a two-element system with 8 mm apertures and 2 mm inter-electrode spacing. Because of the wider apertures, this model had the weakest focusing of all the systems modeled and therefore required the highest potentials to achieve focusing. This can be seen in Figure 3.16, this lens required the highest focusing potentials for each ion beam modeled. Model 3 introduced a relatively low degree of aberration, but because of its weak overall focusing was found to be the least useful of the systems investigated. It could, however, prove useful for low energy beams with an extremely high degree of angular divergence.

Model 4 was a three-element system with 8 mm apertures and 2 mm inter-electrode spacing. This system had the lowest degree of aberration of

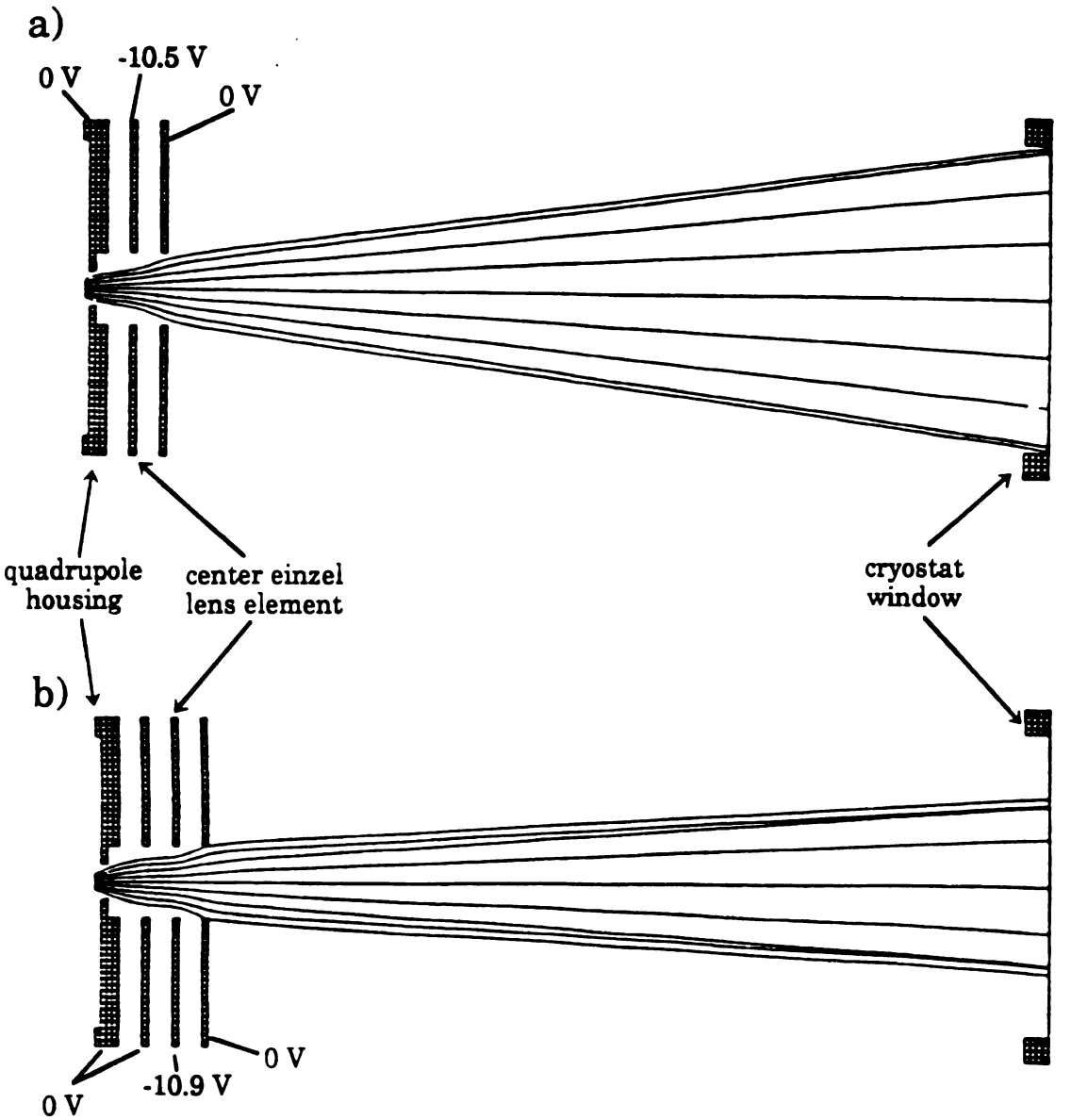

Figure 3.17 SIMION models comparing the degree of aberration produced in focusing a 0-40° divergent beam using a) model 1 and b) model 2.

all the lenses modeled because of the wide aperture size, but also required high potentials to achieve focusing. Model 4 was found to be the best lens system for the focusing of low energy beams with relatively high angular divergence, especially when a smaller spot size is required. Its use with higher energy beams was limited by the relatively high potentials required to achieve focusing. Figure 3.18 shows a comparison between model 2 (a) and model 4 (b) modeling a 3 eV ion beam with 0-40° angular divergence that was focused to ~3 mm in each model. Because of its stronger focusing, model 2 required only -23 V to achieve a ~3 mm beam size, while model 4 required -85 V to focus the beam to 3 mm. Beam focusing with model 2 was accompanied by a high degree of spherical aberration, shown in Figure 3.18a as ion crossover points. Model 4 had a much smaller degree of spherical aberration due to its larger aperture size, and the focused ion beam was much more uniform, as shown in Figure 3.18b.

As mentioned in Chapter 2.III.A, einzel lenses can be operated in decelerate-accelerate as well as accelerate-decelerate mode. In general the operation of an einzel lens in decelerate-accelerate mode requires much lower potentials than operation in accelerate-decelerate mode. To determine if this mode of operation could be used to extend the ion beam energy range of an einzel lens, the performance of model 4 operating in both these modes was investigated. The ion beam profiles produced by model 4 functioning in accelerate-decelerate and decelerate-accelerate modes are shown in Figure 3.19a and Figure 3.19b respectively. A 12 eV beam with 0-40° angular divergence was focused onto the full width of the cryostat window in both models. A potential of -105 V was required to achieve this focusing when the lens was operated in accelerate-decelerate mode, but this mode produced highly uniform focusing. The optimum focusing for the same lens operated in decelerate-accelerate mode was achieved at only +18.5 V, but the ion beam experienced strong aberrations, and loss of ion flux. In general operation in accelerate-decelerate mode was used whenever possible.

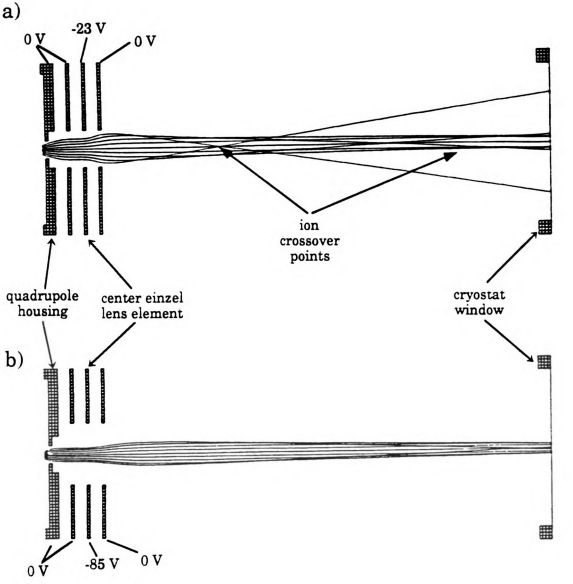

Figure 3.18 SIMION models comparing the degree of aberration produced in focusing a 0-40° divergent beam to 3 mm using a) model 2 and b) model 4.

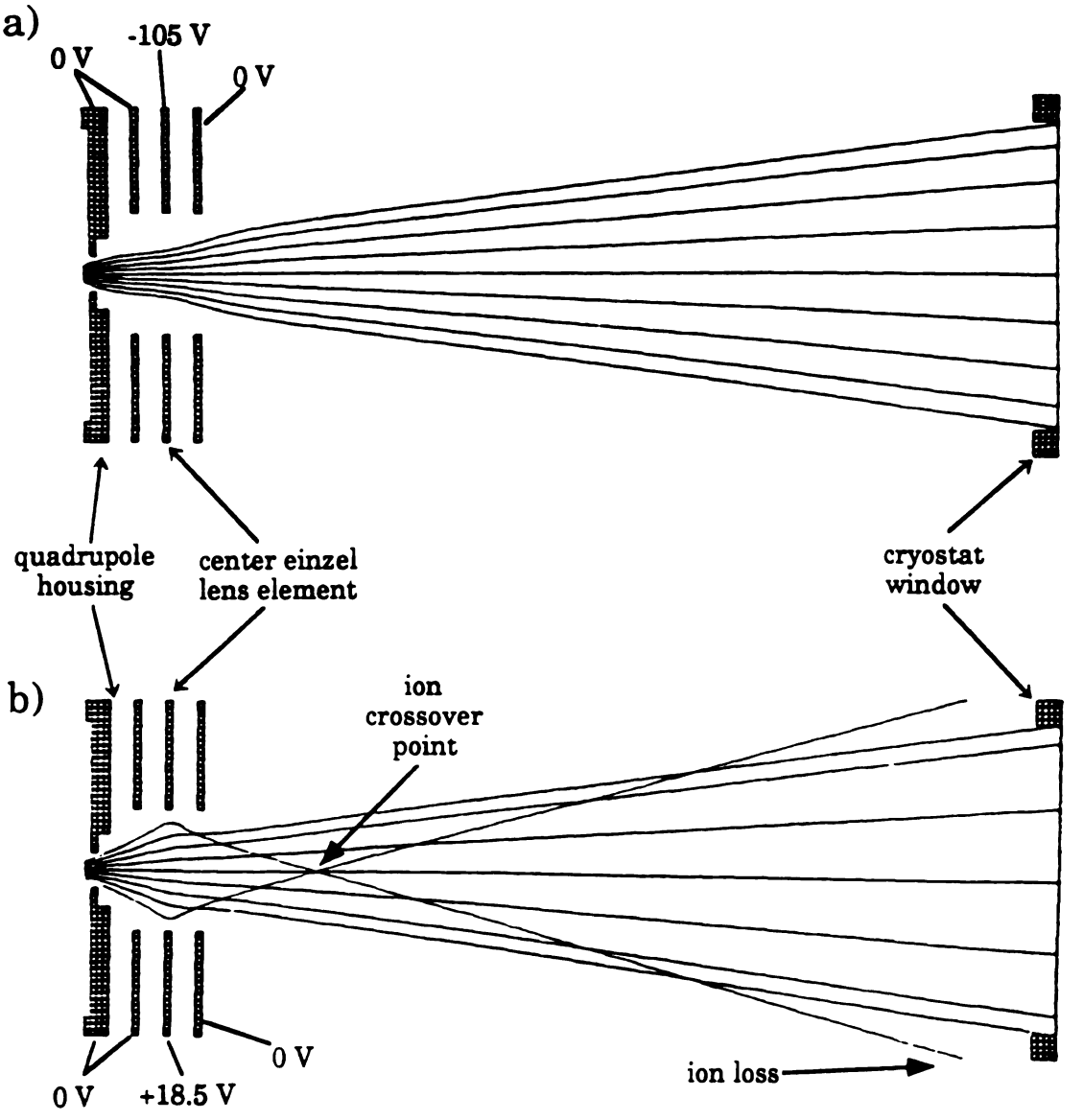

Figure 3.19 SIMION models comparing the degree of aberration produced in focusing a 0-40° divergent beam using an einzel lens in a) accelerate-decelerate mode and b) decelerate-accelerate mode.

The final model, model 5, was a three-elements system with 8 mm apertures and 3 mm inter-electrode spacing. This system had the same overall performance as model 4, with a slightly higher degree of spherical aberration, but stronger focusing. This lens system could prove to be a good general lens, with some limitations when working with highly divergent beams because of the length of the lens system. It should be especially useful for focusing ion beams with slightly higher energy than can be practically controlled with a system based upon model 4.

Several general observations were made from the results of these and other modeling studies: Smaller aperture sizes generally produce stronger focusing, but also introduced a higher degree of spherical aberration. Use of a two-element lens design, with the quadrupole housing as the first lens element, required slightly higher potentials, but allows ions to remain further away from the electrodes. This could prove especially useful when focusing highly divergent ion beams. Increasing the aperture size decreased the degree of spherical aberration that was observed, but also increased the voltage required to achieve focusing. Increasing the spacing between elements increased the focusing power of the lens somewhat, but produced aberrations when manipulating highly divergent beams. Finally, operation in decelerate-accelerate mode required lower potentials than operation in accelerate-decelerate mode, but was accompanied by very high spherical aberration and should, for our purposes, generally be avoided.

A series of deflection plate modeling studies were also performed. Some general conclusions obtained from the results of these studies include: 1. For each deflection direction the use of two plates produced the strongest and most uniform deflection, 2. Operating the deflection plates in push-pull mode produced only slightly more uniform deflection than biasing a single plate and holding the other plate at ground, and 3. The deflection properties of the deflection plates modeled were not especially sensitive to plate length.

In general, a pair of opposing 12 mm long deflection plates located 10 mm away from the beam axis proved satisfactory for beam deflection. In order to simplify the optimization of the system, only one of the two plates used for each axis was biased and the other was connected to ground. For best results, each deflection axis should have an independent pair of opposing deflection plates for allow full control of the beam position.

Rather than constructing a single lens system for focusing and deflecting the ion beam from the quadrupole, a series of elements were machined to allow the user to vary the design of the system to the ion beam of interest. All elements were cut from 0.5 mm stainless steel. Apertures were drilled along with four holes matching the pattern on the mounting bracket of the quadrupole housing. Threaded rod was bolted to the mounting bracket and covered with a ceramic rod. Ceramic insulators were then placed on the rod and used to separate the lens elements. Electrical connections to these elements were made using bolts attached to tabs on the side of each element. Lenses with apertures varying from 5 to 10 mm were manufactured. In general a system using two elements with 6 mm apertures and 2 mm spacing, similar to model 1, was used because of its ability to focus a wide range of both ion energies and angular divergence. When stronger focusing was desired a third 6 mm element was added to reproduce model 2, and if a smaller spot size was desired with low energy ion beams a lens system similar to model 4 was installed.

VI. Performance evaluation of the completed ion source

A. Faraday plate experiments in the matrix chamber

Following the design and construction of the deflection optics, the overall performance of the Anavac mass-selected ion source was evaluated. The original EI source was installed inside the source housing

and attached to the quadrupole. A focusing and deflection system, based upon the design of model 1 detailed in the previous section, was attached to the quadrupole housing mount. This optical system consisted of two additional elements with 6 mm apertures and a spacing of 2 mm. Four 12.5 mm deflection plates were mounted after the focus lens, opposing horizontal elements were mounted 2 mm from the second focus lens element. The opposing vertical deflection pair was positioned 2 mm after the horizontal deflection plates. The electrical and gas connections were made between the analyzer elements and the feedthroughs as described in Chapter 3.IV. The entire unit was installed on the right 6" port of the matrix isolation chamber, and a Keithley 610C electrometer was connected to the movable Faraday plate in the chamber. External power supplies were used to operated all the components of the analyzer except for the quadrupole. A diagram of the power supply and metering scheme used in this study is shown in Figure 3.20.

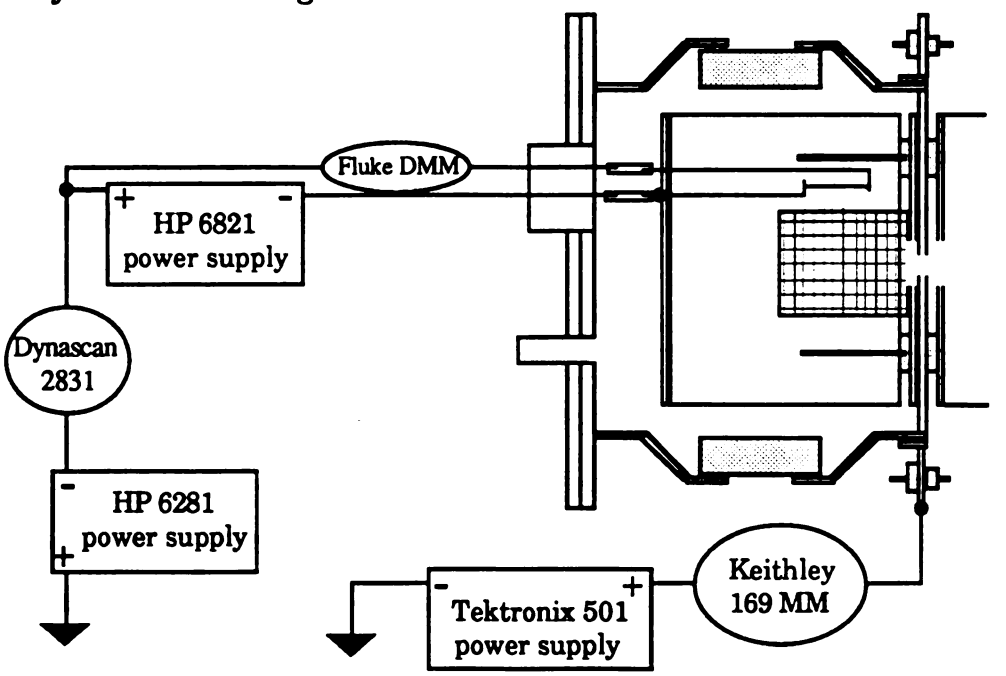

Figure 3.20 The power supply and metering system used to evaluate the performance of the Anavac ion source.

A Hewlett Packard 6821 high current power supply was used to heat the filament with a Fluke DMM connected in line to monitor heating current. The filament bias was supplied by a Hewlett Packard 6281 regulated high voltage power supply capable of producing voltages up to 120 V. A Dynascan 2831 multimeter was connected between the bias and heater power supplies to monitor the total emission from the filament. A Tektronix PS501-1 regulated power supply was used to bias the source plate and a Keithley 169 digital multimeter was connected between the grid bias power supply and the grid element to measure source current. The 1" Faraday plate mounted on the linear motion feedthrough was positioned directly in front of the cryostat window. The filament was slowly heated to 2 mA total emission at a bias of -67 V, and deflection optics were optimized for maximum current with the quadrupole in rf-only mode.

A study was performed to determine the best operating pressure for the ion source. Since no direct measure of source pressure was available, the partial pressure of an introduced gas was evaluated by observing the primary peak in its mass spectrum produced by a Dycor M100 RGA installed on the chamber. A plot of mass-selected ion output current versus chamber partial pressure for the introduction of nitrogen into the chamber is shown in Figure 3.21.

The nitrogen partial pressure was monitored using the intensity of the m/z=28 peak in the RGA spectrum. The filament of the Anavac source was operated at an emission of 0.5 mA. The electron energy for the study was optimized to 70 eV, the ion energy was 12 eV, and the source lens voltage was -40 V. The output of the Anavac source was fairly constant in the $1\text{-}10\text{x}10^{-7}$ torr range. Within this partial pressure range a mass-selected current greater than 1 nA was obtained for nitrogen with a relatively low filament emission. In general the source was operated at the lower end ($\sim 1\text{x}10^{-7}$ torr) of this range to minimize the trapping of neutrals in the matrix.

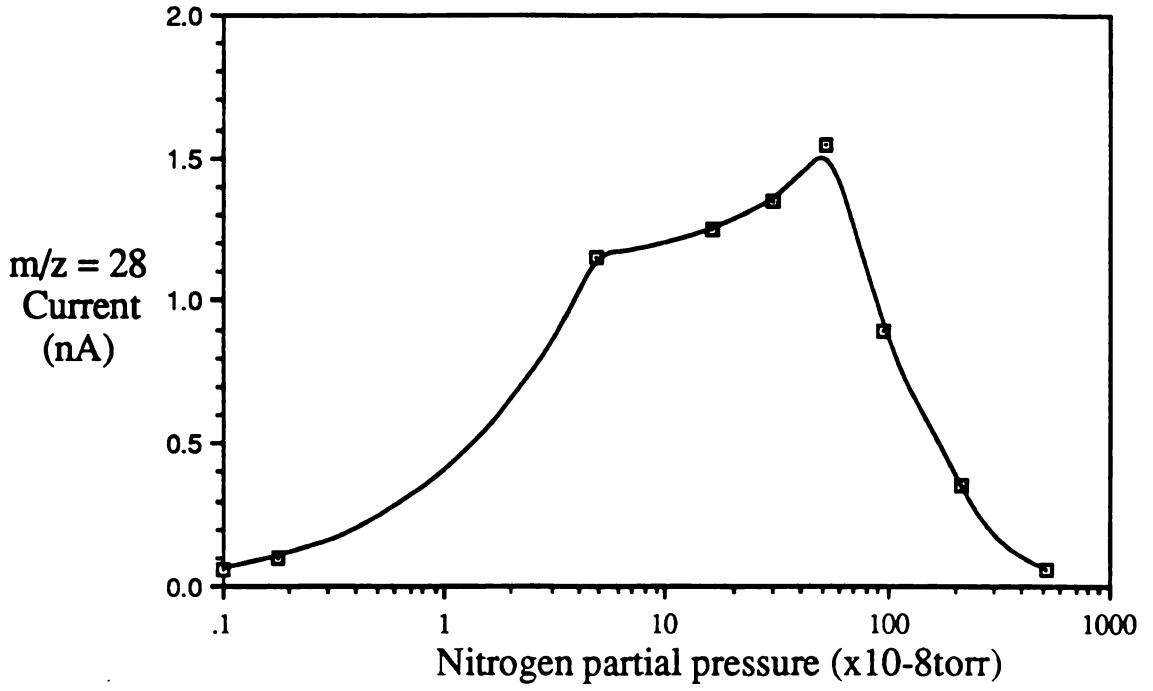

Figure 3.21 Mass-selected ion current at the cryostat window plotted against nitrogen partial pressure in the matrix chamber for the Anavac ion source.

The performance of the quadrupole was evaluated by taking the mass spectrum of several samples. The samples were introduced through a Granville-Phillips model 60 precision leak valve and an evacuated inlet system. Figure 3.22 shows the mass spectrum obtained with an argon leak. The chamber was evacuated to a base pressure of 2.9×10^{-9} torr. Argon was introduced to a partial pressure of 5×10^{-8} torr and a total pressure of 3×10^{-7} torr. The source was operated at an ion energy of 3 eV, electron energy of 70 eV, a focus voltage of -40 V, and an emission of 2 mA. The spectrum was taken at a Y sensitivity of 1" = 1×10^{-10} A, and the principle peak of of the mass spectrum, m/z = 40, produced a maximum current of 1.4 nA which exceeded full scale of the XY recorder. The small peak at m/z = 28 was probably produced by an air leak (N_2) in the inlet system. The peaks at m/z = 18 and 20 corresponding to H_2O^+ (from residual water in the source) and Ar^{2+} were fairly well resolved. The modified quadrupole appeared to be operating at slightly reduced

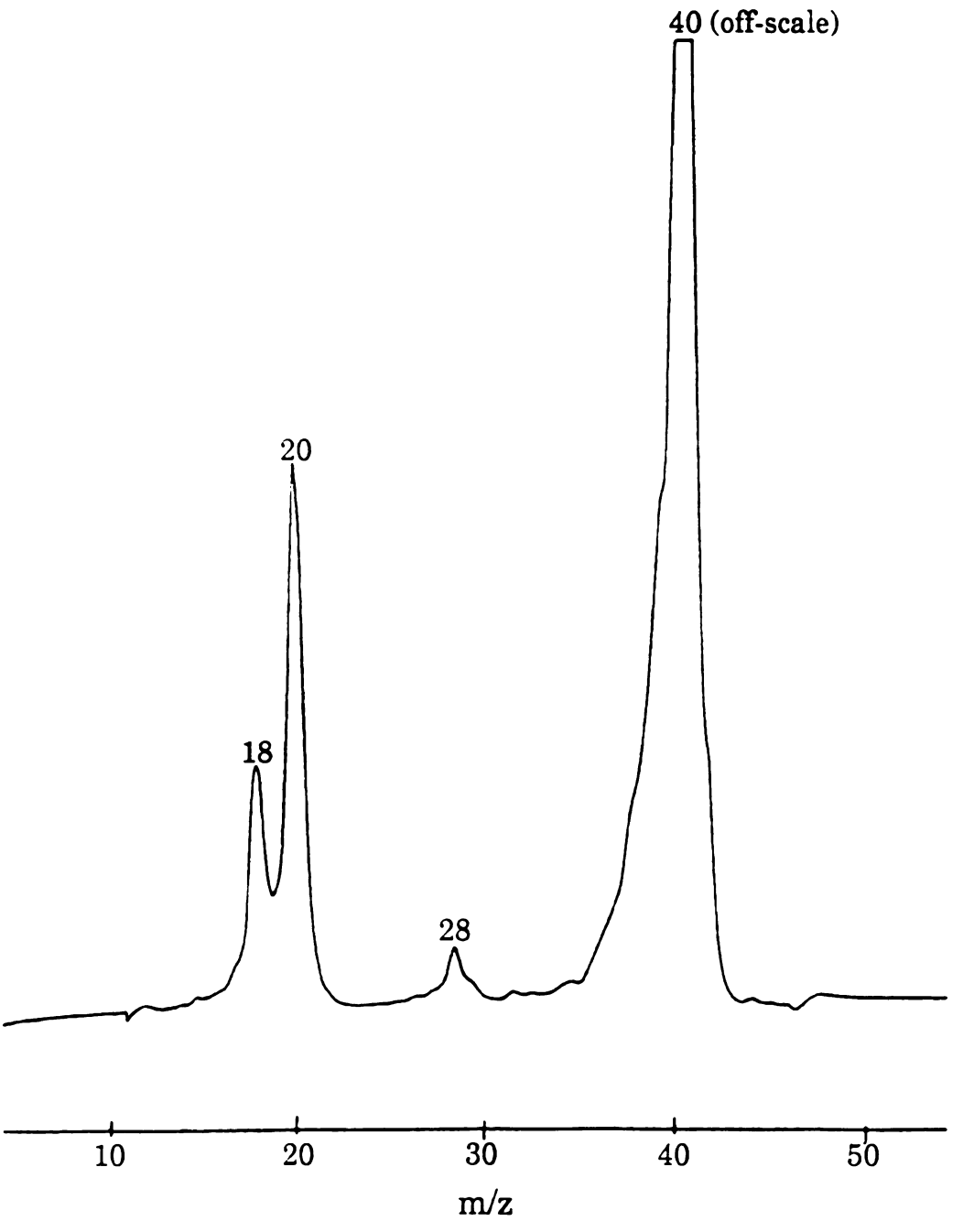

Figure 3.22 The Anavac source mass spectrum of an argon leak detected at the remote faraday plate positioned in front of the cryostat window.

resolution, most likely due to the additional 80 mm flight path of the ion beam. Increasing the dc/rf ratio increased the resolution of the unit, but at the cost of a large loss in ion current.

Another example of the output of the Anavac ion source is shown in Figure 3.23. This spectrum shows a) the spectrum obtained by the M100 RGA and b) the spectrum produced by the Anavac source at the cryostat window with the introduction of propylamine. The chamber base pressure was $1x10^{-8}$ torr. A propylamine bulb was prepared, cleaned with 3 freeze/thaw cycles, and connected to the inlet system. Propylamine was introduced to a total chamber pressure of $1.3x10^{-7}$ torr. The Anavac source was operated with an ion energy of 3 eV, electron energy of 50 eV, focus voltage of -40 V, and filament emission of 2 mA. The maximum ion current with this leak at an ion energy of 3 eV was ~0.1 nA. This was increased to > 1 nA by increasing the ion energy to 12 eV. The peaks at m/z = 30 and 44 were indicative of propylamine. The peak at m/z = 40 was due to argon in the chamber that was present because this spectrum was taken during a matrix-isolation experiment. The peaks at m/z = 28, 27, 26 and 25 are also due to propylamine, with some of the m/z = 28 intensity possibly the result of an air leak. The M100 RGA spectrum showed well-resolved m/z = 26, 27, 28, and 30 peaks while the Anavac spectrum was only able to resolve the m/z = 28 and 30 peaks from this series. This slight loss of resolution in the modified Anavac source is not likely to prove a limitation in the deposition of ions unless the selection of ions only one mass unit from another fragment in the spectrum is required. For most studies the Anavac source resolution could be reduced further by decreasing the dc/rf ratio to increase the output current and decrease the required deposition time.

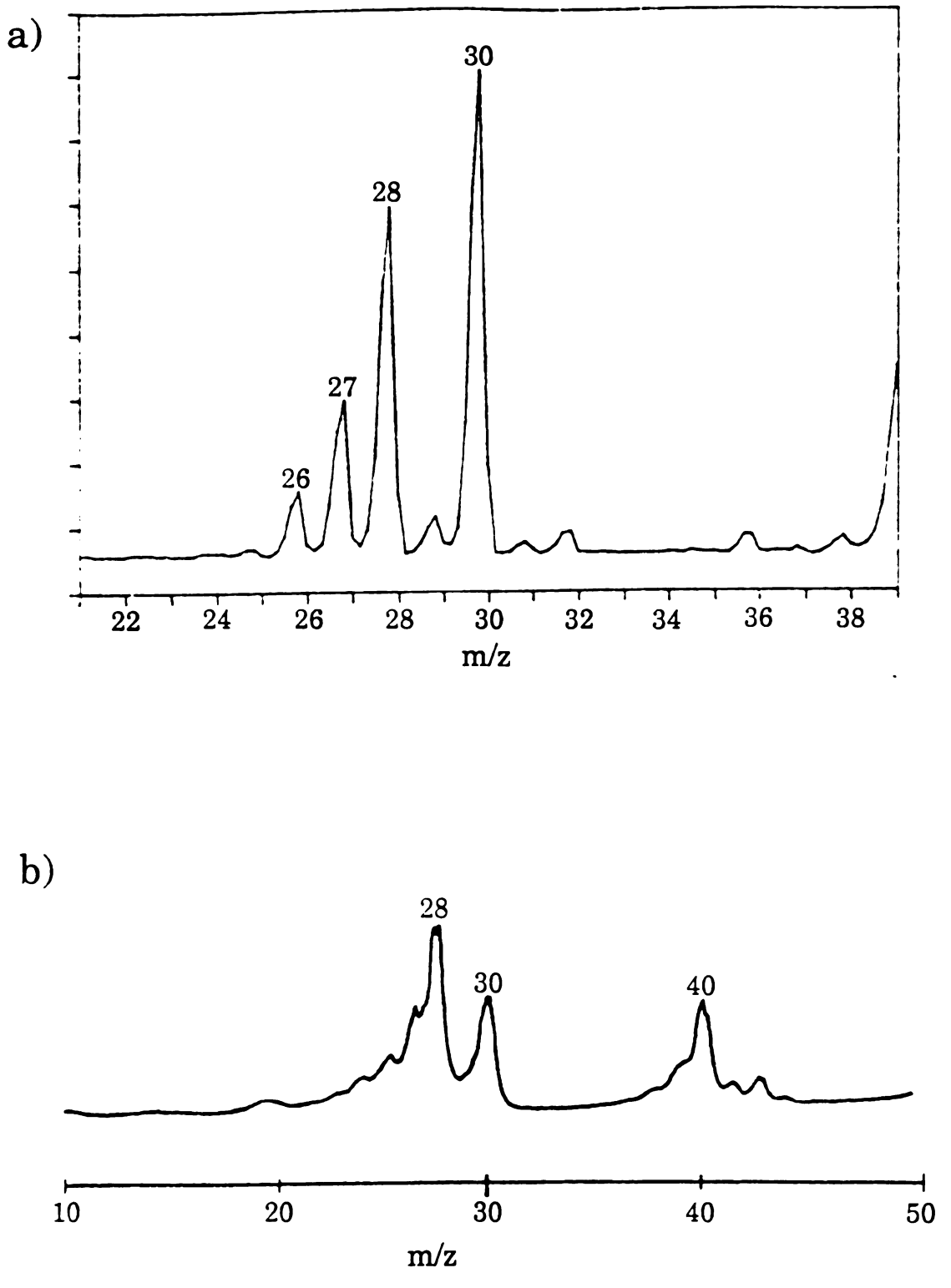

Figure 3.23 The mass spectrum of propylamine taken with a) the Dycor M100 RGA and b) the Anavac source using the remote faraday plate for detection.

B. CEMA visualization at cryostat window

The CEMA detector was also used to observe the beam profile produced by the Anavac source at the cryostat window. A shielded mounting grid/plate was constructed that allowed the CEMA detector to be positioned in place of the cryostat window. This shield was designed to attach to the second stage of the cryostat, and create a field free region between the Anavac source and the CEMA detector. The mount was positioned so that the image on the phosphor screen could be observed through the $2\ ^3/_4$" window/flange generally used to introduce the BOMEM IR beam. The shield plate was designed to clear the inside wall of the chamber by only ~2 cm which reduced field penetration of the potentials applied to the detector. A 40 mm hole was cut in the shield plate at the normal position of the cryostat window and covered with a Buckby-Mears 80% transparent stainless steel grid. The CEMA detector was mounted behind the hole and attached to the shield plate with electrically-isolated threaded rods shielded by copper cages. The CEMA was wired with a 10 MΩ resistor series between the two plates and the back of the second plate was connected to ground. This allowed the CEMA to operate with only two power supplies, one for the front plate and another for the phosphor screen. Potentials were supplied to the detector through a high voltage feedthrough and shielded BNC cables. The chamber was evacuated to a base pressure of $1x10^{-8}$ torr, and a mixed inlet leak of helium ($1x10^{-9}$ torr) and nitrogen ($8x10^{-9}$ torr) was introduced through the source leak valve. The source was operated at an electron energy of 70 eV, ion energy of 12 eV, and focus voltage of -40 V. The channelplate was operated with -1400 V on the front plate and +1600 V on the phosphor screen. Figure 3.24 shows the focused cross pattern produced when the quadrupole was selecting m/z = 4 (helium). This ~ 3 mm focal point was achieved by applying -15.5 V potential to the center einzel lens. In this visualization the Anavac source

Figure 3.24 The mass-selected beam profile for m/z = 4 (He) produced by the Anavac source on the CEMA mounted at the matrix window.

was pointed slightly below the detector, and the application of +5.1 V to the bottom deflection plate was sufficient to successfully deflect the beam onto the detector. The unfocused rf-only beam completely filled the detector window, but could be focused to ~ 6 mm through the application of -39.5 V to the center einzel lens element. The mass-selected m/z = 28 beam from nitrogen had a much higher angular divergence, and attempts to bring the entire cross pattern onto the detector resulted in the strong defocusing of the higher intensity, central portion of the beam. Because of this, a relatively low central element voltage of - 52V to produced the brightest image at the detector for the m/z = 28 beam. These studies indicated that the lens system designed using SIMION was successful in focusing and deflection the ion beam onto the cryostat window. The exact characterization of the mass-selected ion beam at the cryostat window was difficult due to the change in beam profile with increasing m/z. In general, optimization of the ion current through iterative tuning of the optical elements is probably the best technique to get the strongest ion current onto the window. Because the ion beam is fairly diffuse, optimization for FTIR studies should be done using the full size 1" Faraday plate. In LIF studies a smaller Faraday plate could be installed to provide a better overlap between the Faraday plate and the area of the matrix that will be excited by the laser.

VII. Modifications to produce mass-selected ions using alternate sources

A. The modification of a Nermag EI/CI source

A second source was modified for use with the Anavac-2 quadrupole. A Nermag model 1.68 EI/CI ion source was selected for modification to allow the production of ions using high pressure ionization techniques. The Nermag source uses the standard Nier configuration

with the filament residing outside of the source region. This also makes the Nermag source useful for the production of ions from compounds would decompose when directly exposed to the hot filament, and for the use of highly oxidative samples. The Nermag source was designed for high pressure use, and therefore few changes were made to its design. The source is small and cylindrically symmetric making it ideal for coupling with the Anavac quadrupole. A circular repeller located at the rear of the source also serves at the sample introduction port. To allow the use of the source with direct insertion probes, a ~1/4" aperture was located on the side of the source housing. To decrease the conductance from the source, this port was sealed with an aluminium plug. The quadrupole end of the Nermag source is sealed by an endplate that can be removed for source cleaning. To further decrease the source conductance, a series of matching endplates were manufactured with reduced ion exit apertures. The repeller inlet tube was also modified to allow a Teflon line to connect the source inlet to the swagelock gas fitting on the mounting flange. Machined ceramic plugs were installed on the side of the source housing and countersunk to receive the setscrew pins of the pivot mount. These ceramic insulators were used to allow the entire source housing to be biased at the ion energy. Finally a series of additional lens elements of varying aperture sizes were fabricated to allow for the adaptation of the source optics to the system of interest.

A 0.4 mm aperture source endplate was installed on the Nermag source, and the Anavac quadruple was attached to the unit along with the original 3 mm focus and quadrupole entrance apertures. A Galileo model 4700 channeltron detector was adapted to allow it to connect to the exit mount of the quadrupole housing and installed. The entire unit was then installed on the 6" mounting flange. The filament and quadrupole were wired as described in Chapter 3.IV, and the source housing, repeller, collector, and focus potentials were wired to the 8-pin mini-conflat feedthrough using Teflon-coated flexible wire. A Baratron type 170M

capacitance manometer head was attached to the inlet line of the mounting flange to provide a relative measurement of the pressure in the source. The mounting flange was attached to a special 11" adaptor flange that allowed it to be installed on the 11" flange of an o-ring sealed chamber. All the Nermag source studies were performed on an aluminum, o-ring sealed test chamber that was modified from the early Enke triple quadrupole instrument. This test chamber was pumped by a Varian M4 diffusion pump fitted with a liquid nitrogen trap. Base pressure for this chamber was generally on the order of $5x10^{-7}$ torr.

Following the installation of the source mounting flange on the test chamber, high voltage BNC feedthroughs mounted on the side ports of the chamber were connected to the bias and output lines of the channeltron detector. The ion source was operated using external power supplies for all the signals except the quadrupole circuit. The power supply and metering scheme used in these experiments is shown in Figure 3.25.

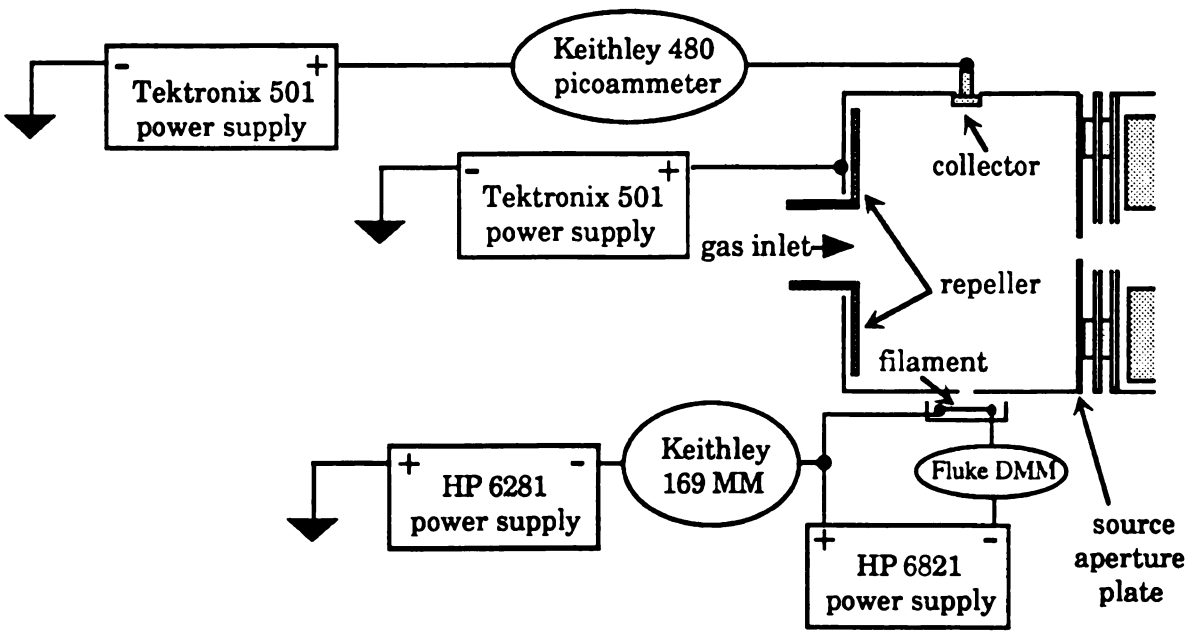

Figure 3.25 The power supply and metering system used with the Nermag source.

The original filament supplied with the Nermag source was heated by a Hewlett Packard 6821 high current power supply. Filament heater current was monitored with a Fluke 23 DMM connected in-line with the heater power supply. A Hewlett Packard 6281 regulated high voltage power supply was referenced to ground and used to supply the filament bias potential. Total filament emission was monitored by a Keithley 169 multimeter connected between the filament bias and heater power supplies. A regulated Tektronix 501 variable power supply was used to supply the collector and source bias potentials. Collector current was monitored with a Keithley 480 picoammeter placed between the collector and the Tektronix power supply. The channeltron detector bias voltage was supplied by a Hewlett Packard 6516A high voltage power supply, and the detector output was monitored with a Keithley 610C electrometer. The other dc potentials required for the operation of the system were supplied by an unregulated variable power supply constructed in-house.

The performance of the Nermag source/Anavac quadrupole combination was first evaluated by operating the source in EI mode. The test chamber was evacuated to a base pressure of 7.8×10^{-7} torr, and a mixture of argon and carbon tetrachloride was introduced through the inlet system. The sample pressure was increases until a capacitance manometer reading of 90 mtorr was obtained which corresponded to partial pressures of 9.2×10^{-6} and 3.7×10^{-6} torr of argon and CCl_4. The operating parameters of the source were optimized, and the best resolution was obtained at ; source = +3.0 V, repeller = +16 V, lens = - 35 V, collector = +5.02 V, x-ray plate = +54.8 V, and detector = - 2.7 kV. The filament was biased at -67 V, setting the electron energy at 70 eV. A heater current was applied across the filament until an total emission of 50 uA was obtained. This corresponded to a collector current of 0.197 uA. With the Anavac control unit in rf-only mode a current of 1.75×10^{-6} A was measured at the detector. The mass spectrum obtained with a mass scan from m/z = 1-60 is shown in Figure 3.26. The dc/rf ratio of the quadrupole was optimized for

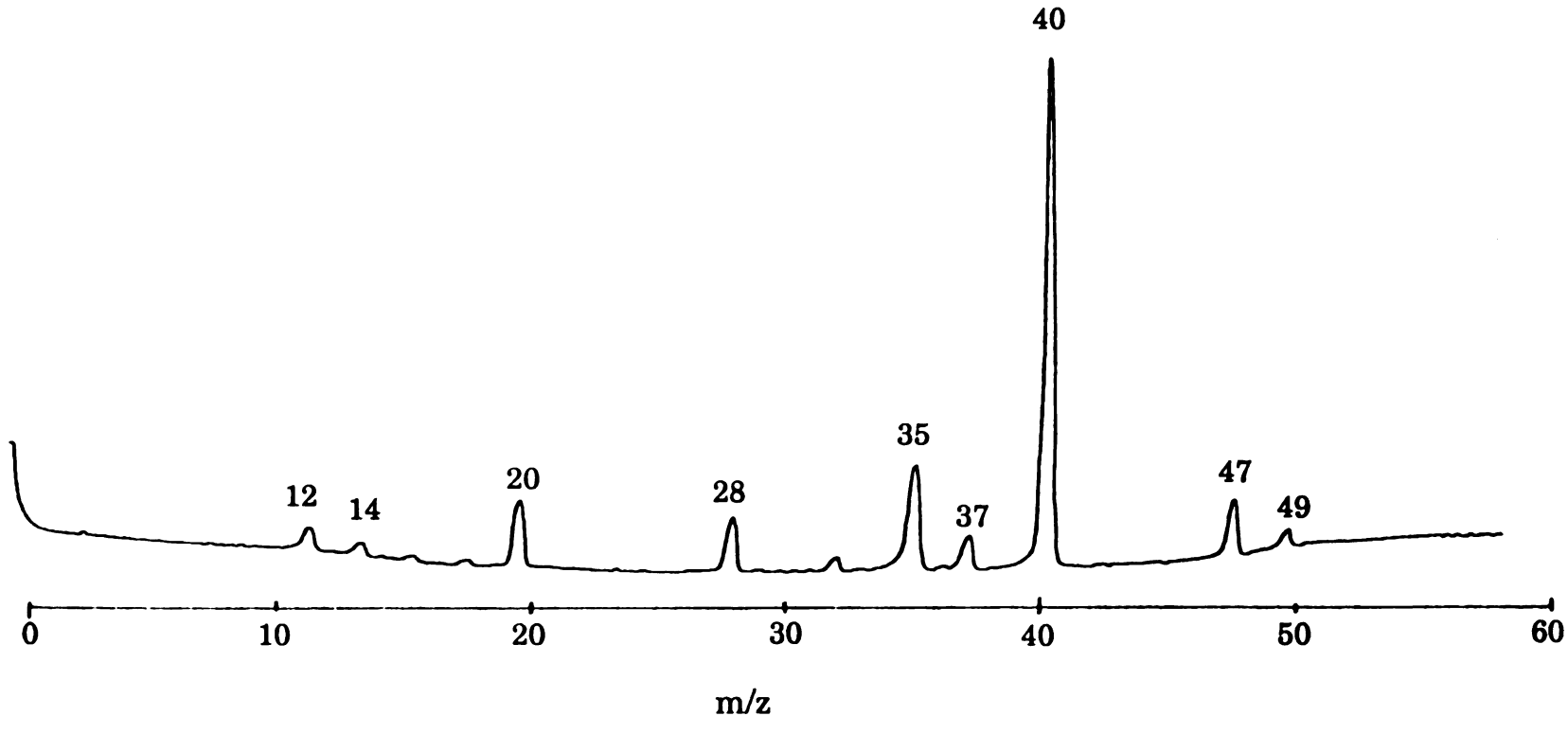

Figure 3.26 The mass spectrum of a mixture of argon and carbon tetrachloride produced using the anavac quadrupole fitted with a modified Nermag EI/CI source.

highest resolution before the scan. The resulting mass spectrum showed very good resolution, with components from Ar, CCl_4, and air resolved to approximately unit mass resolution. The peak intensity for this study was found to be strongly dependent upon dc balance between the quadrupole rod pairs, with the highest output occurring at a slight negative offset. This sensitivity probably corresponded to an optimum alignment of the ion beam in the quadrupole with the quadrupole exit aperture.

A methane leak was introduced into the source region to evaluate the high pressure output of the source. Figure 3.27 shows the mass spectra produced at: a) manometer pressure = 26 mtorr and b) manometer pressure = 400 mtorr. The negative deflection of this mass spectrum was due to the output signal from the detector and could not be reversed using the XY recorder available. The source was operated under the same conditions as the previous study, and the total pressure in the chamber in study a) was 1.7×10^{-6} torr. The total filament emission was regulated at 50 uA at an electron energy of 70 eV. The output from the detector in study a) with the control unit in rf-only mode was 1.3×10^{-6} A. Spectrum a) showed the well resolved methane pattern of m/z = 12, 13, 14, 1516 and a small peak at m/z = 17 indicating the onset of CI conditions. In spectrum b) the total pressure was increased to 6.2×10^{-6} torr which produced an rf-only current of 3×10^{-6} A. This spectrum also showed peaks at m/z = 12, 13,14 ,15, and 16 along with the peaks at m/z = 17 and 29 indicative of high pressure methane CI. All the peaks in this spectrum showed strong splitting. This splitting was first assigned to the imbalance of the quadrupole dc levels. After investigation, this peak splitting was linked to the source pressure, indicating that it is the result of ion/molecule collisions in the quadrupole. The source pressure was reduced until this peak splitting disappeared, and an expanded scale spectrum was taken at a manometer reading of 240 mtorr. This spectrum is shown in Figure 3.28, and clearly showed the presence of peaks at m/z = 17 and 29 that were indicative of the formation of CH_5^+ and $C_2H_5^+$ in methane CI. To increase the intensity of these peaks

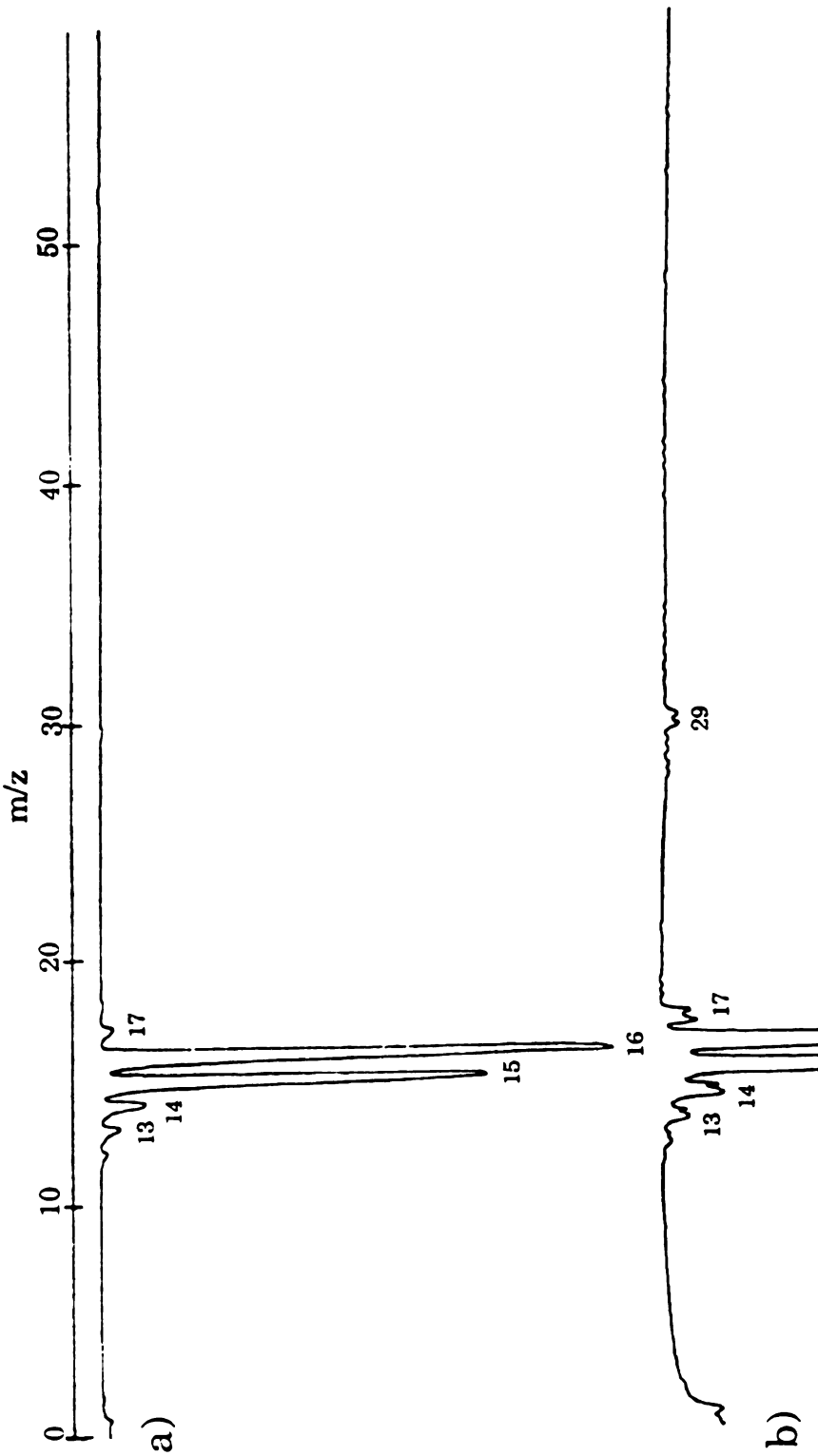

Figure 3.27 The mass spectrum of methane at a source pressure of a) 26 mtorr and b) 400 mtorr produced using the anavac quadrupole fitted with a modified Nermag EI/CI source.

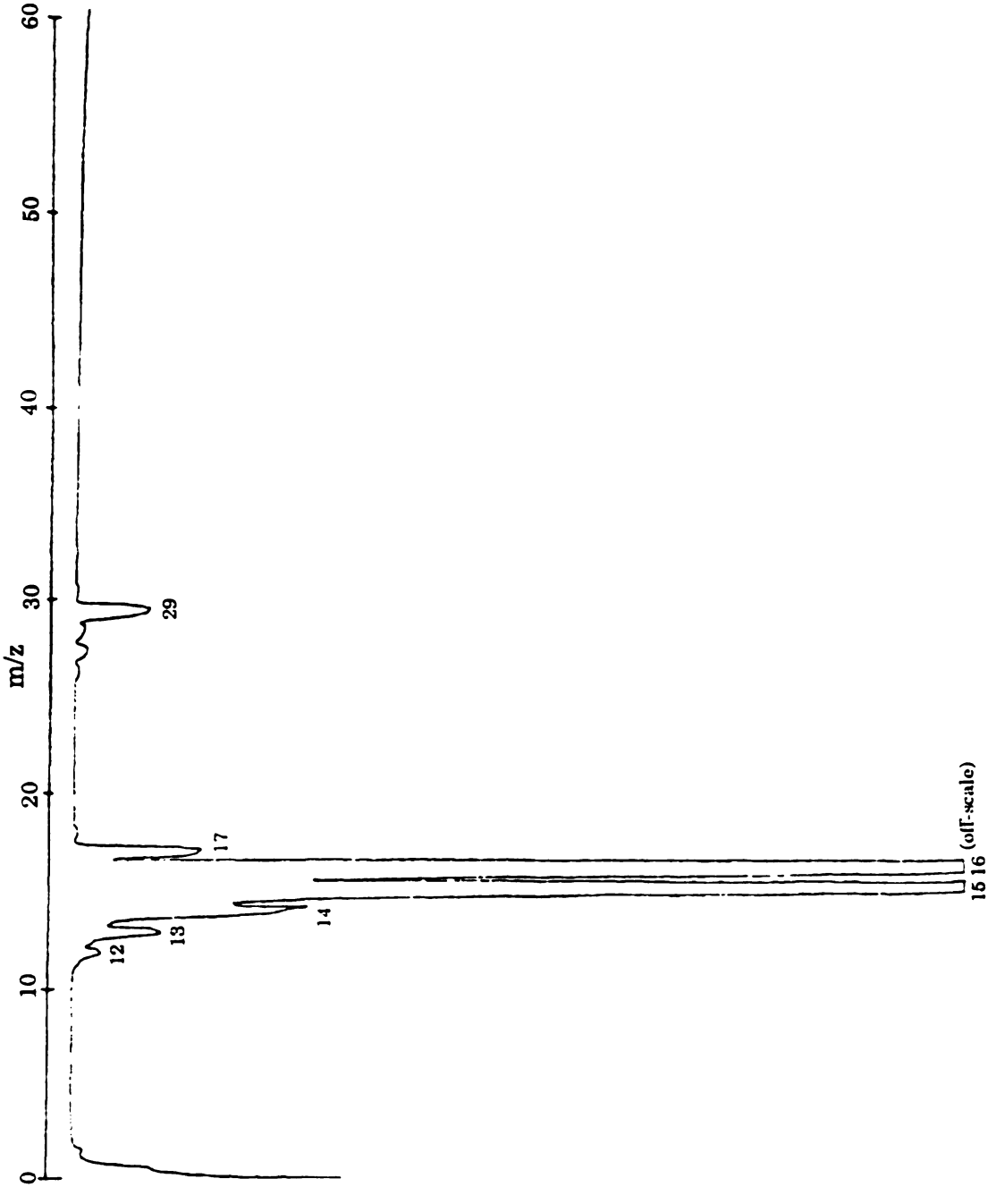

Figure 3.28 An expanded view of the mass spectrum of methane produced at a source pressure of 240 mtorr using the Anavac quadrupole fitted with a modified Nermag EI/CI source.

the pressure at the manometer was slowly increased to > 1 torr and the performance of the quadrupole was observed. Increasing the pressure did increase the intensity of the m/z = 17 and 29 peaks, but was accompanied by a severe loss in resolution. At a manometer pressure of ~1 torr these ions began to dominate the spectrum, but the chamber pressure at this leak rate exceeded $1x10^{-4}$ torr. It was concluded that even with the reduction of the source apertures, the conductance from the source was too high to create true CI conditions within the source region. Increasing the pumping speed in the chamber could improved the performance of the system, but for this source to operate under true CI conditions the source should be adapted for some form differential pumping that is generally used in CI.

The performance of the Nermag source under electron capture conditions was also investigated. The channeltron was modified to allow for the detection of negative ions. The x-ray plate and the detector entrance aperture were isolated, and separate leads were connected to each element. A potential of +3.5 kV was applied to the x-ray plate, -3 V was applied to the detector entrance aperture, and the channeltron was operated at -2.7 kV. Negative ions exiting the quadrupole were strongly attracted to the high positive potential on the x-ray plate and impacted upon the plate at high energies. These high energy collisions resulted in the production of secondary positive ions from the surface which were detected at the channeltron. The conversion process is not well understood, but has been shown to occur at relatively high efficiency for x-ray electrode potentials of > +3 kV [129]. To allow the production of negative ions the source, repeller, and focus potentials were reversed, and the collector was held at the source potential. Figure 3.29 shows an example of the EC-NI mass spectra produced with the Nermag source operating under these conditions. Carbon tetrachloride was introduced into the source to a manometer reading of 400 mtorr, and the source parameters were optimized for ion current in rf-only mode. This

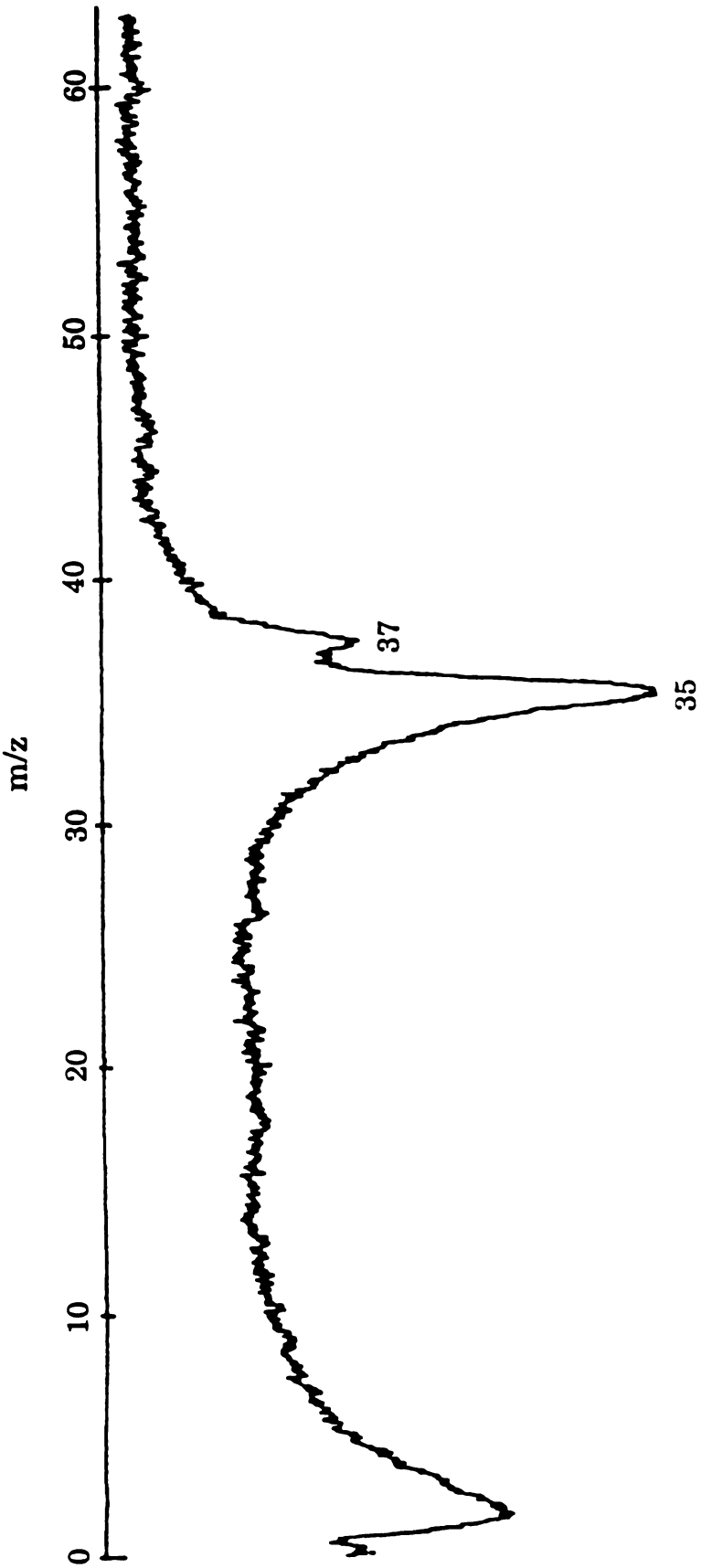

Figure 3.29 An electron capture negative chemical ionization mass spectrum obtained with carbon tectrachloride using the anavac quadrupole with a modified EC/CI source.

spectrum was obtained with the operating potentials: source/collector = -20 V, lens = +70 V, repeller = -45 V, electron energy = 100 eV, and total emission = 60 uA.

The ions produced under these conditions had a transverse energy in excess of 20 eV. This resulted in the poor resolution observed in the mass spectrum. The maximum detector signal obtained with the control unit operating mass-selected mode was ~ 1 nA. At source potentials below 20 eV the ion signal was lost in the baseline noise. Several mixtures of CCl_4 with methane and argon buffer gases were investigated in attempts to improve the output of the unit with little success. Ammonia and nitromethane were also used as electron capture species, but no negative ions were observed with either of these gases. To determine the ion current produced under these conditions prior to multiplication, the channeltron detector was replaced with a shielded Faraday plate. The mass-selected ion currents measured at this Faraday plate under similar conditions were less than $1x10^{-12}$ A. These currents were too low to be used in the matrix isolation studies of interest. The primary reason for the poor efficiency of electron capture ionization using this source was probably insufficient buffer gas pressure in the source. This was compounded by the decreased ion extraction through the small ion exit aperture that had been installed to reduce the source conductance. To make the Nermag source practical for use in EC-NI mode some differential pumping system must again be devised.

Following the high pressure studies, the maximum ion output of the Nermag source was investigated to determine its usefulness for the production of ions from thermally labile and oxidative compounds. The entire source unit was disassembled, and the stock ~3 mm aperture source, focus, and quadrupole entrance plates were replaced. To optimize the total output of the quadrupole, the 3 mm limiting aperture plate at the exit of the quadrupole was removed and the quadrupole dc/rf ratio was adjusted to produced minimum resolution and maximum output. A

shielded Faraday plate was attached to the end of the quadrupole to allow the direct measure of ion output. The unit was wired as described previously, and installed on the test chamber. Figure 3.30 shows a mass spectrum produced from a nitrogen leak. The operating potentials on the systems were; source = +3.0 V, repeller = +16 V, lens = -35 V, collector = +5.0 V, and electron energy = 70 eV. The base pressure of the chamber was 2.4×10^{-6} torr, and nitrogen was introduced through the source inlet to a chamber pressure of 7.1×10^{-6} torr. The filament was heated to 1.7 A which produced an emission current of 14.8 uA and a collector current of 13.95 nA. The ion current at Faraday plate with the control unit operating in rf-only mode was 1.8×10^{-8} A. The maximum m/z = 28 current for the spectrum shown was 8.25×10^{-10} A. The resolution of the system in this study had been substantially reduced, but the source is still capable of resolving peaks at m/z = 28 and 32. The ion output was increased by increasing the filament heater current. A maximum m/z = 28 signal of 5.8 nA was detected on the Faraday plate with a heater current of 2.10 A. Figure 3.31 is a plot of ion output current versus total filament emission under these conditions. Both the rf-only current and m/z = 28 maximum currents are plotted. The output of the source sharply increased with increasing filament emission from 0-50 uA. Above 50 uA emission the source output leveled off. In general, operation of the Nermag filament in the total emission range from 100-200 uA yielded a high, reproducible ion output current at the Faraday plate.

In conclusion, although the attempts to produce high pressure spectra using the modified Nermag source were fairly unsuccessful, the operation of the Nermag source in EI mode produced relatively high ion output currents. The external filament design of this source should make this source especially useful for the production of ions from compounds that would decomposed when directly exposed to the hot filament. Oxidative compounds, such as NO, could also be used with this source for

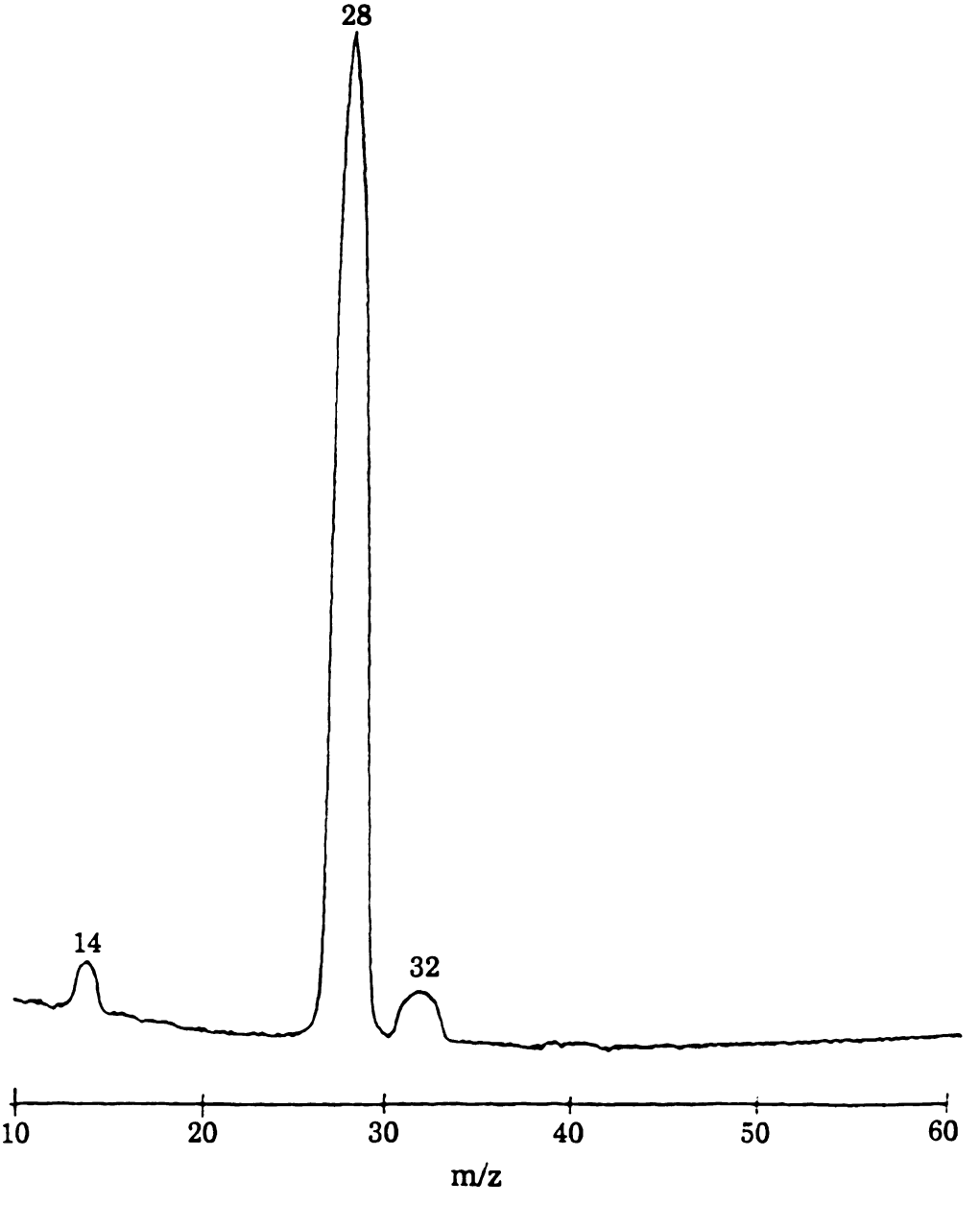

Figure 3.30 The mass spectrum of nitrogen obtained using the Nermag source and Anavac quadrupole with current ouput maximized, maximum m/z 28 current = 5.8 nA.

much longer periods than would be possible using the original Anavac source.

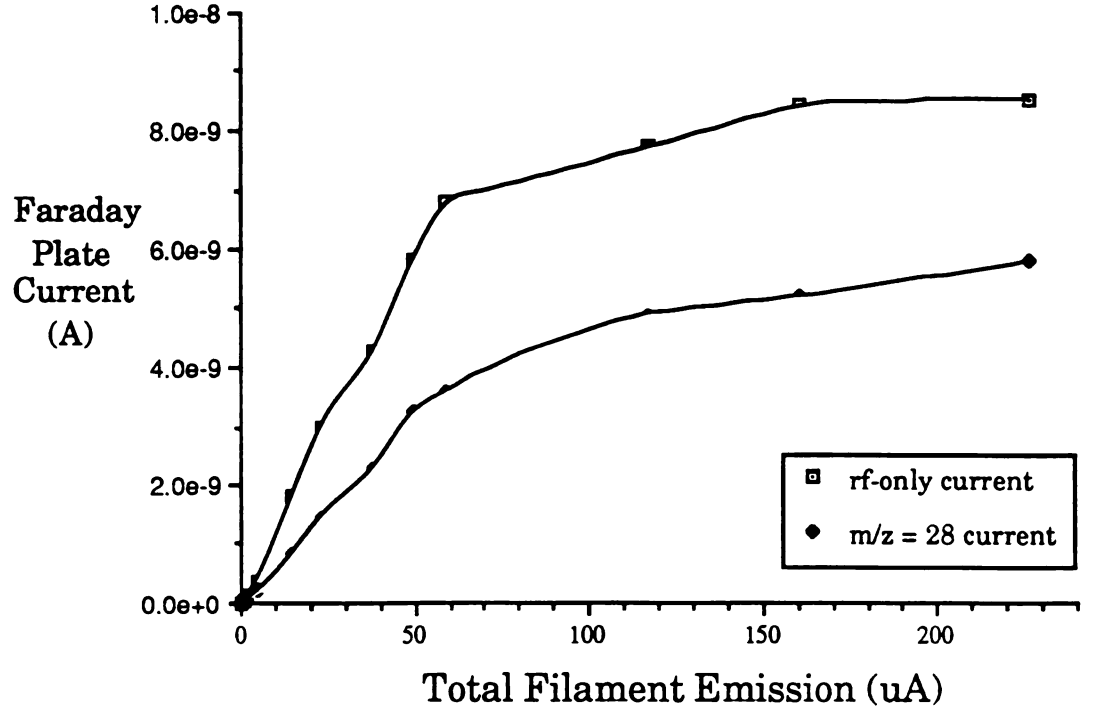

Figure 3.31 The output of the Nermag source versus total filament emission.

B. Surface Ionization in the Anavac source

One area of current research in the Allison group is the use of thermionic emitters for the ionization of thermally labile compounds. Glasses containing potassium and sodium have been shown to produce strong signals of K^+ and Na^+ respectively upon heating [68]. The use of Cs glass surfaces as a means of producing negative ions through negative surface ionization has also been investigated [71]. A series of experiments were performed to determine if the Anavac source could be modified to produce negative ions through NSI using these low work function Cs surfaces.

To study the output from a Cs glass surface, total surface emission experiments were performed on a vacuum rack test chamber. A specially designed test chamber was used that contained high current feedthroughs and could be attached to a standard vacuum rack. To compare the emission from a Cs glass surface against the emission of a rhenium surface two emitters were prepared. The emission of 0.007" diameter bare rhenium wire was compared to that of a Cs glass surface deposited upon a 0.007" rhenium wire. These emitters were prepared by threading the rhenium wire through a ~1/16" diameter, ~1/4 long 2-hole ceramic rod that was used to separated the lengths of wire. A small (~1/16") loop of wire was left at one end of the ceramic tube. The Cs glass surface was prepared from a 2 SiO_2 : 1 Al_2O_3 : 1.58 $CsNO_2$ mixture (by weight) that was suspended in a slurry of acetone. This glass slurry was deposited on the rhenium wire loop and the acetone was removed by heating with a bunsen burner. The heat from the burning acetone also caused the glass mixture to harden sufficiently to remain attached to the wire loop. Following preparation of the two emitters, the free ends of the rhenium wire were attached to alligator clips on the chamber feedthrough wires. To allow the measurement to emission current from the emitters, a ~1" square collector plate was attached to another feedthrough wire and positioned opposite the emitters. The chamber was then assembled and evacuated to a pressure of ~$1x10^{-4}$ torr.

The power supply and detection scheme used in this experiment is shown in Figure 3.32. A Hewlett Packard 6821 high current power supply was used to heat the emitter, and a Hewlett Packard 6281 regulated power supply was used to supply the emitter bias. A Keithley 417 picoammeter was attached to the collector plate lead to measure the total emission from each emitter. A bias of -3.0 volts was applied to each emitter, and the rhenium filament was slowly heated while monitoring emission current at the collector plate. Approximate temperature measurements were also

made using an optical pyrometer. A plot of the collector plate current versus heater current for each of the systems is shown in Figure 3.33.

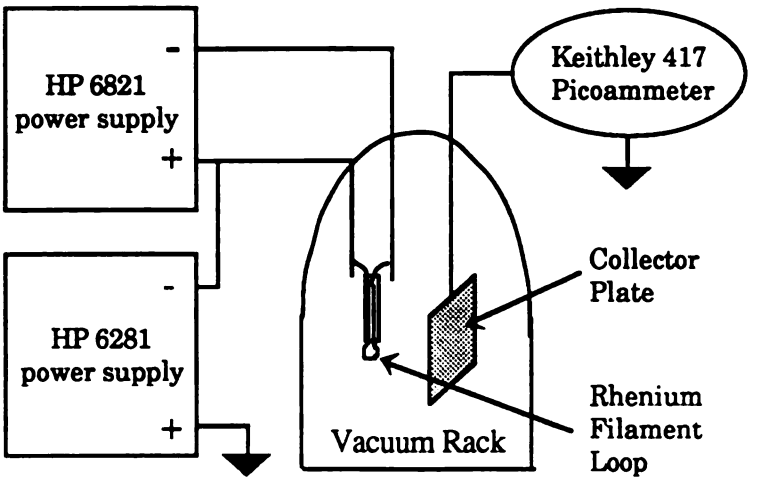

Figure 3.32 The experimental setup used to evaluate the emission of the cesium glass surface.

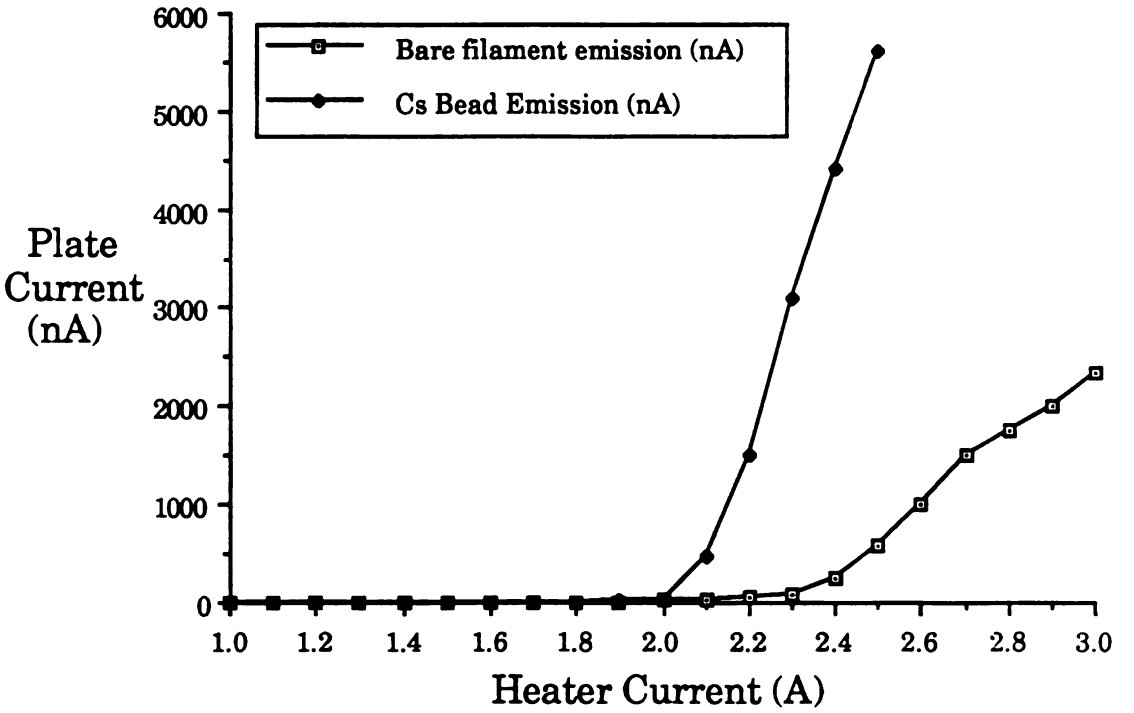

Figure 3.33 Collector plate current versus heater current for both a bare rhenium surface and a cesium glass bead formed on a rhenium wire.

Emission from the bare rhenium wire began at a heater current of ~1.8 A and increased strongly at ~2.2 A which corresponded to a surface temperature ~1255 °C. The output of the bare wire steadily increased from 2.2 to 3.0 A with a collector current of 2 uA produced at 3.0 A (temperature ~ 1750 °C). Emission from the cesium glass surface began at 1.6 A and increased strongly at 2.0 A, which corresponded to a wire temperature of ~1100°C. The emission from the cesium surface increased more rapidly, with a collector plate current of ~6 uA produced with a heater current of only 2.5 A (wire temperature ~1420 °C). The earlier onset and increased overall emission from the cesium bead indicated that this surface had a lower overall work function than the bare rhenium surface. A leak of acetonitrile was introduced into the system and the experiment repeated. With acetonitrile in the system the onset of emission from the cesium surface occurred at a lower heater currents and produced a stronger signal, indicating the possible production of negative ions from NSI.

To determine if the emission signal from the cesium surface was caused by negative ions, or simply electrons, a similar experiment was performed using a mass spectrometer. Previous work in the Allison lab had resulted in the modification of several mass spectrometer direct insertion (DI) probes to accept this type of bead for K^+IDS studies. The modified DI probes contained electrical feedthoughs and leads to allow the biasing and heating of the bead support filament. Another cesium bead was prepared and spot welded to the leads on the end of the DI probe tip. The probe was inserted into the EI/CI source of a Hewlett Packard 5985 quadrupole mass spectrometer and aligned with the exit aperture of the source. The HP5985 used a Galileo 4700 series channeltron detector that had been previously modified to allow detection of negative ions. This was operated at an x-ray plate bias of +3.5 kV and a channeltron bias of -2.2 kV. The base pressure in the source region was $3x10^{-6}$ torr. Carbon tetrachloride was introduced through the sample inlet to a source

chamber pressure of $6x10^{-5}$ torr. A bead bias of -3.0 V was applied, and the total ion current at the detector was optimized at a bead heater current of 2.3 A. The position of bead was also adjusted to create a maximum total ion signal at the detector. The quadrupole was scanned from m/z = 0-200, and the mass spectrum stored. Figure 3.34 shows the average of 290 scans with a total ion current of 6010. The only ions observed from m/z = 0-200 were at 35 and 37 resulting from the formation of $^{35}Cl^-$ and $^{37}Cl^-$ respectively. This NSI production of strong signals of Cl^- from the cesium surface indicated that these cesium surfaces could prove useful for negative ion beam formation using the Anavac source. Other gases were investigated for negative ion production including acetonitrile and nitromethane, but the strongest negative ion output was obtained with CCl_4.

Following these studies, the original Anavac EI source was modified for use as a surface ionization source. This was accomplished by removing the source grid plate and installing a mount for the cesium bead. A high current feedthrough from a gas chromatograph thermal conductivity detector (TCD) was spot welded in the center of the filament housing endplate as shown in Figure 3.35. The free ends of the cesium bead were spot welded to the inside leads of the TCD feedthrough, allowing the bead to be positioned directly over the source exit aperture. The outside leads of the TCD feedthrough were connected to two of the pins on the source housing flange feedthrough. The filament housing could be biased separately from the bead using another lead on the source housing feedthrough flange.

A SIMION modeling study was performed to determine the best operating conditions for the Anavac NSI source. The dimensions of the source assembly were measured and a 9,200 point cylindrically symmetric array was used to construct a model of the source electrodes. This array was refined, and the potentials on each element were optimized to produce high ion transmission for 3 eV negative ions emitted from the bead

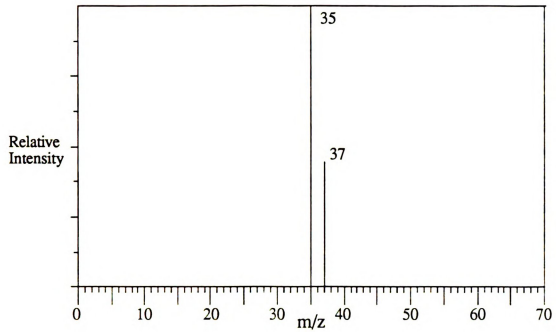

Figure 3.34 The mass spectrum produced from NSI of CCl_4 on a cesium surface, this spectrum was taken on an HP5985 mass spectrometer.

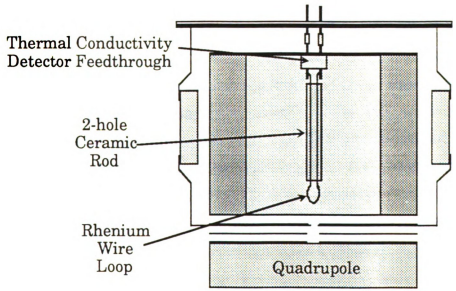

Figure 3.35 The original Anavac source adapted for surface ionization.

surface. The resulting SIMION model is shown in Figure 3.36. The best compromise between ion transmission and ion energy was obtained with the potentials: filament housing = -9.0 V, bead = -3.0 V, source plate = 0 V, and lens = -40 V. The source plate was maintained at 0 V to simulate the use of a picoammeter to monitor the source plate current. The model Figure 3.36 shows 5 V contours from 0 to -40V and 2 V contours from 0 to 10 V. Strong focusing fields were created by the source einzel lens similar to that observed in previous source models. The field lines behind the bead illustrated the field created by applying a -9 V potential to the source housing. This field helps push ions toward the exit aperture of the source. The field line in front of the bead showed the surface extraction field present in the system which aids in the detachment of an ion from the bead surface. The trajectories of ions emitted along the bead surface are also shown in Figure 3.36. Ions formed along the sides of the bead failed to exit the source aperture, but ions formed along the front of the bead successfully exited the source aperture and were injected into the quadrupole.

Using these modeling results, a study was performed to optimize the operating conditions of the Anavac NSI source. The output of K^+ from potassium glass surface is very strong, and this system was selected to allow the easy optimization of source conditions. Once these operating potentials were determined they were reversed for use with NSI. A potassium glass bead was prepared using the methods described earlier. A 0.007" rhenium filament was looped through a 1/4" length of 2-hole ceramic rod and spot welded to the TCD feedthrough. A mixture of potassium glass, 1 K_2O : 1 Al_2O_3 : 2 SiO_2 by weight, was suspended in an acetone slurry, deposited on the wire loop, and heated with a bunsen burner. The grid plate was removed from the source and the filament housing and endplate containing the bead were installed, allowing the filament housing to be electrically isolated. In this configuration the bead surface was located directly over the source exit aperture at a distance of

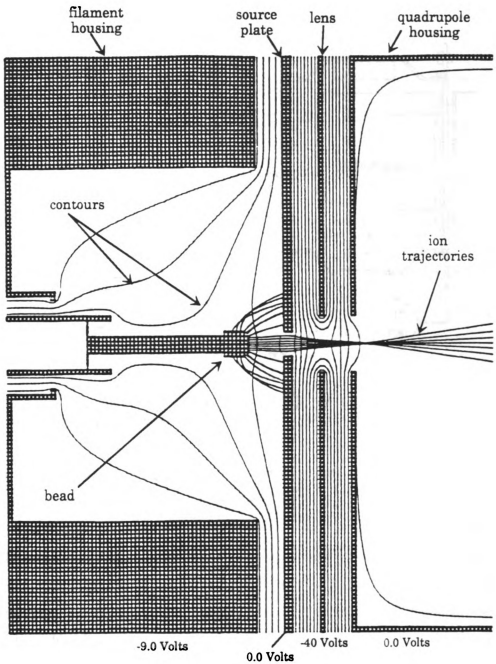

Figure 3.36 A SIMION model of the Anavac source modifed for surface ionization.

~ 2 mm. The entire source was assembled, wired, and installed on the test chamber. External power supplies were used to bias the components, the diagram of the power supply and metering setup used in this study is shown in Figure 3.37.

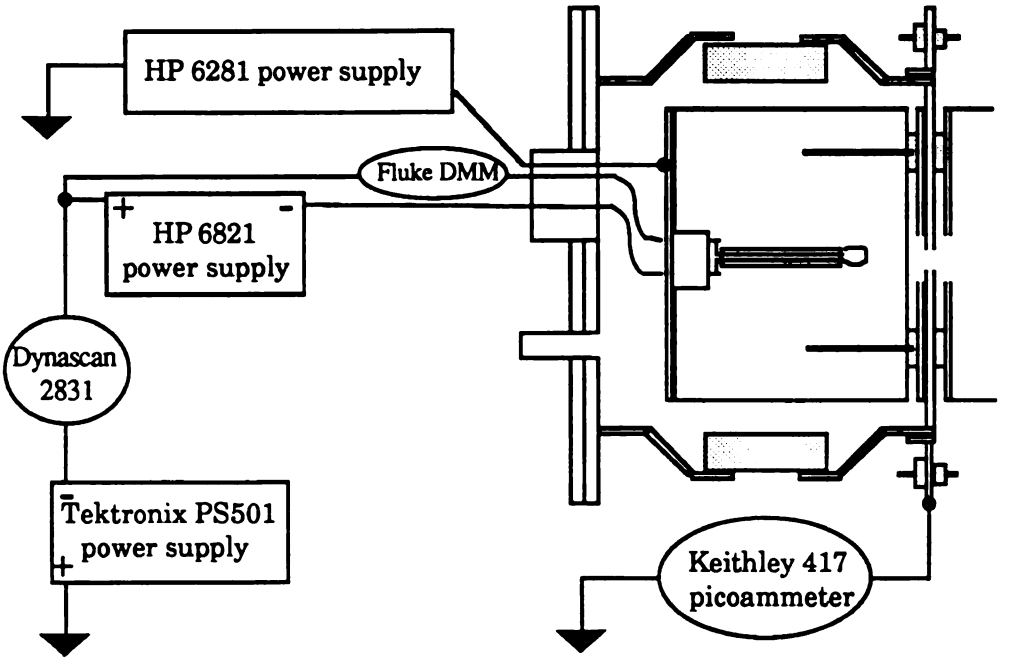

Figure 3.37 The power supply and metering setup used to operated the Anavac surface ionization source.

A Hewlett Packard 6821 high current power supply was again used to head the bead filament and a Fluke 23 DMM was used to monitor heater current. A Tektronix 501 regulated power supply provided the bead bias and a Dynascan 2831 multimeter was connected between the bead bias supply and the emitter to measure total bead emission. A Hewlett Packard 6281 regulated power supply was used to supply the filament housing potential. A Keithley 417 picoammeter was connected to the source plate to monitor source current, and a Keithely 610C electrometer was connected to the shielded Faraday plate at the end of the quadrupole to measure ion current produced by the quadrupole. Other operating potentials were supplied by an unregulated variable voltage power supply not shown.

The bead support filament was heated and the filament housing and lens potentials were optimized for maximum rf-only output with a bead bias of -3.0 V. The control unit was then switched to mass scan mode and a mass spectrum was taken from m/z = 1-60. The spectrum recorded on an XY recorded is shown in Figure 3.38a. The operating conditions for this study were: source = +3.0 V, filament housing = +9.0 V, and lens = -40 V. The filament heater current was 0.95 A which produced a total emission of 0.972 uA, and source current of 140.7 nA. The rf-only signal obtained prior to this scan was 1.31×10^{-8} A and the maximum m/z = 40 current of 1.46×10^{-9} A was measured. This scan was obtained with the 3 mm quadrupole exit aperture in place, the dc balance on the quadrupole offset with +dc 10% above -dc, and the dc/rf ratio set to a central position within the range of VR2. A series of source output measurements were performed at different heater currents, and a close relationship between source current and mass-selected output current was observed. This relationship proved useful for monitoring the output of the source during matrix isolation experiments. The strong output from this potassium surface allowed the easy optimization of source operating conditions, and could prove useful if matrix isolation studies are performed that require a strong current of K^+ ions.

The optimum source operating conditions determined using the potassium emitter were reversed for use in negative surface emission. A cesium bead was prepared by applying 2 SiO_2 : 1 Al_2O_3 : 1.58 $CsNO_2$ mixture suspended on a acetone slurry to another 0.007" Re wire loop. This was spot welded to the TCD feedthrough and installed in the source. The unit was attached to the test chamber and the same power supply and metering setup was connected, with the polarity of the outputs reversed. The chamber was pumped down to a base pressure of 1.6×10^{-6} torr and a leak of CCl_4 was introduced through the source inlet to 5×10^{-6} torr. The filament was heated and the source operating potentials were optimized for maximum rf-only output. The optimized operating conditions were:

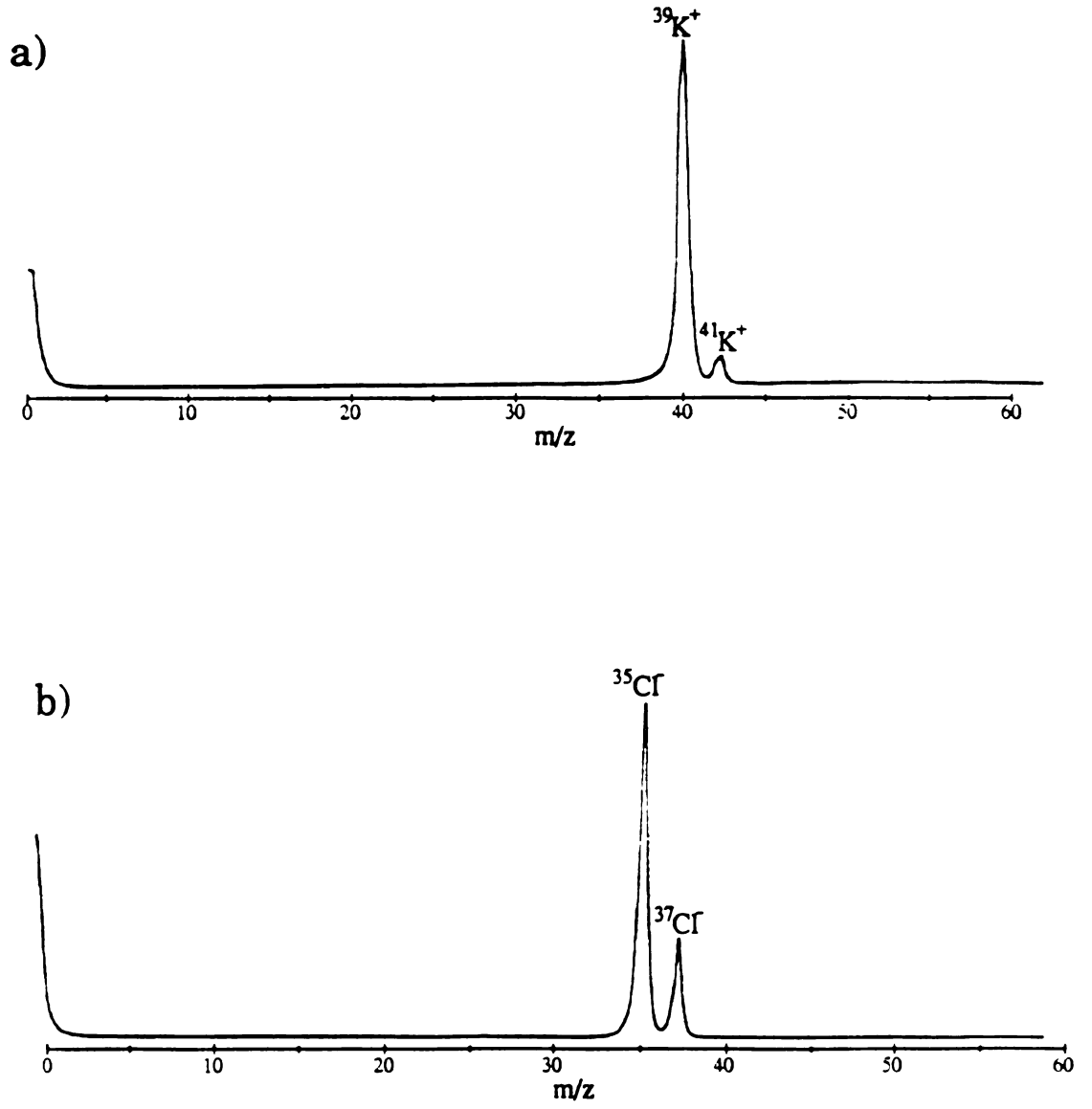

Figure 3.38 Surface ionization spectra produced by the modified Anavac ion source showing a) the output from potassium glass, and b) the output from Cs glass with CCl_4

bead = -2.0 V, filament housing = -13.7 V, and lens = +43 V. The control unit was switched to mass scan mode and the mass spectrum was obtained, which is shown in Figure 3.38b. This scan was taken at a scale of 1" = 0.1 nA, with a heater current of 1.9 A which produced a source current of 10 nA, and total emission of 0.1 uA. Pressure and heater current optimization studies were performed, and a mass-selected output in excess of 1 nA was produced. Once again the current at the source plate proved to be a good indicator of both the rf-only and mass-selected outputs from the source. At higher filament emission levels the total filament emission also proved to be a good indicator of source output, and was somewhat more stable indicator than source plate current.

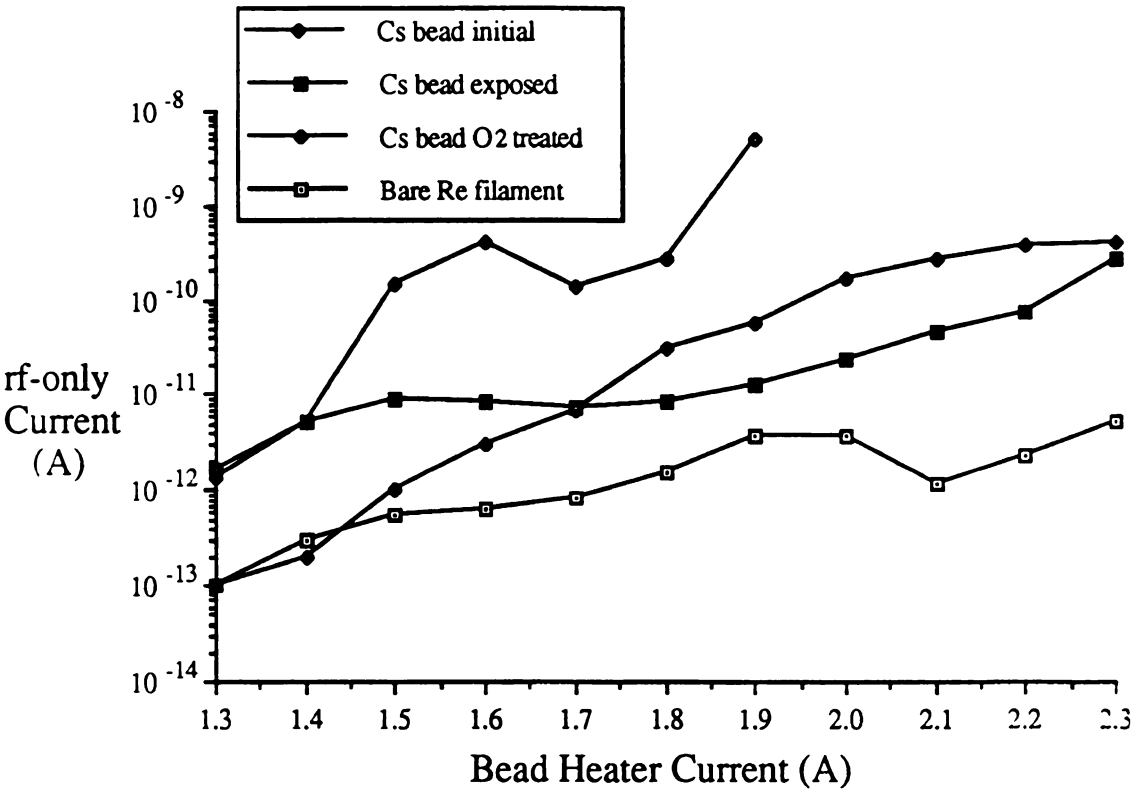

Figure 3.39 A comparison of the NSI rf-only output for several surfaces.

After several hours of exposure to CCl_4 the maximum output from the source decreased to ~0.2 nA. This decrease in performance was accompanied by a decrease in source current. Increasing the filament

accompanied by a decrease in source current. Increasing the filament heater current only increased the mass-selected ion output nominally. To attempt to regenerate the surface, the aged bead was heated and exposed to oxygen at a pressure of $3x10^{-7}$ torr for 10 minutes. The output of the surface under a CCl_4 leak was then tested. Finally the output of the fresh Cs surface, aged Cs surface, and O_2 treated surface were compared to that of a bare rhenium wire installed in the source and operated under the same conditions. The results of these studies are shown in Figure 3.39 which shows the rf-only output for each surface plotted against filament heater current. The highest output was observed with the fresh cesium bead. After several hours of exposure to CCl_4 the output from the same surface decreased to the level shown as 'Cs bead exposed'. This same surface was exposed to oxygen which improved its output at higher heater currents and is shown as 'Cs bead O_2 treated' in Figure 3.39. Finally, a bare 0.007" rhenium loop was studied and its output observed to be much lower than any of the cesium surfaces.

A study was also performed to determine the long term stability of the NSI source using a cesium surface, the results of this study are shown in Figure 3.40. The source was operated at: bead bias = -2.5 V, filament housing = -10.0 V, and lens = +35 V. Prior to this study a new cesium bead was installed, heated, and exposed to CCl_4 for ~ 1 hour. The base pressure of the system was $1.6x10^{-6}$ torr and CCl_4 was introduced to $5x10^{-6}$ torr. The filament heater current was maintained at 2.6 A to simulate unmonitored operation of the source. The output of the source was monitored for over one hour and the source current, rf-only current, and m/z = 35 current were measured at 10 minute intervals. Figure 3.40 shows plots of a) rf-only and source current with time, and b) m/z = 35 and source current with time. The source current was somewhat unstable with time, and the rf-only and m/z = 35 currents reflect this change in total surface emission. Although the source output was not very stable with time, mass-selected ion currents in excess of 0.2 nA were produced over the length of the study.

This study was repeated, and by manually regulating the source current both the rf-only and m/z = 35 currents could be maintained at a relatively constant level.

These preliminary studies indicate that negative surface ionization will prove useful for producing mass-selected negative ion beams for matrix isolation experiments. Further studies to improve the output and stability of these systems need to be made. Some areas that could be investigated to improve the performance of these sources include:

1. Investigating the influence of bead alignment with the source aperture.

2. Studying the use of other types of surfaces such a LaB_6 and Th-Ir with other gases and/or solids.

3. Investigating the effect of treating the surface with oxygen as a means to regenerate the surface while under vacuum.

4. Changing the ion exit aperture size to increase the total ion output from the source

5. Investigating the use of a floatable picoammeter to allow the application of a bias to the source plate which could be used to create stronger electric fields at the surface of the bead.

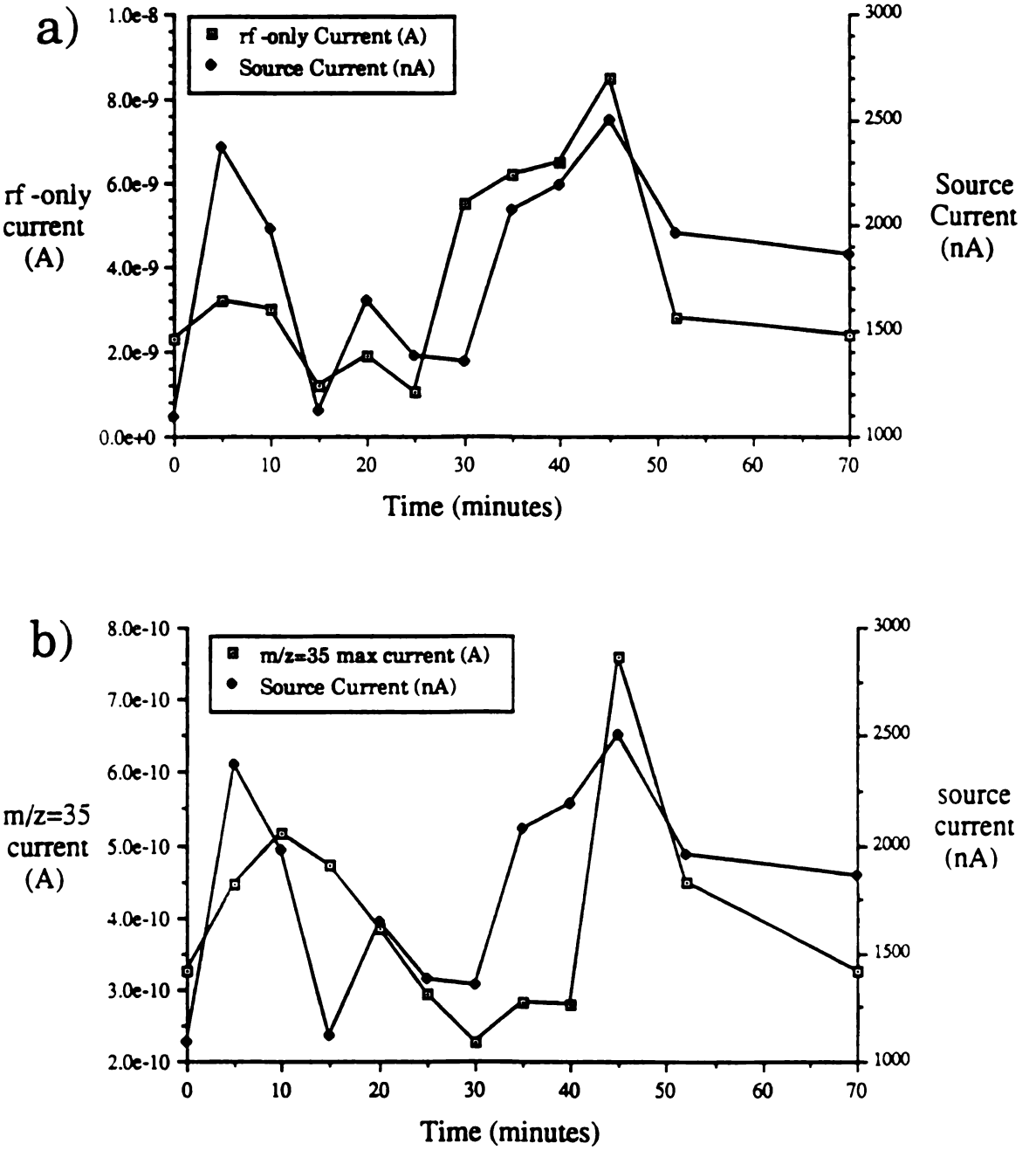

Figure 3.40 Time stability data for the production of negative ions from a Cs glass surface with the modified Anavac source monitoring a) rf-only and b) m/z = 35 currents with time and source current.

Chapter 4. Dycor M200 Ion Source Modifications

I. The design and performance of the Dycor M200 source

The second residual gas analyzer selected for modification was a Dycor Ametek model M200 RGA. This RGA was designed to analyze background residual gases from pressures of $1x10^{-3}$ to $1x10^{-11}$ torr. The Dycor M200 has a larger quadrupole than the Anavac-2 and produces higher amplitude rf signals which allow it to mass-select ions from m/z 1-200. The source sensitivity of the unit is quoted at $2.0x10^{-4}$ A/torr for nitrogen, taken at a resolution of 10% valley. The minimum peak width the Dycor M200 can achieve is 0.5 amu at 10% valley with a drift of <0.1 amu per hour following warmup. This RGA was originally purchased for ~$5,000, and was selected primarily due to its low cost and extended mass range.

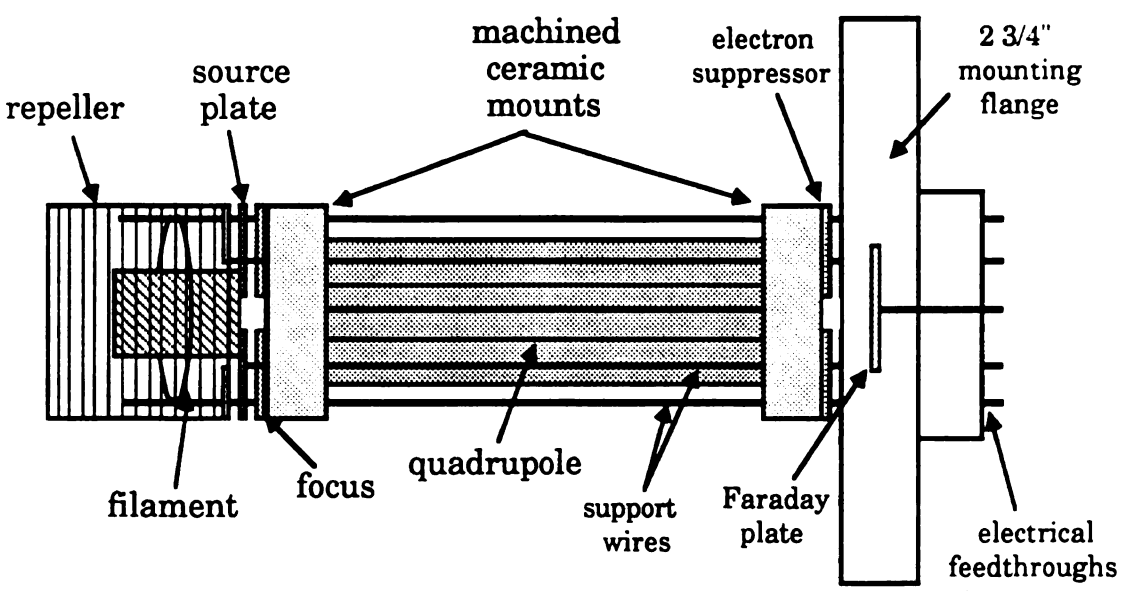

Figure 4.1 A block diagram of the Dycor M200 analyzer head.

The RGA consists of four units; the analyzer head, the power supply, the electrometer/amplifier remote head, and the control unit. The analyzer head includes all components that are inserted into the vacuum chamber. It was designed to mount on a 2 $^3/_4$" conflat flange, and the source, quadrupole and detector components were originally housed in a ~160 mm long tube fitted with 2 $^3/_4$" conflat flanges. The total length of the unit from the feedthrough flange to the end of the source was 171 mm, and the diameter of the system was 34 mm. The components of the source include the: electron repeller, source grid/plate, focus lens, quadrupole, electron suppressor, and Faraday plate. These are shown in Figure 4.1. All the components except for the Faraday plate are connected to the feedthroughs in the mounting flange by 1/16" stainless steel rods. These rods provide both physical support and electrical contact for each component. The unit is disassembled by loosening the connectors that couple these support rods to the electrical feedthroughs in the mounting flange.

The Dycor M200 uses an EI source similar to the Anavac-2 source, but of a more open design. The source components include the repeller, filament, source plate, and focus lens shown in Figure 4.1. Instead of a solid filament housing surrounding the filament, the Dycor M200 uses a repeller grid (32 mm diameter, 41 mm length) that is biased negative with respect to the filament to create an electric field that causes the electrons to travel toward the source grid. This open grid design is used to increase conductance into the source and thereby increase the source sensitivity for residual chamber gases. The filament is mounted inside the repeller grid on two filament support rods connected to feedthroughs on the mounting flange. The filament is a loop ~ 20 mm in diameter that is spot welded to the two support rods. This design effectively gives the source two filaments. If one arm of the filament loop burns out, the other side can still operate, extending the period between filament replacement. This filament loop design also increases the total emission surface of the

filament and better matches the circular symmetry present in the source. The source plate/grid is similar in design, but larger than, the source plate/grid in the Anavac-2 source and normally is positioned with the grid inserted inside the repeller cage and the source plate 2.4 mm from the end of the repeller. The wire grid is cylindrical with a 14.5 mm diameter and length of 26 mm. It is spot welded to the source plate which is a 0.5 mm thick cylindrical plate with an outside diameter of 32 mm and has a central 6.3 mm diameter ion exit aperture. The focus lens is positioned 2.4 mm from the source plate and is also a 32 mm diameter cylindrical plate with a central 6.3 mm diameter aperture. The focus lens also has a set of fine cross wires spot welded across the central aperture. These are installed to eliminate ions that would enter the quadrupole from those initial positions. The cross wires are aligned so that they lie along the axes between the quadrupole rods, by eliminating these initial ion entry positions the amount of peak tailing in the mass spectrum is reduced as discussed in Chapter 2.II.C.

The Dycor M200 quadrupole is much larger that the Anavac-2 quadrupole with a rod length of 114 mm, rod diameter of 10.0 mm, and rod spacing of 6.0 mm. The four rods are mounted in machined ceramic mounts that also contain holes through which the component support rods are inserted, thereby further ensuring the proper positioning of the source components. These quadrupole dimensions yield a r/r_o of 1.67, which is close to the ideal value of 1.148 discussed in Chapter 2.II.C. The quadrupole is normally operated with a maximum of 1000 $V_{p\text{-}p}$, 2.27 MHz rf signal and an average ion energy of 7 eV. The ultimate performance that can be achieved with system can be calculated using the theoretical equations described in Chapter 2.II.C for maximum mass (M_m) and minimum peak width (ΔM_{min}) as:

$$M_m = \frac{7\text{x}10^6 V_m}{f^2 r_o^2} = \frac{7\text{x}10^6 (2000\ \text{V})}{(2.27\text{x}10^6\ \text{Hz})^2\ (3.0\text{x}10^{-3}\ \text{m})^2} = 302\ \text{daltons}$$

$$\Delta M_{min} = \frac{4x10^9 V_z}{f^2 L^2} = \frac{4x10^9 (7\ eV)}{(2.27x10^6)^2 (0.114\ m)^2} = 0.42\ daltons$$

These calculations indicate that the Dycor M200 quadrupole is operating well below its ultimate maximum mass, but at approximately the best resolution that could be achieved. This is most likely some compromise between sensitivity, construction costs, mechanical tolerance in quadrupole manufacture, and user needs.

An electron suppressor plate is mounted after the quadrupole and serves as the quadrupole exit aperture. This component is a 32 mm diameter cylindrical plate with a central 6.3 mm aperture, and is normally biased at -120 Volts to suppress electron noise from the source. The ions are detected by a shielded Faraday plate that is mounted within the 2 $^3/_4$" mounting flange.

The power supply unit provides dc voltages to the analyzer head, generates the rf and dc signals used to operate the quadrupole, and contains the power supplies and emission control necessary for the operation of the filament. It also houses the analog-to-digital converters that convert the analog signals from the electrometer head and analyzer into the digital format for manipulation and display by the control unit. The power supply can produce a 1 to 5 V potential, across the filament leads, which is regulated to produce an emission current (monitored at the source plate) determined by the control unit. The rf power supply is frequency-variable from 2 to 3 MHz, controlled by the control unit, and fed to the electrometer head through a BNC cable. All other potentials are fed to the electrometer head and analyzer through a ribbon cable.

The electrometer/amplifier remote head attaches to the 2 $^3/_4$" mounting flange on the analyzer head. Most of the operating potentials for the analyzer simply pass through this unit with some added dc capacitive filtering. This remote head also houses the sensitive, optically coupled

amplifier for detecting ion currents at the Faraday plate, and the rf transformer used to increase the amplitude of the rf signal produced by the power supply unit.

The control unit is used to display and control the operation of the entire system. It is microprocessor controlled, and contains a CRT that allows the user to display and change the value of a series of operational parameters that are used to control the power supply unit. It also allows the operator to store two 600 point intensity files, or spectra, which can be displayed, printed, or uploaded through an RS232 port. The RS232 port can also be used to modify the value of the operational parameters of the RGA, making remote control and data acquisition possible with a personal computer. The control unit operation parameters control all the functions of the RGA, a description of their function is given below and a list of their initial values is given in Table 4.1.

TOTAL PRESSURE - turns on the total pressure mode for the RGA, in this mode the RGA will switch to rf-only mode between scans and also display the filament resistance, voltage, current, and RF TUNE values

LO MASS - sets the lower limit of the scan range for the quadrupole

HI MASS - sets the upper limit of the scan range for the quadrupole

SAMP/AMU - sets the number of stored data points per amu for the mass scan

DWELL - sets the sampling time for each data point in the mass spectrum

EMISSION - sets the filament emission regulation level, monitored at the source grid, and displayed as ELECT CUR on the control unit

EL ENERGY - sets the potential difference between the source grid and the filament rods, which varies if the source potential changes with m/z

FOCUS - sets the potential energy applied to the focus lens

REPELLER - sets the potential applied to the repeller surrounding the source

FREQUENCY - sets the rf frequency of the power supply, in TOTAL mode the user can observe the RF TUNE parameter to monitor reflected rf power

FIL PROT - sets upper pressure limit for overpressure protection of filament

ANALOG MODE - scans the quadrupole between LO MASS and HI MASS values, records and displays analog intensity vs m/z spectrum

BAR MODE - scans quadrupole between LO MASS and HI MASS values, records analog intensity vs m/z spectrum, integrates points within 1/4 amu of peak mass for bar intensity display.

TAB MODE - selected ion monitoring for up to 12 masses

LO RES and HI RES - sets rf/dc ratio on quadrupole at the low and high ends of mass spectrum

LO POS and HI POS - allows user to align mass spectrum with the display mass axis

LO SENS and HI SENS - sets ion energy (1 to 10 eV) at the low and high ends of the mass range, ion energy is varied linearly between these values during a mass scan allowing the user to operate the unit in constant sensitivity or constant peak width modes

Table 4.1 The initial values of the Dycor M200 operating parameters for the original thoriated iridium filament.

EMISSION = 1.0E-03	EL ENERGY = -70.0 V	FOCUS = -31.0 V
REPELLER = -72.0 V	FREQUENCY = 2.27E+06	RF TUNE = 6.552
LO RES = 4048	HI RES = 2427	LO SENS = 6.00
HI SENS = 8.30	FIL PROT = 1.0E-03 torr	FIL = ON
FIL VOLTS = 2.0 V	FIL CUR = 2.9 A	FIL RES = 0.68

A study was performed to evaluate the resolution and mass range performance of the Dycor M200 RGA prior to modification. Both the Dycor M200 and another Dycor M100 RGA (1-100 m/z range) were mounted on the matrix isolation chamber. The chamber was evacuated to a base pressure of 4×10^{-9} torr, and a leak of perfluorotributylamine was introduced into the system to a pressure of 5.8×10^{-6} torr measured by the

M100. The M200 was set to DWELL = 1.0 seconds, and 6 SAMP/AMU and scanned from m/z = 1-200 in ANALOG mode. A plot of the mass spectrum produced by the M200 is shown in Figure 4.2. The highest mass that was observed in the spectrum was m/z = 181, but the unit appeared to operate properly to m/z = 200, at which point the scan was automatically reset. The unit produced ~20% valley resolution throughout the entire mass range, with a slight increase in peak width at higher masses. The peak width increase at higher masses resulted from the operation of the quadrupole with the ion energy increasing from 6 eV at m/z = 1 to 8.3 eV at m/z = 200.

II. Modification of the Dycor M200

Following evaluation of the original performance of the Dycor M200 RGA, the analyzer head was modified to produce a beam of mass-selected ions. To allow the introduction of sample gas directly into and minimize conductance from the source region, a source housing was designed similar to the source housing used with the Anavac-2. The design was based upon results from SIMION modeling studies of the Dycor M200 EI source. The source elements were carefully measured, and a 16,000 point circular symmetry SIMION electrode array was constructed that closely reproduced these dimensions. The SIMION array was refined, and the standard operating potentials for the source were applied to the electrodes. Figure 4.3a shows the refined SIMION model of the original source with the repeller = -72 V, source grid = +6.0 V, focus lens = -31 V, and quadrupole at 0.0 V. Equipotential contour lines were displayed to illustrate the penetration of the extraction field from the focus element into the source grid and the focal properties of the lens system. The trajectories of electrons formed at the filament position were modeled to determine the region within the source grid of highest electron density. The trajectories of 75 ions formed within this region are shown in Figure 4.3a. All the ions

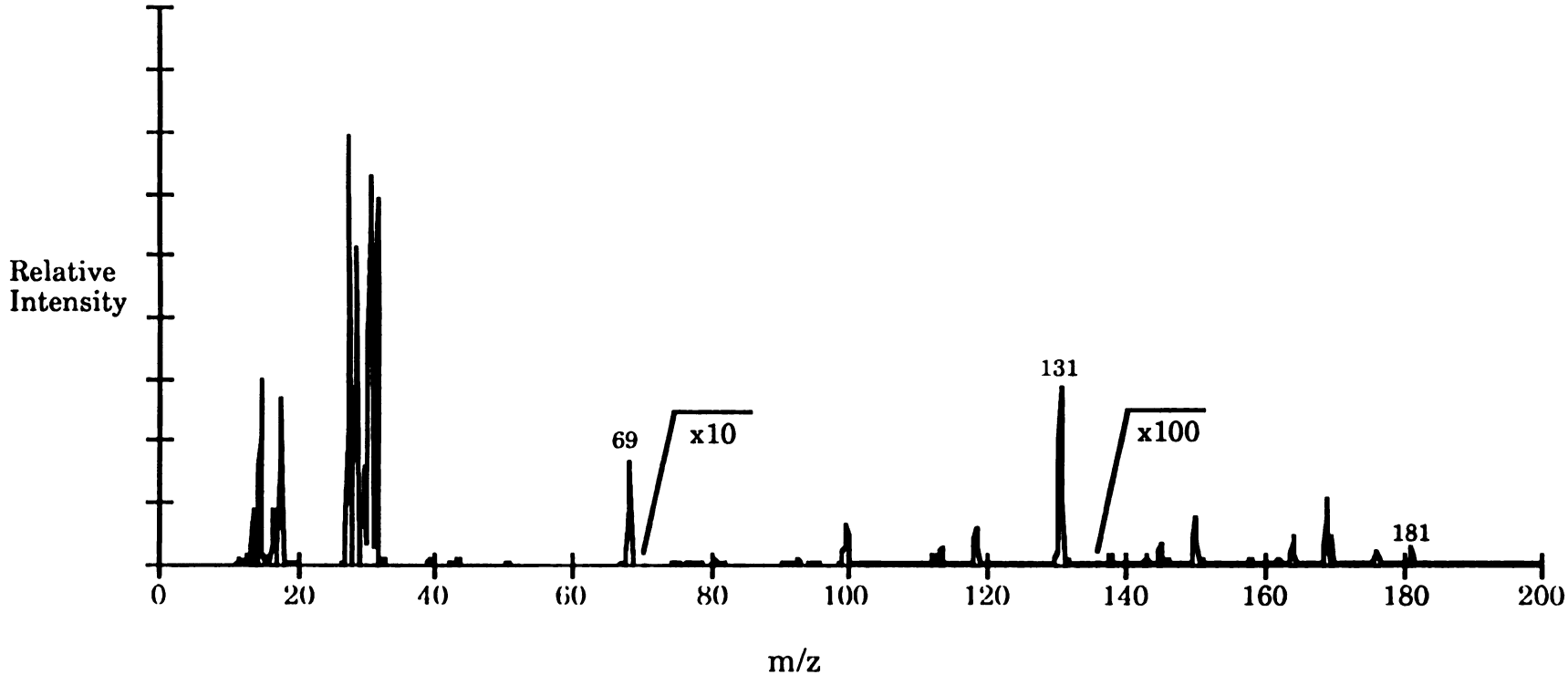

Figure 4.2 The mass spectrum produced by the original Dycor M200 RGA for perfluorotributylamine.

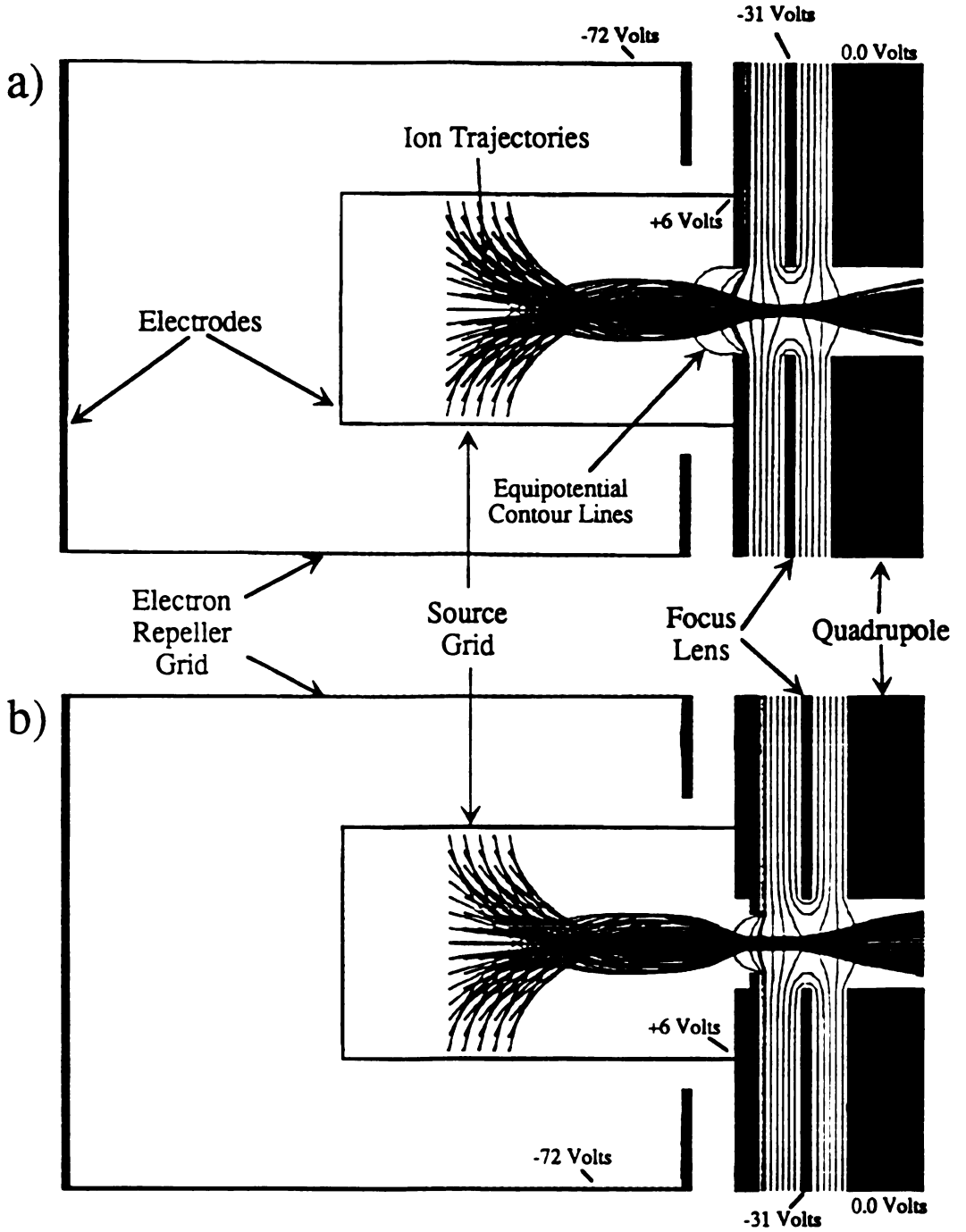

Figure 4.3 SIMION models of the Dycor M200 source a) before modification and b) following enclosure in a source housing.

that were modeled experienced sufficient drawout potential from the focus element to be extracted from the source and injected into the quadrupole, producing the ion beam profile shown. A second SIMION model was constructed based on this model, but with a reduced ion exit aperture and additional lens thickness that represented the placement of the source within a source housing. The model, shown in Figure 4.3b, was refined, the elements were biased at the same operating potentials, and the contour lines and trajectories calculated for the previous model were recalculated and displayed. The contour lines in Figure 4.3b clearly shows a reduction in the penetration of the extraction field due to the smaller ion exit aperture in this model. The ion trajectories calculated for this model were almost identical to those calculated in Figure 4.3a, indicating that enclosing the source should effect the ion beam injected into the quadrupole only slightly. These results were similar to those observed earlier in the SIMION modeling studies of the Anavac-2 source housing.

Following the SIMION modeling of the Dycor M200 EI source, a source mount was designed and constructed to enclose the EI source, turn around the unit so that the ion beam was directed inward toward the matrix experiment, and feed the electrical and gas lines to the various analyzer components. Figure 4.4 shows a mechanical drawing of the completed analyzer chamber with the analyzer components installed. The EI source housing was constructed using a Ceramaseal 807A0296-1 metal/ceramic/envelope for the housing body. The upper end of this envelope was welded to a 4 $^1/_2$"-to-6" conflat conversion flange, labeled as the support flange in Figure 4.4. A 0.5 mm thick stainless steel plate was welded to the lower end of the envelope and a 6.3 mm aperture was drilled in the center of this plate to serve as the ion exit aperture. Threaded rods extending 10 mm inside the source housing were silver soldered into this plate. The support rod attached to the Dycor source plate was sheared off, and the source plate was bolted onto these threaded rods. This configuration allowed the source grid/plate to be mounted within the

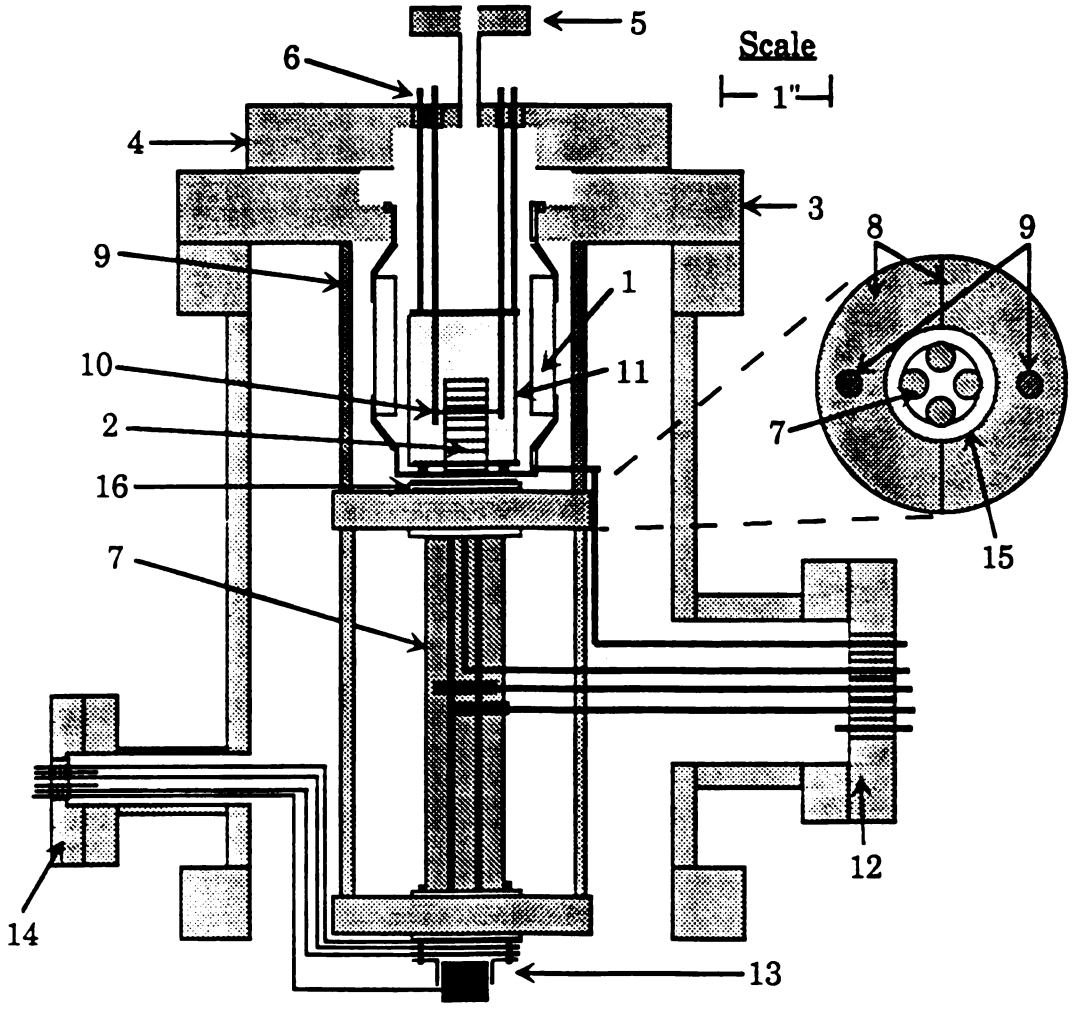

Fig. 4.4 The modified Dycor M200 RGA mass selected ion source. Components include; (1) enclosed source housing, (2) source grid, (3) support flange, (4) feedthrough flange, (5) gas inlet, (6) source electrical feedthroughs, (7) quadrupole rods, (8) clamp rings, (9) support rods, (10) filament, (11) electron repeller, (12) original RGA mounting flange, (13) focusing/deflection optics, (14) multi-pin feedthrough, (15) ceramic mount for quadrupole rods.

enclosed source housing while adding only the additional thickness of the housing endplate to the ion optical system.

A 4 1/2" conflat flange was used as a mount for the repeller, filament, and sample inlet lines. A miniconflat flange connected to a 1/4" stainless steel tube was welded into the center of this flange to serve as the sample inlet line. Four Ceramaseal 809B8030-1 high current BNC vacuum feedthroughs were mounted around the inlet line, and arranged to reproduce the original positioning of the filament and repeller components in the Dycor RGA. The support rods for the filament and repeller were shortened by ~50 mm, and connected to these feedthroughs using the original RGA connectors. The repeller was positioned to extend 84 mm from the face of the 4 1/2" flange. When the unit was inserted, this distance closely reproduced the original 2.4 mm spacing between the repeller and the source plate. Ceramic sheaths were placed over the upper half of the filament support rods to insulate them from the repeller, a 0.005" rhenium wire loop was spot welded to the rods, and they were fed through the repeller and connected to the feedthroughs on the 4 $^1/_2$" flange. The fourth feedthrough on this flange was connected to the source plate using flexible, Teflon-coated wire. With these connections completed, the feedthrough flange was carefully installed on the 6" mounting flange and tightened down. This mounting system closely reproduced the 2.4 mm spacing between the repeller and source plate elements, while enclosing the source in a low conductance housing. The potentials to the source plate, repeller, and filament could be fed via BNC feedthroughs in the 4 $^1/_2$" flange, and sample gas could be directly introduced into the source housing.

Two 1/4" stainless steel support rods were installed in the mounting flange as shown in Figure 4.4. These were used to support two sets of clamp rings that fit around the ceramic quadrupole mount. The focus lens was installed through the quadrupole ceramic, and both components were inserted inside the clamp rings. Tightening two setscrews, mounted

in the clamp rings, allowed the quadrupole ceramic to be locked into a position that placed the focus element at a distance of 2.4 mm from the bottom plate of the source housing. A 193 mm long chamber was constructed to house the source and quadrupole. Each end of this chamber was welded to rotatable 6" conflat flanges, with the support flange attaching to the upper flange, as shown in Figure 4.4, and the lower flange connecting the unit to the matrix isolation chamber. Two ports, a 2 $^{3}/_{4}$" and a miniconflat port, were installed on opposite sides of this chamber. The 2 $^{3}/_{4}$" port was positioned opposite the quadrupole connection rods at a distance that closely reproduced the original, ~ 75 mm, distance from these rods to the Dycor mounting flange. The support rods on the quadrupole were shortened, and the original Dycor connectors were modified so that these lines could be sent out the 2 $^{3}/_{4}$" port where they were connected to the feedthroughs on the original Dycor mounting flange. The focus element was also wired through this feedthrough flange using flexible Teflon-coated wire. This connection scheme closely reproduced the original wiring used to supply the rf and dc potentials to the quadrupole rods, minimizing the change in the resonant frequency of this quadrupole circuit.

A Ceramaseal 808B9340-1 8-pin miniconflat electrical feedthrough was mounted on the opposite port and the feedthrough pins were connected to flexible Teflon-coated wires to supply potentials to the lens system. A series of deflection optics were fabricated that were designed to mount at the exit end of of the ceramic quadrupole mount as shown in Figure 4.4. Circular einzel lens elements were machined from 0.5 mm stainless steel stock to an outside diameter of 32 mm. Elements with several center aperture sizes were machined including; 1/4"(6.3 mm), 7/32" (5.5 mm), 3/16"(4.8 mm), and 9/32" (7.1 mm). Two sets of four deflection plates were manufactured that were 1/2" wide and 1/2" and 3/4" long. All of these elements were designed to attach to threaded rods installed through the quadrupole ceramic mount. These threaded rods

were isolated from the lens components by glass sheath rods, and the distance between components was determined by the ceramic spacers used to separate the individual elements.

The source filament used following modification was 0.005" rhenium wire, this was chosen because of its low cost and availability. A minor modification was made to the control board of the power supply unit to allow it to create the higher heater current necessary to operate with this higher work function material. A 3 kΩ resistor was added parallel to R22 on the power supply control board which is shown circled in Figure 4.5. This modification allowed the filament to operate at higher current levels than before modification, which were necessary to heat the rhenium wire to the 1-3 mA emission levels for normal operation of the RGA.

It was also necessary to patch into the ribbon cable connecting the power supply to the electrometer head to allow the source, filament, and repeller lines to connect to the BNC feedthroughs on the 4 $^1/_2$" feedthrough flange. A bud box was installed which connected to the ribbon cable connector on the back of the power supply unit. All connections except for the repeller, source, and filament lines were fed through this box to the ribbon cable. The repeller, source and filament lines were connected to high voltage BNC feedthroughs on the box. High voltage BNC cables were made that connected to another bud box attached to the source chamber. This box contained 0.01 uF capacitors used as noise filters on the source components. One end of the BNC cables fed through this box was connected to the power supply patch box, and the other to the feedthroughs on the source feedthrough flange. These modifications allowed the remote electrometer head to attach to the original Dycor mounting flange, supplying the rf/dc potentials to the quadrupole and the dc potential to the focus element, while the the patch boxes allowed the repeller, filament, and source potentials to be fed through BNC cables to the removable feedthrough flange.

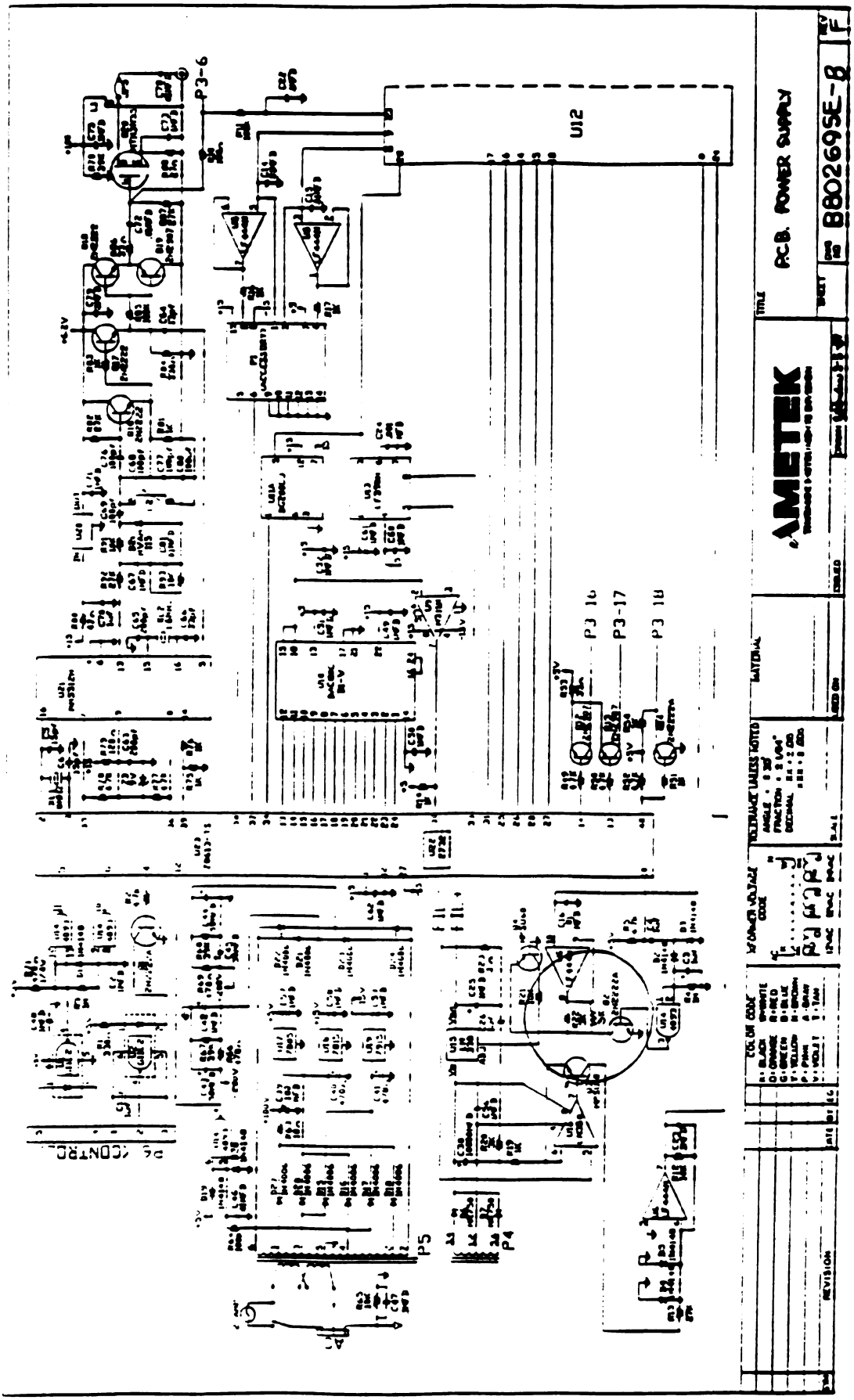

Figure 4.5 A schematic diagram of the Dycor M200 power supply board including the addition of a resistor (circled) to allow the use of 0.005" rhenium filament wire.

III. Performance evaluation of the completed ion source

Following fabrication of the components of the source mount, a 0.005" rhenium filament was spot welded to the filament support rods and the source feedthrough flange was installed. The quadrupole and focus lines were connected to the original Dycor flange, and a shielded Faraday plate was installed after the quadrupole. The Faraday plate was connected to a miniconflat electrical BNC feedthrough flange mounted on the miniconflat port of the source housing. A Granville Phillips model 60 leak valve was installed on the source inlet line, and the entire assembly was connected to the left 6" port on the matrix isolation chamber. The chamber was evacuated, and the electrometer head and BNC lines from the patch boxes were connected to the source mount. A Keithley 610C electrometer was connected to the miniconflat BNC port to monitor Faraday plate current.

Both the power supply and control unit were switched on, and the rf frequency of the system was optimized. With the filament off, the unit was switched to total pressure (rf-only) mode which caused the control unit to display the value of the RF TUNE parameter. This parameter is a measure of the rf power that is reflected back from the rf transformer into the power supply. The RF TUNE parameter can vary from 0 to 10, and in the original configuration the unit had an RF TUNE of 6.552. With an rf frequency of 2.27 MHz the value of RF TUNE displayed on the control unit following modification was 10.0, indicating a high level of reflected rf power and poor rf power transfer to the quadrupole. The frequency of the rf power was varied at the control unit using the FREQUENCY parameter while observing the value of the RF TUNE parameter. A plot of RF TUNE verses FREQUENCY is shown in Figure 4.6a. The FREQUENCY parameter was varied from 2.27 MHz to 2.35 MHz, and a minimum RF TUNE value of 6.493 was obtained at a FREQUENCY of 2.308 MHz. This

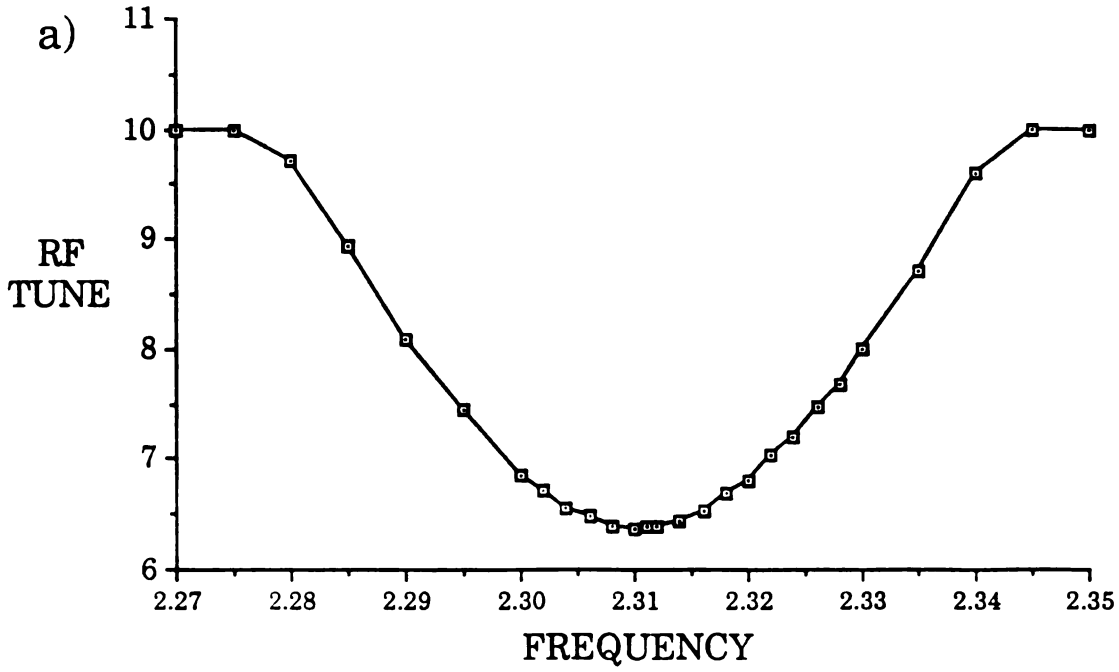

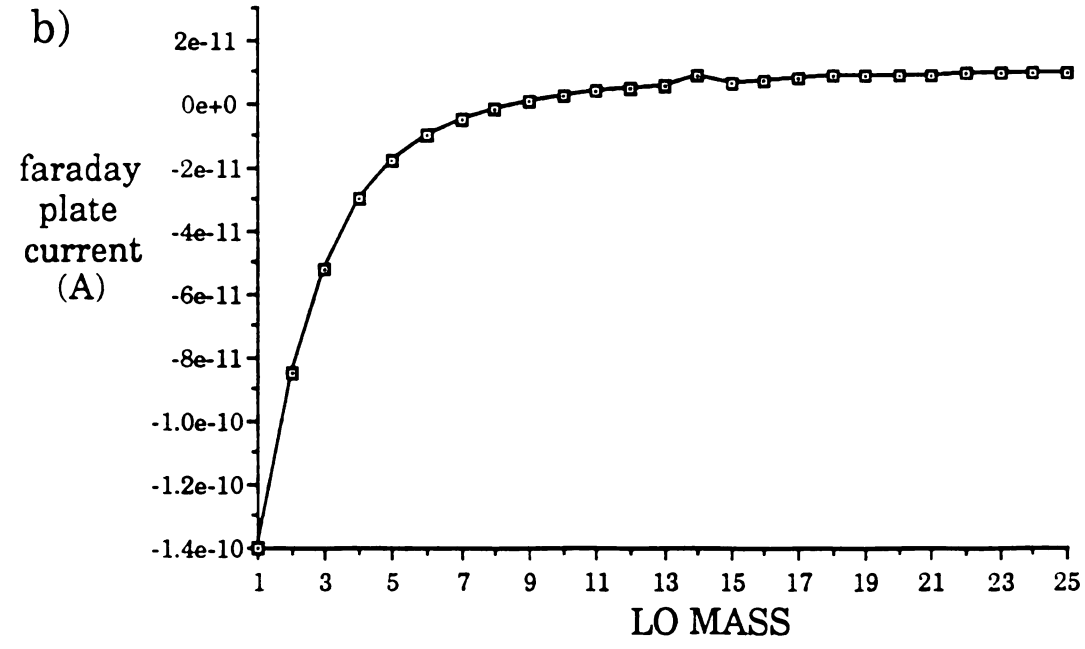

Figure 4.6 Graph of both the RF TUNE parameter versus FREQUENCY (a), and the faraday plate curent vs LO MASS setting (b) for the modified DYCOR M200.

RF TUNE value was lower than the original setting, indicating that the rf reflected power had been decreased through the quadrupole wiring modifications and that the unit should operate properly.

After the rf frequency was optimized, the total mode was switched off, and the unit was switched to mass scan mode. The filament was turned on, and set to an EMISSION level of 1 mA, the source was operated with EL ENERGY = 70.0, REPELLER = -72 V, and FOCUS = -31 V. The LO MASS parameter was set to 1 and the HI MASS parameter set to 100. As soon as the filament was switched on, a signal of -1.4×10^{-10} A was detected at the Faraday plate, indicating that electrons from the filament were passing through the quadrupole and hitting the Faraday plate. In the original Dycor these electrons were eliminated by placing a suppressor plate before the Faraday plate and biasing it at -120 V. The modified M200 source no longer utilized any electron suppression, and a study was performed to determine if the quadrupole could discriminate against electrons at high mass settings. The LO MASS parameter was varied while observing the sign and magnitude of the signal at the Faraday plate. A plot of the Faraday plate current verses LO MASS setting obtained from this study is shown in Figure 4.6b. The LO MASS parameter was varied from 1 to 25 which determined the initial mass that the quadrupole was selecting. A negative current, indicating electrons hitting the Faraday plate, was measured for LO MASS settings less than 10. Above LO MASS setting of 10 the Faraday plate signal was relatively constant, with a slight positive deflection at m/z = 14. This indicated that the quadrupole was effective at discriminating against electrons at settings above m/z = 10, and the positive deflection at m/z = 14 was determined to be the result of a small air leak (N^+ and N_2^{2+}) in the source inlet that was later sealed. As a general rule this source should not be used to mass-select ions lower than m/z = 10 unless a suppressor plate is installed after the quadrupole, or the presence of a background electron current can be tolerated.

The ability of the system to produce mass-selected ions was evaluated by introducing samples into the source, scanning the quadrupole, and observing the current at the Faraday plate. The base pressure of the chamber was $3x10^{-8}$ torr. Argon was introduced through the leak valve to a total chamber pressure of $4.5x10^{-7}$ torr. The Dycor M200 was scanned at a dwell of 2.0 sec with 10 samp/amu and the ion current was detected by a Keithley 610C electrometer which was used to drive an XY recorder that used a time sweep for the x axis.. The source was operated with 1 mA emission, 70 eV electrons, repeller = -72 V, and focus = -31 V. This produced a maximum signal of 11.0 nA at the Faraday plate for m/z = 40. The argon leak was removed, and nitrogen was introduced into the source to a chamber pressure of $4.0x10^{-7}$ torr. With the source operating under the same conditions, a maximum mass selected signal of 10.0 nA was measured at the Faraday plate for m/z = 28.

The nitrogen leak was removed, and a leak of perfluorotributylamine (PFTBA) was introduced to evaluate the resolution and mass range of the modified Dycor M200 source. A PFTBA bulb was cleaned and prepared with three freeze/thaw cycles. This was connected to the source inlet which was evacuated to 50 mtorr. The bulb valve and source leak valve were opened to introduce PFTBA into the source to a chamber pressure of $4x10^{-7}$ torr. The source was operated under the same conditions, and the quadrupole was scanned from m/z 15-190 at a dwell of 2.0 seconds and 10 samples/amu. The spectrum recorded at the XY recorder is shown in Figure 4.7. The bottom trace shows the scan from m/z = 15-105 at a sensitivity of full scale = 10 nA, the central trace show a scan from m/z = 90-160 at full scale = 1 nA, and the upper trace shows a scan from m/z = 150-190 at a sensitivity of full scale = 0.1 nA. The maximum current at the Faraday plate in this spectrum was 2.23 nA at m/z = 69. The spectrum shows well-resolved peaks through the range from m/z = 15-140, above this range the peak width increased dramatically, but ion peaks were observed above m/z = 170. The intensity of the ion peaks

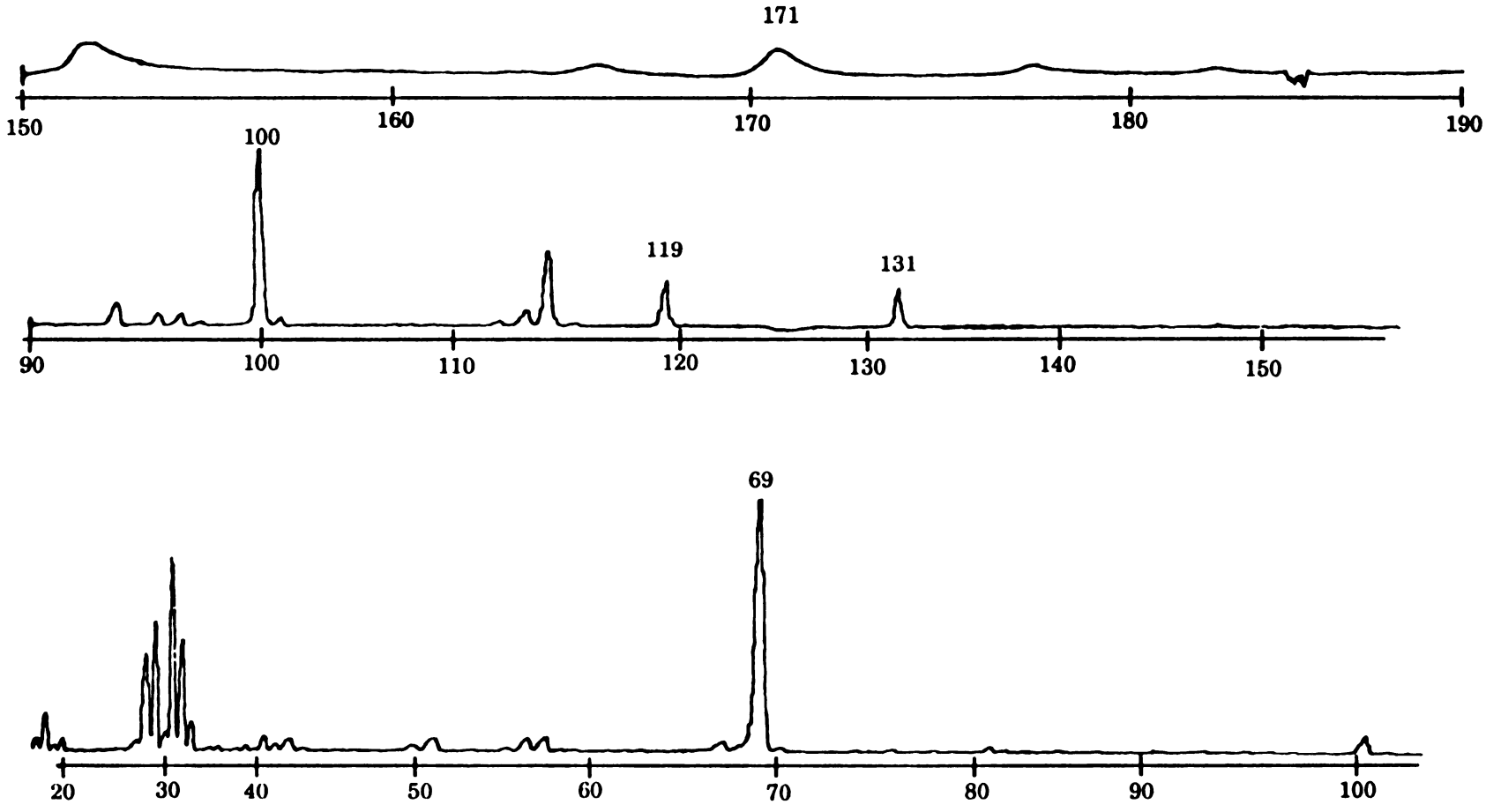

Figure 4.7 The mass spectrum of perfluorotributylamine produced by the modified Dycor M200 source and measured at a faraday plate mounted at the exit of the quadrupole.

in the upper mass range was reduced slightly relative to the PFTBA spectrum taken with the original Dycor M200 RGA. To further evaluate the mass range performance of the unit, the PFTBA leak was replaced with a leak of perfluorokerosene introduced through the source inlet to a pressure of 4.7×10^{-7} torr. The resolution of the unit was reduced from the original HI RES value of 2427 to a value of 2200 to allow better observation of high mass peaks in the mass spectrum. The source was operated under the same conditions, and the quadrupole was scanned from m/z = 20-200 at a dwell of 1.0 second and 15 samp/amu. The spectrum recorded on the XY chart recorded is shown in Figure 4.8. The maximum current obtained in this scan was 2.22 nA at m/z = 69. This spectrum clearly shows peaks up to m/z = 181 indicating that the mass range of the Dycor M200 had not been degraded by the design modifications. The resolution at higher mass values was slightly reduced due to the change in HI RES setting, but approximate unit mass resolution was still observed. This resolution was higher than required for most matrix isolation studies, and in most cases the HI RES and LO RES settings could be decreased to increase ion output from the source.

The ability of the source to produce a mass-selected beam at a remote Faraday plate was evaluated by removing the Faraday plate from the end of the quadrupole, installing a focusing/deflection optics systems after the quadrupole, and monitoring the ion current at the Faraday plate mounted on the linear motion feedthrough 203 mm from the end of the quadrupole. The lens system installed after the quadrupole was based on the design of model 1 from the SIMION deflection optics studies in Chapter 3.V.B. Three lens elements were used to function as an einzel lens. The first two elements had central aperture of 6.3 mm and the third element had an aperture of 7.1 mm. The spacing between these elements was set with 2 mm ceramic insulators, and the first and third elements were connected to ground. Two pairs of $^1/_2$" long deflection plates were placed after the einzel lens. These were offset with the horizontal pair preceding the

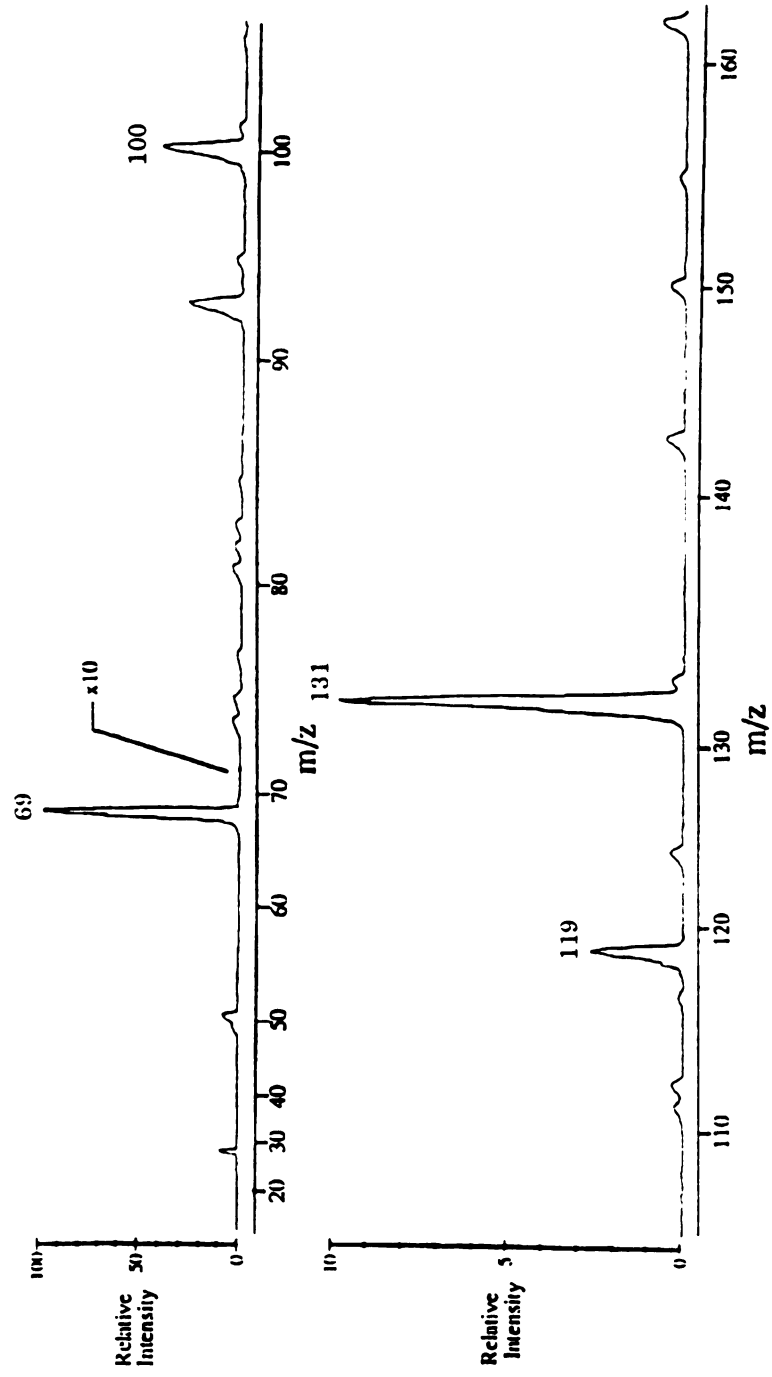

Figure 4.8 The mass spectrum of perfluorokerosene produced by the Dycor M200 source.

vertical pair, and the spacing between each plate pair was also set at 2 mm. This system was installed on the quadrupole ceramic, and flexible Teflon-coated wire was used to connect each element to a feedthrough pin on the 8-pin miniconflat feedthrough. The unit was then installed on the left 6" flange of the matrix isolation chamber and the chamber was evacuated. The linear motion feedthrough was inserted to 0.95" which positioned the 1" diameter Faraday plate mounted at the end of the feedthrough directly in front of the cryostat window, at a distance to 203 mm from the lens system. The lead from the Faraday plate was fed through a BNC miniconflat electrical feedthrough and connected to a Keithley 610C electrometer used to measure ion current and drive an XY recorder.

The base pressure in the chamber was 3.0×10^{-9} torr, and a leak of argon was introduced through the source inlet to a chamber pressure of 6.8×10^{-7} torr. The electrometer head and BNC cables were connected to the source and the unit was turned on. The source was operated at: repeller = -72 V, electron energy = 70 eV, focus lens = -31 V, and filament emission = 1 mA. The unit was set to scan over m/z = 28 and the potentials on the deflection optics were optimized for maximum ion current at the Faraday plate. The optimum values were; center einzel lens = -25 V, lower deflection plate = +1.4 V, right deflection plate = 1.6 V, all other elements were kept at 0.0 V. The quadrupole was scanned from m/z = 1-60 at a dwell of 250 msec with 15 samples/amu. The spectrum recorded on the XY chart recorder is shown in Figure 4.9. This spectrum was recorded at a sensitivity of full scale = 1 nA and the maximum signal for this scan was 0.64 nA at m/z = 40. The ion optics were re-optimized, and a m/z = 40 signal maximum greater than 1 nA was obtained. This spectrum showed some decrease in resolution compared to earlier studies where the Faraday plate was placed at the end of the quadrupole.

A comparison study was performed to evaluate the loss in resolution that occurred when the Faraday plate was located 203 mm from the exit of

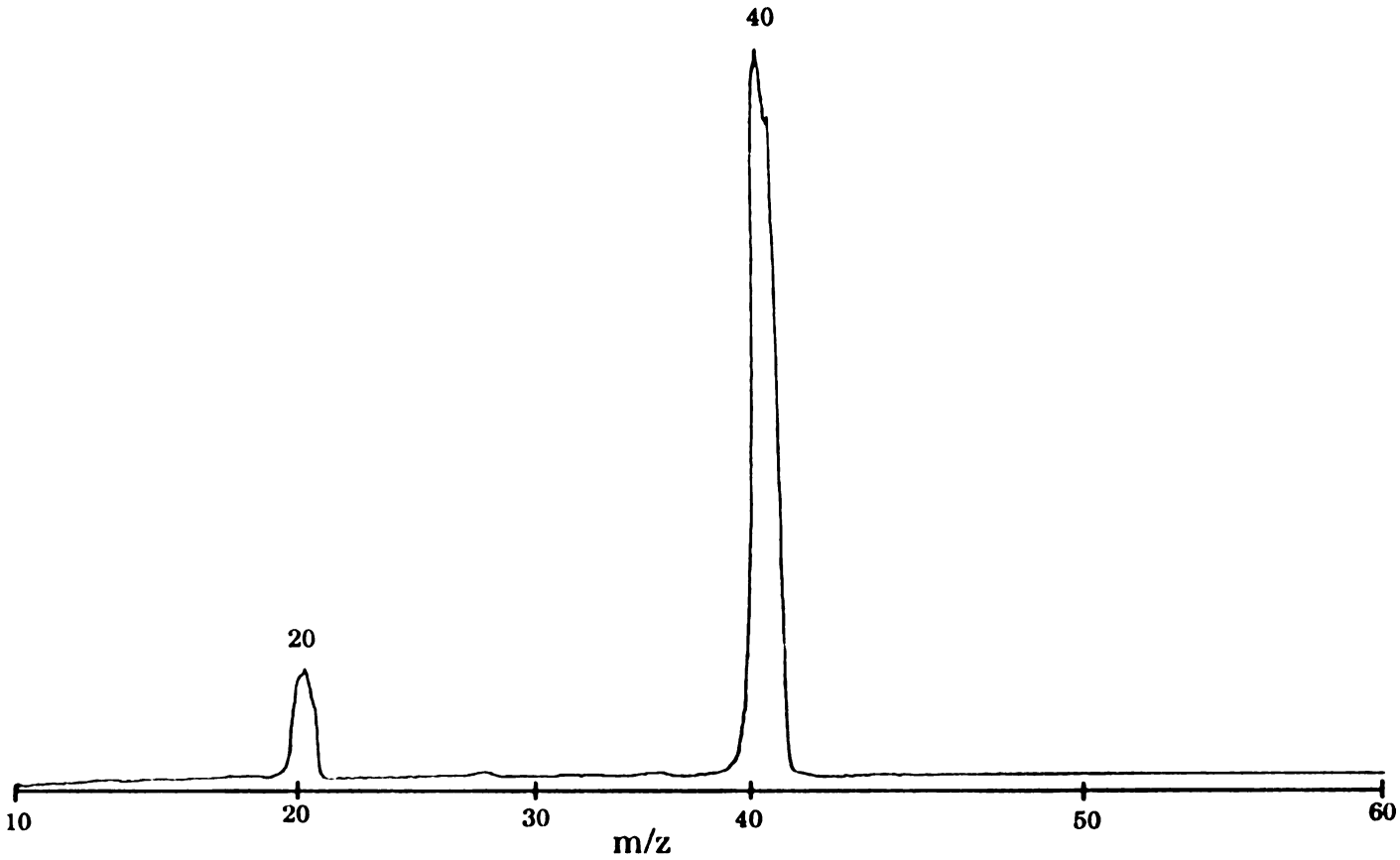

Figure 4.9 The mass spectrum of argon produced by the Dycor M200 source and measured at a 1 in. faraday plate positioned in front of the cryostat window, 203 mm from the exit of the quadrupole.

the quadrupole. A shielded Faraday plate was installed on the end of the quadrupole and connected to one of the pins on the 8-pin miniconflat feedthrough. The unit was installed on the diffusion pump test chamber and evacuated to a base pressure of $1x10^{-6}$ torr. A bulb of CS_2 was prepared, using three freeze/thaw cycles to remove volatile contaminants. This was connected to the source inlet, evacuated, and CS_2 was introduced into the source chamber to a pressure of $3.0x10^{-6}$ torr. Ion current was measured by a Keithley 610C electrometer, connected to the Faraday plate feedthrough, which was used to drive an XY chart recorder. The source was operated at 1 mA emission, repeller = -72 V, focus -31 V, and with 70 eV electron energy. The quadrupole was scanned from m/z = 10-100 at a dwell of 250 msec with 15 samples/amu. Figure 4.10 shows the mass spectrum produced at the XY recorder. The lower trace was made at full scale = 10 nA and the upper trace was taken at full scale = 1 nA. The spectrum shows that the quadrupole was able to effectively resolve ion separated by two mass units, but true unit mass resolution was not observed. This was probably due to the fact that the HI RES parameter was set to 2100 for this scan. The quadrupole was able to resolve the important peaks in the spectrum of CS_2, of particular significance was the ability to mass-select the peaks at m/z = 76 and 78, the molecular ion of CS_2. This was important for the CS_2^+ ion deposition studies that were conducted using this source.

The unit was then removed from the test chamber, and the Faraday plate was taken off the quadrupole ceramic mount. The three element (apertures = 6.3, 6.3, and 7.1 mm) lens system with four (1/2" long) deflection plates described earlier was installed after the quadrupole and the elements were connected to the 8-pin feedthrough miniconflat flange leads. The unit was installed on the left 6" port of the matrix chamber, and the chamber was evacuated to a base pressure of $8.1x10^{-8}$ torr. The linear motion feedthrough was inserted to 0.95", placing the Faraday plate directly in front of the cryostat window. The Faraday plate feedthrough

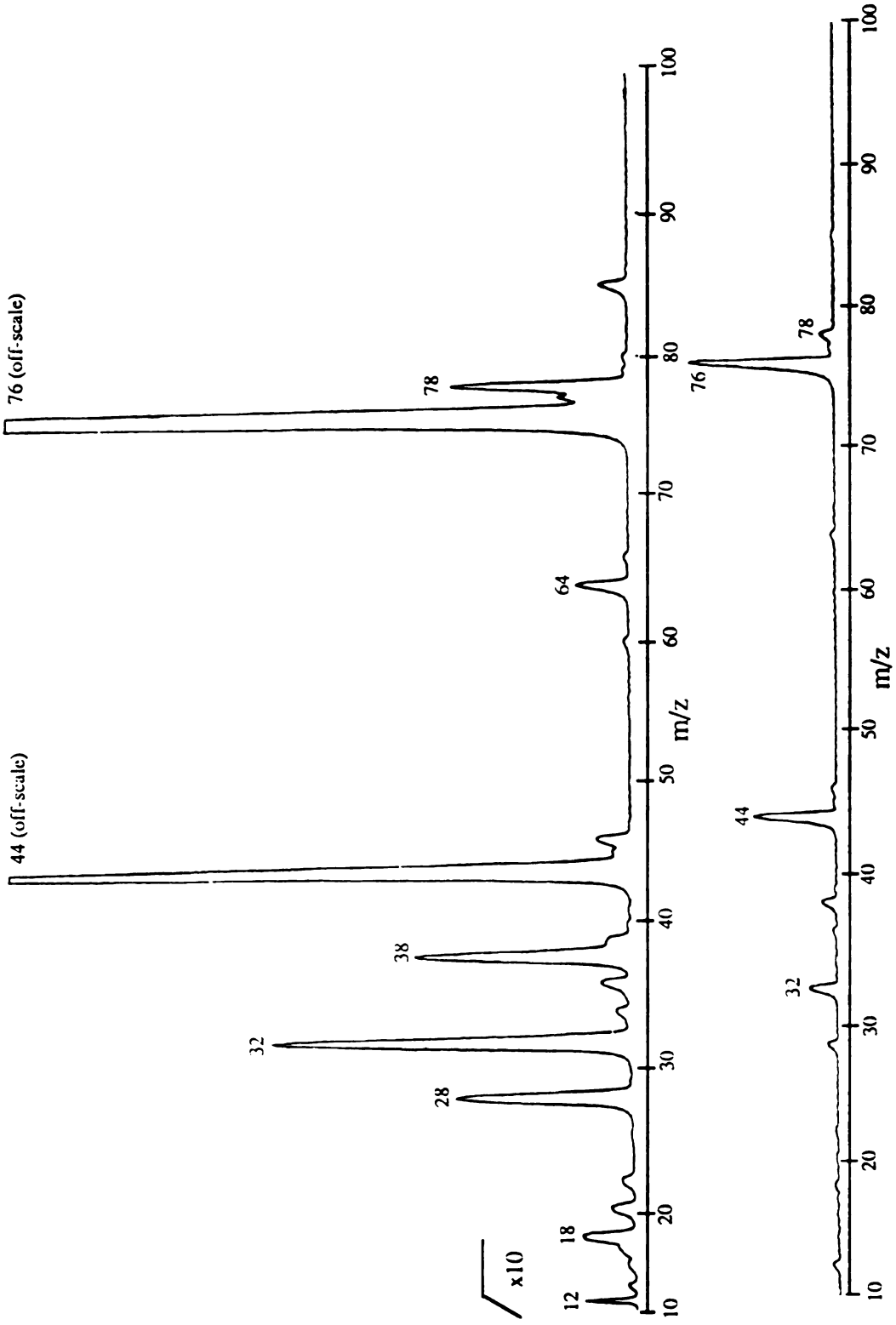

Figure 4.10 The mass spectrum of carbon disulfide produced by the Dycor M200 source and measured at a faraday plate mounted at the exit of the quadrupole.

was again connected to a Keithley 610C electrometer which was used to drive an XY chart recorder. The CS_2 bulb from the previous study was connected to the source inlet, the inlet was evacuated, and the source leak valve was opened until a total pressure of $3x10^{-6}$ torr was measure in the chamber. This corresponded to a CS_2 partial pressure peak at m/z = 76 of $4x10^{-7}$ torr measured by the Dycor M100 RGA mounted on the chamber. The source was operated under the same conditions, and the quadrupole was scanned from m/z = 10-100 at a dwell of 250 msec and 15 samples/amu. The potentials applied to the deflection optics were optimized for ion current at m/z = 76 current, and the optimum settings were: center einzel lens = -25 V, right deflection plate = -1.8 V, bottom deflection plate = -1.58 V, and all other elements = 0.0 V. Figure 4.11 shows two consecutive mass spectra recorded on the XY recorder at a sensitivity of full scale = 10 nA. the maximum signal measured at m/z = 76 was ~5.6 nA. These spectra showed that the resolution of the system had been degraded by placing the Faraday plate 203 mm away from the quadrupole. This loss in resolution indicated that the system in its current configuration was no longer capable of resolving ions that were separated by only a single mass unit, and this must be taken into account when planning matrix isolation studies. Fortunately the source was able to resolve ions that differ by 2 mass units, as indicated by the effective separation of ions at m/z = 76 and 78, the molecular ions of CS_2. This resolution proved sufficient for most matrix isolation studies, and was occasionally degraded further to increase ion current.

To evaluate the shape of the ion beam produced by the modified Dycor M200 source, the shielded CEMA detector mount described in Chapter 3.VI.B was installed in place of the cryostat head. This allowed the visualization of the ion beam profile produced by the source at the same position as the cryostat window. The output from the phosphor screen was observed through the 2 $^3/_4$" window flange normally used to introduced the FTIR beam. A 10 MΩ resistor network was installed across the CEMA

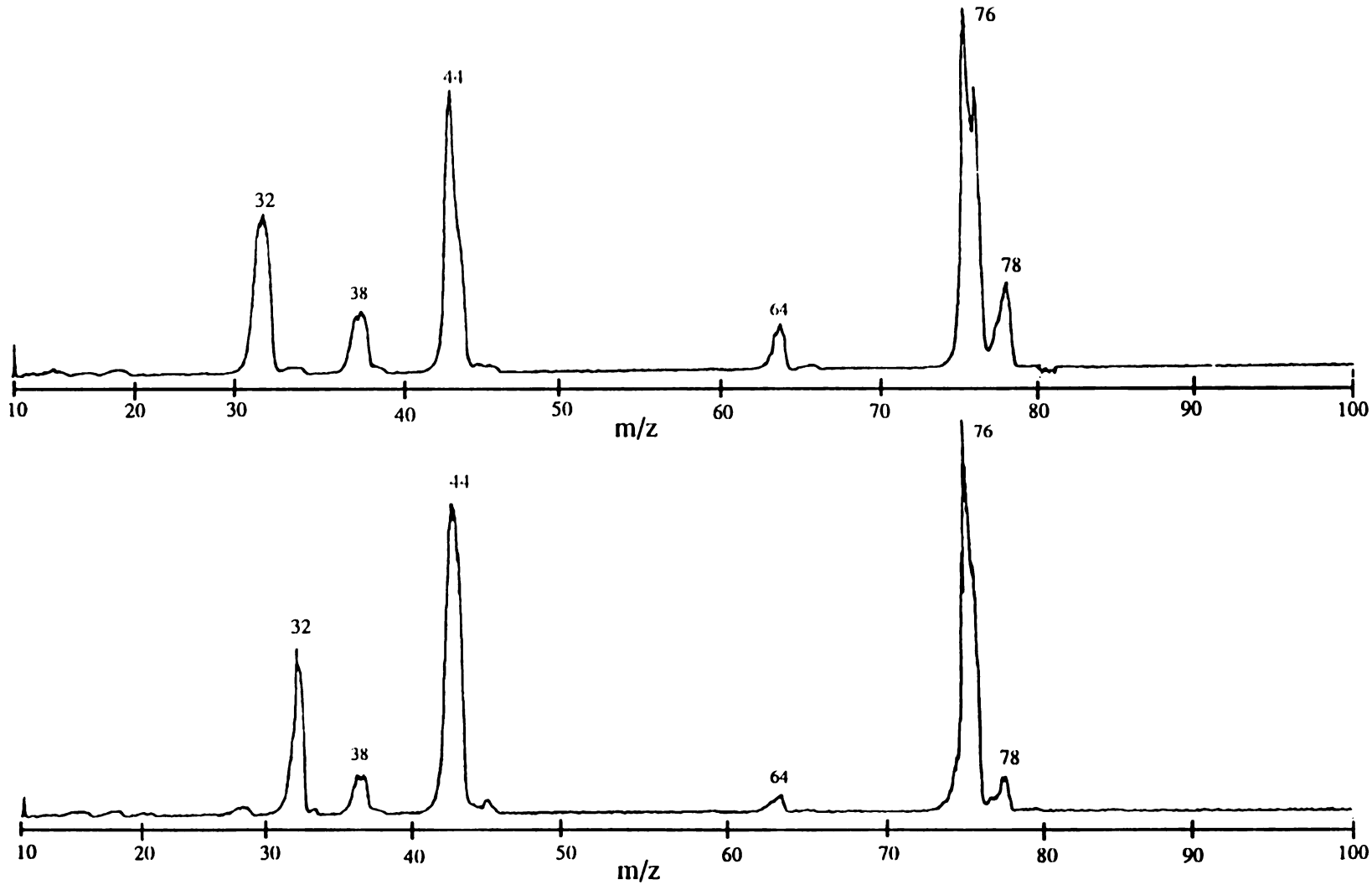

Figure 4.11 Two repeat scans of the mass spectrum of carbon disulfide produced by the Dycor M200 source and measured at a faraday plate mounted in front of the cryostat window, 203 mm from the exit of the quadrupole.

plates and the rear plate was connected through a Fluke 23 DMM to ground. The high voltage operating potentials were supplied to the CEMA detector from a high voltage feedthrough flange using shielded BNC cables. The CEMA was normally operated with -1400 V on the front plate of the detector and +1800 V on the phosphor screen. These conditions produced a current at the DMM of less than 0.1 mA indicating proper operation of the channelplate detector.

Several lens systems were investigated for use with the Dycor M200 source. Einzel lenses using three 6.3 mm apertures, a 6.3 and two 7.1 mm apertures, and two 6.3 mm apertures followed by a 7.1 mm aperture systems were installed and visualized with the CEMA. Two versions of each of these systems were installed, one with 2 mm and another with 4 mm inter-element spacing. Each of these systems were followed by a set of four offset, 1/2" long deflection plates. The beam profiles of these six systems were evaluated for m/z = 4 (He^+), m/z = 28 (N_2^+), and m/z = 40 (Ar^+). The potential applied to the central einzel lens element was varied from -120 to + 120 V, and none of the lens systems were able to focus the entire mass-selected ion beams within the 1" diameter of the detector. This most likely due to the fact that the source ion beam travels a much larger distance, 203 mm, from the end of the quadrupole to the window than with the Anavac-2 source. As a result a potential that correctly focuses some portion of the complex ion beam exiting the quadrupole, will defocus another portion. By operating the einzel lenses in accellerate-decelerate mode, a clear cross pattern was produced with each of the lens systems, but some portion of the beam was lost. The most intense and clearly focused cross patterns was produced using the 6.3, 6.3, 6.3 mm aperture system with 2 mm inter-element spacing. The first and third elements of this system were held at ground and the center element was biased at -60.5 V. To determine whether these values actually produced the highest ion current at the matrix window, the CEMA detector was removed and the linear motion feedthrough was inserted to 0.95" to position the 1" Faraday

plate in front of the cryostat window. With the 6.3, 6.3, 6.3 mm aperture, 2 mm spacing einzel lens, and two sets of offset $^1/_2$" long deflection plates installed, the potentials applied to the lens elements were optimized for mass selected ion current (m/z = 40 with an argon leak) at the Faraday plate. Several such studies were repeated during the process of conducting matrix isolation studies with this lens system. The best average optimal settings were: center einzel lens element = -25 V, right deflection plate = -1.8 V, bottom deflection plate = -1.58 V, and all other lens elements maintained at 0.0 V. At these settings mass-selected ion currents of more that 1 nA were maintained with only minor adjustment for several hours during the course of the matrix isolation studies.

Chapter 5. Conclusions and suggested future studies

The ion sources constructed through the modification of the Anavac-2 and Dycor M200 residual gas analyzers have proved reliable for the production of mass-selected ion beams. These devices have been used in several matrix isolation studies with good success. We have successfully trapped and spectroscopically observed via laser induced fluorescence spectroscopy mass-selected ions within a low temperature argon matrix. An example of the LIF spectrum of CS_2^+ isolated in an argon matrix is shown in Appendix XV. The LIF technique is much more sensitive than is infrared analysis; IR spectroscopy requires the accumulation of higher numbers of absorbers for effective detection. To minimize the time required for the IR experiments it would be desirable to increase the mass-selected ion current produced by these sources.

I. Possible modifications to the original Anavac EI source

Several possible studies and could be performed to determine which modifications would increase the ion output from the modified RGAs. The total ion flux from the original Anavac-2 EI source was reduced by approximately 79% by enclosing the unit in the sealed source housing. Most of this current loss was probably due to the reduction of the ion exit aperture. If a higher flux of neutrals from the source could be tolerated, increasing the source housing aperture size should result in an increase in ion current at the cryostat window. It might also be useful to install a repeller electrode within the cylindrical grid. This could be used to increase the electric field within the ionization region, thereby increasing the total output of the source. Disadvantages to using this type of repeller include: difficulty in installing a repeller in the small cylindrical grid region, increased ion energy due the higher electric potentials within the

ionization region, and difficulties in electrically isolating and biasing the repeller electrode. The Anavac source was also used for the deposition of NO^+ from NO. The 0.005" rhenium filament installed in the source was able to survive in the highly oxidative NO environment for only a few hours. If the Anavac EI source is used under chemically reactive conditions, a more robust filament material, such as thoriated-iridium should be used.

II. Differential pumping of the Nermag source

The modified Nermag EI/CI source proved unacceptable for use as a CI source with the present vacuum system. However, it was able to produce very strong mass-selected ion beams when coupled to the Anavac quadrupole and operating in EI mode with the original 4 mm apertures in place. Differential pumping could be employed to allow this source to produce ion beams under high pressure CI conditions . A source chamber could be constructed to enclose the source assembly. The new chamber could be placed between the 6" source flange and the matrix chamber 6" flange as shown in Figure 5.1.

By installing a separate pump, possibly a turbomolecular pump, and an aperture plate after the quadrupole, this type of chamber could greatly reduce the flow of sample gas from the source into the matrix chamber. The aperture plate would have to be sealed to the chamber walls; it would allow ions to pass through a small conductance-limiting aperture located close to the quadruple entrance aperture, while discriminating against the flow of neutrals from the source region into the matrix isolation chamber. Because this aperture plate would have to be permanently attached to the walls of the chamber, the pivoting feature of the source could no longer be utilized. This should not prove to be a difficulty; the source could be permanently positioned off-axis and the ions deflected onto the cryostat window using deflection and focusing optics.

Also, the differential pumping provided by this type of chamber would greatly reduce the total flux of neutrals into the matrix chamber, possibly making off-axis orientation unnecessary. One disadvantage to using this type of differential pumping would be that the ion beam would need to travel a greater distance between the quadrupole exit aperture and the cryostat window, which could result in some loss of ion current.

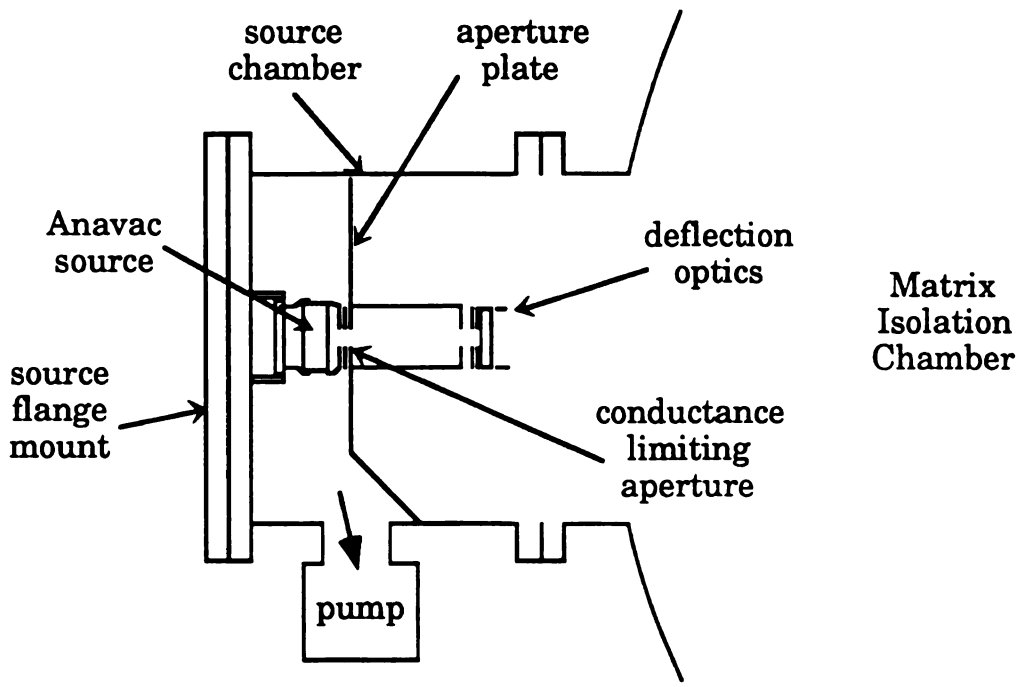

Figure 5.1 One possible design for a source chamber to allow differential pumping of the source region.

III. Water cooling of the Nermag source

Matrix isolation studies were performed using the Nermag source with the Anavac quadrupole in the matrix isolation of Co^+ from the $Co(CO)_3NO$ precursor. Early attempts to form Co^+ using the Dycor M200 EI source were unsuccessful because the compound decomposed when directly exposed to the hot filament. The maximum current of Co^+ (m/z = 59) produced by the Dycor M200 source was only ~$5x10^{-11}$ A, this mass spectrum is shown in Figure 5.2. The modified Nermag source with 4 mm

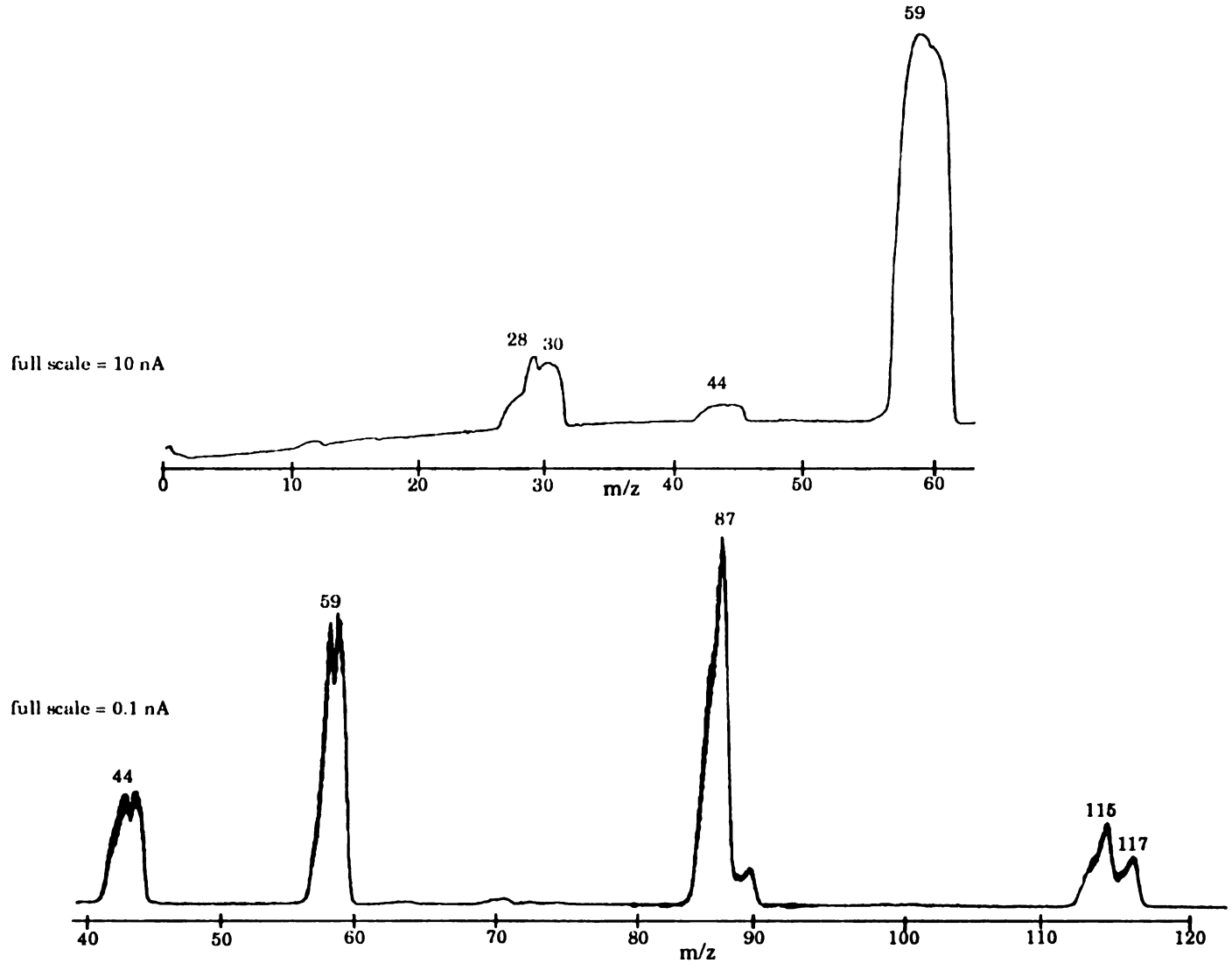

Figure 5.2 The mass spectrum of $Co(CO)_3NO$ produced with the Nermag source/Anavac quadrupole (top) and the Dycor M200 source (bottom). The ions were detected at the Faraday plate positioned at the cryostat window.

apertures produced much higher currents of Co^+ because the sample was not directly exposed to the heated filament. An example of the output from the Nermag source is also shown in Figure 5.2; the m/z = 59 current in this spectrum was ~ 0.5 nA. When this source was initially turned on a strong Co^+ signal was observed, which decreased with time. This falloff was attributed to the slow radiative heating of the Nermag source by the filament which increased the degree of sample pyrolysis. To increase output from this source with such labile compounds, the system could be adapted to allow the source to be water-cooled. Inlet and outlet water feedthrough lines could be installed in the 6" mounting flange, and coupled to swagelock fittings on both the vacuum and atmosphere ends of the lines. A short length of ~1/8" stainless steel tubing could be brazed to the body of the Nermag source and terminated with swagelock fittings. Teflon lines could be used to connect the source housing to the swagelock fittings on the flange, while maintaining the necessary electrical isolation between the two components. Using this system, water could flow through the inlet line, remove heat from the source, and flow out through the outlet line, cooling the body of the Nermag source. If this type of cooling system is used, care must be taken to ensure that water leaks into the vacuum system are prevented.

IV. Improving the output of the Anavac NSI source

Several methods could be investigated to improve the negative ion output current from the Anavac source operating in NSI mode. In the Cs glass bead NSI studies performed, the Cs bead wire was spot-welded to the TCD feedthrough and inserted into the Anavac source housing. This method of mounting made it difficult to precisely align the Cs glass surface with the source exit aperture. Poor alignment of these elements could cause most of the negative ions emitted from the surface of the bead to be neutralized on the source aperture plate, resulting in low negative ion

output from the source. Alternate bead mounting methods should be investigated to ensure proper alignment of these elements. Several alternate NSI surfaces and neutral molecules have been successfully used by other researchers to produce high currents of negative ions as mentioned in Chapter 2.I.C. Low work function surfaces such as thoriated iridium or LaB_6 could be adapted for use in the NSI source as alternatives to the Cs glass system used in these studies. Other neutral precursor molecules, such as $KCl_{(s)}$ coated on the NSI surface or $Cl_{2(g)}$, could also be studied to determine if they could be utilized for the production of high currents of negative ions through NSI. The output of the Anavac NSI source may also be limited by the size of the ion exit aperture. Increasing the size of this aperture could result in a stronger output of negative ions, but would also increase conductance from the source. Finally, the use of a stronger extraction field at the NSI surface could be investigated. By placing a bias on the source aperture plate, the electric field at the surface of the NSI bead could be varied. Increasing this surface extraction field may increase the current of negative ions exiting the ion source.

V. Emission regulation for the Anavac system

One of the advantages to using the Dycor M200 mass-selected ion source is that the modifications made to this unit allowed the original filament emission controls to be retained. The ion sources adapted for use with the Anavac quadrupole were connected to external power supplies which had to be regulated manually. This was not a difficulty for the source optimization studies, but became a limiting factor when the sources were operated for the extended matrix isolation experiments. To make these sources practical for such experiments, regulated power supplies should be constructed. To design these supplies the method of filament heater current regulation must first be determined, or the power supplies

must be designed to function using several modes of emission regulation. The original Anavac EI source could be operated by regulating filament heater current through monitoring the total emission of the power supply, or by monitoring the current of electrons at the source grid. The original Anavac control unit filament regulation circuit could be adapted for use if the filament heater current was monitored at the grid element. The filament on the Nermag source could regulated by monitoring total emission from the power supply or current at the collector, depending upon whether the source is operated in CI or EI modes. The filament in the Anavac NSI source could be regulated through monitoring total filament emission, or by monitoring the electron/negative ion current at the source plate. The source plate current proved to be a more sensitive measure of total ion output, but varied with changes in sample pressure within the source.

VI. Differential pumping of the Dycor source

The modified Dycor mass-selected ion source would also benefit from modifications, similar to those shown in Figure 5.1, to provide differential pumping. During a normal matrix isolation experiment the pressure within the deposition chamber was generally maintained below $5x10^{-7}$ torr. To maintain these pressures, the leak into the Dycor source was controlled at a level that produced a partial pressure reading of $2x10^{-7}$ torr for the sample gas. At these low pressures the maximum mass-selected ion current that could be measured at the cryostat window was ~1 nA. Studies performed at higher source pressures indicated that stronger ion currents could be maintained, up to ~5 nA, if the ion source pressure was increased. By implementing differential pumping between the EI source and the matrix chamber, higher pressure source conditions could be utilized without substantially elevating the pressure in the matrix isolation chamber. This could be accomplished by installing a pump on

the source chamber housing and sealing this chamber with a plate positioned between the ion source and the quadrupole. Such differential pumping of the source chamber would remove most of the sample gas leaking from the ion source, while still allowing the mass-selected ion beam produced by the quadrupole to be directed onto the cryostat window.

VII. Alternate filament materials

To lower the operating temperature of the Dycor source a lower work function filament material, such as thoriated iridium, could be used in place of a rhenium filament. This type of filament is more difficult to prepare, but operates at a lower temperature and is more resistive to oxidation. Pre-fabricated Th-Ir filaments mounted on the Dycor filament support rods can be purchased directly from the manufacturer. To increase the output from the Dycor source the filament could also be operated at higher emission levels, but this could reduce the lifetime of the filament. In general this parameter, along with the repeller voltage, electron energy, and focus voltages were optimized at regular intervals during a matrix isolation experiment to maintain maximum ion current.

VIII. Low resolution operation of the source quadrupoles

To further increase the mass-selected ion output from both of the sources, the operation of their quadrupoles could be modified. The remote electronics head of the Anavac system allows the user to decrease the resolution of the quadrupole. This is accomplished by varying VR2 on the remote head, which determines the dc/rf ratio on the quadrupole. The setting of VR2 could be varied to decrease the resolution of the quadrupole, resulting in a strong increase in the ion current at the matrix window. Increasing the ion energy, and removing the 3 mm exit aperture on the Anavac quadrupole housing could also be used to increase the ion current

at the cryostat window. The resolution of the Dycor unit could be reduced by decreasing the HI RES and LO RES settings on the control unit. Ion energy could be increased using the LO SENS and HI SENS parameters, and the operation of the unit in BAR or TAB modes could also be investigated.

VIX. Post-quadrupole optics optimization

Finally, modifications to the ion optics after the quadrupole should be further investigated to determine whether the ion current at the cryostat window can be increased. The Dycor source, in particular, could benefit from improved transfer of the mass-selected beam from the quadrupole to the cryostat window. The energy and m/z dependence of the mass-selected ion beam produced by Dycor quadrupole should be investigated by visualizing the ion beam produced after the quadrupole using the CEMA detector. It is possible that the use of a multistage optics system could increase efficiency of the transfer of the ion beam onto the cryostat window. A lens system which employs two sets of einzel lenses, coupled by a tube element for physical support, is one system that might be considered. Although it would be complex, an rf-multipole beam guide could also be used to transfer the mass-selected beam onto the cryostat window.

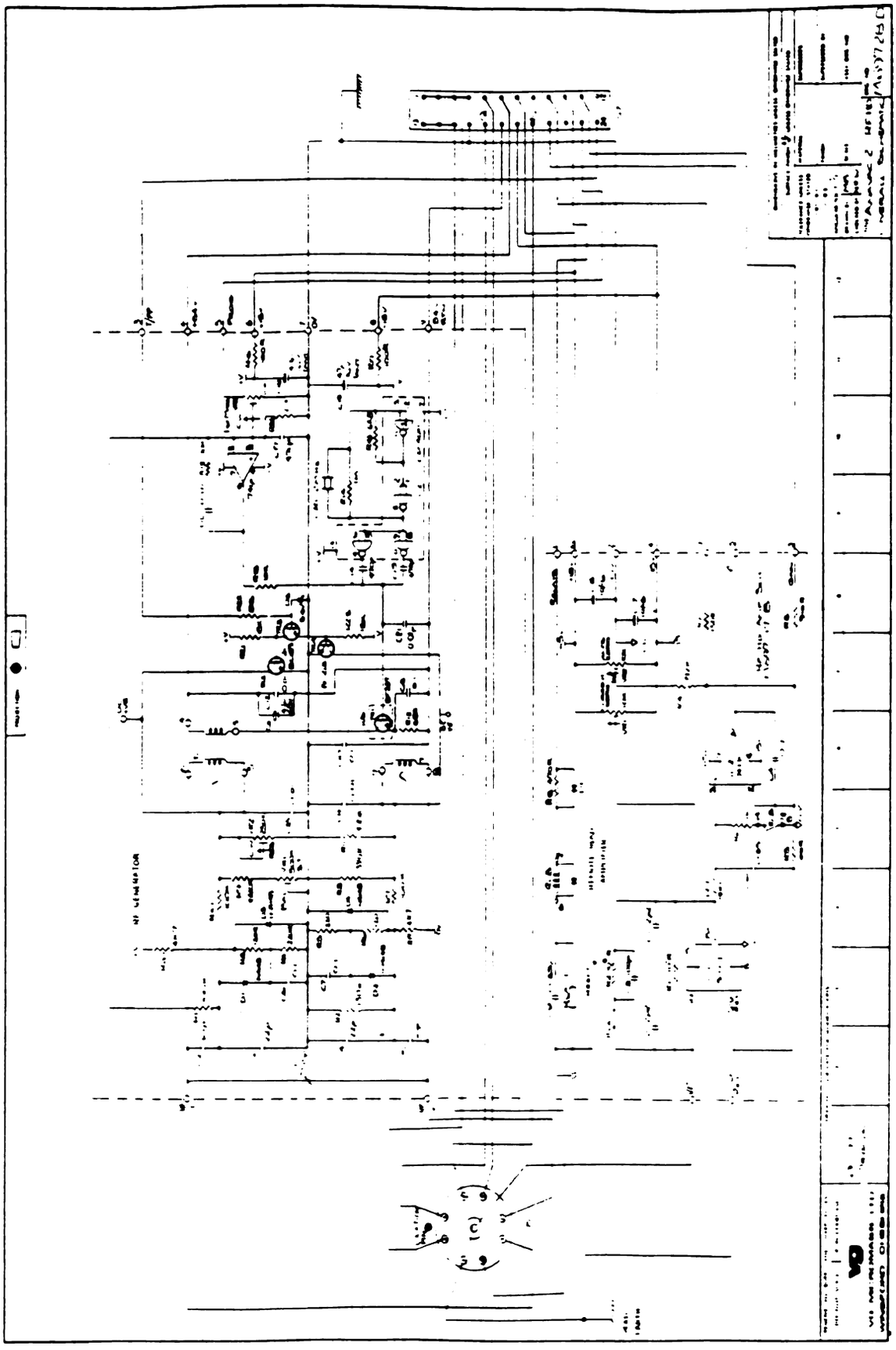

Appendix I. A schematic diagram of the Anavac-2 remote electronics head.

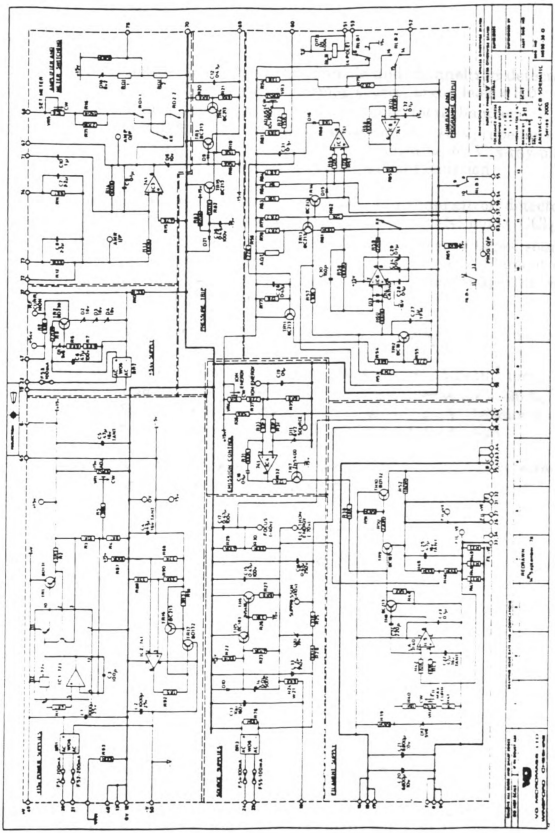

Appendix II. A schematic diagram of the Anavac-2 main control unit.

Appendix III - Experimental conditions for the optimization studies shown in Appendices IV - XIV

Appendix

IV Nermag source with Anavac quadrupole and channeltron detector 0.5 mm aperture exit plate on Nermag source, argon leak = 5.0 mtorr, chamber base pressure = 5.7×10^{-7} torr, total chamber pressure = 6.3×10^{-7} torr, initial voltages: source = +3 V, repeller = +15 V, collector = +5.02 V, Lens = -40 V, filament = -67 V, x-ray plate = +50 V, detector = -2.7 kV, 50 μA total filament emission

V Nermag source with Anavac quadrupole and channeltron detector 0.5 mm aperture exit plate on Nermag source, EC-NI mode, CCl_4 leak , chamber base pressure = 5.2×10^{-7} torr, initial voltages: source = -20 V, repeller = -45 V, collector = -20 V, Lens = +50 V, filament = -120 V, x-ray plate = +3.5 kV, detector = -2.7 kV, detector aperture = -3 V, 50 μA total filament emission

VI Nermag source with Anavac quadrupole and channeltron detector 0.5 mm aperture exit plate on Nermag source, EC-NI mode, CCl_4 and 100:1 Ar:CCl_4 leaks, chamber base pressure = 5.2×10^{-7} torr, initial voltages: source = -20 V, repeller = -60 V, collector = -20 V, Lens = +50 V, filament = -120 V, x-ray plate = +3.5 kV, detector = -2.7 kV, detector aperture = -3 V, 50 μA total filament emission

VII Anavac surface source and quadrupole with channeltron detector surface ionization with KNO_3 bead, chamber pressure = 1.6×10^{-6} torr, initial voltages: bead = +3.0 V, filament housing = +9.0 V, lens = - 40 V, x-ray plate = +50 V, detector = -2.7 kV,filament I = 0.8 A

VIII Anavac surface source and quadrupole with channeltron detector surface ionization with KNO_3 bead, chamber pressure = 1.6×10^{-6} torr, initial voltages: bead = +3.0 V, filament housing = +9.0 V, lens = - 40 V, x-ray plate = +50 V, detector = -1.2 kV,filament I = 0.8 A

IX Anavac surface source and quadrupole with Faraday plate detector surface ionization with KNO_3 bead, chamber pressure = 2.5×10^{-6} torr, initial voltages: bead = +3.0 V, filament housing = +9.0 V, lens = - 40 V, source = 0.0 V, filament current = 0.8 A

X Anavac surface source and quadrupole with Faraday plate detector negative surface ionization with cesium bead, chamber base pressure = 1.4×10^{-6} torr, CCl_4 chamber pressure = 5.0×10^{-6} torr, source pressure = 18 mtorr, bead = -2.0 V, initial filament housing = -8.5 V, lens = +43 V, source = 0.0 V, filament current = 2.35 A

Appendix III (continued)

Appendix

XI Anavac surface source and quadrupole with Faraday plate detector negative surface ionization with cesium bead, chamber base pressure = 1.4×10^{-6} torr, CCl_4 chamber pressure = 6.3×10^{-6} torr, source pressure = 20 mtorr, bead = -2.5 V, initial filament housing = -11 V, lens = +43 V, source = 0.0 V, filament current = 2.2 A

XII Anavac surface source and quadrupole with Faraday plate detector negative surface ionization with cesium bead, chamber base pressure = 1.4×10^{-6} torr, CCl_4 chamber pressure = 6.3×10^{-6} torr, source pressure = 20 mtorr, bead = -2.5 V, initial filament housing = -11 V, lens = +43 V, source = 0.0 V, filament current = 2.2 A

XIII Anavac surface source and quadrupole with Faraday plate detector negative surface ionization with cesium bead, chamber base pressure = 1.4×10^{-6} torr, CCl_4 chamber pressure = 5.0×10^{-6} torr, source pressure = 18 mtorr, bead = -3.0 V, initial filament housing = -8.5 V, lens = +43 V, source = 0.0 V, filament current = 2.2 A

IV Anavac surface source and quadrupole with Faraday plate detector negative surface ionization, compating old Cs surface with cesium bead after exposure to oxygen at 2.0×10^{-6} torr, chamber base pressure = 1.0×10^{-6} torr, CCl_4 chamber pressure = 5.8×10^{-6} torr, source pressure = 18 mtorr, bead = -2.5 V, initial filament housing = -11 V, lens = +35 V, source = 0.0 V

Appendix IV - Optimization studies for the Nermag source with 0.5 mm source aperture coupled to the Anavac quadrupole, ion current measured with a channeltron detector.

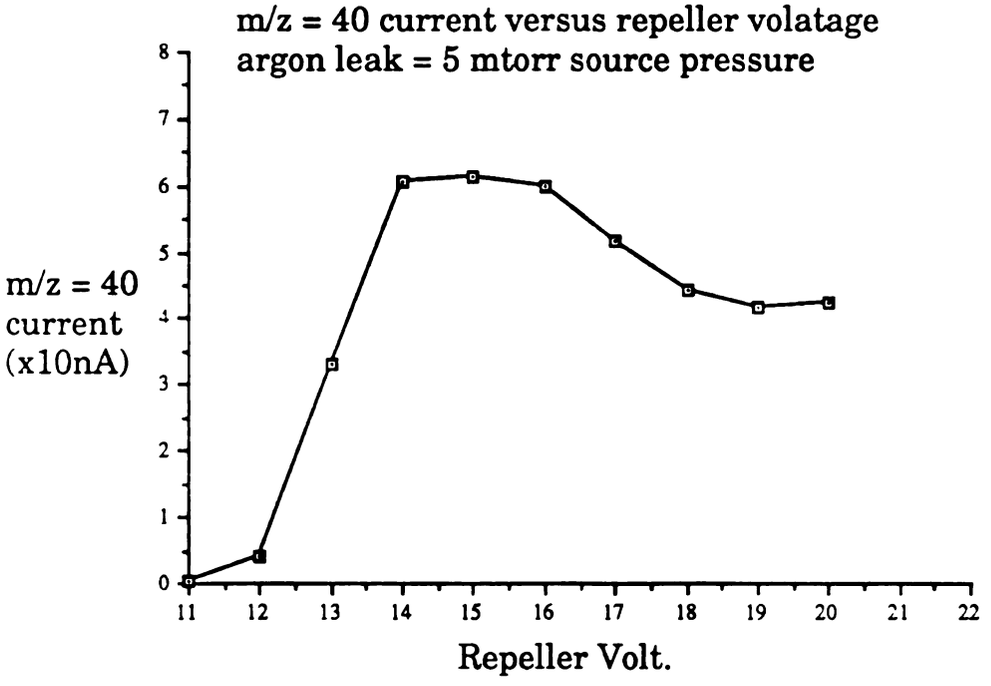

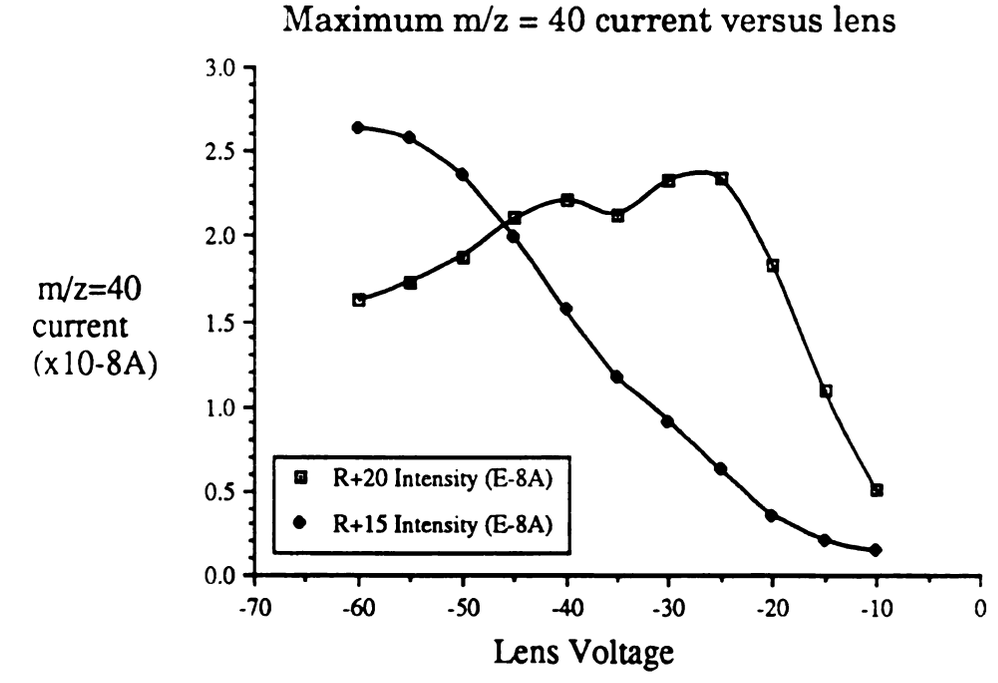

Appendix V - Optimization studies for the Nermag source (with 0.5 mm source aperture) coupled to the Anavac quadrupole, ion current was measured with a channeltron detector. The spectrum was taken under EC-CI conditions using carbon tetrachloride.

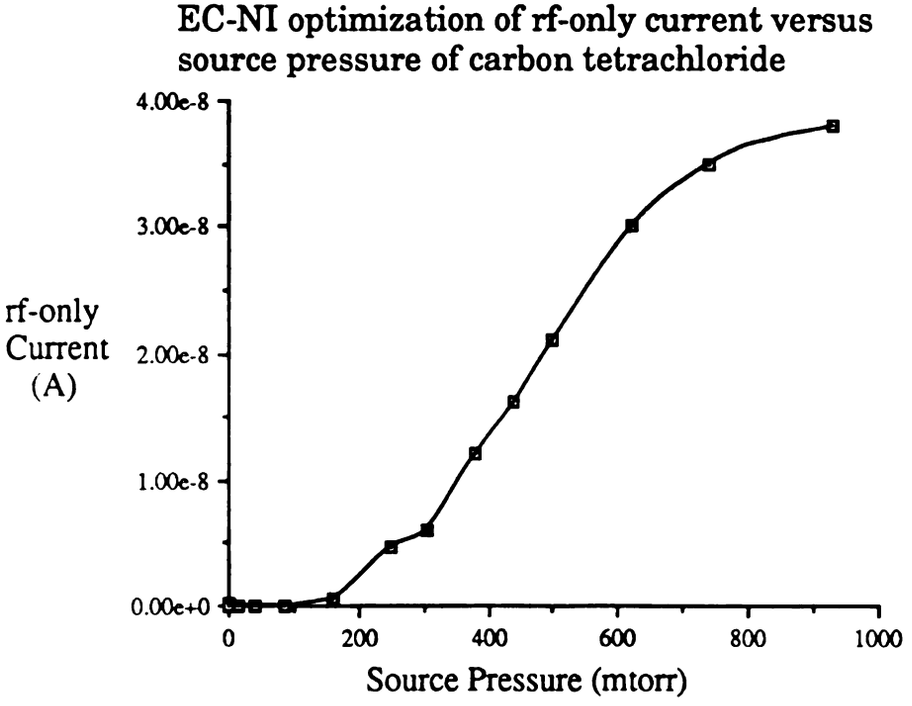

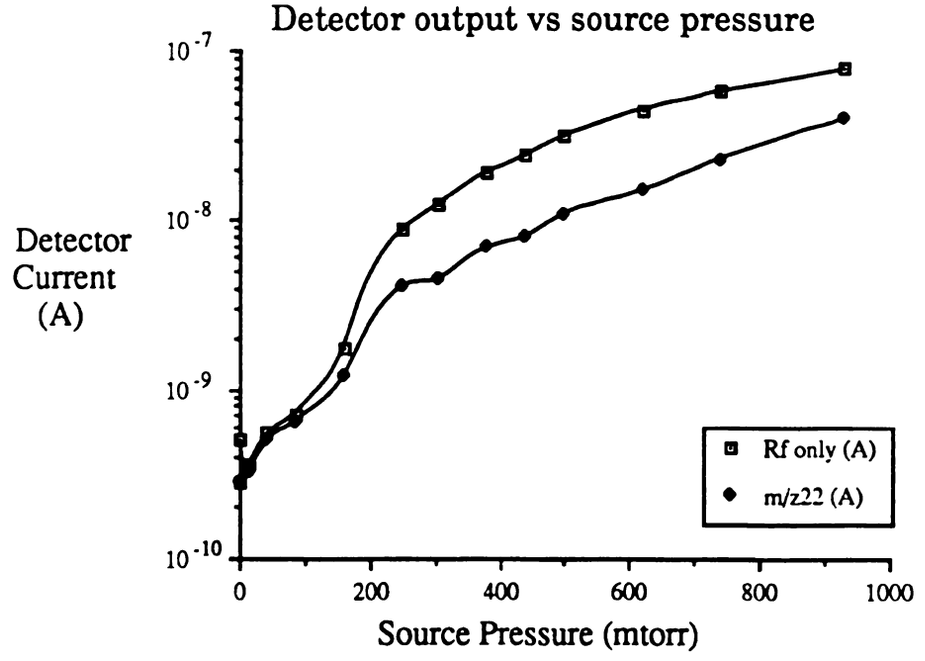

Appendix VI - Optimization studies for the Nermag source (with 0.5 mm source aperture) coupled to the Anavac quadrupole, ion current was measured with a channeltron detector. EC-CI conditions were maintained using carbon tetrachloride and argon:carbon tetrachloride mixtures.

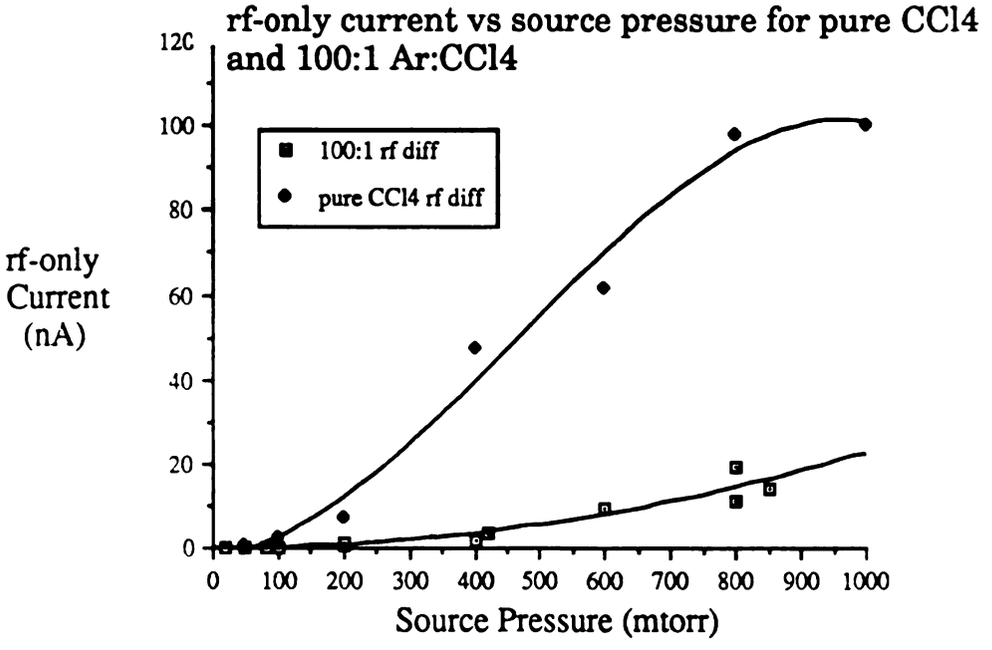

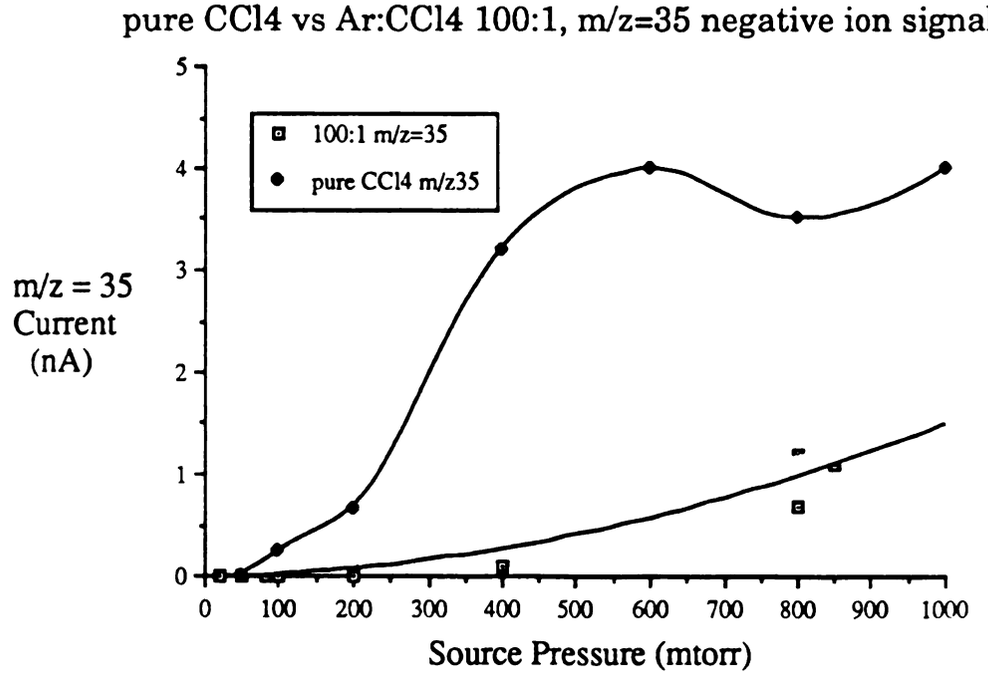

Appendix VII - Optimization studies for the Anavac source and quadrupole. The source was configured for surface ionization using a potassium bead, and ions were detected by a channeltron detector.

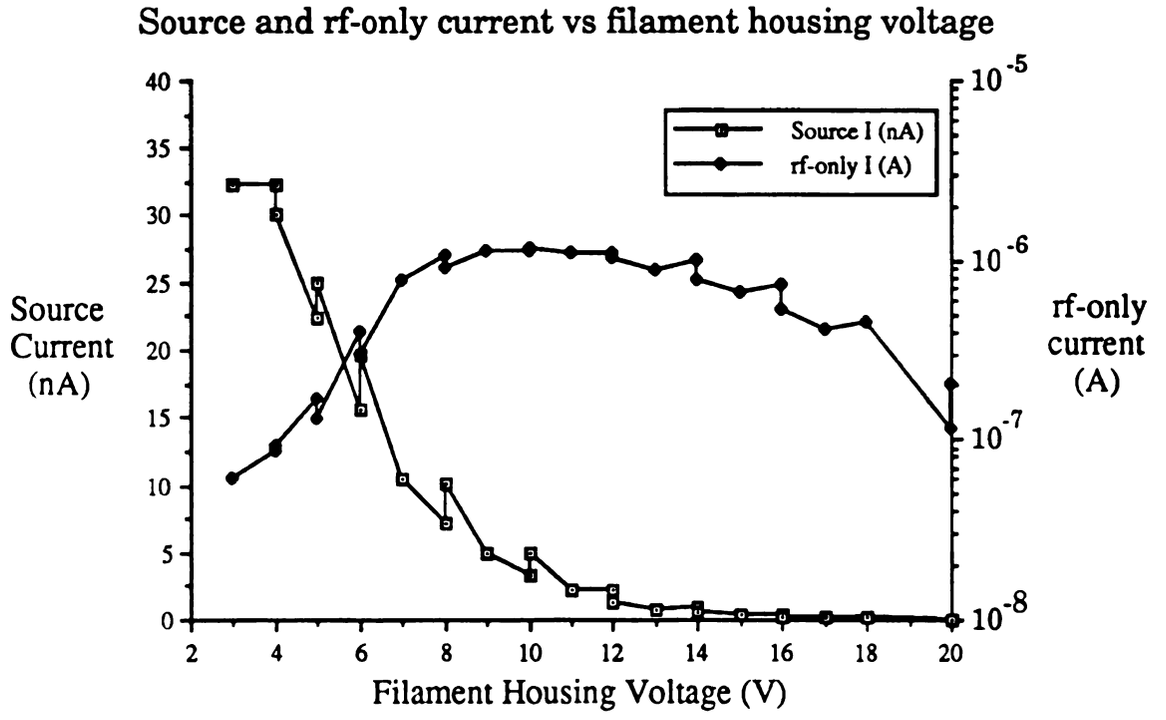

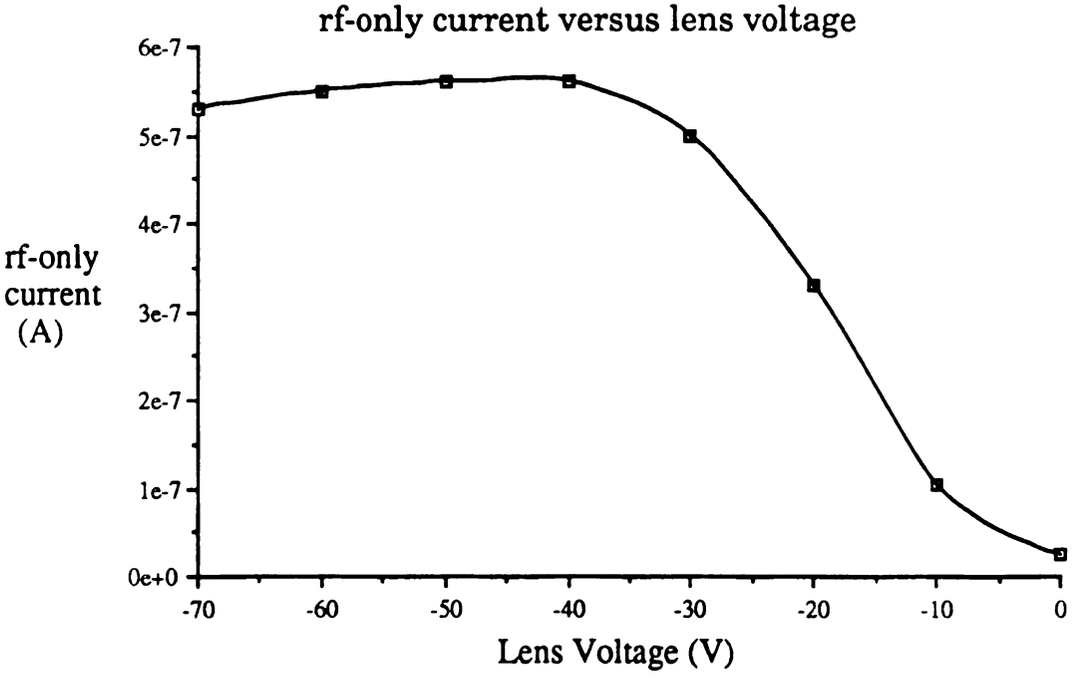

Appendix VIII - Optimization study for the Anavac source and quadrupole. The source was configured for surface ionization using a potassium bead, and ions were detected by a channeltron detector.

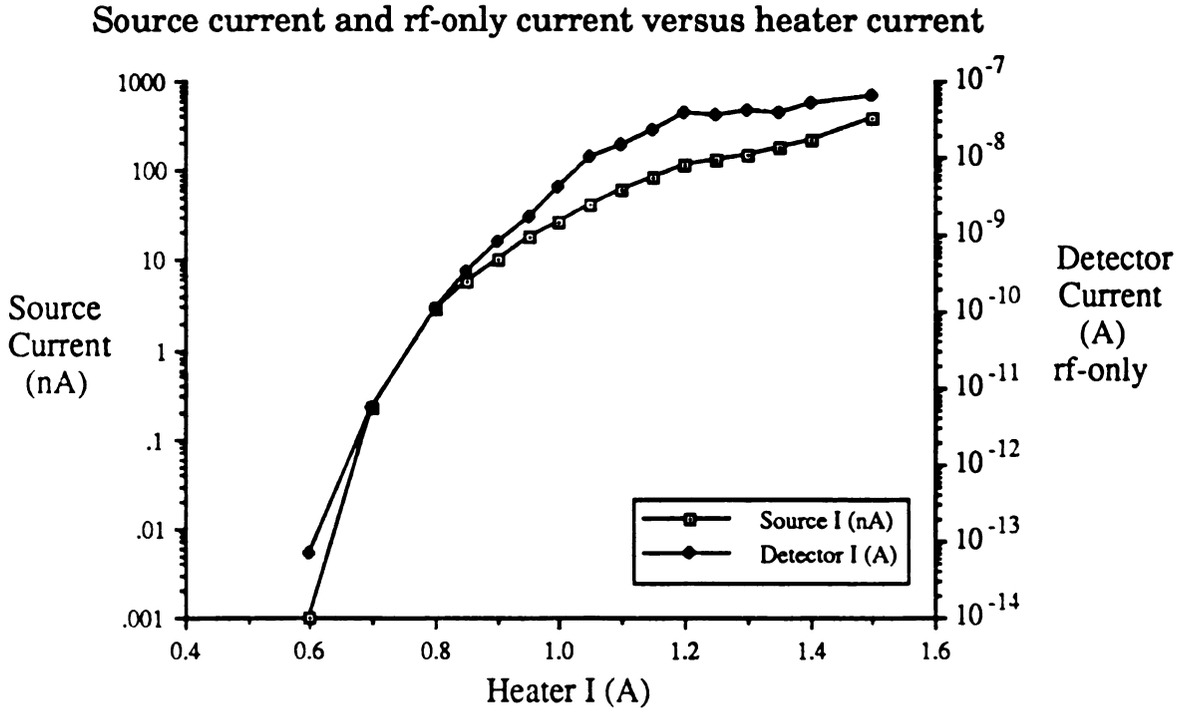

Appendix IX - Optimization study for the Anavac source and quadrupole. The source was configured for surface ionization using a potassium bead, and ions were detected at a faraday plate mounted after the quadrupole.

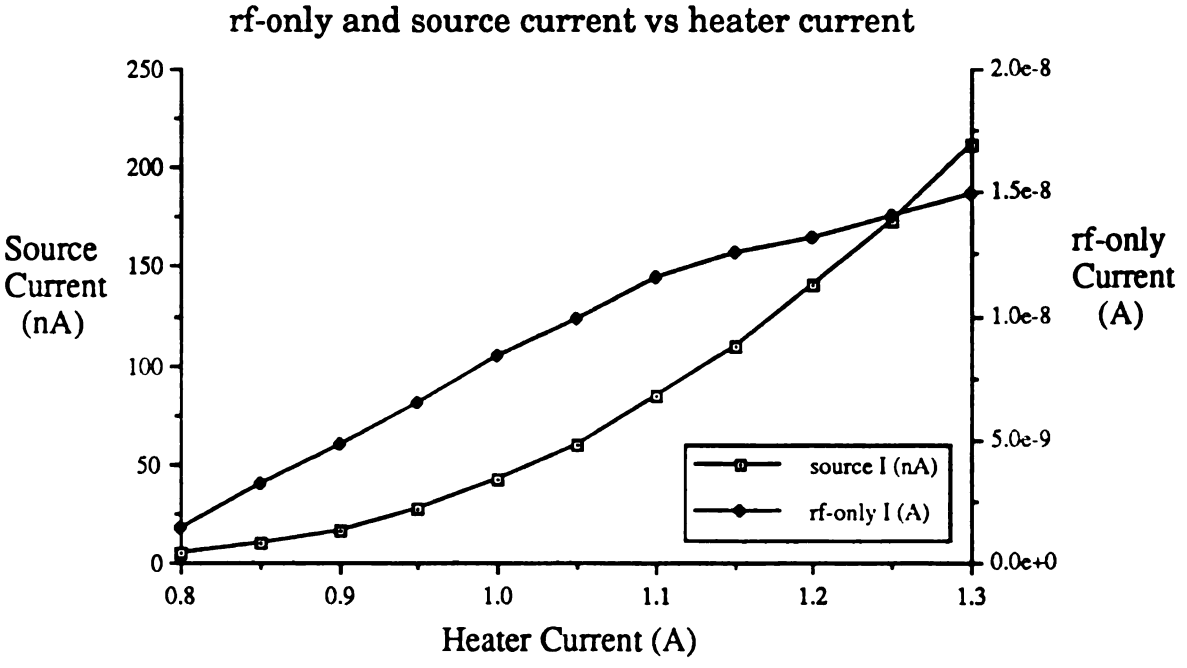

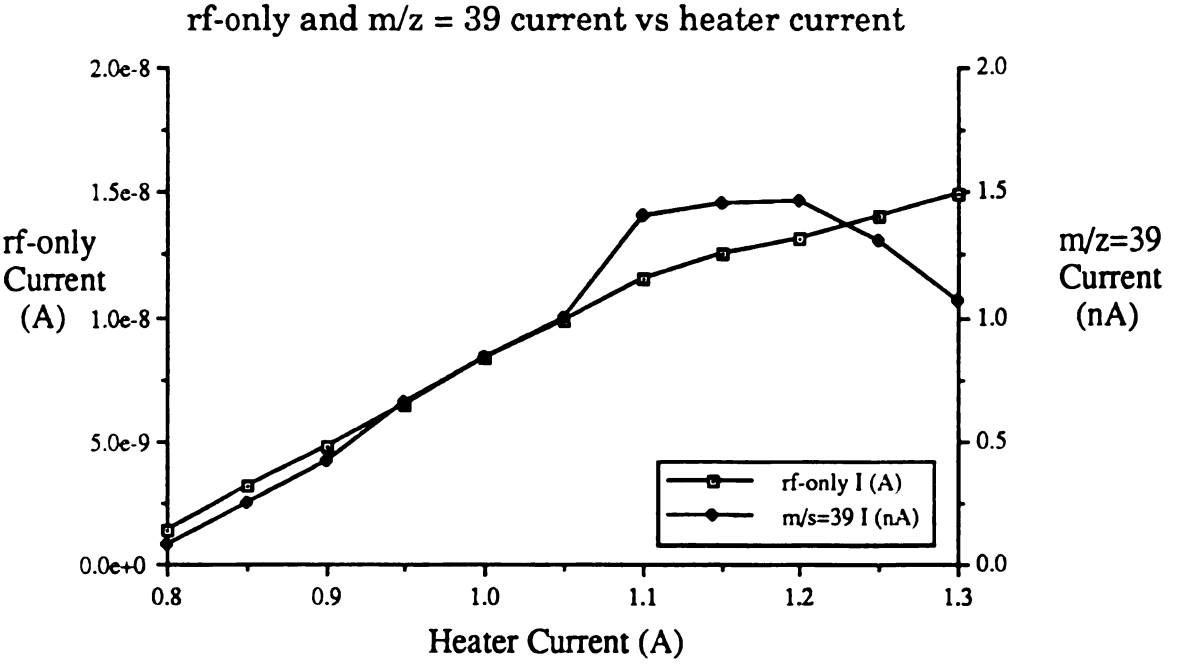

Appendix X - Optimization study for the Anavac source and quadrupole. The source was configured for surface ionization using a cesium bead biased at -2.0 V, with a leak of carbon tetrachloride. Ions were detected at a Faraday plate mounted after the quadrupole.

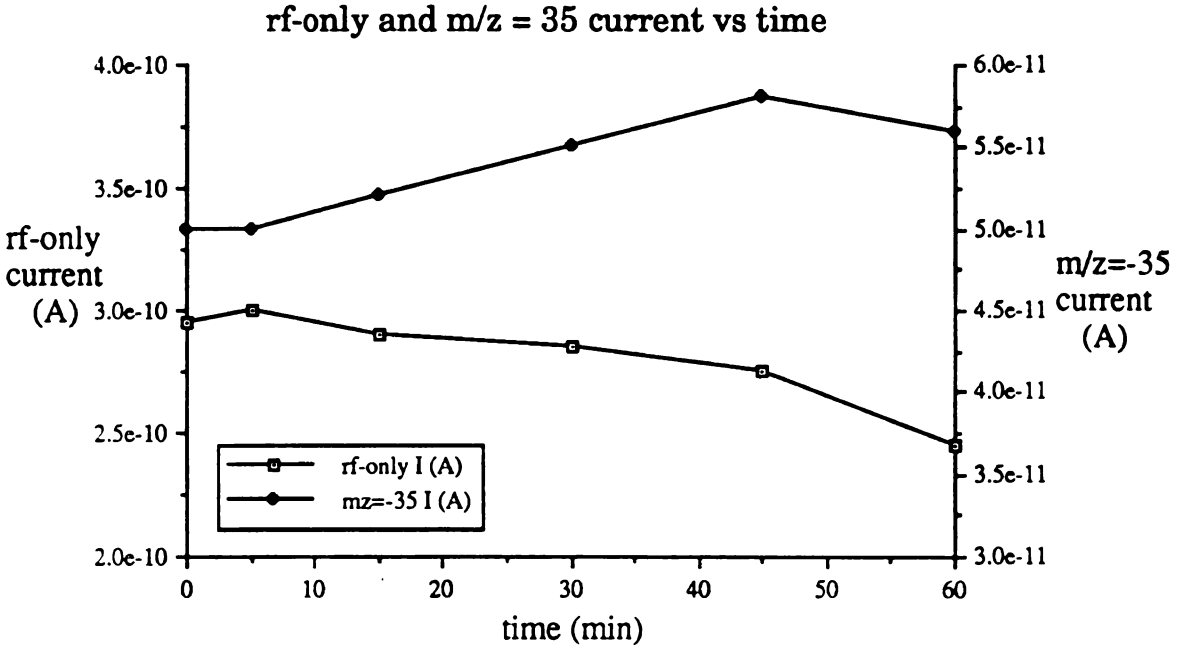

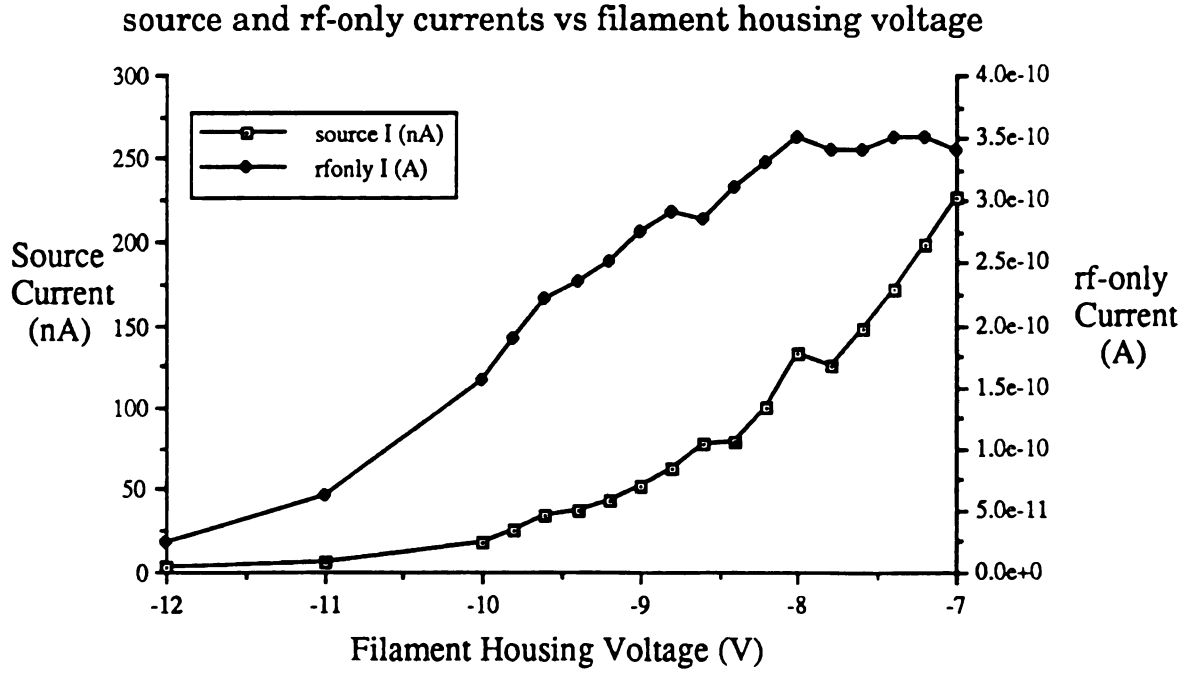

Appendix XI - Optimization study for the Anavac source and quadrupole. The source was configured for surface ionization using a cesium bead biased at -2.5 V, with a leak of carbon tetrachloride. Ions were detected at a Faraday plate mounted after the quadrupole.

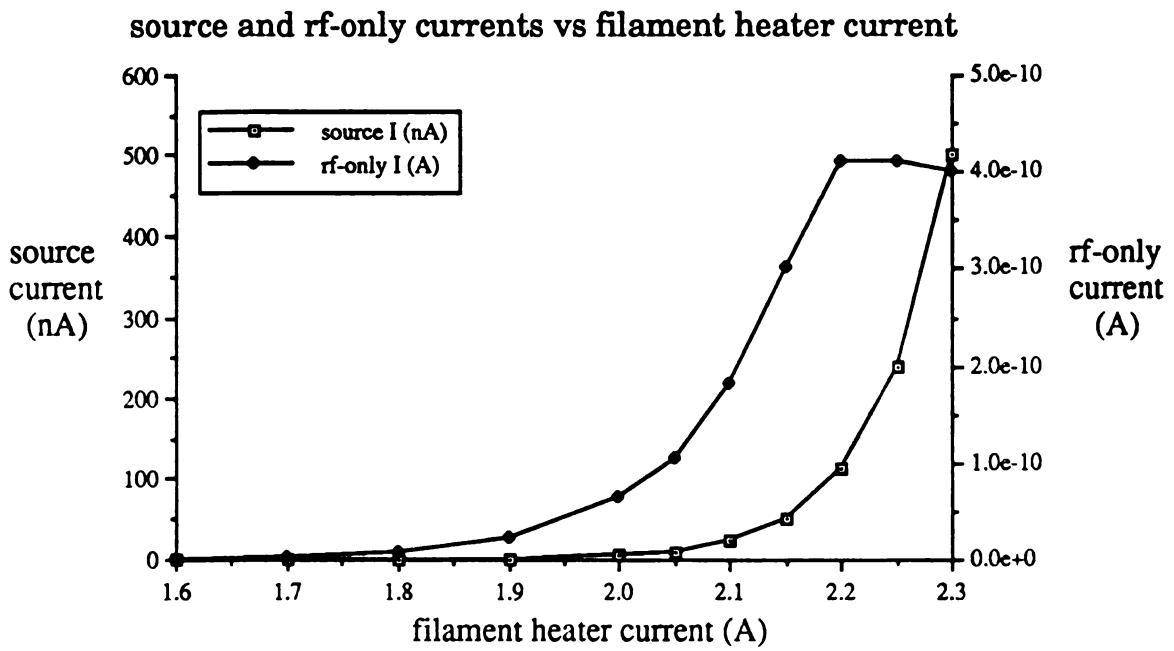

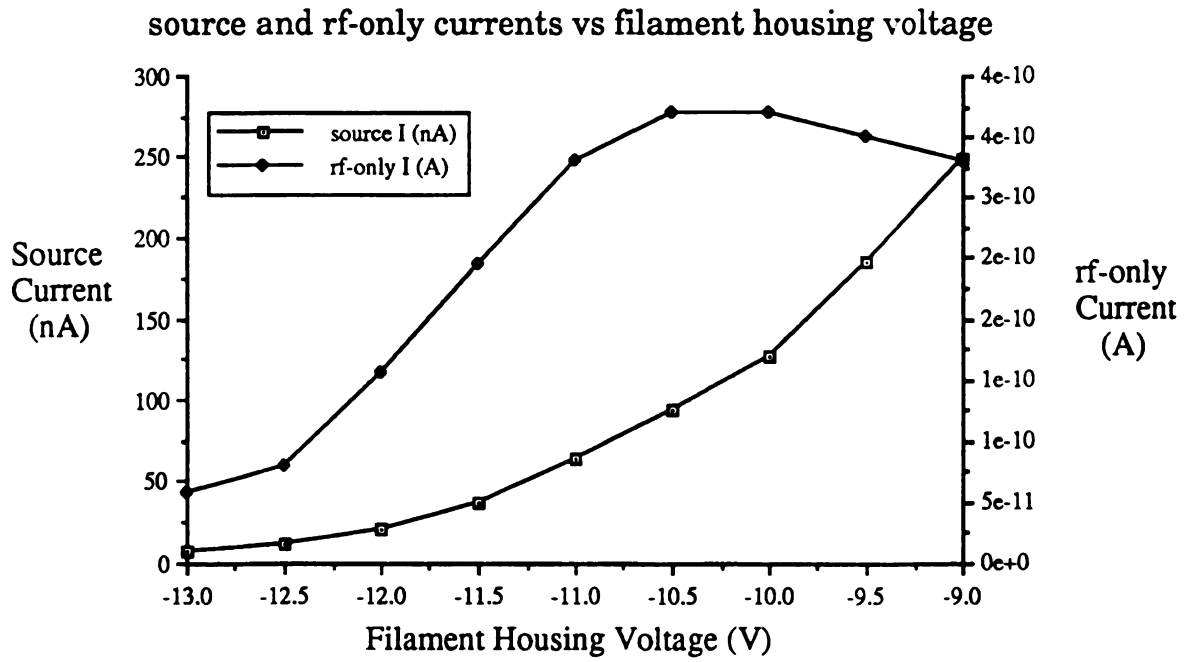

Appendix XII - Optimization study for the Anavac source and quadrupole. The source was configured for surface ionization using a cesium bead biased at -2.5 V, with a leak of carbon tetrachloride. Ions were detected at a Faraday plate mounted after the quadrupole.

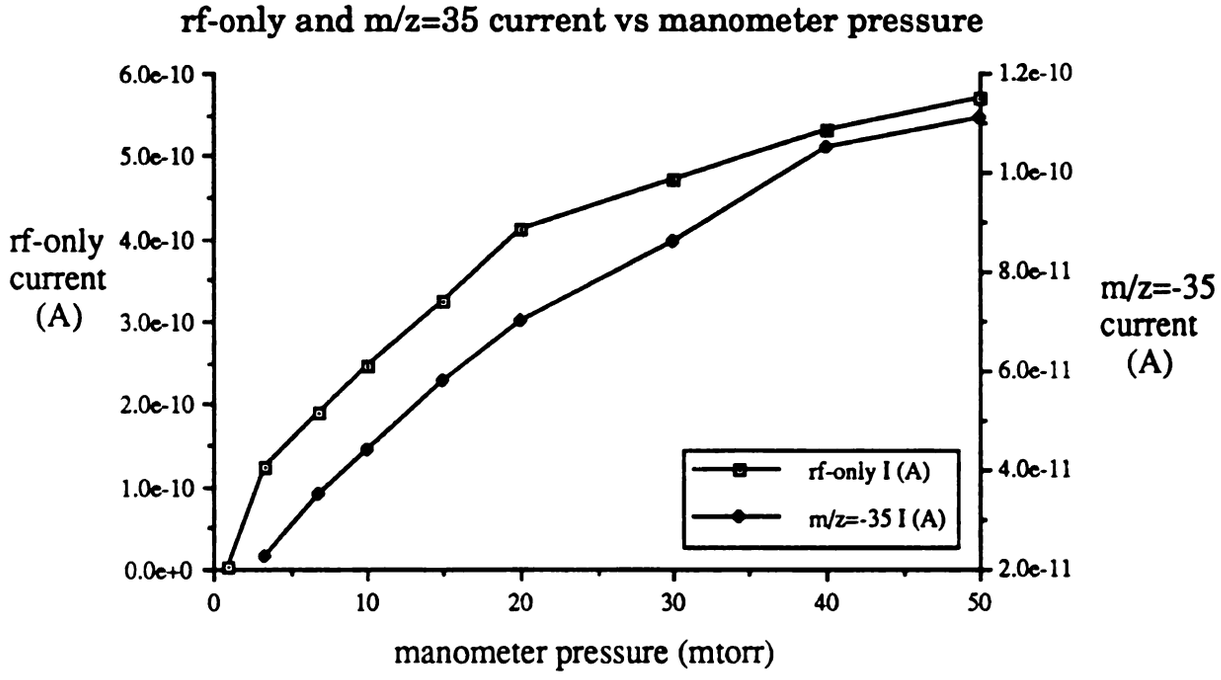

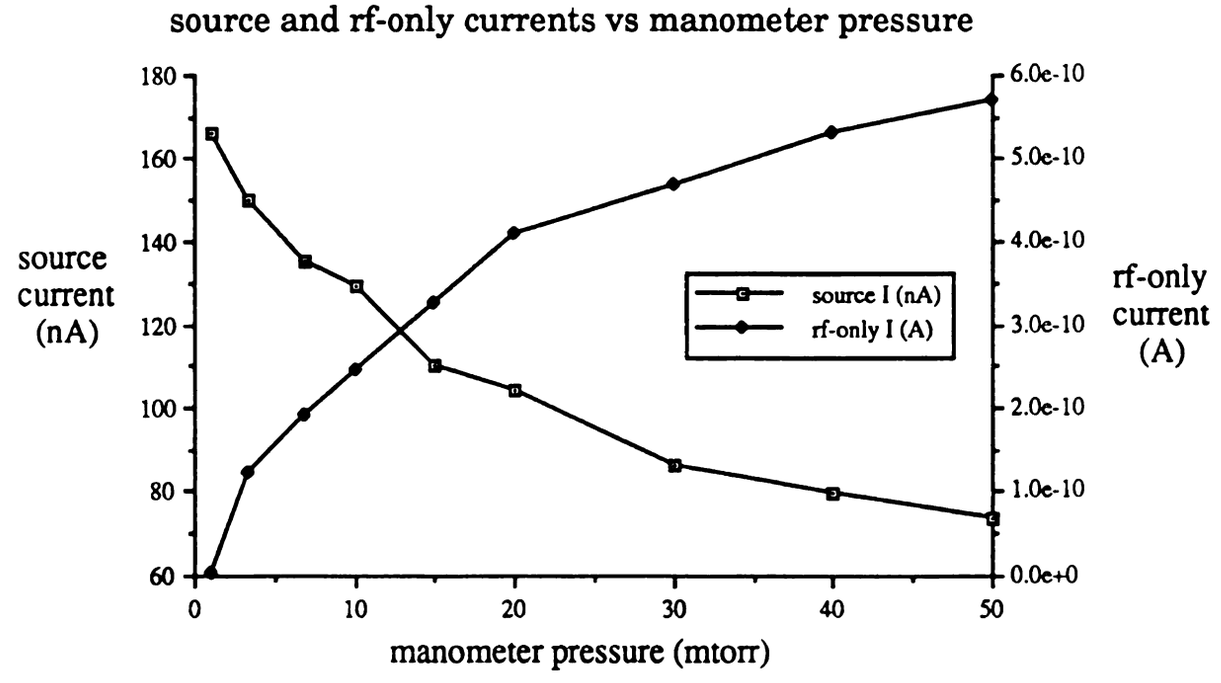

Appendix XIII - Optimization study for the Anavac source and quadrupole. The source was configured for surface ionization using a cesium bead biased at -3.0 V, with a leak of carbon tetrachloride. Ions were detected at a Faraday plate mounted after the quadrupole.

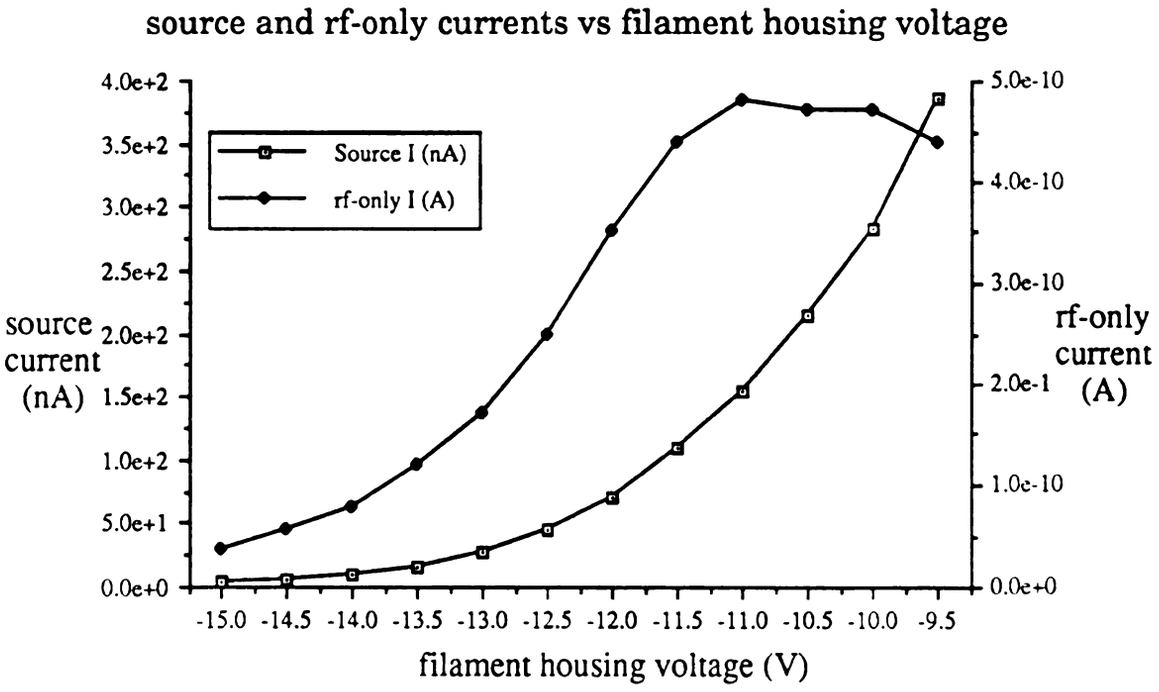

Appendix XIV - Optimization study for the Anavac source and quadrupole the source was configured for surface ionization using a cesium bead biased at -2.5 V, the aged Cs surface (no O2) and the same surface after exposure to oxygen (w/O2) are shown.

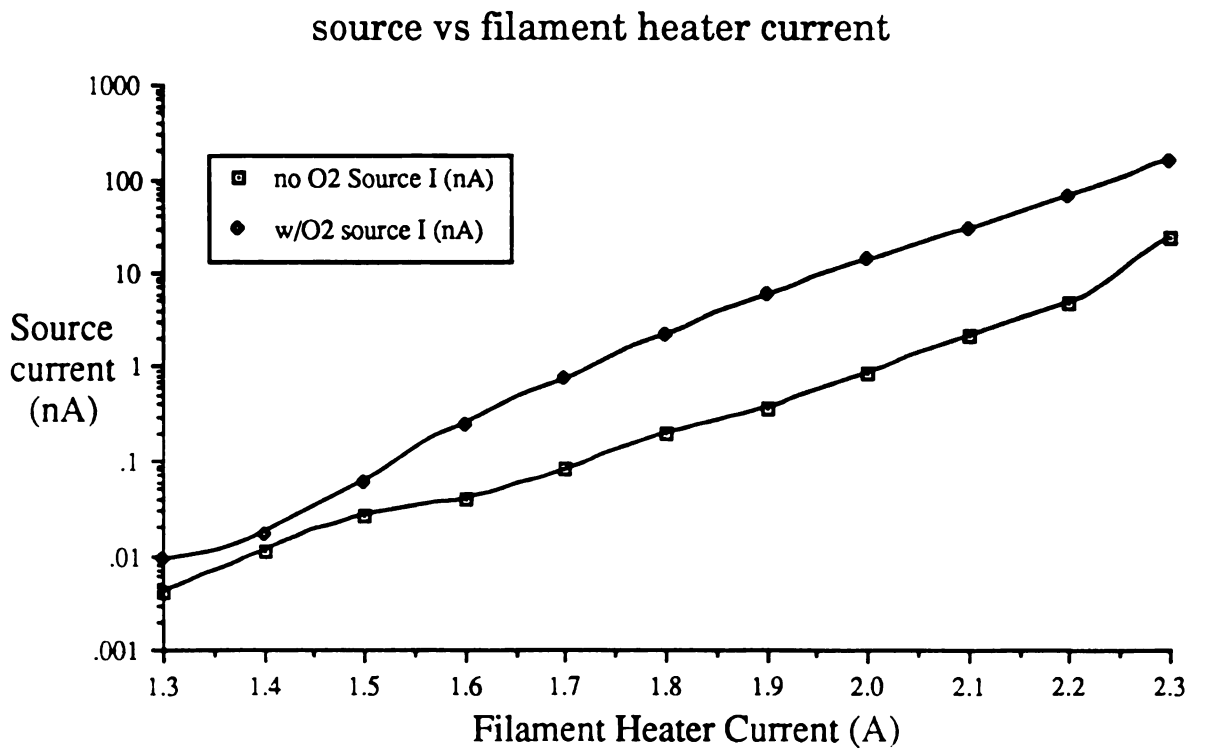

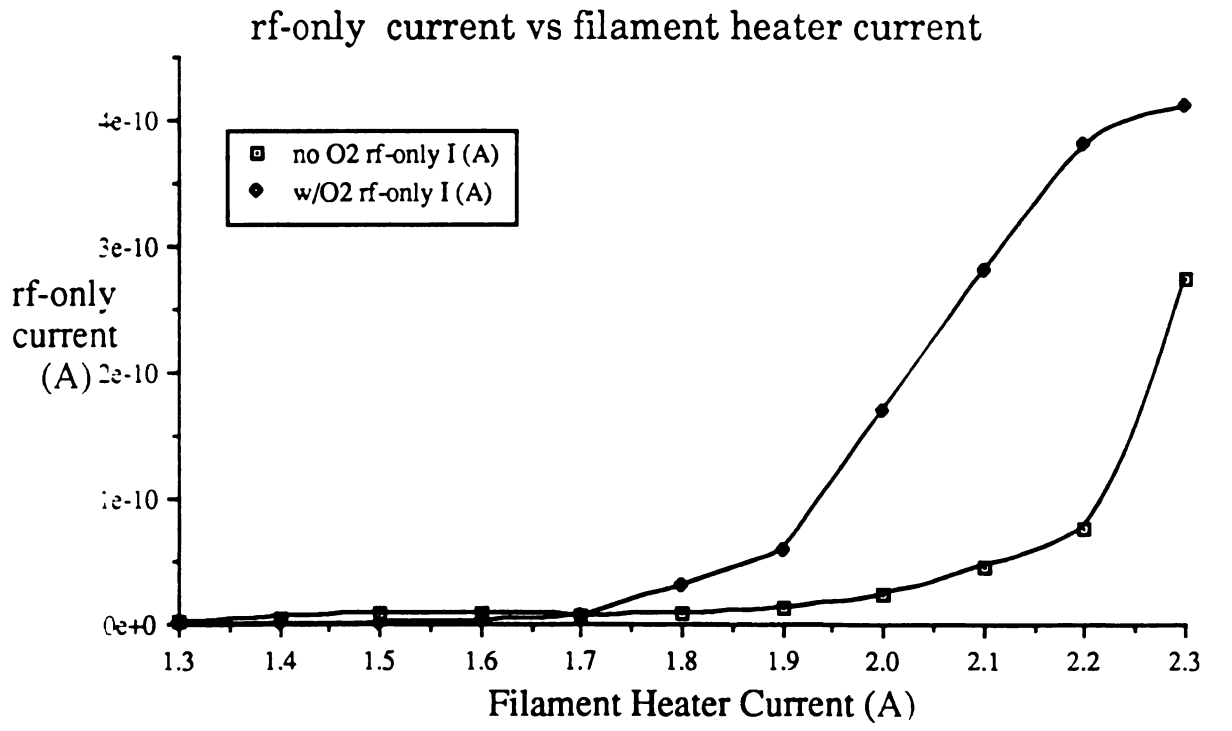

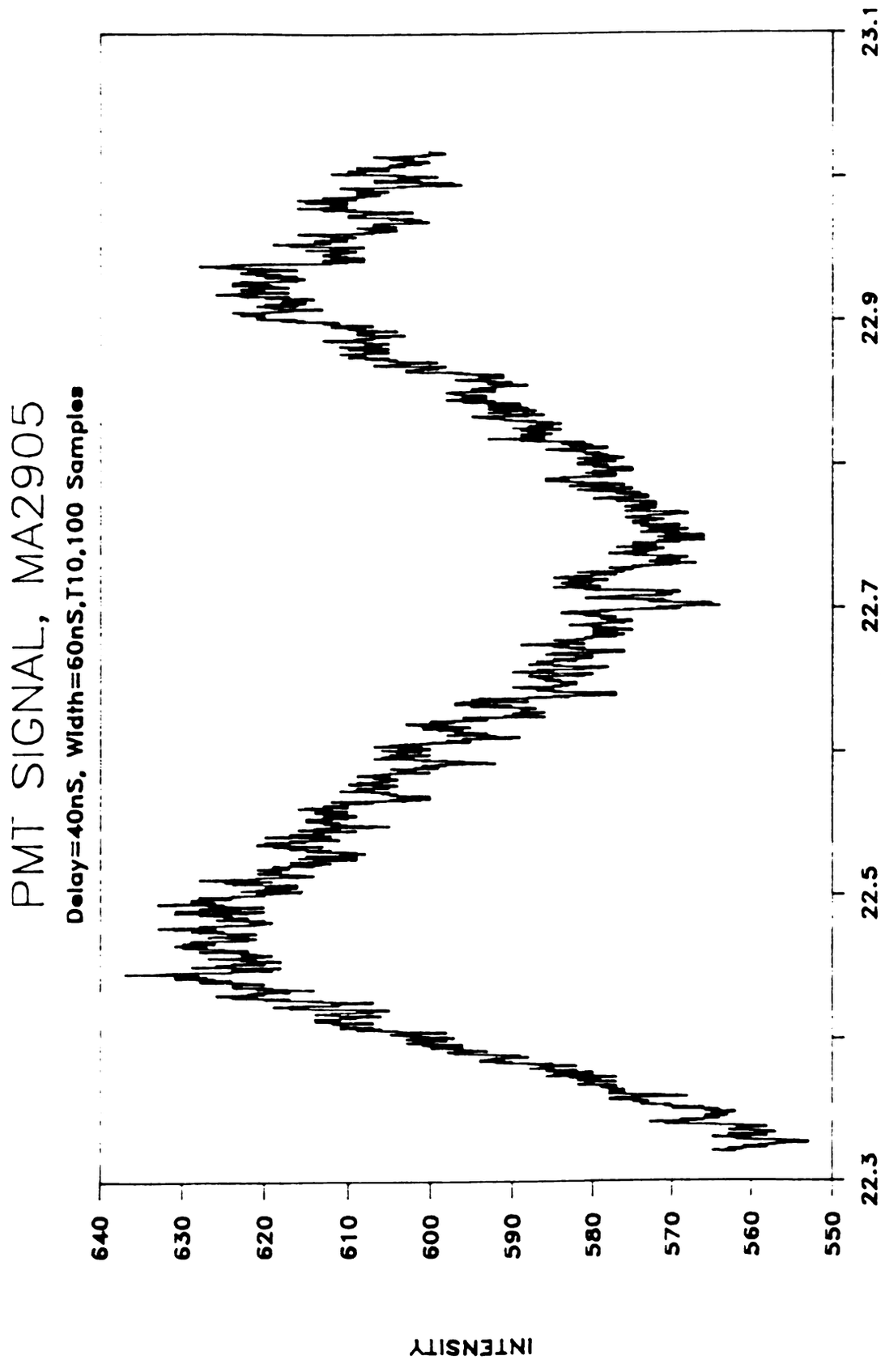

Appendix XV. The LIF spectrum of CS_2^+ trapped in solid argon

LIST OF REFERENCES

1. L.F. Halle, R. Houriet, M.M. Kappes, R.H. Staley, and J.L. Beauchamp, J. Am. Chem. Soc., 104, 6293 (1982).

2. D.B. Jacobson and B.S. Freiser, J. Am. Chem. Soc, 105, 5197 (1983).

3. M.M. Kappes and R.H.J. Staley, J. Am. Chem. Soc., 104, 1813 (1982).

4. D.B. Jacobson, and B.S. Freiser, J. Am. Chem. Soc., 105, 736 (1983).

5. K.L Busch, G.L. Glish, and S.A. McLuckey, *Mass Spectrometry / Mass Spectrometry: Techniques and Applications of Tandem Mass Spectrometry*, VCH Publishers Inc, New York, 1988, 107-151.

6. J.L. Holmes, Org. Mass Spectrom., 20, 169 (1985).

7. J.D. Morrison, in M.T.P. International Review of Science, Physical Chemistry Series One, Vol. 3: Mass Spectrometry, A. Maccoll, ed., Chap. 2, Butterworths, London (1972).

8. P.C. Burgers and J.L. Holmes, Org. Mass Spectrom., 17, 123 (1982).

9. J. Berkowitz and K.O. Groeneveld, eds., *Molecular Ions; Geometric and Electronic Structures*, Plenium Press, New York, 1980.

10. J.P. Maier, Chem. Soc. Rev., 17, 45 (1988).

11. R.C. Woods, *Ion and Cluster Ion Spectroscopy and Structure*, J.P. Maier, ed., Elsevier, New York, 1989, 27-58.

12. Z. Vager, R. Naaman, and E.P. Kanter, *Ion and Cluster Ion Spectroscopy and Structure*, J.P. Maier, ed., Elsevier, New York, 1989, 1-26.

13. M.E. Jacox, J. Phys. Chem. Ref. Data, 17, 269 (1988).

14. T. Amano, Phil. Trans. R. Soc. Lond. A, 324, 163 (1988).

15. E. Whittle, D.A. Dows, and G.C. Pimentel, J. Chem. Phys., 22, 1954 (1943).

16. M.C.R. Symons, Chem. Soc. Rev, 13, 393 (1984).

17. R.N. Perutz, Chem. Rev., 85, 97 (1985).

18. J.V. Coe and R.J. Saykally, *Ion and Cluster Ion Spectroscopy and Structure*, J.P. Maier, ed., Elsevier, New York, 1989, 131-154.

19. L. Andrews, *Advances in Infrared and Raman Spectroscopy*, R.J.H. Clark and R.E. Hester, eds., Vol. 7, Heyden, London, 1980, 59-85.

20. M.J. Almond and A.J. Downs, *Advances in Spectroscopy,* R.J.H. Clark and R.E. Hester, eds., Vol. 17, John Wiley & Sons, New York, 1989, 107-185.

21. L.B. Knight Jr., Acc. Chem. Res., 19, 313, (1986).

22. L. Andrews, *Absorption Spectroscopy of Molecular Ions and Complexes in Noble-Gas Matrices*, L. Andrews and M. Moskovits, eds., Elsevier, Oxford, 1989.

23. L. Andrews, Ann. Rev. Phys. Chem., 30, 79 (1979).

24. D. E. Milligan and M.E. Jacox, J. Chem. Phys, 51, 1952 (1969).

25. J.R. Morton and K.F. Preston, Inorg. Chem., 24, 3317 (1985).

26. C.A. Wight, B.S. Ault, and L. Andrews, J. Chem. Phys., 65, 1244 (1976).

27. L. Andrews, J.M. Gryzbowski, and R. O. Allen, J. Phys. Chem., 79, 904 (1975).

28. L.B. Knight Jr., J.M. Bostick, J.R. Woodward, and J.J. Steadman, J. Chem., Phys., 78, 6415 (1983).

29. L.B. Knight Jr., P.K. Miller, and J.J. Steadman, J. Chem. Phys., 80, 4587, (1984).

30. L.B. Knight Jr. and J.O. Herlong, J. Chem. Phys., 91, 69 (1989).

31. J. Hacaloglu and L. Andrews, Chem. Phys. Lett., 160, 274 (1989).

32. D. Forney, M. Jakobi, and J.P. Maier, J. Chem. Phys., 90, 600 (1989).

33. M.S. Sabo, Ph.D. Dissertation, Michigan State University, 1990.

34. P. Lenard, Ann. d. Phys., 8, 149 (1902).

35. T. D. Märk and G. H. Dunn, eds., *Electron Impact Ionization*, Springer-Verlag, Vienna (1985).

36. M. E. Rose and R. E. W. Johnstone, *Mass Spectrometry for Chemists and Biochemists*, Cambridge University Press, Cambridge, England (1982).

37. T. D. Märk in *Gaseous Ion Chemistry and Mass Spectrometry*, Jean H. Futrell, ed., John Wiley & Sons, New York (1986) p 61-93.

38. T.D. Märk, F.Egger, and M. Cheret, J. Chem. Phys, 67, 2629 (1977).

39. K. Biemann, *Mass Spectrometry: Organic Chemical Applications*, McGraw Hill, New York (1962).

40. F. Pichou , R. I. Hall, M. Landau, and C. Scherman, J. Phys., B16, 2445 (1983).

41. L. J. Kieffer and G. H. Dunn, Rev. Mod. Phys., 38, 1 (1966).

42. A.J. Dempster, Phys Rev., II, 316 (1918).

43. A. O. Nier, Rev. Sci. Instrum., II, 212 (1940).

44. H. E. Duckworth, *Mass Spectrometry*, Cambridge University Press, 1958, 37-41.

45. J. T. Watson, *Introduction to Mass spectrometry*, Raven Press, New York 1985.

46. T. D. Märk, Int. J. Mass Spectrom. Ion Phys., 45, 125 (1982).

47. A. O. Nier, Rev. Sci. Instrum., 18, 398 (1947).

48. W. Paul, H. P. Reinhard and U. von Zahn, *Z. Phys.*, 152, 132 (1958).

49. J. H. Batey, Vacuum, 37, 659 (1987).

50. F.H. Field and M.S.B. Munson, J. Amer. Chem. Soc., 87, 3289 (1965).

51. M.S.B. Munson and F.H. Field, J. Amer. Chem. Soc., 88, 2621 (1966).

52. F. Hunt , Adv. Mass. Spectrom., 6, 359 (1973).

53. B.L. Jelus, B. Munson, and C. Fenselau, Biomed. Mass. Spectrometry., 1, 96 (1974).

54. F. H. Field, Chemical ionization mass spectrometry, Accounts Chem. Res., 1, 42 (1968).

55. C. E. Melton, *Principles of Mass Spectrometry and Negative Ions*, Marcel Dekker Inc., New York, 1970.

56. D. F. Hunt, G.C. Stafford, F.W. Crow, and J.W. Russell, Anal. Chem., 48, 2098 (1976).

57. E.A. Stemmer and R.A. Hites, Anal. Chem., 57, 684 (1985).

58. C.E. Klotz, *Fundamental Processes in Radiation Chemistry*, P. Ausloos, Ed., John Wiley and Sons, New York, 1968, p 40.

59. R.C. Dougherty, Anal. Chem., 53, 625 (1981).

60. J.H. Bowie, Mass Spectrom. Rev., 3, 161 (1984).

61. H.P. Tannenbaum, J.D. Roberts, and R.C. Dougherty, Anal. Chem., 47, 49 (1975).

62. M. Deinzer, D. Griffin, T. Miller, J. Lamberton, P. Freeman, and V. Jonas, Mass Spectrom., 9, 85, (1982).

63. A.G. Harrison, *Chemical Ionization Mass Spectrometry*, CRC Press, Boca Raton, Fla, (1983).

64. H.E. Duckworth, Mass Spectroscopy, Cambridge University Press, Cambridge, 1960, p 35.

65. J. Elster and H. Geitel, Ann. Phys., Chem., 37, 315 (1889).

66. J. C. Beattie, Philos. Mag., 48, 97 (1899).

67. J.J. Thomson, Proc. Cambridge Philos. Soc., 15, 64 (1908).

68. J.P. Blewett and E.J. Jones, Phys. Rev., 50, 464 (1936).

69. J.C. Blais, A. Brunot, and M. Cottin, Int. J. Mass Spectr. Ion Phys., 22, 71 (1976).

70. R.Grosser, K.G. Heumann, and W. Schindlmeier, Adv. Mass Spectr., J.F.J. Todd, ed., B, 1057 (1985).

71. D.Bombick,Ph.D. Dissertation, Michigan State University, 1986.

72. J.B. Moreau, Rev. Phys. Appl., 3 , 286 (1968).

73. N.I. Ionov, Prog. Surf. Sci., 1, 237 (1972).

74. T. Fujii and H. Jimba, Int. J. Mass Spectrom. Ion Phys., 79, 221 (1987).

75. G. Owen, Proc. Cambridge Philos. Soc., 12, 493 (1904).

76. O.W. Richardson, Phys Rev., 34, 386 (1912).

77. M.J. Cardillo, M.S. Chou, E.F. Green, and D.B. Sheen, J. Chem. Phys., 54, 3054 (1971).

78. H. Kawano, Shinku, Vacuum, 23, 1 (1980).

79. H. Kawano, Shinku, Vacuum, 23, 229 (1980).

80. H. Kawano, and F.M. Page, Int. J. Mass Spectrom. Ion Phys. , 50, 1 (1983).

81. H. Kawano, Y. Hidaka, and F.M. Page, Int. J. Mass Spectrom. Ion Phys. , 50, 34 (1983).

82. H. Kawano, Y. Hidaka, M. Suga, and F.M. Page,Int. J. Mass Spectrom. Ion Phys. , 50, 77 (1983).

83. H. Hotop and W.C. Lineberger, J. Phys. Chem. Ref. Data, 4, 539 (1975).

84. A. Persky, E.F. Green, and A. Kuppermann, J. Chem. Phys., 49, 2347 (1968).

85. J.C. Blais and G. Bolbach, Int. J. Mass Spectr. Ion Phys., 24, 412 (1977).

86. J.M. Lafferty, J. Appl. Phys., 22, 299 (1951).

87. L.J. Favreau, Rev. Sci. Instr., 36, 856 (1965).

88. H. Kishi and H. Kawano, Int. J. Mass Spectr. Ion Phys., 85, 301 (1988).

89. N. Kashihira, E. Vietzke, and G. Zellerman, Rev. Sci. Instrum., 48, 171 (1977).

90. S. Dushman, Rev. Mod. Phys., 2, 381 (1930).

91. D. Bombick and J. Allison, J. Chrom. Sci., 27, 612 (1989).

92. W. Geiger, Z. Phys., 140, 608 (1955).

93. H. Kawano, J. Chem. Phys., 75, 3471 (1971).

94. J.W. Trischka, D.T.F. Marple, and A. White, Phys. Rev., 85, 136 (1952).

95. J.T. Cheng and S. Datz, J. Chem. Phys, 71, 1814 (1979).

96. J.F.J. Todd and G. Lawson, *Int. Rev. Sci. Mass Spectrometry, Physical Chemistry Series two* V5, A. Maccoll and A.D. Buckingham, eds., Butterworths, London, 1975.

97. P.H. Dawson, Mass Spectrometry Reviews, 1986, John Wiley & Sons Inc., 5, 1 (1986).

98. Extrell Corporation 1978 short course, theory and operation of quadrupoles.

99. P. E. Miller and M. B. Denton, J. Chem. Ed., 63, 7 (1986).

100. D.W. McLachlan, "Theory and Applications of Mathieu Functions", Clarendon: Oxford, 1947.

101. F.M. Mao and J.H. Leck, Vacuum, 37 , 669 (1987).

102. N. Ierokomos, 20th ASTM Meeting on Mass Spectrometry and Allied Topics, 221, Dallas, Texas.

103. The ARRL handbook for the Radio Amateur, B.S. Hale, ed., American Radio Relay League, Newington, Ct, 1989.

104. R.G. Wilson and G.R. Brewer, *Ion Beams*, John Wiley and Sons, 1973.

105. J.E. Delmore, Int. J. Mass Spectrom. Ion Processes, 56, 151 (1984).

106. P. Grivet, *Electron Optics*, Pergamon Press, New York, 1965.

107. A.O.C. Nier, Rev. Sci. Instrum., 18, 336 (1947).

108. L.A. Dietz, Rev. Sci. Instrum., 30, 235 (1959).

109. Hsi-men, and Chi-yeh, Advances in Electronics and Electron Optics, J. Ximan, ed., Supplement 17, (1986).

110. E. Harding and F.H. Read, *Electrostatic Lenses*, Sydney and Machenster, 1974.

111. T. Matsuo, Jpn. J. Appl. Phys., 23, 1518 (1984)

112. H. Wollnick, J. Brezina, and M. Berz, Nucl. Instrum. Methods A, 258, 408 (1987).

113. R.J. Ryba and G.J. Mains, Int. J. Mass Spectrom. Ion Physics, 42, 169 (1982).

114. A. Vertes, P. Juhasz, and L. Matus, Int. J. Mass Spectrom. Ion Processes, 73, 109 (1986).

115. A. Vertes, P. Juhasz, L. Balazs, M. de Wolf, and R. Gijbels, Int. J. Mass Spectrom. Ion Processes, 84, 255 (1988).

116. H.T. Shaw, S. Niemeyer, and G.F. Hunt, Int. J. Mass Spectrom. Ion Processes, 68, 317 (1986).

117. D.C. McGilvery, Ph.D. Dissertation, LaTrobe University, 1978.

118. D.A. Dahl and J.E. Delmore, presented at the 34th annual A.S.M.S. conference 1986 (pg 304).

119. D. A. Dahl, J. E. Delmore, and A. D. Appelhans, Rev. Sci. Instrum., 61, 607 (1990).

120. D.C. McGilvery and R.J.S. Morrison, MacSIMION, PTY LTD, Clayton, Victoria, Australia, 1988.

121. J.E. Delmore, Int. J. Mass Spectrom. Ion Processes, 56, 151 (1984).

122. H.S. McKown, D.H. Smith, and R.L. Sherman, Int. J. Mass Spectrom. Ion Phys., 51, 39 (1983).

123. Wright, M. C., Inst. Phys. Conf. Ser., 94, 363 (1989).

124. J.E. Delmore, Int. J. Mass Spectrom. Ion Processes, 67, 121 (1985).

125. W.C. Wiley and C.F. Hendee, IRE Trans. Nucl. Sci., NS-9, 103 (1962).

126. J. L. Wiza, Nucl. Instrum. Methods, 162, 587 (1979).

127. J.G. Timothy and R.L. Bybee, Rev. Sci. Instrum., 48, 202 (1977).

128. C.E. Griffin, H.G. Boettger, and D.D. Norris, Int. J. Mass Spectrom. Ion Phys., 15, 437 (1974).

129. Guor-Rong Her, Ph.D. Dissertation , Michigan State University, 1985.